Erosion Mitigation via Bio-Mediated Soil Improvement

Thesis submitted in partial fulfilment of the requirements for the degree of

Doctor of Philosophy

by

Anant Aishwarya Dubey

Department of Civil Engineering
Indian Institute of Technology
Guwahati-781039
India

School of Civil & Mechanical Engineering
Curtin University
Perth- 6102
Australia

October 2022

Erosion Mitigation via Bio-Mediated Soil Improvement

Thesis submitted in partial fulfilment of the requirements for the degree of

Doctor of Philosophy

by

Anant Aishwarya Dubey

Department of Civil Engineering
Indian Institute of Technology
Guwahati-781039
India

School of Civil & Mechanical Engineering
Curtin University
Perth- 6102
Australia

October 2022

Candidate's Declaration

The work reported in this thesis is original and was carried out by me during my tenure as a collaborative PhD student at the Department of Civil Engineering, Indian Institute of Technology, Guwahati and School of Civil & Mechanical Engineering, Curtin University, Perth, Australia. This thesis has not formed the basis for the award of any degree, diploma, associateship, membership or similar title of any university or institution.

Date: 20-10-2022

Anant Aishwarya Dubey
Collaborative PhD Candidate
1. Registration No. 166104011
Department of Civil Engineering
Indian Institute of Technology Guwahati
2. Registration No. 19733654
School of Civil and Mechanical Engineering
Curtin University

CERTIFICATE

It is certified that the work described in this thesis titled **"Erosion Mitigation via Bio-Mediated Soil Improvement"** by Mr Anant Aishwarya Dubey for the award of the degree of Doctor of Philosophy is an authentic record of the results obtained from research work carried out under our supervision at the Department of Civil Engineering, Indian Institute of Technology Guwahati (India) and School of Civil & Mechanical Engineering, Curtin University (Australia). To the best of our knowledge, this work is not submitted elsewhere for the award of any other degree or diploma.

Dr K Ravi
Associate Professor
Department of Civil Engineering,
Indian Institute of Technology,
Guwahati

Prof. Abhijit Mukherjee
Professor
School of Civil &
Mechanical Engineering,
Curtin University

Dr Navdeep K Dhami
Senior Research Fellow
School of Civil &
Mechanical Engineering,
Curtin University

Acknowledgements

I am grateful to many people who have supported me during the realisation of my doctoral research. I am fortunate to be a part of the collaborative doctoral program at Indian Institute of Technology Guwahati and Curtin University, Australia.

First and foremost, my sincere thanks go to my supervisors, Dr K Ravi (Associate professor, IIT Guwahati), Prof. Abhijit Mukherjee (Professor, Curtin University) and Dr Navdeep K. Dhami (Senior Research Fellow, Curtin University). I consider myself fortunate to have Dr K Ravi as my principal research supervisor. He did not only introduce me to the field of bio-mediated soil improvement and geo-environmental engineering but also trained me to assess the existing real-life geotechnical challenges around us. During my stay at Curtin University, Prof. Abhijit Mukherjee imparted to me the valuable skills of time management, efficient designing of a research plan and sophisticated scientific communication. I am grateful to Dr Navdeep K Dhami for always being available for discussions and for the motivation that I required most for my research, especially in tough times. I will be forever indebted to their excellent guidance, encouragement, and affection. My supervisors contributed a great deal to my understanding of the research area through valuable discussions, ideas, and useful comments. I am lucky to have them as my technical guardians.

I express my sincere thanks to the members of my Doctoral Committee, Prof. Sreedeep S., Prof. Vibin Ramakrishnan, and Dr Abhishek Kumar, for their valuable suggestions and continuous encouragement at various stages of the research work. My sincere thank goes to Prof. Mohamed A. Shahin and Prof. Lingaraj Sahoo for their valuable insights on the research objectives.

I appreciate the Head of the department, faculty members, and technical staff of the Department of Civil Engineering at both institutes for providing support and facilities during

the course of my research work. I also thank Prof. T. V. Bharat and Prof. Ankit Garg for their excellent classes on unsaturated soil mechanics and geo-environmental engineering.

I would like to thank my seniors Dr Rohini C Kale, Dr Subhra Majhi, Dr Asha L Ramachandran, Dr Shiv Shankar Kumar, Dr Pradeep K Dammala, Mr Chandrabhanu Gupt, Dr Jay Kumar Shah, Dr Abiala Moses, Dr Sanjeev Kumar and Dr Surbhi Jain for giving their precious motivations and remarks related to my research work.

I am obliged to Mr Rituraj Devrani and Mr Jack Hooper-Lewis for helping me during my experimental work.

I sincerely acknowledge the affectionate forbearance and continuous motivations received from my friends Mr Deepak Patwa, Mr Rahul Raoniar, Mr Rajeev Gandhi BG, Mr Saroj Kumar Sahu, Dr Abhisekh Saha, Dr Jinesh Machale, Mr Krushna Sonar, Ms Sakshi Tiwari, Dr Sukrit Kumar De, Dr Nimrat Pal Kaur, Dr Abhijit Mistri, and Dr Aparna Harichandran.

I will be forever indebted to Indian Institute of Technology Guwahati and Curtin University for the wonderful ambience bestowed upon me, which helped me to understand the significance and magnificence of research.

My family has been my greatest source of joy and comfort. I am grateful to my parents, Mr Pawan K. Dubey and Mrs Neelam Dubey, for their prayers, unconditional love and support. I can never forget the support I received from my sister Ms Anu A Dubey, during the tough times. I am forever indebted to my wife, Mrs Aparna Dubey, for her sacrifices, support, love, and unconditional supply of coffee. I am also grateful to Prof. S K Pandey (IIT-BHU), my uncle, who consistently inspired me during my PhD. Above all, I owe it all to almighty God for granting me the wisdom, health, and strength to undertake this research task and enabling me to its completion.

Anant Aishwarya Dubey

Abstract

Existing soil erosion mitigation practices that focus on cement-based hard structures and chemical grouts have limitations in terms of their environmental impact and effectiveness. Recently bio-mediated soil improvement has been proposed by several researchers as a promising eco-friendly solution for mitigating erosion. However, the bio-mediated soil improvement techniques have their own limitations, such as bacteria transportation to the site, non-uniform distribution of bio-precipitates, and generation of ammonia as a by-product.

In the current study, biocementation is employed in soil with the aim of investigating its influence on aeolian erosion, riverbank erosion and coastal erosion using soil microbes isolated from three different local sites. The thesis is comprised of five stages. First, it was revealed via 16S rRNA analysis that the isolated soil Firmicutes prevalently belong to *Sporosarcina* and *Pseudogracilibacillus* genera. The availability of the calcifying microbes in local soil reduces the liability of transporting extraneous microbes to the site.

Second, in a preliminary investigation to check the efficiency of the isolated strain, the desert sand was subjected to biocementation treatment at various concentrations of cementation media (CM), ranging from 250 to 1000 mM. A high unconfined compressive strength (UCS) value of around 900 kPa was observed with a low calcium carbonate content of 1.3%. The wind erosion resistance is observed to be maximum with 1000 mM cementation solution treatment withstanding the maximum wind velocity above 55 km/h.

The third objective was designed to formulate optimal concentration for cementation for improving surficial binding. The microbes liable for bio-augmentation, stimulation, and selective stimulation have been compared for their binding performance via needle penetration test against CM, ranging from 250 to 2000 mM concentration of CM. Maximum needle penetration resistance was observed at 500 mM concentration of CM for all the microbes. The findings revealed that the different microbes respond distinctively to different concentrations

of CM. Detailed microstructure analysis of the precipitated $CaCO_3$ crystals suggested that the morphology and quantity are major parameters influencing surficial strength.

Fourth, the Brahmaputra soil isolate (BS3) was employed for a selective stimulation-based treatment for the mitigation of current-induced riverbank erosion. Soil treated with up to four cycles of biocementation treatment (500 mM) has been tested on three different slopes (30°, 45° and 53°) in a flow-controlled hydraulic flume subjected to a critical current profile ranging from 0.06 to 0.62 m/s. Up to a four-fold reduction in the erosion rate was observed with biocementation treatment. However, cementation beyond a threshold (around 7% $CaCO_3$) led to the formation of brittle chunks. Thus, a bio-composite was devised by a pre-treatment of low-viscosity biopolymer along with biocementation. The bio-composite was found to effectively mitigate the current-induced erosion with 36% lower ammonia production. The dual characteristics of the bio-composite were confirmed with the microstructural analysis.

Fifth, the erosion characteristics of soil treated with various levels of biocementation are investigated against waves combined with the hydraulic current, similar to coastal erosion. It was observed that soil erosion declined exponentially with the increase in $CaCO_3$ content against the perpendicular waves. However, the brittle fracture beyond a threshold limits the efficacy of biocementation against the tangential waves. The findings from the current study will be helpful for the transition of bio-mediated treatment toward field-scale applications for erosion control.

Keywords: Bacteria Isolation, Biostimulation based MICP, Desert erosion, Riverbank erosion, coastal erosion, Bio-mediated soil improvement.

CONTENTS

CHAPTER 3 MATERIALS AND METHODS

CHAPTER 4 ENRICHMENT, ISOLATION, AND CHARACTERISATION OF BIOCEMENTATION POTENT MICROBES FROM LOCAL SOILS

CHAPTER 5 INFLUENCE OF BIOCEMENTATION ON GEOTECHNICAL PROPERTIES AND AEOLIAN EROSION CHARACTERISTICS OF DESERT SOIL

CHAPTER 6 THE IMPACT OF CEMENTATION MEDIA CONCENTRATION ON BIOCEMENT PROPERTIES UNDER-STIMULATION AND AUGMENTATION

List of figures

List of tables

List of symbols/abbreviations

Symbol/ Abbreviation	Description
BS	Brahmaputra sand
BRS	Brahmaputra river stream
LS	Soil from the local slope
RS	Rajasthan Desert Sand
D_{50}	Mean particle size (mm)
C_u	Coefficient of uniformity
C_c	Coefficient of curvature
UCS	Unconfined compressive strength (MPa)
K_{sat}	Coefficient of permeability (m/s)
$O.D._{600}$	Optical density at 600 nm
mM	Millimoles (Molar concentration)
M	Moles (Molar concentration)
NB5U	Enrichment media
NBU	Growth media
FM	Fixation media

Symbol/ Abbreviation	Description
CM	Cementation media
SP	*Sporosarcina pasteurii*
BS3	Isolated strain from Brahmaputra riverbank
C	Consortia
TDV	Threshold detachment velocity (km/h)
v_c	Critical flow velocity (m/s)
NPI	Needle penetration index (N/mm)
C or $CaCO_3$	Calcium carbonate
A_s	Surface area of the specimen
D	Total eroded depth
v	Current/Flow velocity (m/s)
A	Cross-sectional area of flow (m^2)
t	Total test duration
E_R	Cumulative erosion rate
P_S	Specific power of current (W/m^2)

Symbol/ Abbreviation	Description
S35	35° soil slope (1 horizontal to 0.7 vertical)
S45	45° soil slope (1 horizontal to 1 vertical)
S53	53° soil slope (1 horizontal to 1.32 vertical)
E_w	Wave energy as per linear shallow water wave theory
E_D	Wave energy density
ρ	Density of the water (997 kg/m^3 at 25 °C)
ρ_s	Density of sand (in kg/m^3)
ρ_a	Density of air (in kg/m^3)
d	Effective diameter of the particles
g	Gravitational acceleration
h_w	Wave height
f	Frequency of waves
A_s	The exposed surface area of the soil

Symbol/ Abbreviation	Description
φ	Friction factor
V	Total volume eroded
V_i	Initial volume of the treated specimen
V_t	Volume of retained soil at time 't'
m_L	Soil mass loss
m_i	Initial mass of treated soil
m_r	Mass of the residual soil
m_t	Mass of biocemented specimen prior to acid washing
m_a	Mass of the soil after acid-washing

CHAPTER 1

INTRODUCTION

1.1 Overview

Soil is one of the major resources for life, along with air and water (García-Ruiz et al. 2015). A drastic soil loss of greater than 24 billion tonnes per year is reported around the globe (United Nations 2019). Aeolian, riverbank, and coastal erosion are the major contributors to global soil loss.

The majority of the deserts around the globe are vulnerable to aeolian erosion (D'Odorico et al. 2013). Around 12% of the dryland is found vulnerable to degradation accounting for an area of around 5 million square kilometres (Burrell et al. 2020). In India, 73% of the Thar desert has a vulnerability to wind-induced erosion (Moharana et al. 2016; Chlachula 2021). The majority of desert soil consists of dry and cohesionless loose sand, which is subjected to surface erosion due to aeolian processes. The erosion is generally initiated by sediment detachment followed by entrainment, transport, and deposition of the detached particles. Every so often, the aeolian processes are also liable to the formation of some of the majestic aeolian landforms such as crescent sand dunes and pinnacle Karst. In Figure 1 (a), the pinnacle karst of Nambung National Park, Western Australia, is shown. The pinnacles have formed in the Limestones due to cyclic aeolian erosion processes (Lipar and Webb 2015). However, the dust and sand particles are also released into the air due to the aeolian erosion, which adversely impacts human health and essential infrastructural services such as transportation, telecommunication, and electricity.

(a)

(b)

(c)

Figure 1.1 (a). Aeolian erosion induced pinnacles karst in Nambung National Park, Western Australia; (b). Bank erosion along the Brahmaputra River, Guwahati region, India (c). Coastal erosion at eagle-bay, Rottnest Island, Australia. (Photographs taken by Authors)

Riverbank erosion also contributes significantly to global land degradation. The majority of the banks along the mega rivers have been reported to lose substantial land due to erosion (Latrubesse 2008; Das et al. 2014). One such mega river is the Brahmaputra, which caused a land loss of 2358.57 square kilometres in the Assam valley between 1912 and 1996 in India (Sarma 2005). The collapse of the riverbank due to bank erosion, as shown in Figure 1 (b), is common. Brahmaputra river is eroding the North-eastern Assam shoreline with an erosion rate of 80 square km per year (Phukan et al. 2012).

On the other hand, around 40% global population is impacted by coastal erosion, and an overall surface loss of 28,000 square kilometres is recorded over a period of 32 years (1984-2015). The coasts are enduring severe erosion leading to loss of land and infrastructure. One such coastal bank is situated near eagle bay, Rottnest Island, Australia. The photo of the beach is shown in Figure 1 (c). The marks of erosion induced by the sea waves can be observed clearly in the photograph.

The erosion control measures can be classified broadly into two categories, including deviating/attenuating the erosive forces with rigid structures and improving soil resilience by chemical binders. The attenuation of erosive forces such as wind, river currents and hydraulic waves is accomplished by means of hard structures, which are often costly and counterproductive as they lead to sediment imbalance and harm the ecology (Florsheim et al. 2008; D'Odorico et al. 2013). The other method to improve soil resilience includes chemical and cementitious binders. However, it is to be noted that synthetic grout materials, including micro-fine cement, epoxy, and silicates, have been reported to be toxic to the geo-environment (Karol 2003; DeJong et al. 2010) and, hence they can negatively impact the flora, fauna, and crop productivity of the soil. Therefore, an alternative riverbank erosion mitigation strategy with minimum intervention to the ecology is urgently needed.

1.2 Mechanism of surficial soil erosion

Aeolian, riverbank, or coastal erosion initiates with the detachment of soil particles from the surface. Figure 1.2 demonstrates the mechanics of surficial erosion initiation.

The surficial erosion begins once the erosive stress (τ) on the soil caused by the action of wind or water exceeds the critical stress (τ_c). The critical shear stress or critical velocity for soil grains majorly depends on the interparticle electrical forces (f_e), Interparticle contact forces (f_c), saturation /suction (u_w/-u_w), and weight of the particles (Briaud 2008). Later, the detached particles are entrained and transported with wind or water prior to their deposition. In the case of wind or water, the flow velocity at which critical stresses are generated and detachment of particle initiates is termed as critical velocity or threshold frictional velocity.

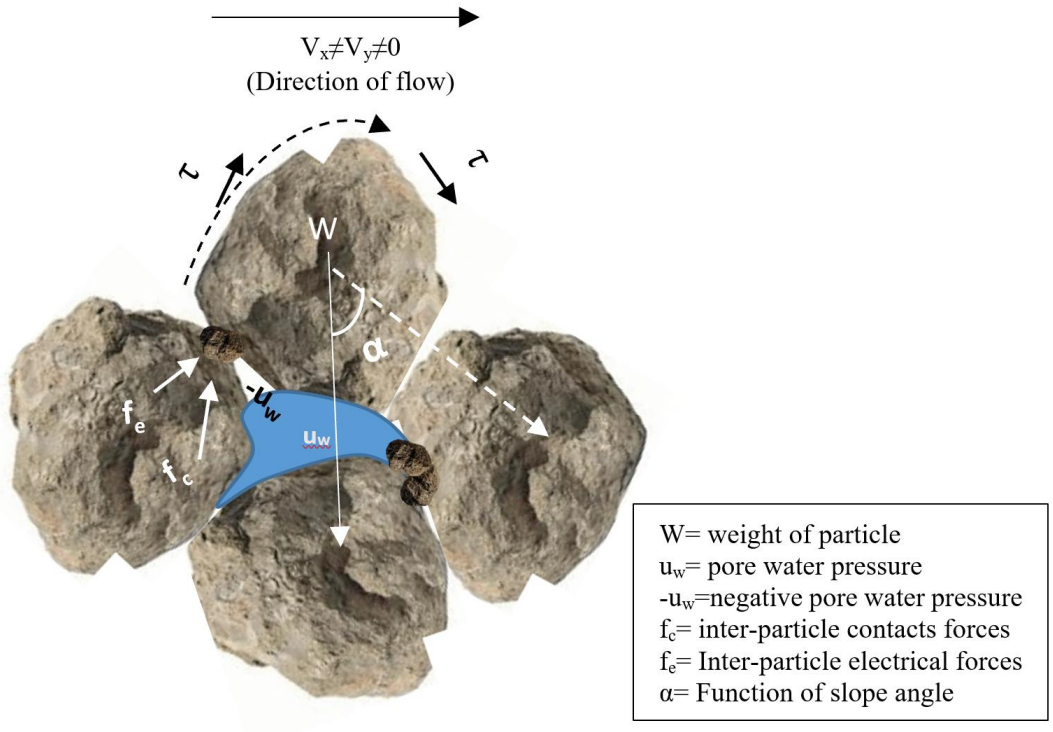

Figure 1.2 Mechanics of surficial erosion

1.3 Biocementation as a potential solution

Nature has been forming biominerals and cemented aggregates for millions of years, as seen in the case of anthills, cave speleothems, beach rocks and corals (Baskar et al. 2009; Dhami et al. 2013b). Figure 1.3 (a) shows an anthill formed nearby the department of civil engineering, while Figure 1.3 (b) illustrates Speleothems from Mawsmai Caves, Meghalaya, India. Figure 1.3 (c) illustrates a freestanding natural beach rock at Eagle-bay, Rottenest Island of Western Australia, withstanding erosion forces.

(a)

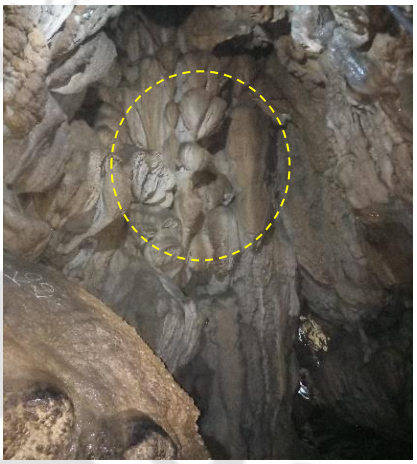

(b)

(c)

Figure 1.3 Example of naturally formed minerals, (a). Anthills near Civil Engineering Department, IIT Guwahati campus, (b). Speleothems from Mawsmai Caves, Meghalaya, India, and (c). Natural beach rock withstanding coastal erosion at Rottnest Island, Australia. (Photographs taken by Authors)

Previous literature has unravelled the biogenic and abiogenic biocementation processes responsible for such formations and emulated them in the laboratory (van Paassen et al. 2010a; Gomez et al. 2017; Ramachandran et al. 2020). The major pathways to biocementation are urea hydrolysis, denitrification, sulphate and iron reduction (DeJong et al. 2010). However, a calcite precipitation approach via the urea hydrolysis pathway, also known as microbially induced calcite precipitation (MICP), has found popularity in laboratory simulations due to the ease of control, durability and rapid soil strength improvement (Dhami et al. 2013b; Mujah et al. 2017; Terzis and Laloui 2019). Therefore, mimicking the natural biocementation via urea hydrolysis might also provide an eco-friendly solution for soil erosion mitigation.

1.4 Need of the study

The major challenges associated with biocementation via the urea hydrolysis pathway are ammonium by-production, non-uniformity of precipitation, and transport of healthy ureolytic bacteria in large quantities to the site (DeJong et al. 2010). The presence of native ureolytic bacteria and their on-site enrichment can tackle the challenge of bacteria transport (Dhami et al. 2017; Gomez et al. 2017; Graddy et al. 2021).

While soil bacteria may have the advantage in terms of their survival, their performance for improvement in erosion resistance of soil has not been addressed largely. Most of the previous studies have considered the exogenous microbe *Sporosarcina pasteurii* for limiting wind-induced erosion, tangential hydraulic-flow-induced erosion and wave-induced erosion (Maleki et al. 2016; Tian et al. 2018; Wang et al. 2018a; Zomorodian et al. 2019; Kou et al. 2020; Shahin et al. 2020; Clarà Saracho et al. 2021; Do et al. 2021; Liu et al. 2021b). Further, the biocementation process could be improved by controlling the uniformity and amount of generated ammonia. The biopolymers are found to provide an ambient micro-environment and moisture to the biocementing microbes (Wang et al. 2018a). Therefore, biopolymer-biocement composites can improve conventional biocementation through uniform precipitation. Based on

the gaps in the literature, it is of paramount importance to investigate the role of such biopolymer-biocement composite in mitigating soil erosion.

1.5 Broad objectives of the study

MICP treatment has proven its potential to improve soil strength. However, there are only a handful of studies that have investigated its potential for controlling the soil erosion induced by wind (aeolian erosion), hydraulic current (riverbank erosion) and hydraulic waves (coastal erosion). The potential of locally available soil microbes in controlling soil erosion has largely been unaddressed in literature. The broad objective of the current study is to investigate the efficiency of soil microbes in preventing erosion in different environments via biocementation. Broadly, the following objectives have been identified for this study-

- To examine the influence of biocementation on the geotechnical properties of soil.
- To examine the efficiency of biocementation in mitigating aeolian erosion.
- To examine the efficiency of biocementation in mitigating current-induced soil erosion at riverbanks.
- To examine the efficiency of biocementation in mitigating hydraulic wave-induced soil erosion at coasts.

The proposed assessment is expected to provide a better understanding of the biocementation process for designing large-scale applications to mitigate soil erosion.

1.6 Organisation of thesis

After the introductory chapter, the details of the previous works have been reported in **Chapter 2** in the form of a literature review. The literature review chapter has been further subdivided to specifically discuss the studies relevant to the defined objectives. After performing a critical appraisal of the literature, the statement of purpose has been described along with the objectives and scope of the work.

Chapter 3 provides details about the materials and methodologies required for fulfilling the defined objectives.

Chapter 4 presents an investigation of the enrichment and isolation of biocementation-potent soil microbes from different local soil environments. The isolated bacteria are characterised by their biochemical characteristics and compared with the standard calcifying culture of *Sporosarcina pasteurii*. Chapter 4 substantiates the presence of calcifying microbes in local soils. The availability of calcifying microbes in local soil not only makes the requirement of extraneous microbes redundant but also helps in minimal intervention to the soil biodiversity.

Chapter 5 presents a preliminary investigation of the efficiency of one of the isolated strains (LS2) in the microbial treatment of the Thar desert soil to study the influence on strength and wind erosion characteristics. LS2 was isolated from a vegetative slope inside the Indian Institute of Technology Guwahati campus, nearby the basin of the Brahmaputra River. The selection of a low-performing isolated microbe was to ensure the biocementing capabilities of the isolated strains. The aeolian erosion was simulated in a laboratory-scale wind tunnel. The findings have been supported by microstructural and mineralogical analysis.

Chapter 6 presents an investigation on determining the most suitable concentration of cementation media (CM) for microbes liable for bio-augmentation, stimulation, and selective stimulation after confirming that even the low-performing isolated strain is able to improve soil properties via grain binding. Thus, the best-performing microbe, bacterial consortium and widely used microbe, *Sporosarcina pasteurii* (SP), has been compared for the precipitation and soil binding capacity via the needle penetration tests at different concentrations of CM. The strength enhancement in the biocemented soil was assessed via the needle penetration test. The needle penetration test was chosen over UCS to evaluate the local strength enhancement of

spray-treated biocemented specimens. The findings are supported by the microstructural analysis.

Chapter 7 presents an investigation of the performance of biocement and biopolymer-biocement composite in the mitigation of the current induced erosion. A soil microbe (BS3) isolated from the banks of the Brahmaputra River was employed for a selective stimulation-based treatment via a spraying strategy for controlling the current-induced riverbank erosion. The strength of stabilised soil is assessed by needle penetration tests and $CaCO_3$ contents. The riverbank erosion process is simulated in a flow-controlled hydraulic flume. The eroded depth and erosion rates are evaluated with image analysis.

Chapter 8 presents an investigation of erosion characteristics of soil treated with biocement and biopolymer-biocement composite against waves combined with the hydraulic current, similar to coastal erosion, using the best-performing isolated strain BS3. The samples were subjected to hydraulic flow in both tangential and perpendicular directions to simulate riverlike- and coastal erosion scenarios. Soil mass loss, eroded volume, and erosion rates of the treated soil against the applied hydraulic energy density have been reported. The strength of the residual soil was examined with the needle penetration test. The cost of the proposed treatment has been compared with the existing erosion mitigation techniques.

Chapter 9 summarises the major conclusions of the study.

CHAPTER 2

LITERATURE REVIEW

2.1 Introduction

Soil erosion triggers when the erosive stress (τ) on the soil caused by the action of wind or water exceeds the critical stress (τ_c) or critical velocity (v_c). The critical stress is usually calculated with the help of the velocity of wind or water. The critical velocity of wind is also termed threshold frictional velocity and can be theoretically estimated for cohesionless soil in dry conditions (Bagnold 1984; Ravi et al. 2006), as shown in Equation (2.1).

$$v_c = A\sqrt{\frac{(\rho_s - \rho_a)}{\rho_a} gd} \tag{2.1}$$

Here, v_c stands for threshold frictional/detachment velocity (in m/s), ρ_s and ρ_a denote the density of sand particles and air (in kg/m^3), g is the gravitational acceleration (9.81 m/s^2), and "d" stands for the diameter of the particles. A is a dimensionless parameter that depends on the shape factor, drag coefficient and ratio of the moment arms lengths to the soil grain diameter. For cohesive soil, the critical wind velocity (Ravi et al. 2006) is proposed as-

$$v_C = A\sqrt{\frac{(\rho_s - \rho_a)}{\rho_a} gd} \cdot \sqrt{1 + \frac{F_c.B}{(\rho_s - \rho_a)gd^3}} \tag{2.2}$$

Here, F_c stands for interparticle cohesive forces, and B is a parameter depending on the shape factor of the particles.

On the other hand, Briaud (2008) proposed the critical velocity of cohesionless soil can be estimated from Equation (2.3).

$$v_C = 0.35\ (D_{50})^{0.45} \tag{2.3}$$

In the case of the cohesive soils of particle size lesser than 100 microns, the following Equations (2.4 and 2.5) are proposed as lower and upper bounds-

$$v_C = 0.1\ (D_{50})^{-0.2} \tag{2.4}$$

$$v_C = 0.03\ (D_{50})^{-1} \tag{2.5}$$

Here D_{50} is the mean grain size in mm. These equations can be used in designing the experimental flow velocity to simulate erosion in the wind-tunnel or flume. From these empirical equations, it is clear that the critical velocity of soil can be enhanced with the coagulation of soil particles as the effective diameter increases upon grain bridging.

The erosive stresses (τ) on the soil due to the action of wind can be calculated in Equation 2.6 (Bagnold 1984)-

$$\tau = \rho_a (V_D)^2 \tag{2.6}$$

Here, ρ_a is the density of air, and V_D is the drag velocity.

The erosive stresses (τ) on the wall of an open channel, such as a flume due to hydraulic flow, can be calculated from Equation 2.7 (Briaud 2013; Clarà Saracho et al. 2021).

$$\tau = \frac{1}{8}\ \varphi . \rho_w\ v^2 \tag{2.7}$$

Here, φ (friction factor) is a function of the flow regime and can be estimated with the help of pipe roughness, and Reynolds number and v is the velocity of the hydraulic flume.

Soil erosion can be controlled either by minimising the erosive stress or improving the critical stress of the soil particles. The grain bonding can be enhanced with synthetic and natural binders. Most synthetic binders and grout materials, including micro-fine cement, silicates and epoxy, are found to be harmful to the ecology (Karol 2003; DeJong et al. 2010). Rigid and

cement-based structures are found to be counterproductive to the ecology. The cement industry contributes more than 7% to global anthropogenic CO_2 emissions, which are increasing rapidly (Ali et al. 2011). Around 0.92 tonnes of CO_2 is emitted into the environment for each tonne of clinker produced in the cement-making process (Habert et al. 2010). With the target of controlling global warming, the united nations have proposed a "net zero" carbon footprint by 2050 (Intergovernmental Panel on Climate Changes; United Nations 2018). Therefore, it is of paramount importance to investigate novel low-carbon-producing binding materials such as biocement and biopolymers. Their potential to mitigate the surficial erosion in aeolian, riverbank and coastal environments is worth exploring.

2.2 Biocementation: an alternative solution

The naturally formed minerals with biocement are almost everywhere, including teeth, bones, kidney stones, seashells, desert karsts, anthills, caves, beach rocks, and corals (Dhami et al. 2013b). Naturally formed karsts and beach rocks are observed to resist the erosive actions of wind and water up to a great extent, as shown in Figure 1.1 (a) and Figure 1.2 (c) when compared with naturally available loose soil. Emulating these techniques in the laboratory could provide the key to an ecologically conscious technique for controlling soil erosion. The basic mechanism by which biocementation can improve soil erosion resistance is by improving interparticle forces due to interlocking caused friction and particle bridging. Particle bridging enlarges the effective diameter of the grains (Clarà Saracho et al. 2021), which results in higher critical velocity.

2.2.1 Different pathways of biocementation

Previous studies have emulated natural biocementation in the laboratory via different pathways. The governing chemical reactions derived from the previous literature for the bio-mediated processes have been presented in Table 2.1 (van Paassen et al. 2010a; Castro-Alonso et al. 2019; Jain et al. 2021). The biominerals present in nature are classified as biologically

induced mineralisation and biologically controlled mineralisation (Lowenstam 1981). The biologically induced minerals are developed extracellularly through the metabolic activities of the prokaryotes, while the biologically controlled minerals are precipitated inside or around the cell of the microorganisms. Previous studies demonstrated that biologically induced precipitation has the potential to offer solutions for various engineering challenges such as bioremediation, soil stabilisation, leakage control, advanced building materials and erosion control (Fujita et al. 2010; van Paassen et al. 2010a; van Paassen et al. 2010b; DeJong et al. 2013; Dhami et al. 2013b; Al Qabany and Soga 2013; Chu et al. 2014; Montoya and DeJong 2015; Stabnikov et al. 2015; Feng and Montoya 2016; Maleki et al. 2016; Ivanov and Stabnikov 2017; Jiang and Soga 2017; Mujah et al. 2017; Porter et al. 2017a; Porter et al. 2017b; Graddy et al. 2018; Wang et al. 2018a; Terzis and Laloui 2019; Shahin et al. 2020; Graddy et al. 2021). The different pathways can be compared on the basis of spontaneity, solubility, rate, yield, and by-products of the governing chemical reactions. It is to be noted that in Table 2.1, Calcium sources have been considered for the precipitation of calcium carbonate. However, these chemical reactions can be harnessed to precipitate most of the divalent metal ions. Several studies have reported the application of biologically induced mineralisation for the bioremediation of soil by immobilising heavy metals such as Pb^{2+}, Sr^{2+}, and As^{2+}(Fujita et al. 2010; Achal et al. 2012; Yang et al. 2016; Sharma et al. 2020).

2.2.1.1 Autotrophic pathways

The autotrophic pathways for biocementation include photosynthesis and methane oxidation. The autotrophic pathways are underexplored for engineering applications due to the challenges observed during the laboratory simulations. Nature has been forming stromatolites for billions of years with photosynthesis reactions through cyanobacteria (Arp et al. 1999; Altermann et al. 2006; Rodríguez-Martínez et al. 2012). Almost three-quarters (70%) of the carbonate rocks of the earth's crust are formed via photosynthesis (Altermann et al. 2006). The

major reason for the limited studies on photosynthesis for biocementation can be attributed to the continuous requirement of light and CO_2 for the metabolic activity of cyanobacteria.

On the other hand, in the methane oxidation pathway, complex microbial/enzymatic activity results in the production of formate ($HCOO^-$), which lead to the generation of CO_3^{2-} in alkaline conditions (Ganendra et al. 2014; Caesar et al. 2019). The CO_3^{2-} ions precipitate with the divalent metal ions such as Ca^{2+} and Mg^{2+}. Further research in a controlled environment is required to determine suitable strategies for their emulation for in situ engineering applications.

2.2.1.2 Heterotrophic pathways

Although previous studies have discovered a handful of pathways for heterotrophic bio-mineralisation in nature, urea hydrolysis has gained the most popularity in laboratories due to its high solubility, precipitation rate and yield. Sulphate reduction, aerobic oxidation and ammonification pathways are not recommended for ground improvement due to the poor solubility of reagents (van Paassen et al. 2010a; Jain et al. 2021). In the case of denitrification, calcium acetate and calcium nitrate are considerably soluble and have a similar precipitation rate and yield to the urea hydrolysis pathway; however, there are only a few studies based on denitrification. Both urea hydrolysis and denitrification have their advantages and limitations. The denitrification pathway is largely anaerobic, and therefore, it is viable for most of the deep geotechnical applications; however, denitrification is a multistep process, and the intermediate products such as nitric oxide (NO_2^-) and nitrous oxide (NO_2) are toxic (DeJong et al. 2010; van Paassen et al. 2010a). Accumulation of the intermediate products must be carefully manged carefully managed by maintaining lower concentrations of reagents.

Table 2.1 Biocementation techniques and the governing chemical reactions.

	S. N.	Processes	Governing Chemical Reactions		Reported mediating microbial species	Key References
Autotrophic	1.	Photo-synthesis	$CO_2 + H_2O \rightarrow CH_2O + O_2$ $HCO_3 \rightarrow CO_2 + OH^-$ $Ca^{2+} + 2HCO_3^- \rightarrow \mathbf{CaCO_3}\downarrow + CO_2 + H_2O$ $Ca^{2+} + HCO^{-2} + OH^- \rightarrow \mathbf{CaCO_3}\downarrow + 2H_2O$		Cyanobacteria such as *Nostoc punctiforme, Microcoleus vaginatus, Synechococcus sp.* PCC 7002	Arp et al. (1999); Rodríguez-Martínez et al. (2012); Colica et al. (2014); Fattahi et al. (2020); Heveran et al. (2020)
	2.	Methane Oxidation	**Aerobic** $CH_4+O_2 \leftrightarrow CH_3OH+ H_2O$ $CH_3OH \rightarrow CHOH$ $CHOH+ H_2O \rightarrow HCOO^- + H^+$ $HCOO^- + H_2O \leftrightarrow HCOOH+ OH^-$ $HCOOH \rightarrow CO_2 + 2\ H^+$ $Ca^{2+} + CO_2 + 2OH^- \leftrightarrow \mathbf{CaCO_3} + H2O$	**Anaerobic** $CH_3^{2-} + H_2O \leftrightarrow HCO_3^-$ $CH_4 + SO_4^{2-} \rightarrow HCO_3 + HS^- + H_2O$	*Methylocystis parvus* OBBP	Arp et al. (1999); Ganendra et al. (2014); Caesar et al. (2019)
Heterotrophic	3.	Urea Hydrolysis	$NH_2\text{-}CO\text{-}NH_2 + 2H_2O + CaCl_2 \rightarrow \mathbf{CaCO_3}\downarrow + 2NH_4Cl$		*Sporosarcina pasteurii, Bacillus Megaterium, Sporosarcina Ureae, Bacillus sphaericus, Bacillus sp.*	Stocks-Fischer et al. (1999); Ivanov and Chu (2008); Montoya and DeJong (2015); Nassar et al. (2018)
	4.	Nitrate reduction	$5Ca(C_2H_3O_2)_2 + 8Ca(NO_3)_2 \rightarrow 13\mathbf{CaCO_3}\downarrow + 8N_2 + 7CO_2$		*Pseudomonas denitrifican, Diaphorobacter nitroreducens, Castellaniella denitrifican*	van Paassen et al. (2010a); Erşan et al. (2015)
	5.	Sulphate Reduction	$6CaSO_4 + 4H_2O + 6CO_2 \rightarrow \mathbf{CaCO_3}\downarrow + 4H_2S + 2S + 11O_2$		*Desulfovibrio sp.*, Sulphate-reducing bacteria/ SRB (Anaerobic)	Alshalif et al. (2016); Tambunan et al. (2019)
	6.	Aerobic oxidation	$Ca(C_2H_3O_2)_2 + 4O_2 \rightarrow \mathbf{CaCO_3}\downarrow + 3CO_2 + 3H_2O$		*Halomonas pacifica, Halomonas venusta*	Sánchez-Román et al. (2011), van Paassen et al. (2010a)
	7.	Nitrogen cycle	Amino acid + O_2 +CO_2+ H_2O + $Ca(C_2H_3O_2)_2 \rightarrow \mathbf{CaCO_3}\downarrow + H^+$		*Myxococcus xanthus, Alcanivorax borkumensis.*	Rodriguez-Navarro et al. (2003), (2012); Ben Chekroun et al. (2004)

In a recent study by Gao et al. (2022), a large-volume circulation strategy was used following the denitrification pathway and the formation of cavities due to gas bubbles was reported. Therefore, the urea hydrolysis pathway is the most suitable candidate for surficial erosion control applications, as oxygen availability is not a concern at shallow depths. In aerobic conditions, the urea hydrolysis path has been established for its high yield precipitation rate, carbonate yield and ease of control (DeJong et al. 2010; van Paassen et al. 2010a). The challenge with urea hydrolysis lies with the management/removal of the by-product, i.e., ammonium chloride/ammonia.

2.3 Biocementation via urea hydrolysis and its engineering applications

Biocementation based on the urea hydrolysis pathway is often termed microbially induced calcite precipitation (MICP). The principle of MICP is to utilise the urease enzyme-producing bacteria to catalyse urea hydrolysis, as shown in Equation (2.8). It is to be noted that for the engineering application of MICP, the required urease enzyme can be supplemented either by supplying exogenous urease-producing microbes or by stimulating the native biocementing microbial community. The strategy for applying exogenous ureolytic microbes in soil is termed bio-augmentation while stimulating the indigenous microbial community for biocementation is known as bio-augmentation. One of the most popular bacteria used for bio-augmentation-based MICP is *Sporosarcina pasteurii* (SP). The ammonia gets converted to ammonium and hydroxide ions in the aqueous solution, which makes the system alkaline, as displayed in Equation (2.9).

$$CO(NH_2)_2 + 2H_2O \xrightarrow{Ureolytic\ microbe/Urease} H_2CO_3 + 2NH_3 \quad (2.8)$$

$$NH_3 + H_2O \rightarrow NH_4^+ + OH^- \quad (2.9)$$

The produced bicarbonate breaks down to form carbonate ions in the solution, as described in Equation (2.10). In the presence of free calcium ions and an alkaline environment,

$CaCO_3$ is precipitated in the soil pores (Stocks-Fischer et al. 1999; DeJong et al. 2010), as illustrated in Equation (2.11).

$$H_2CO_3 \rightarrow 2H^+ + CO_3^{2-} \quad (2.10)$$

$$Ca^{2+} + CO_3^{2-} \rightarrow CaCO_3 \downarrow (K_{sp}= 3.8\times10^{-9}) \quad (2.11)$$

In Equation (2.11), K_{sp} denotes the solubility product. The precipitated calcium carbonate in the soil pores bridges the sand grains and substantially improves soil strength (Al Qabany and Soga 2013; Montoya and DeJong 2015; Cheng and Shahin 2016; Feng and Montoya 2016). Therefore, the MICP treatment has the potential to reduce soil erodibility. The soil grain binding with $CaCO_3$ precipitation through the MICP process is illustrated in Figure 2.1. There are certain advantages of MICP over existing grouting practices, such as easy permeation through soil media due to the water-like viscosity of the cementation solution and comparatively negotiable impact on the geo-environment (DeJong et al. 2010; Dhami et al. 2013b; Ivanov and Stabnikov 2017).

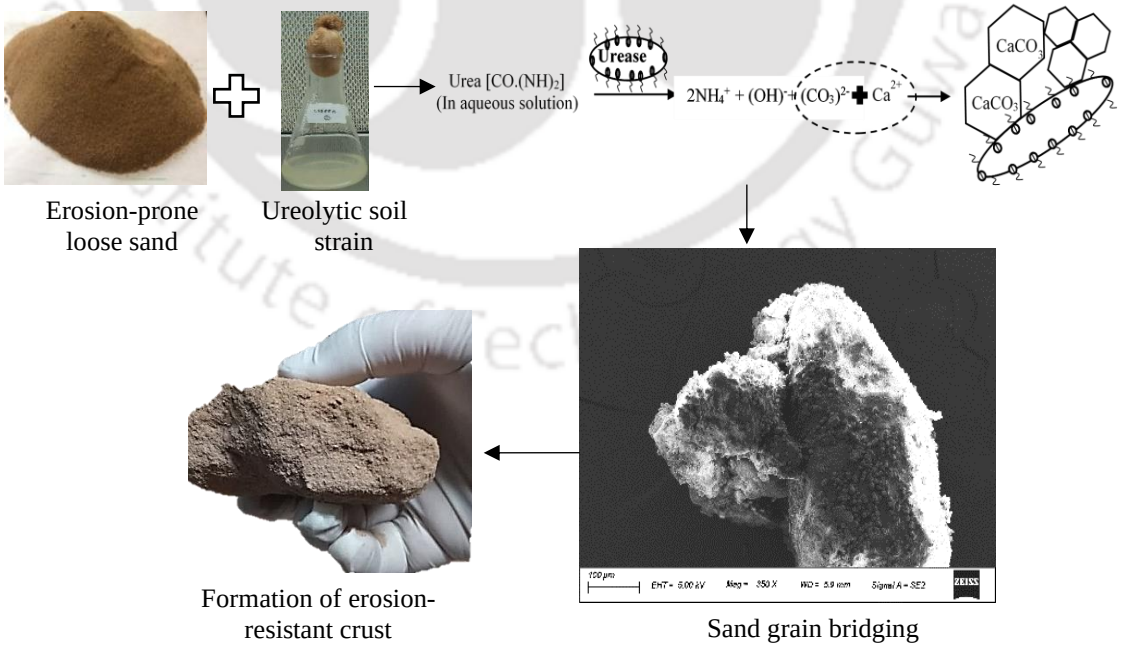

Figure 2.1 Soil grain bridging with MICP.

2.3.1 Factors affecting the efficiency of MICP

Although biocementation via urea hydrolysis is a straightforward pathway for the precipitation of $CaCO_3$, there are several factors that control its efficiency in soil binding. The efficiency of MICP is chiefly controlled by the quality and quantity of precipitates. The quality of precipitates implies for their morphology, microstructure, and strength, which is reported to be influenced by the saturation state, temperature, pH and concentrations of urea and $CaCl_2$ in the system. It is necessary that the saturation index (SI) is greater than 1 for $CaCO_3$ precipitation (Arp et al. 1999; Dhami et al. 2013b). The supersaturation index is defined in Equation (2.12).

$$SI = \log \Omega = \log \frac{IAP}{K_s} \qquad (2.12)$$

IAP stands for ionic activity product, and K_s stands for solubility product. In the literature, precipitation of calcite, vaterite and aragonite polymorphs is reported with the MICP technique (Cizer et al. 2012; Rodriguez-Navarro et al. 2012). The rhombohedral-shaped calcite with epitaxial growth is often observed with the MICP technique (Hammes et al. 2003; Cizer et al. 2012; Cuthbert et al. 2012). Vaterite is a less stable polymorph of $CaCO_3$ and is known for its cauliflower-like spheroidal morphology. In contrast, aragonite is identified by its morning-star shaped morphology bounded by curved prismatic faces (Mayorga et al. 2019) and is rarely reported with MICP.

The factors influencing the MICP process can be further subdivided as follows-

2.3.1.1 Type of microbes, their growth stage and urease activity

The rate of a chemical reaction depends upon the threshold activation energy that is required to move the chemical reaction in the forward direction. Microbes can efficiently reduce this energy barrier from the application of "specialised enzyme activity", which is generally excreted out of their cell membrane or cytoplasm. The microbial activity can increase

the rate of reaction up to 10^{20} times by reducing the energy barrier (Mitchell and Santamarina 2005).

Several microorganisms have been reported for MICP, including fungi and bacteria (Ivanov and Chu 2008; Li et al. 2014; Bindschedler et al. 2016; Mujah et al. 2017). However, most of the studies have considered MICP through bacteria due to ease of control and their compatibility for permeation through soil pores (DeJong et al. 2010). Bacteria from various genera have been reported for biocementation, including *Bacillus*, *Sporosarcina*, *Lysinibacillus*, *Pseudogracilibacillus* and *Proteus* family (Whiffin 2004; Cheng et al. 2013a; Dhami et al. 2013a; Omoregie 2016). A significant proportion of the soil microbes exhibit ureolytic activity (Hammes et al. 2003; Burbank et al. 2011). The population of cells in the bacterial solution play a key role in hydrolysing urea and precipitation of $CaCO_3$ crystals. The bacterial population is often assessed in terms of the optical density ($O.D._{600}$) of the bacterial solution at a light intensity of 600 nm. The four phases of bacterial growth are the lag phase, exponential phase, stationary phase and death phase (Konhauser 2007). Previous studies have suggested utilising the bacterial cells in the exponential phase ($0.5 \leq O.D._{600} \leq 1.2$) for optimum biocementation (Dhami et al. 2013a; Chu et al. 2014; Zhao et al. 2014; Mujah et al. 2019; Konstantinou et al. 2021; Lai et al. 2021). The young cells in the exponential phase are expected to reproduce rapidly and are supposed to have maximum metabolic activity. In a recent study, Wang et al. (2021) reported that bacteria at lower density (0.6×10^8 cells/ml) produce lesser numbers of bigger $CaCO_3$ crystals (8000 μm^3); however, at higher density (5.2×10^8 cells/ml), higher numbers of $CaCO_3$ crystals of small size (450 μm^3) are produced.

The biocementation potential of the ureolytic bacteria is often predicted by its urease activity. In simple words, the capability of bacteria to break down urea per unit time is termed urease activity. The urease activity of the microbes is evaluated by measuring the generated ammonia via the phenol-hypochlorite method (Weatherburn 1967; Dhami et al. 2013a) or by

measuring the electrical conductivity method (Whiffin 2004). The urease activity of bacterial solution per unit $O.D._{600}$ is termed as specific urease activity. Several studies have reported that the specific urease activity of standard biocementing microbe SP can vary from 1.1 to 29 mM urea/minute/$O.D._{600}$ depending upon the availability of nutrients and microenvironment (Whiffin 2004; van Paassen et al. 2010b; Jiang and Soga 2017). On the other hand, although the soil microbes are reported to have a considerable proportion of ureolytic communities (Hammes et al. 2003; Mitchell and Santamarina 2005; Burbank et al. 2012), their specific urease activity is reported to vary according to their origin. Burbank et al. (2012) demonstrated that at least one isolated microbe from six different soil was ureolytic and cultivable.

A high ureolytic bacteria is considered to be a better alternative for biocementation as it would lead to quicker precipitation, but prior studies have also reported that slow urease-producing microbes lead to the formation of larger calcite crystals with higher strength moduli (Chu et al. 2014; Heveran et al. 2019; Konstantinou et al. 2021; Wang et al. 2021). Recently, Mujah et al. (2019) interestingly reported that the unconfined compressive strength (UCS) of the soil treated with the lowest concentrations of cementation media (0.25 M) and highest urease activity (32 U/ml, $O.D._{600}$=4.46) was maximum when compared to other combinations, including low urease activity (8 U/ml) and moderate urease activity (16 U/ml). Here, 1 U/ml represents the amount of urease in 1 ml of culture to hydrolyse 1 μmol of urea hydrolysed/minute. It is to be noted that the recharge of the bacterial solution is also a critical factor in improving the efficiency of the MICP process. Several studies have shown that multiple applications of cementation solution over a single bacteria solution deteriorate the calcium conversion efficiency (Mujah et al. 2019; Lai et al. 2021). However, with multiple bacterial recharge strategies, a close to 100% precipitation rate is maintained (Lai et al. 2021; Murugan et al. 2021).

It is to be noted that although attempts have been made to determine the influence of urease activity on soil binding, there are several aspects that are still unclear. Microbes are living organisms, and it is possible that they behave distinctively under different conditions, such as concentration of cementation media, temperature and pH.

2.3.1.2 The concentration of cementation media

Most of the previous studies investigating the influence of the concentration of cementation media as the controlling parameters have considered the application of the bio-augmentation approach, which utilises exogenous biocementing microbes SP for MICP. Al Qabany and Soga (2013) demonstrated that for equivalent calcite content produced by standard microbe SP (ATCC 11859) with the injection strategy, a low concentration (0.1 M) of cementation solution produced significantly higher UCS for the biocemented soil than the higher concentrations of cementation solution. Interestingly, with the same strain (ATCC 11859) but a different treatment strategy utilising a batch reactor, Zhao et al. (2014) demonstrated a consistent increase in UCS values with concentrations of cementation solution (0.25M to 1.5 M) and an increase in the urease activity. On the other hand, Mujah et al. (2019) reported that a low concentration of cementation media (0.25 M) resulted in considerably stronger biocemented soil in comparison with the combinations. Sharma et al. (2020) reported the maximum UCS strength and lead immobilisation capacity for an artificially lead-contaminated soil with 0.5 M cementation solution when treated with a consortium made up of green-blue algae in combination with SP and *Bacillus sphaericus* individually.

In a recent study, Lai et al. (2021) reported maximum soil strength at 0.5 M cementation media with a single dose of SP bacterial solution. Above 1 M concentration of cementation media, a retarding pattern was observed, and the precipitation ceased when the concentration of cementation media was 2.5 M or higher. Although with the above-mentioned studies, the

influence of concentration of cementation media on the efficiency of MICP has been explored for SP, its comparison with soil microbes has been largely unaddressed in the literature.

2.3.1.3 Temperature and pH

Biogeochemical reactions are usually affected by temperature. Ferris et al. (2004) reported that the kinetic rate constant decreased from 0.91 per day to 0.09 per day when the temperature varied from 20 °C to 10 °C. The pH raised from 6.5 to 9.3 (in less than one day) at all the temperatures varying in a range of 10 °C to 20 °C. However, Whiffin (2004) reported that the urease activity of SP was stable in a temperature range of 15 °C to 25 °C, increased linearly in a range of 25 °C to 60 °C and had a maximum value at 70 °C. The findings indicated that the biocementing microbe SP could be used for field application in a wide range of temperatures. However, Rebata-Landa (2007) asserted that the $CaCO_3$ precipitation ceases above 60 °C. This is mainly due to the reduction in the population of active microorganisms. Cheng et al. (2014) reported that although $CaCO_3$ precipitation at 50 °C was three times higher compared to room temperature (25 °C), the UCS strength developed in the treated soil sample at a higher temperature was found to be much lesser than in the treated sample at room temperature. The scanning electron microscopy later indicated that the $CaCO_3$ crystals formed at room temperature were bigger in size and were placed at the soil throat. The larger size of $CaCO_3$ crystals led to more contact area between the soil particles, and hence more strength was developed at room temperature.

Urea hydrolysis favours an alkaline environment (Stocks-Fischer et al. 1999; DeJong et al. 2010). Stocks-Fischer et al. 1999 reported maximum urease activity of *Bacillus pasteurii* at pH 8. Whiffin (2004) also reported that although optimum growth of SP was observed at pH 9.25, the maximum specific activity of the resuspended cells was observed in a pH range of 7 to 8. In agreement with the above-mentioned finding, Cheng et al. (2014) reported that both the acidic and alkaline conditions of the soil were reported to be detrimental to the strength of

MICP-treated soil. They also reported a maximum UCS at pH 7. However, Keykha et al. (2017) reported an increase in UCS and $CaCO_3$ precipitation with an increase in the pH of the biocementation solution ($5 \leq pH \leq 9$).

The initial pH of soil and temperature during the biocementation process are both critical parameters for influencing the biocementation process. Both acidic and alkaline soils are abundant in nature. Therefore, a large-scale test is required to accurately predict the improvement in the soil properties as per site conditions.

2.3.1.4 Availability of oxygen

For construction practices, facultative anaerobic and microaerophilic microbes are recommended (Ivanov and Chu 2008) as they can grow and precipitate under low oxygen in the subsurface. Past studies have been unclear about the characterisation of SP as facultative anaerobic (Mortensen et al. 2011; Tobler et al. 2011; Martin et al. 2012) or aerobic (Benini et al. 1998; DeJong et al. 2006; Mitchell et al. 2019).

Prior studies have reported that SP demonstrates recognisable urease activity under anoxic conditions (Mortensen et al. 2011; Martin et al. 2012). However, the duration of the ureolytic activity is uncertain in anoxic conditions. Jain and Arnepalli (2019) reported inhibition of the MICP process in the absence of oxygen. Mortensen et al. (2011) reported that the ureolytic activity of SP is not inhibited for a test on a time scale of an hour in the anoxic condition. With 0.07 $O.D._{600}$ of SP, Tobler et al. (2011) reported no practical difference in the ureolytic activity and precipitation in the oxic and anoxic conditions. On the contrary, Martin et al. (2012) reported poor growth and questioned whether the ureolytic activity of SP could be maintained for the long-term under anoxic conditions. In agreement with this, Mitchell et al. (2019) reported that although the growth of SP was not sustainable in an oxygen-free environment, their ureolytic activity has no practical difference in oxic and anoxic conditions.

The adaptability of the microbe to precipitate in anoxic conditions also depend on their species. Jiang et al. (2016) reported that the ureolytic activity of bacterial pallets was unaffected in anoxic conditions for another ureolytic microbe, i.e., *Bacillus megaterium*. However, it is to be noted that for surficial erosion mitigation, this might not be a concern due to the availability of oxygen near the surface.

2.3.1.5 Type of soil and treatment strategy

The biocementation technique is geometrically restricted to coarse-grained materials (sand and gravels) due to the pore size compatibility of microbes in soil for transport in both stimulation and augmentation approaches (Mitchell and Santamarina 2005; DeJong et al. 2010). Typically, the size of bacteria is observed to be around 0.5- 3μm (Konhauser 2007). The precipitation through MICP is quick, and therefore, a low permeation of biocementation solutions might lead to non-uniform precipitation or precipitation over the surface. Therefore, clays are observed not to be suitable for MICP treatment, specifically with grouting or percolation. Mortensen et al. (2011) reported that poorly graded gravel and poorly graded silt take a much longer time for improvement in shear wave velocity than well-graded coarse and fine sand. However, there are a handful of recent studies that have attempted to use MICP for treatments of expansive soils and desiccation cracking of clays (Kwon et al. 2019; Zhu et al. 2019; Liu et al. 2021a; Tiwari et al. 2021) using a mixing strategy.

Majorly the proposed strategies for MICP application include injection/grouting, surface percolation/spraying and premixing. Whiffin et al. (2007) employed an injection method for a 5 m-long sand column and reported non-uniform $CaCO_3$ precipitation and strength. They reported a low injection with a relatively low flow rate (< 10 meters per day) for bio-mediated ground improvement. van Paassen et al. (2010b) attempted a horizontal flow-based injection strategy with low pressure in a large-scale biocementation of a 100 m^3 sample. The shear wave velocity and UCS were compared after treatment showing significant variation.

Soon et al. (2014) investigated injection strategies with different pressure (0.2, 1.1 and 2 bar). The authors proposed 1.1 bar pressure for 0.5 M cementation reagent flow for 48 hours for uniform precipitation. At lower pressure, the precipitation is reported to occur close to the inlet and prohibits the flow of the reagents. Amin et al. (2017) investigated different injection strategies with aeration and reported that an injection strategy with aeration and 0.5 M cementation solution resulted in reasonably uniform $CaCO_3$ precipitation and resulted in a five-fold increase in critical stress value compared to the untreated sand.

Surface percolation is another method for the application of bacteria to the soil without disturbing the soil matrix. The bacterial solution, along with cementation solutions, is allowed to permeate through the soil by the action of gravity and soil grains' capillary action only. Cheng and Cord-Ruwisch (2012) reported that the percolation method is suitable for unsaturated soil up to 1 m depth. Extending this strategy, Cheng and Cord-Ruwisch (2014) reported with laboratory larger-scale experiments that the surface percolation strategy is indeed suitable for coarse-grained soil (D_{50}>0.3 mm) due to their high permeability, which leads to uniform precipitation. Terzis and Laloui (2017) reported that mixing the biocementing solutions in a triangular grid induces more homogenous calcite distribution than the surface percolation method. In contrast, there are limited studies on spraying strategies (Wang et al. 2018b; Jiang et al. 2019; Zomorodian et al. 2019; Chek et al. 2021) that have shown potential in mitigating the surficial erosion against wind and rainfall.

Most of the studies on fine-clayey soil have considered a mixing strategy for the application of MICP. Mixing techniques provide uniform calcification in the soil pores, but the field application of mixing techniques tends to be costly and non-feasible as the soil is disturbed. Cheng and Shahin (2016) utilised the bacterial suspension with urea and calcium sources and formed a bio-slurry. A high amount (more than 95%) of bio-slurry was reported to be retained in the soil, providing uniform precipitation. In a recent study, Won et al. (2021)

demonstrated that a kaolinite suspension along with a biocementation solution facilitates uniform precipitation of $CaCO_3$ as the kaolinite acts as a nucleation site. Similar observations were reported with bentonite-assisted MICP (Ma et al. 2021). It is to be noted that both of the above-mentioned studies have proposed injecting clay suspension along with bacterial and cementation solutions to enhance MICP; however, that will reduce the soil hydraulic conductivity continuously with treatment leading to clogging in the upper layers. Moreover, the soil is heterogeneous in nature, containing different proportions of sand, clay, and gravel. Therefore, further studies on potential strategies of MICP on fine-grained soils are necessitated.

2.3.2 Influence of MICP on permeability and strength of soil

The permeability and strength characteristics of biocemented soil have been extensively studied in the literature. The key findings from the literature have been summarised in Table 2.2. It is to be noted that a one to two-order decrease in hydraulic conductivity of soil (specifically fine sand) has been reported in literature upon MICP treatment (Al Qabany and Soga 2013; Chu et al. 2014; Cheng and Shahin 2016; Ma et al. 2021). Enhancement in soil strength without clogging the soil pores is one of the desirous features of MICP that allows easy drainage of pore liquid (Mujah et al. 2017) and might avoid the generation of excess pore water pressure.

Several studies have reported substantial improvement in soil strength via MICP, as mentioned in Table 2.2. Most of these studies have utilised injection strategy for treatment and evaluated soil strength via UCS and triaxial tests. The range of UCS variation with MICP treatment is reported to be as high as 12 MPa with 27% $CaCO_3$ content in fine sands of a mean diameter of 0.17 mm (van Paassen et al. 2010b). On the other hand, Terzis and Laloui (2018) reported a UCS strength of up to 11.3 MPa for fine sands of a mean diameter of 0.3 mm. It is to be noted that primarily it was reported that the strength of MICP-treated soil is dependent on the quality and quantity of precipitate. Quality of precipitate is termed for its morphology,

size and microstructure, whereas quantity is referred to as the total amount of precipitated $CaCO_3$ content. However, Cheng and Shahin (2016) reported that the location of precipitate in the soil matrix plays a vital role in the development of strength. They reported that treating specimens with 30% pore volumes of biocementation treatment may result in optimum strength.

Drained and undrained triaxial tests have also been conducted extensively for biocemented soils. Both friction angle and cohesion are reported to improve substantially with biocementation. In a recent study, Wu et al. (2021) proposed that the effective friction angle of the biocemented soil improves only up to 5% $CaCO_3$ precipitation. While investigating fine sand in $CaCO_3$ precipitation ranging from 0 to 14.25%, it was determined that the major contributor to the improvement in the shear strength of biocemented sand above 5% $CaCO_3$ content is cohesion. The study also reported an increase in the dilatancy behaviour of sand with the increase in $CaCO_3$ content.

The improvement is the shear modulus of soil can also be measured non-destructively with bender elements, which could also be installed in triaxial instruments. In one of the studies, the shear wave velocity was found to improve from 107 m/s to 370 m/s when $CaCO_3$ content varied from 12 to 27% (van Paassen et al. 2010b). In another study, Montoya and DeJong (2015)reported that the shear wave velocity of MICP-treated fine sand improved from 190 m/s to 1400 m/s. The differences in their findings are influenced by the confinement conditions and type of soil. In a large-scale test on biocementation with stimulation and augmentation approaches, Gomez et al. (2017) reported that the shear wave velocity improved from 107 m/s to 1028 m/s for MICP-treated sand and maximum $CaCO_3$ content of 5.3%. Although researchers have demonstrated that the MICP treatment can be monitored through bender elements, more insights are required for predicting the relationship between shear wave velocity, $CaCO_3$ content, strength parameters and intrinsic properties of soil.

Table 2.2 Key findings in the literature on the improvement of soil strength.

Reference	Micro-organism	Urease Activity & ($O.D._{600}$)	Urea & $CaCl_2$ (Number of cycles)	$CaCO_3$ content (w/w %)	Type of Soil & (D_{50} in mm)	Improvement after treatment					Remarks
						K_{sat} in 10^{-5} m/s	UCS in kPa	Shear Strength parameter		V_s (m/s)	
								c'	ϕ'		
van Paassen et al. (2010b)	SP DSM 33	1.1 M urea/ litre/hour (NA)	1 M Urea and $CaCl_2$ (10)	12 to 27	Fine sand (0.17)	NA	700 to 12000	NA	NA	107 to 395	-Large-scale experiment was conducted on a 100 m^3 sample.
Al Qabany and Soga (2013)	SP ATCC 11859	NA (0.8-1.2)	0.1 to 1 M Urea and $CaCl_2$ (multiple)	0 to 8	Fine sand (0.15)	15 to 1	0 to 3000	NA	NA	NA	-At lower concentrations of cementation media with injection strategy, uniform precipitation was observed.
Cheng et al. (2013a)	*B. sphaericus* MCP-11	10 U/ml (1.5-2.0)	1 M Urea and $CaCl_2$ (multiple)	1 to 14	Fine & Medium sand (0.23 & 0.70)	9 to 2 (fine) 45 to 10 (medium)	150 to 2300	0 to 290 kPa	23° to 40°	NA	-Soil was treated at various levels of saturation. -Optimum strength was observed at 30% saturation.
Montoya and DeJong (2015)	SP ATCC 11859	NA (0.8-1)	333 mM Urea & 50 mM $CaCl_2$ (6 to 16)	0 to 5.31	Ottawa 50-70 Sand (0.22)	NA	NA	NA	33° to 44°	190-1400	- Samples were treated in triaxial apparatus with constant monitoring by bender elements.
Terzis and Laloui (2018)	SP ATCC 11859 Lyophilised	104 mM urea/ litre/hour - Rehydrated	1 M	3 to 10	Fine sand (0.19 & 0.30)	NA	0 to 11300	NA	NA	NA	- A cell-free mechanism for MICP was proposed that reduces the costs.
Mujah et al. (2019)	*Bacillus sp.* (Isolated in a prior study)	8.3 to 32.1 U/ml (1.2 to 4.46)	0.25 to 1M	0 to 8.5	Fine Sand (0.23)	NA	0 to 4000	NA	NA	NA	-The combination of 32 U/ml urease and 0.25 M of cementation solution resulted in maximum UCS.
Wu et al. (2021)	*Bacillus sp.* (Isolated in a prior study)	2-4 mM urea/minute (1.2)	1 M urea and 0.75 M $CaCl_2$ (10 to 40)	0 to 14.25	Ottawa 30-100 Sand (0.30)	NA	NA	0 to 550 kPa	33° to 44°	NA	-The increase in shear strength was attributed to an increase in effective cohesion as friction increased only up to 5% $CaCO_3$.

Another method for correlating $CaCO_3$ content with the local strength of the formed crust of soil is the needle penetration test Chung et al. (2020), which is relatively underexplored. The authors utilised sand fractions varying from 75-150 μm, 150-200 μm, 300-355 μm, and 500-1000 μm and reported good consistency in the increase in penetration index with the $CaCO_3$ content. However, a relationship was not proposed. Bender elements are relatively costly alternatives for non-destructively evaluating soil strength. The needle penetrometer can provide a cheaper non-destructive alternative for monitoring the soil strength of the developed crust. Therefore, further research to establish a correlation between needle penetration index and $CaCO_3$ content is necessary.

2.3.3 Influence of MICP on wind erosion resistance of soil

The current wind erosion control practices are watering, mulching, cement lining, geo-polymers, biopolymers and micro-wind breakers in the drylands and deserts (Kar et al. 2009; D'Odorico et al. 2013). The above-mentioned techniques are not viable due to their cost, environmental impact and their durability. Moreover, these techniques negatively impact the natural aesthetics of natural sand landforms. It is not feasible to water the drylands due to the scarcity of water caused by low rainfall and the poor water retention capacity of sandy terrain (Singh et al. 2018). Vegetation is also not feasible due to the same reason.

In the past few years, several studies have investigated the potential of biocementation to control aeolian erosion (Maleki et al. 2016; Duo et al. 2018; Tian et al. 2018; Zomorodian et al. 2019). Most of the studies have utilised exogenous strain SP for soil erosion mitigation. The studies have considered desert regions of China and Iran. The application of MICP for aeolian erosion mitigation at the Thar desert of India is limitedly explored. In a recent study by Devrani et al. (2021), *Bacillus megaterium* (*Bm*) was employed for the MICP process. However, the improvement in UCS was not reported. The key findings on aeolian erosion mitigation with MICP in literature are summarised in Table 2.3.

Table 2.3 Key findings in the literature on aeolian erosion mitigation with MICP.

Reference & Region of Study	Micro-organism	Urease Activity & ($O.D._{600}$)	Urea & $CaCl_2$. (Number of cycles)	$CaCO_3$ content (w/w %)	Type of Soil (D_{50} in mm)	Major Findings
Maleki et al. (2016) (Yazd Desert, Iran)	SP PTCC 1645	2.2 mM/Litre/ Minute (1.5 g /l - dry)	0.1 to 1 M Urea and $CaCl_2$ (1)	NA	Desert Sand (NA)	- Soil erosion reduced to more than 96.5% at wind velocity 55 km with penetration resistance≥ 50 kPa.
Duo et al. (2018) and Tian et al. (2018) (Tengger Desert, China)	SP ATCC 11859	8.62 mM/Litre/ Minute (≈1.9)	0.5 to 2.5 M Urea and $CaCl_2$ (8)	10 to 19.5	Fine Sand (0.15)	- A maximum UCS value of 18 MPa is reported at 19.5% calcium Carbonate content (Duo et al. 2018). - Samples treated with three cycles of 0.5M cementation solution (or more) exhibited no erosion at 16 m/s wind velocity. (Tian et al. 2018).
Li et al. (2018) (Kubuqi Desert, China)	SP ATCC 11859	NA (0.5 to 0.8)	0.5 M Urea and $CaCl_2$ (NA)	NA	Mixture of desert and silica sand (0.17 to 0.90)	- Samples were treated continuously in a batch reactor for seven days. - A maximum UCS of 780 kPa was reported with 0.5 $O.D._{600}$. -For a well-graded mixture of aeolian sand and silica sand, maximum shear strength (ϕ) was observed around 44° for a well-graded specimen at bacterial $O.D._{600}$=0.5.
Zomorodian et al. (2019) (Silicate sand from Mines and Khormoj, Iran)	SP PTCC 1645	NA (1 to 2.5)	0.5 M Urea and $CaCl_2$ (1)	NA	Three types of sand (0.20 to 0.28)	- soil erosion ceased with 0.5 M cementation solution, and O.D.= 1.5 treated sand cured for 28 days at 28ºC against wind velocity of 20 m/s was observed. -The crust's strength was reported as 39 kPa for silica sand and 69 kPa for silty carbonate sand after 28 days of curing period with 1.5 $O.D._{600}$ of bacteria.
Devrani et al. (2021) (Thar desert, India)	*B. megaterium* NCIM 5472	250 U/ml (≈0.8)	0.25 to 1 M Urea and $CaCl_2$ (1)	1.94 to 4.1	Fine sand (0.15)	- Negligible wind erosion was observed for soil specimens with 2.97% of calcium carbonate and with 0.25% of Biopolymer treatment at a wind velocity of 45 km/h.

These studies have suggested that a low $CaCO_3$ content of up to 4% can cease erosion against wind velocity up to 45-55 km/h. Such studies have not been conducted utilising soil microbes.

2.3.4 Influence of MICP on hydraulic-erosion resistance of soil

The existing riverbank and coastal erosion control practices are inclined toward rigid structures such as aprons, sea walls, concrete revetments, geomembranes/geotextiles, sandbags filters, artificial reefs gabions, and check dams, which can irretrievably damage the riparian and coastal ecology (Florsheim et al. 2008). In the case of riverbanks, these structures may drastically impact the features of the river channel and induce floods downstream (Florsheim et al. 2008; Das et al. 2014). One of the options for a sustainable erosion mitigation technique is vegetation. However, vegetation and its influence on the erodibility of soil is too complex to predict due to its uncertain life cycle and dense root structures, which is dependent on the type of vegetation, available nutrition, and climatic conditions (van Dijk et al. 2013; Krzeminska et al. 2019). The key findings from the literature on hydraulic-erosion mitigation via biocementation have been summarised in Table 2.4.

The studies on the mitigation of soil erosion via MICP subjected to tangential flow conditions are limited in the literature. Amin et al. (2017) investigated the different injection strategies along with aeration to ensure uniform calcium carbonate precipitation and reported that the critical shear stress increased five-fold upon MICP treatment. On the other hand, Wang et al. (2018a) employed polyvinyl alcohol-modified MICP treatment and reported that the polymer is useful in anchoring the $CaCO_3$ crystals. In a recent study by Clarà Saracho et al. (2021), it was reported that although biocementation can mitigate soil erosion against the tangential flow with a 0.08M cementation solution, the treated specimen cracks along with the tangential flow due to brittleness. The studies based on indigenous soil microbes in the context of mitigating riverbank erosion have been largely unaddressed.

In a related investigation, biocemented soil slope has been investigated in the case of rainfall-induced soil erosion (Jiang et al. 2019; Chung et al. 2021). Jiang et al. (2019) reported that a high concentration of cementation solution (2M) could be detrimental to the $CaCO_3$ precipitation. Behzadipour and Sadrekarimi (2021) have investigated the direct shear strength of biochar-assisted biocemented sand of the Karoon riverbank of southwest Iran via stimulated indigenous strain. There was no identification and characterisation of the microbial colonies.

There are only a handful of reports on biocementation-mediated erosion mitigation against hydraulic waves. Shahin et al. (2020) reported less than 5% erosion with a calcite content of 1.52% against erosional wave action for two hours. Kou et al. (2020) have reported that the minimum soil erosion occurred in a sample containing 30.1% calcite content against the hydraulic waves in a 30-minute test. On the other hand, Liu et al. (2021b) reported that two cycles of MICP treatment were inefficient in preventing erosion for a 2-hour test duration without quantifying the precipitated calcite content. Behzadipour and Sadrekarimi (2021) reported that negligible erosion occurred in a physical riverbank model treated with 20 cycles of biochar-assisted biocementation treatment against 600 strong waves. It is evident from these studies that the number of cycles of biocementation treatment, i.e., the quantity of $CaCO_3$ precipitates, is one of the deciding factors in controlling erosion. Moreover, these studies have reported the erosion characteristics against the wave features such as dimension, frequency and test duration. For upscaling the laboratory results to the field, a study correlating the erosion traits of the biocemented soil against wave energy is imperative.

Table 2.4 Key findings in the literature on hydraulic erosion mitigation with MICP.

Reference & Subject of study	Urea & $CaCl_2$ (no. of cycles)	$CaCO_3$ content (w/w %)	Type of Soil (D_{50} in mm)	Major Findings
Salifu et al. (2016) (Tidal flow-induced erosion)	0.7 M urea and $CaCl_2$ (18)	≈10%	Fine sand (0.33)	- The MICP-treated soil (9.9% pore volume filled with $CaCO_3$) exhibited almost no erosion for a slope of 35° and 53° against 30 tidal cycles. A corresponding UCS of around 450 kPa was observed.
Jiang and Soga (2017) (Internal erosion)	0.2 to 2 M of Urea and $CaCl_2$ (1)	0 to 0.95	Gravel-sand Blend (1)	- At least 0.28% $CaCO_3$ was suggested for erosion control against a water pressure up to 50 kPa.
Amin et al. (2017) (Surficial- erosion)	0.5 & 0.75 M of Urea and $CaCl_2$ (1 to 2)	2.7 to 8	Fine sand (0.28)	- The soil treated with two cycles of 0.5 M cementation solution with aeration with 6-day drainage resulted in 6.1% $CaCO_3$ and 95% reduction in erodibility coefficient.
Wang et al. (2018a) (Tangential flow-induced erosion)	0.5 to 1.5 M of Urea and $CaCl_2$ (1)	1.3 to 2	Fine sand (0.33)	- The sand was immersed in the PVA-modified cementation solution and SP bacterial solution. - 1 M PVA polymer-modified cementation solution was suggested for erosion control.
Jiang et al. (2019) (Rainfall induced erosion)	0.2 M,1M and 2 M of Urea and $CaCl_2$ (4)	NA	Fine sand (0.23)	-2 M cementation solution was found to be not effective against erosion. -Maximum erosion resistance was observed with a 1 M cementation solution.
Chung et al. (2020) (Rainfall induced erosion)	0.45 M Urea and $CaCl_2$ (1 to 13)	0 to 12%	Sand and sandy loam (multiple)	-Soil erosion rate (g/m^2-minute) almost ceases for MICP stabilised slope up to 15° against rainfall intensity up to 75 mm/hour with more than three cycles of treatment on the sand and more than five treatment cycles for the sandy loan.
Shahin et al. (2020) (Coastal erosion)	1 M Urea and $CaCl_2$ (1-2)	0 to 1.52%	Medium sand (0.4)	-1.52% $CaCO_3$ with 2 treatment cycles of 1 M cementation solution can cease soil erosion (<5% soil mass loss) and the wave-induced erosion for a 2-hour test.
Kou et al. (2020) (Coastal erosion)	1 M Urea and $CaCl_2$ (1 to 4)	0 to 30% (residual)	Qingdao Sea sand (0.75)	-With 2 to 4 cycles of MICP treatment, soil erosion can be reduced to less than 50%.
Clarà Saracho et al. (2021) (Flow-induced erosion)	0.02 to 0.1 M Urea and $CaCl_2$ (10)	0.4 to 2%	Fine and Coarse sand (0.21& 1.61)	-A treatment with 0.8 M cementation solution brings down the soil erosion to a legible level for surficial flow ranging from 0·033–0·18 m/s.
Do et al. (2021) (Scour)	0.333 M Urea & 0.25 M $CaCl_2$ (18)	0 to 20%	Medium sand (0.49)	-The MICP-treated specimen exhibited lesser changes in landforms. - The MICP treated specimen became brittle and eroded in brittle chunks rather than smooth particle transport observed in the untreated sand.
Liu et al. (2021b) (Coastal erosion)	0.5 M urea and 0.25 M $CaCl_2$ (1-2)	NA	Calcareous sand (≈0.7)	-Both MICP and EICP (Enzyme induced carbonate precipitation) were observed to be not effective for long-term (2 hours) big wave (0.8 cm) attacks.

2.4 Challenges with Biocementation

Although biocementation holds potential for ground improvement, there are several challenges associated with it, such as non-uniformity, ammonia, cost, and upscaling for the formulation of a standard protocol for field applications.

2.4.1 Non-Uniformity

Non-uniformity is one of the obvious constraints of MICP. Attempts have been made to make the precipitation more uniform apart from the investigation of different treatment strategies. Harkes et al. (2010) proposed a two-phase treatment with a pre-application of fixation solution (50 mM $CaCl_2$) and reported more uniform precipitation. Al Qabany and Soga (2013) reported that a more uniform precipitation and strength improvement could be achieved using a low-concentration cementation solution; however, it will also increase the required time, cost, and number of treatment cycles for the targeted $CaCO_3$ content. In another study, Cheng and Shahin (2016) reported a urease active bio-slurry that retains more than 95% bacteria upon mixing with soil and uniform precipitation was observed for 300 mm soil cylinders. Cheng et al. (2019) reported a one-phase low-pH injection method for MICP. They reported a uniform soil strength for low-urease activity (< 5 U/ml) and all in one low pH biocementation solution. Konstantinou et al. (2021) also reported more uniform precipitation of $CaCO_3$ with low urease activity (10 mM/L/h/O.D.$_{600}$). The overall proposed mechanism for uniform precipitation is to slow down the MICP process so that the soil is not clogged near the injection points and reagents can be uniformly distributed for precipitation. Biopolymers can be added to modify the conventional MICP to control the location and depth of precipitation, as biopolymers not only provide an ambient micro-environment to the microbes but also anchor the $CaCO_3$ crystals (Wang et al. 2018a).

2.4.2 Ammonia/Ammonium

Ammonia/Ammonium (NH_3/NH_4^+) is a by-product of the MICP technique that might be harmful to the environment, specifically with large-scale applications. In order to reduce the ammonia release, Li et al. (2015) suggested replacing urea with an asparaginase-based MICP process with *B. megaterium* and reported significantly lesser ammonia with comparable strength to conventional MICP. On the other hand, Yu et al. (2016) reported eco-friendly struvite precipitation using $MgCl_2$ (2 M) and $K_2HPO_4.3H_2O$ (3 M) along with 1 M urea for minimum ammonia release. Keykha et al. (2019) reported an ammonia-free cementation solution by filtering the biocementing solution (bacteria & urea) through a 40 cm zeolite column. They reported that the ammonium ion concentration decreased from 14700 mg/l to less than 1 mg/l with the proposed treatment. Lee et al. (2019a) investigated 3.7 m long columns and reported that rinsing of the soil column with 525 L was of high pH and ionic strength solution (200 mM $CaCl_2$, pH ≈10.0), resulted in 97.9% removal of NH_4^+. The one-phase low-pH cementation technique proposed by Cheng et al. (2019) is reported to remove 90% ammonia. The proposed methods have the potential to remove ammonia up to a great extent, and they must be adopted for field-scale application as per the requirement. However, in the case of the site of ecological importance, most of them have limitations in terms of cost, effectiveness and applicability. More research on large-scale models is required to confirm if they also influence the uniformity of the precipitation.

2.4.3 Cost

There is limited literature on the cost aspect of biocementation. Ivanov and Chu (2008) reported that the cost of materials for biocementation treatment could vary from 0.5 US$/m^3 to 9 US$/m^3, which is competitive with the cost of existing grout material (2 to 72 US$/m^3) such as sodium silicates, polyurethane, and acrylamides. In contrast, the estimates are also reported in a wide range of 25 to 500 US$/m^3 (DeJong et al. 2013). These costs are in a vast range due

to the uncertainty in miscellaneous costs, including labour, electricity and transport. The material cost could be further brought down by utilising commercial-grade materials for cementation solutions and waste materials for microbial cultivation. However, to establish a fair estimation of cost, a collaborative filed-scale investigation must be conducted.

2.4.4 Upscaling

Extending the laboratory knowledge of biocementation techniques to the field is the most formidable challenge. Many peers consider that biocementation can never replace the conventional grouting system (DeJong et al. 2013), which is rational as, in the current state, there is uncertainty over its service life, monitoring tools and durability. There is very limited literature on field-scale models based on biocementation. However, a few field-scale applications have been reported utilising bio-augmentation and bio-stimulation. van Paassen (2011), in collaboration with contractors Visser & Smit Hanab, reported the first pilot study for the stabilisation of gravel to support horizontal directional drilling for a gas pipeline in the Netherlands. Despite several flushes, the calcite precipitation was heterogeneous; however, improvement in shear strength was significant, and the horizontal drilling was successful. Another field application was reported (Fujita et al. 2010; Smith et al. 2012) to evaluate the capacity bio-stimulation process to immobilise heavy metals, strontium-90, along with calcium carbonate. Another study by Gomez et al. (2015) conducted a field-scale study on four plots 2.4×4.9 m and reported that the lowest concentration of cementation media, including 15 g/l urea and 13.875 g/l $CaCl_2$, developed a thick crust of 2.5 cm and performed optimum on the dynamic cone penetration (DCP) test. However, in a recent study, Zeng et al. (2021) reported no significant improvement in the cone penetration resistance upon MICP treatment of three plots each of 125 m^3 via injection strategy and reasoned it with the heterogenous profile of the soil and inhibition of urease activity due to high amount of natural calcium salts and low pH of the soil. These studies have provided uncertainty on the possibility of profit-making with the

MICP technique for field-scale applications. Currently, three start-ups, namely, Medusoil, BioMason and Basilisk, based on biocementation techniques, are operational. Their projects could provide more insights on the commercialisation of biocementation technique. Nonetheless, further studies are required addressing the cost-benefit, service life and durability of biocementation for field-scale applications and replace existing grouting techniques.

2.5 Statement of Purpose

The potential of locally available soil microbes in controlling soil erosion has been largely unaddressed in literature. Soil is rich in microbial diversity, with approximately 10^9-10^{12} microorganisms per kilogram of soil nearby the ground surface (Mitchell and Santamarina 2005). Any supplemented foreign bacteria have to compete with the native microorganisms for their survival in the new environment. Hence, utilising the indigenous microorganisms over the bio-augmentation approach for soil improvement has definite advantages in terms of minimum intervention to native biodiversity. However, with the conventional biostimulation approach, there is a likelihood of stimulating the undesired and non-participating bacterial communities, which may slow down the biocementation process (Gomez et al. 2017). Moreover, with conventional stimulation, it is necessary to identify and profile the enriched communities, as there is a threat of stimulating pathogenic ureolytic bacteria such as *Mycobacterium tuberculosis*, which are reported to be present in natural soils (Velayati et al. 2015). Therefore, an approach with selective stimulation of ureolytic microorganisms with identification from the indigenous biodiversity is imperative.

Moreover, indigenous soil strains have an advantage over exogenous strains in terms of survivability and adaptability in the soil environment (Dhami et al. 2017; Graddy et al. 2018). There are limited studies on the indigenous biocementation potent strains as their availability in desert soils is uncertain due to the harsh environment, low nutrient availability, and scarcity of moisture content (Bibi et al. 2018; Rajabi Agereh et al. 2019). The influence of

biocementation on geotechnical properties of desert soils in terms of UCS and hydraulic conductivity with a single cycle of MICP treatment is necessary to investigate along with the aeolian erosion mitigation potential, which has been limitedly explored in the literature (Maleki et al. 2016; Zomorodian et al. 2019; Devrani et al. 2021). Moreover, the focus of previous studies has shifted towards injection and percolation strategies for uniform precipitation. However, the spraying strategy might be more effective for a field-scale application, which is relatively underexplored.

The biocementing microbes are living organisms, and it is plausible that the response to various concentrations of cementation media varies due to their adaptability in different environments. While the augmentation and stimulation approaches have been investigated independently in previous studies, a comparative analysis of these techniques and the response of liable microbial communities to the exposure of various concentrations of cementation solution on the soil strength improvement have not been addressed largely. Moreover, in literature, more focus has been given to bulk strength properties such as unconfined compressive strength. However, with MICP treatment, the soil strength improves heterogeneously. The depth of the developed crust is often lower than the recommended depth of the cylindrical specimen required for UCS/triaxial tests. For the evaluation of the local strength of weak rocks and cemented soils, the needle penetration test is recommended by the International Society of Rock Mechanics (Ulusay and Erguler 2012; Dipova 2018). This method could also be used to evaluate the heterogenous surficial strength of biocemented soils.

In the context of mitigation of riverbank erosion via MICP, there are very few studies in the literature that have investigated the performance of biocemented soil against the tangential flow (Amin et al. 2017; Wang et al. 2018a; Clarà Saracho et al. 2021; Do et al. 2021). Most of these studies have reported cracking along with the tangential flow due to brittleness.

There is another way to improve biocementation via the incorporation of biopolymers, which might avoid brittle fracture of MICP-stabilised soil.

Laboratory investigations have been conducted to simulate coastal conditions in hydraulic flumes (Faure et al. 2010; Gu et al. 2020; Kou et al. 2020; Shahin et al. 2020; Liu et al. 2021b). In nature, a complex interaction of current and wave derives the erosion process at coasts and riverbanks. There are limited studies in the literature on coastal erosion mitigation against hydraulic waves via biocementation (Kou et al. 2020; Shahin et al. 2020; Liu et al. 2021b). Most of these studies have reported the erosion characteristics of biocemented soil against wave characteristics such as frequency, dimension, and duration of exposure/tests. A study correlating the erosion traits of the biocemented soil against wave energy is imperative for upscaling the laboratory results to the field.

The current study is designed to explore the above-mentioned gaps in the literature with the aim of facilitating the transition of biocementation technology from laboratories to the field. The study will provide crucial insights into the applicability and potential of soil microbes for aeolian, riverbank and coastal erosion control.

2.6 Objectives of the thesis

The objectives of the thesis have been defined as per the gaps in the literature. The objectives of the study are encapsulated as follows-

1. To study enrichment, isolation, and characterisation of biocementation potent microbial communities from local soils.
2. To study the influence of biocementation on geotechnical properties and aeolian erosion characteristics of desert soil.
3. To investigate the impact of cementation media concentration on properties of biocement under-stimulation and augmentation approaches.

4. To investigate the efficiency of the biocement, biopolymer, and their composites for mitigation of current-induced soil erosion.
5. To investigate the efficiency of biocement, biopolymer, and their composites for mitigation of hydraulic wave-induced soil erosion.

2.7 Scope of thesis

The scope of the thesis is confined to studying the applicability of soil microbes for the improvement of strength and erosion characteristics of sandy soils in different environments. As transport of healthy microbes in huge quantities to the site is a challenge. Therefore, it is of paramount importance to find alternate ways to supply biocement-potent microbes for this purpose. The scope of the thesis is defined as follows-

- Soil microbes have been isolated from three sources in the vicinity of the Brahmaputra riverbank. Their biocementation potential has been investigated along with their essential biochemical characterisation. 16S rRNA sequencing was carried out for the identification of isolates.
- The study is confined to the biocementation of poorly graded fine sand, as it predominantly exists in deserts, riverbanks, and beaches. Another reason to prefer the fine sand was due to their size compatibility for their transport. In the current study, a spraying strategy has been employed for supplying microbes and cementation solution to the soil as it is convenient for large-scale applications, and a few studies in the literature have demonstrated its applicability in reducing wind-induced and rainfall-induced erosion.
- There is the possibility of heterogeneity in the local strength of the soil with the adopted spray strategy. A thin crust of biocemented layer has been reported in the literature with the spraying strategy. Therefore, the needle penetration test

has been adopted in the current study to investigate the local strength of soil at various points.

- The wind erosion was investigated in a laboratory-scale flume where the wind velocity was restricted to up to 55 kilometres per hour. The wind velocity in the Thar desert is reported to be in this range except in the case of extreme events like dust storms.
- The riverbank erosion due to tangential flow was simulated in a hydraulic flume. The maximum hydraulic-flow velocity in the laboratory flume was restricted up to 0.75 m/s. The designed critical flow varied from 0.06 to 0.62 m/s based on the theoretical critical velocity, which was estimated based on the mean diameter of the soil.
- The coastal erosion is also simulated in the hydraulic flume. The erosion characteristics of biocemented soil are reported against waves travelling in tangential and perpendicular directions. The wave energy is calculated by the simplified shallow wave energy theory, which would be helpful to upscale the proposed treatment.
- A novel biopolymer-biocement composite has also been devised to avoid brittle fractures of MICP-treated specimens.

The treated soil and precipitated crystals have been investigated qualitatively and quantitively based on their mineralogy, microstructure, and weight. Overall, the current study will facilitate the transition of biocementation from laboratory to pilot-scale studies, specifically in the area of erosion mitigation.

CHAPTER 3

MATERIALS AND METHODS

In order to achieve the stipulated objective, various experimental procedures were adopted. The soils were collected from various locations to investigate the presence of biocementation potent microbes and their applicability in mitigating soil erosion. The details of materials and methodology are described in this chapter.

3.1 Materials

3.1.1 Soil for bacteria isolation

Bacteria were isolated from three different sources, including the Brahmaputra River stream (BRS), Brahmaputra Soil (BS) and locally available soil from a natural slope (LS) in the vicinity of the Indian Institute of Technology, Guwahati campus. Topsoil (10 mm) was removed, and the soil beneath was collected in a sterile tube and kept in an ice bucket for isolation purposes. The soil was collected separately for geotechnical classification within 500 mm depth.

The engineering properties and physicochemical characterisation of soil (Table 3.1) are evaluated following American Society for Testing and Materials standards (ASTM D4254-16 2006; ASTM D854-14 2014; ASTM D6913/D6913M-17 2017; ASTM D4972-19 2019). As per the USCS (Unified Soil Classification System), the soil collected at Brahmaputra bank is characterised as poorly graded fine sand, while the soil collected from the nearby slope is identified as clayey sand. It is to be noted that Brahmaputra Sand (BS) is used in this study to investigate hydraulic erosion. Both the Brahmaputra soil and the river stream had a pH of around 7.5±0.3, whereas the local soil exhibited a pH of around 8.5±0.5. The specific gravity of Brahmaputra riverbank sand was 2.7, whereas the specific gravity of local soil was found to be 2.65.

Table 3.1 Properties of soils used in microbial isolation.

Properties	Site 1 (BS) (Brahmaputra Riverbank)	Site 2 (LS) (Natural slope near IIT Guwahati)
Coordinates	26°10'50" N; 91°41'26" E	26°11'05" N; 91°41'32" E
pH	7.5	8
Predominant Minerals	Quartz, Mica	Quartz, Hematite, Kaolinite
Environmental Temperature	32±3°C	32±3°C
Specific Gravity	2.7	2.65
Coarse sand content% (2 mm - 4.75 mm)	0	1
Medium sand content% (0.425 mm- 2 mm)	1	26
Fine sand content% (0.075mm - 0.425 mm)	94	54
Silt content % (0.002 mm - 0.075 mm)	5	14
Clay content % (≤ 0.002 mm)	0	5
Coefficient of uniformity (C_u)	1.67	18.75
Coefficient of Curvature (C_c)	1.06	4.68
Maximum Dry Density (kN/m^3)	15.36	16.75

3.1.2 Soil for aeolian erosion experiments

Additionally, to evaluate the influence of biocementation on the aeolian erosion characteristics, desert soil (RS) has also been procured from a dune of the Jaisalmer district (27.27° N, 70.79° E) of the Thar Desert situated in Rajasthan, India. The evaluated engineering properties of soil have been encapsulated in Table 3.2. The desert soil was also classified as poorly graded fine sand as per the USCS classification. The desert sand contained 5% fine content. The pH of Rajasthan soil was found to be 7.5, and specific gravity was determined as 2.67.

Table 3.2 Properties of Rajasthan Desert Sand (RS).

Characteristics	Values
pH	7.5
Predominant Minerals	Quartz
Specific Gravity	2.67
Fine sand content% (0.075mm - 0.425 mm)	95
Silt content % (0.002 mm - 0.075 mm)	5
Coefficient of uniformity (C_u)	2.21
Coefficient of Curvature (C_c)	0.88
Maximum dry density (kN/m^3)	15.50

3.1.3 Soil for hydraulic-current and wave-induced erosion experiments

Fine-grained soil equivalent to the soil collected from Brahmaputra Riverbank (BS) was used to study the impact of hydraulic current and wave-induced erosion. The property of BS is mentioned in Table 3.1. Biocementation with isolated microbes in BS is conducive to the selective stimulation approach since the native microbes are being utilised for $CaCO_3$ precipitation. Equivalent fine-grained sand with similar gradations is also prevalent on coastal banks (Kou et al. 2020; Shahin et al. 2020; Liu et al. 2021b). Therefore, to study the potential of MICP in improving erosion resistance against coastal waves, soils equivalent to BS were considered intentionally. Another notable reason for using fine sand in the current study is that it has compatibility with the size of the pore throats of fine sand for microbial migration (DeJong et al. 2010).

3.1.4 Biocementing microbes

The standard biocementing microbe *Sporosarcina pasteurii* (ATCC 11859) was procured from American Type Culture Collection (ATCC) for benchmarking the performance of the isolated strains. In this study, biocementing microbes were isolated from three different soil environments, the Brahmaputra riverbank soil (BS), the Brahmaputra river stream (BRS) and a local vegetative slope (LS) of a hill nearby the

Indian Institute of Technology Guwahati Campus as mentioned in section 3.1.1. The two best-performing isolates from each source were characterised based on their biocementation capabilities. In a preliminary investigation, to ensure that the isolated strains have the potential to bind the soil, the low-performing strain (LS2) has been employed in Objective 2 to confirm the ability of isolated microbes to improve the soil properties, including unconfined compressive strength and hydraulic conductivity. After confirmation, the best-performing isolated microbe (BS3) has been compared with the conventionally used microbe SP and consortia in Objective 3 to find out the most suitable concentration of cementation media for soil binding. Afterwards, the best-performing isolated strain (BS3) was used to investigate their potential to improve soil erosion resistance in Objectives 4 and 5. Another reason for choosing BS3 for investigating hydraulic erosion over other microbes was due to its isolation from the Brahmaputra riverbank, which is liable for the selective-stimulation approach.

The details of the isolation methodologies are discussed in subsequent sections. The isolated microbes are reported to have better resilience and viability in soil environments in previous studies (Dhami et al. 2017; Graddy et al. 2021). Moreover, isolation from local soil is expected to result in transport-related cost savings.

3.1.5 Biopolymer

Xanthan gum, a commercially available biopolymer (BP), was also used in the current study with the aim of developing a biopolymer-biocement composite treatment for soils. Laboratory-grade powdered xanthan gum (XG) manufactured by Sigma Aldrich was used in this study. XG is a well-established biopolymer used for soil strength improvement (Chang et al. 2015; Chang et al. 2016). XG is characterised as a hydrophilic non-toxic polysaccharide produced from *Xanthomonas campestris* (Casas et al. 2000; Rosalam and England 2006).

3.1.6 Microbial growth and Cementation media

For making the liquid growth media for microbes, nutrient broth (Sigma Aldrich) in powdered form was utilised. For making cementation reagents, analytical grade of dihydrate calcium chloride ($CaCl_2$. $2H_2O$, molecular weight 147.01 grams per mole) and urea (NH_2-CO-NH_2, molecular weight 60.06 grams per mole) were used. The details of each of the media (sterile) used in the current study are summarised in Table 3.3.

Table 3.3 Details of the media used for enrichment, isolation, and cementation.

Media/Components	Identifier	Nutrient Broth	Urea	$CaCl_2$
Enrichment media	NB5U	13 g/l	5%	NA
Growth Media	NBU	13 g/l	2%	NA
Precipitation Media	PM	1 g/l	2%	50 mM
Fixation Media	FM	-	-	25 mM
Cementation Media	CM	1 g/l	250-1000 mM	250-1000 mM

It is to be noted that for objective 5 (chapter 8), the bacteria were grown in the yeast extract-ammonium sulphate (YE) media instead of NBU media based on the past studies conducted on coastal erosion mitigation with MICP treatment (Shahin et al. 2020; Liu et al. 2021b; Wang et al. 2022). The growth media consisted of yeast extract (20g/l), tris buffer (0.13 M), and ammonium sulphate (10 g/l).

3.2 Methods

A summary of the required experiments for the objectives is illustrated in Table 3.4. In Table 3.4, FESEM, EDX, and XRD stand for Field Emission Scanning Electron Microscopy, Energy Dispersive X-ray spectroscopy and X-ray Diffraction, respectively. The details of test methodologies are described in the following sections.

Table 3.4 Experimental Summary.

S.N.	Objective	Tests
1	Enrichment, isolation, and characterisation of biocementation potent microbes from local soils.	Enrichment of soils in flasks, Serial Dilution of consortia, Isolating pure culture, Biochemical analysis and 16S rRNA identification of isolates.
2	Influence of biocementation on geotechnical properties and aeolian erosion characteristics of desert soil.	Permeability, Unconfined compressive strength (UCS), Wind erosion test, $CaCO_3$ content, FESEM, EDX, and XRD.
3	Impact of cementation media concentration on biocement properties under-stimulation and augmentation.	Flask batch test for Urea and Calcium depletion monitoring, Needle penetration test, $CaCO_3$ content, FESEM, EDX, and XRD.
4	Evaluation of biocement, biopolymer, and their composites for mitigation of current-induced soil erosion.	Needle penetration test, Current erosion test in the flume, $CaCO_3$ content, FESEM, EDX, and XRD.
5	Evaluation of biocement, biopolymer, and their composites for mitigation of hydraulic wave-induced soil erosion.	Needle penetration test, Hydraulic wave erosion test in the flume, $CaCO_3$, FESEM, EDX, and XRD.

3.2.1 Isolation and characterisation of biocementing microbes from the soils

3.2.1.1 Enrichment of ureolytic communities

One gram of the collected soil (BS & LS) was inoculated into the 100 ml enrichment media containing 13 g/l of Nutrient Broth (NB) and 5% Urea in a shaking incubator at 37° C and 120 rpm for five days. This was followed by two subcultures of the enriched communities into new enrichment media. Confirmation of the ureolytic capability of these communities was verified by inoculating the bacterial culture into the urea agar base, wherein the change in colour was recorded within 12 hours.

3.2.1.2 Identification and characterisation of the isolates

After the enrichment of ureolytic communities, the most efficient ureolytic cultures were isolated from the consortia. For this purpose, the enriched consortia were serially diluted and inoculated on Nutrient Broth- 2% Urea (NBU) agar plates, and single colonies were obtained following standard protocols (Dhami et al. 2013a). These colonies were then screened for qualitative urease assay on urea agar plates (Christensen 1946). Six highly ureolytic cultures were screened. Then, the preliminary gram staining and endospore formation capabilities were evaluated following standard protocols (Smith and Hussey 2005; Hussey 2013). The gram staining is usually conducted for the phenotypic characterisation of bacteria based on their cell wall characteristics. Gram-positive microbes exhibit blue to purple colour, whereas Gram-negative cells illustrate red to pink shade after the staining protocol. Endospore formation is evaluated to check the capability of microbes to form dormant cells in unfavourable conditions for microbes' survival. The biochemical properties of the isolates were evaluated using the Microbact 12 A, 12B, and 24 E kit. This was followed by the identification of these cultures via 16S rRNA genomic sequencing. The 16S rRNA sequencing was conducted at NCMR (National Centre for Microbial Research, India). The sequences of the isolated strains were analysed and compared with the highly similar sequences available on the NCBI database utilising nucleotide BLAST. The DNA sequences of the isolated strains were aligned with the reference sequences of the obtained highly similar strains by the MUSCLE algorithm, and the phylogenetic tree was constructed by the neighbour-joining method using Mega-X software (Kumar et al. 2018).

The screened isolates were further characterised based on their biochemical properties, growth characteristics, urease activity, and calcium utilisation potential. The isolates were grown in the NBU media for four days at 37°C and 120 rpm in a shaking

incubator to evaluate growth characteristics and urease activity. The performance of isolates was compared with the comprehensively used SP (*Sporosarcina pasteurii* ATCC 11859) and the artificial consortia. The artificial consortia were created by mixing an equal proportion of the isolated strains from site 1.

3.2.1.3 Growth, pH and Specific urease activity of isolated microbes

1% of overnight cultivated microbe ($O.D._{600}$ =1) was added to fresh NBU media to record their growth characteristics. The pH of the bacterial solution was measured along with their growth with the help of the Eutech pH meter. The urease activity (mM urea hydrolysed per hour) of the bacterial isolates was evaluated following the electrical conductivity method (Whiffin et al. 2007). For the assay of urease activity, 1 ml of bacteria was mixed with 9 ml of 1.11 M urea, and the change in electrical conductivity was measured for 5 minutes at room temperature (25±3 °C). The electrical conductivity (EC) of the bacterial solution was measured along with their growth with the help of the Eutech EC meter. The ratio of the urease activity and the bacterial optical density ($O.D._{600}$) is defined as the specific urease activity (mM urea hydrolysed h^{-1} $O.D._{600}^{-1}$).

3.2.2 Methods for evaluation of the biocementation potential of the isolates

The preliminary comparison of the isolated microbes for their biocementation potential was carried out by a modified method from previous literature (Dhami et al. 2013a; Dhami et al. 2016). One percentage of the volume of the overnight grown bacterial culture ($O.D._{600}\approx1$) was added to the precipitation media (PM) in a shaking incubator at 37° C and 120 rpm. A negative control set consisting of only flask cementation media was also observed for the test duration to check the possibility of abiotic precipitation.

To investigate further, the biocementation potential of the different microbes at various concentrations of cementation media (CM) was evaluated by monitoring the biochemical reaction. The concentration of the urea and soluble Ca^{2+} was measured at

regular time intervals. For this purpose, 2.5% of the bacterial cultures in the exponential phase (O.D. $_{600}$ ≈1) were inoculated in the CM (for 250 mM to 2000 mM) in a shaking incubator set at 37 °C and 120 rpm. A negative control set consisting of only cementation media was also kept for the test duration to confirm the abiogenic $CaCO_3$ precipitation and the possibility of contaminant growth. 15 ml samples were collected from the inoculated flasks at regular time intervals and centrifuged at 4°C and 8000 rpm for 5 minutes before the measurements.

3.2.2.1 Measurement of Soluble Ca^{2+} concentration

The concentration of the soluble Ca^{2+} was measured by the modified Ethylenediaminetetraacetic acid (EDTA) titration method (Stocks-Fischer et al. 1999). From the centrifuged supernatant, an adequate amount of sample (10 µL to 100 µL) was diluted into 10 mL of distilled water. Around 400 µL of 1N NaOH solution was added to increase the pH to the hyper alkaline range (≈13). After the pH adjustment, a few drops of 1 % (W/V) hydroxy-naphthol blue indicator was added, and the sample was titrated against the 1 mM EDTA solution. The required EDTA volume to change colour from pink to blue was noted and compared with the standard calibration plot for $CaCl_2$ solutions.

At the end of four days, the precipitates were collected on Whatman no. 1 filter paper and washed with sterile water as per Dhami et al. (2016). The precipitates were air-dried after filtration at room temperature for 48 hours, weighed, and analysed for gravimetric, microstructural, and mineralogical analysis.

3.2.2.2 Measurement of urea concentration

The hydrolysed urea was measured by the colourimetric p-Dimethyl- amino benzaldehyde (DMAB) method (IS:1479-1 1960; Murugan et al. 2021). The reagent was prepared by mixing 1.6 g of DMAB in a 100 mL solution containing concentrated absolute ethanol and hydrochloric acid in a 1:9 ratio. From the centrifuged supernatant, 50 µL of

the appropriately diluted samples were mixed with a mixture of 50 µL of a trichloroacetic acid solution (12%) and 100 µL of DMAB reagent. The finally mixed solution was incubated at room temperature for 5 min. After the incubation, the optical density of the mixtures was measured at 425 nm, and the concentration of urea was estimated using the standard calibration plot.

3.2.3 Permeability and unconfined compressive strength

Test setup schematics for the permeability and unconfined compressive strength are illustrated in Figure 3.1. For evaluating the permeability and unconfined compressive strength of the untreated and treated soil samples, cylindrical soil specimens of 40 mm diameter and 80 mm length were prepared in an acrylic pipe. The soil samples were prepared at a density of 1.56 Mg/m^3 (Megagrams per m^3) by the dry pluviation method. The sand was sterilised before sample preparation to avoid the possible undesired influence of contaminants. 10 mm of gravel filter was kept at the top and bottom of the soil sample along with the Whatman Grade 42 filter papers for uniform flow of the cementation reagents. The soil was saturated utilising deionised water with backpressure, and permeability was measured by the falling head permeability technique in the first step. Prior to each step of introducing the mentioned solutions, the specimens were allowed to drain first by opening the outlet valve, and then the new solutions were introduced at the top of the specimen. In the second step, fixation media (FM) was injected for uniform precipitation (Harkes et al. 2010), followed by the third step, which includes supplementing the one pore volume (40 ml) of bacteria solution of $O.D._{600}$ equivalent to 1**.** In the fourth step, after 24 hours of the bacterial retention period, one pore volume (40 ml) of cementation media (CM) comprising equimolar urea, calcium chloride (250 mM, 500 mM, and 1000 mM) and nutrient broth (1 g/l) are passed through the soil media and the outlet valve was closed for 7-day reaction period. After seven days of the reaction

period, the treated soil column was washed with deionised water as the final step of the treatment. The permeability of treated soil was measured again.

The soil was saturated utilising deionised water with backpressure, and permeability was measured by the falling head permeability technique. The saturated hydraulic conductivity (k_{sat}) of the soil is measured by the following equation 3.1

$$k_{sat} = \frac{aL}{At} \ln\left(\frac{h_2}{h_1}\right) \qquad (3.1)$$

Where 'a' represents the area of the stand tube/burette (in square meters), 'L' is the length of the soil sample (in meters), 'A' represents the cross-sectional area of the soil sample (in square meters), 't' is the time taken (in seconds) for the hydraulic head to fall from h_2 (in mm) to h_1 (in mm).

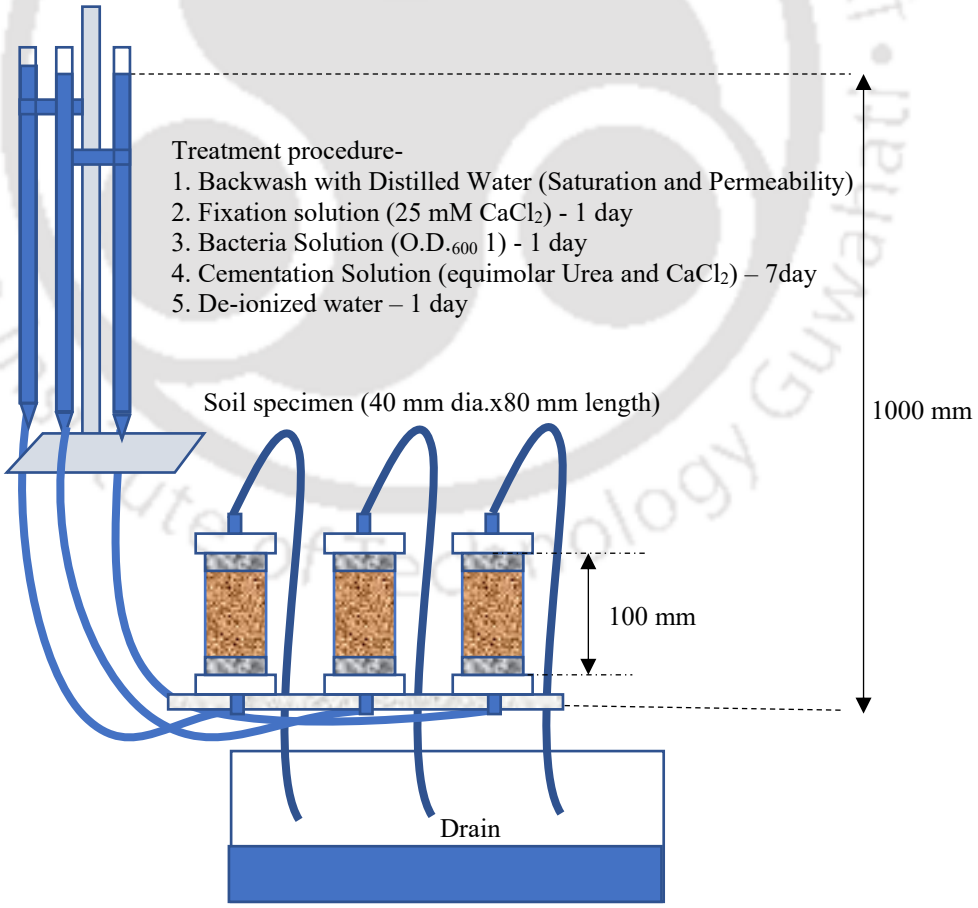

Figure 3.1 Test setup schematics for the permeability and unconfined compressive strength.

The treated soil columns of 40 mm diameter and 80 mm height were extruded and oven-dried for the unconfined compressive strength (UCS) test at a strain rate of 1 mm/min.

3.2.4 Needle penetration tests

The soil strength improvement of the treated specimens was compared with the resistance index of the soil against needle penetration. The needle penetration resistance was employed to evaluate the local strength of soil grains upon biocementation as a spraying strategy is adopted for the treatment in the current study. As recommended by the International Society of Rock Mechanics (ISRM), the needle penetration test is an emerging non-destructive technique for a quick comparison of the strength of weak rocks and cemented soils (Ulusay et al. 2014; Dipova 2018; Chung et al. 2021). The ratio of penetration resistance (N) to penetrated depth (mm) is defined as the needle penetration index (NPI). A needle of diameter 0.86 mm manufactured by the Chenille brand (needle #22) was installed on a universal testing machine (Shimadzu AGS-X). The penetration rate was set as 15 mm/minute for every test. The penetration was conducted up to a penetration depth of 5 mm. To negate the undesired influence from the boundaries of the Petri dishes, all the penetrations were carried out at least 10 mm away (>ten times the diameter of the needle) from the boundary and from the other penetration points based on the conducted trials. The penetration depths were also restricted to half of the soil sample depth to avoid influence from the bottom boundary of the Petri dish. The penetrations were carried out at least on 15 distinct points on the developed biocemented crust for each sample. The average needle penetration resistance from these 15 points has been reported with standard deviation, as suggested by Dipova (2018), to determine the non-uniformity in the biocemented samples.

The needle penetration tests were conducted on two types of samples in this study. First, to investigate the impact of different microbes and cementation media concentrations in Chapter 6, the samples were prepared in Petri dishes. The soil was washed with ultrapure water, dried, and later sterilised to highlight the influence of the intended treatment. After the sterilisation, the sand was filled in 16 Petri dishes of 60 mm diameter and 10 mm depth in sets of four. The dry density of the sand was maintained at 1.56 megagrams per cubic meter (Mg/m^3). The biocementation treatment was conducted via a three-staged spraying strategy with a spraying rate of 50 ml per minute. The employed spraying strategy is recommended as one of the most viable strategies for surficial biocementation applications considering field application, similar to agricultural irrigation (Wang et al. 2018a)). First, one pore volume (15 ml) of the fixation solution (FM) was sprayed in all 16 specimens. In the second stage, 15 ml of the specific microbial cultures were sprayed in four Petri dishes each. One set of 4 Petri dishes was kept as a negative control (without any bacteria) to evaluate the strength improvement in soil with possible precipitation of the abiogenic calcium carbonate. In the third stage, the samples were sprayed with cementation media (CM) of intended concentrations. Four different concentrations of cementation media of molarity 250, 500, 1000 and 2000 mM were investigated. The samples were retained and dried in a fan-equipped oven at the temperature of 37 degrees Celsius for 24 hours after the completion of each stage. Multiple cycles of cementation media were applied to produce equivalent theoretical calcite (7.12%) in all the specimens. The equivalent theoretical calcium carbonate content was aimed to evaluate the influence of the number of treatment cycles on the efficiency of bacteria in producing calcium carbonate and binding soil grains. Treatment with less than 250 mM concentration of CM was not considered because a large number of CM treatment cycles would be required to achieve the equivalent $CaCO_3$ content. It is to be noted that

the bacteria samples were supplied only once, and the multiple numbers of cementation treatments have an adverse influence on the $CaCO_3$ precipitation efficiency of the microbes (Mujah et al. 2019).

Secondly, the samples were also checked for their strength using a needle penetration test for duplicate samples that were investigated for their erosion resistance against hydraulic current and waves in the hydraulic flume. The dry sterilised sand was pluviated at a density of 1.56 megagram per cubic meter (Mg/m^3) in a cuboidal container of dimensions 92.5 mm × 58 mm × 40 mm. For biocementation treatment, one pore volume of each, i.e., fixation solution, bacterial solution (at optical density ≥ 1) and 500 mM cementation solution (two times) were sprayed consecutively with a retention period of 24 hours for each step to complete one biocementation cycle for soil treatment. The sand sample treated with one biocementation cycle is termed BC1, and similarly, samples treated with 2, 3, and 4 biocementation cycles are termed BC2, BC3, and BC4, respectively. One cycle of biocementation is assumed to precipitate 2.5% of average calcite by the weight of the untreated sand. The untreated sand (BC0) was reported as a control. For the treatment with biopolymer, a low-viscosity xanthan gum (1 g/l) was sprayed on the untreated soil. The low concentration of xanthan gum was selected in this study to have a sprayable viscosity of the solution that can penetrate the soil matrix without disturbing the surficial soil structure based on the previous studies, which have considered biopolymer treatment for mitigating aeolian erosion (Kavazanjian et al. 2009; Devrani et al. 2021). Samples sprayed with one pore volume of xanthan gum solution are termed BP1. The samples BP2 and BP4 are prepared by spraying one pore volume of the solution for 2 and 4 days consecutively at an interval of 24 hours. All samples were kept in an air-circulating temperature-controlled chamber at 37°C after spraying the required treatment solutions. One spray of biopolymer theoretically adds 0.025% of biopolymer by weight of

the dry weight of soil. It is to be noted that theoretically, around a 5% reduction in the initial pore volume was estimated after the successful completion of each biocementation cycle, based on which the pore volume of cementation solutions for each cycle was decided. For samples BC1, BC2, BC3, and BC4, one pore volume means 100, 95, 90, and 85 ml of corresponding solutions, respectively. No significant change in the pore space was anticipated with biopolymer treatment. Three biopolymer-biocement composite samples, BP1BC1, BP1BC2, BP2BC2, and BP4BC2, were prepared by treating two additional cycles of biocementation after the intended biopolymer treatment.

3.2.5 Wind erosion tests

The samples were filled in a shallow cylindrical pan of 280 mm diameter and 45 mm depth at 1.56 Mg/m^3 for wind erosion test. The soil was treated with one pore volume of fixation fluid and bacteria solution by spraying with a hand atomiser at a rate of 50 ml/min. The samples were air-dried for 24 hours. After that, one pore volume of cementation media (250 mM, 500 mM, and 1000 mM) was sprayed on the sample, and the sample was kept for air drying for seven days.

The samples were then tested in the basic wind tunnel apparatus (0.3m x0.3 m flow area) situated in the Water Resource Engineering Laboratory, Department of Civil Engineering, IIT Guwahati. First, the soil threshold detachment velocity (TDV) of the soil was observed visually by gradually increasing the wind velocity and observing the particle movement. TDV is defined as the wind velocity at which erosion initiates. After noting the TDV, the fan speed is gradually increased to a wind velocity of 32 km/h and 55 km/h consecutively for an exposure period of 5 minutes each, the methodology described by Devrani et al. (2021). The configuration for the wind erosion test is shown in Figure 3.2.

The selected wind velocity profile is based on the average wind velocities in the Thar region, which is reported to be in the range of 25-45 km/hour in the erosion-prone zones (Ramakrishna et al. 1990, 1994, Worldweatheronline.com 2020).

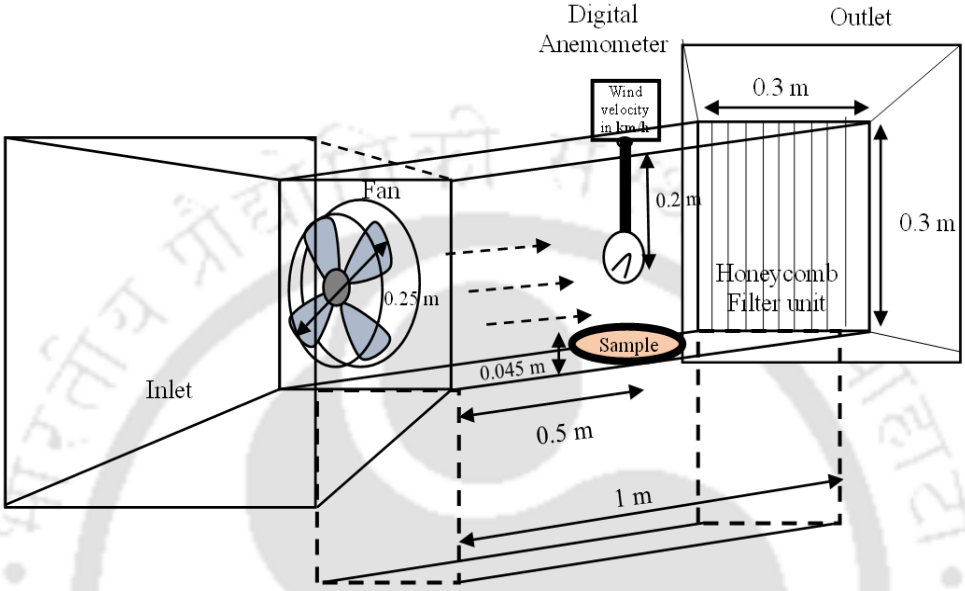

Figure 3.2 Schematics for wind erosion test.

3.2.6 Hydraulic-current-induced erosion tests

A total of 32 soil samples were prepared in a cuboidal container of dimensions 92.5 mm × 58 mm × 40 mm for a flume erosion test against the hydraulic current. Biocemented samples BC1, BC2, BC3 and BC4 were prepared as mentioned in section 3.2.4. Biopolymer-stabilised samples BP1, BP2 and BP4, were also tested. Biopolymer biocement composite specimens BP1BC2, BP2BC2, and BP4BC2 were also prepared for the flume erosion test. Each specimen of composite material is considered to have 5% of calcium carbonate by weight of soil along with the above-mentioned biopolymer content. In the presented study, the biocement levels were kept constant in the composite samples

to specifically investigate the influence of varying the biopolymer content on the composite.

The fluvial erosion tests were conducted in a 12 m long glass-walled tilting flume manufactured by Armfield Engineering Ltd. with a dimension of 320 mm height and 300 mm internal width of the flow channel placed in the School of Civil and Mechanical Engineering, Curtin University. The plan and front section of the flume is shown in Figures 3.3 (a) and (b).

All samples were saturated first by spraying one pore volume of deionised water before placing it on the acrylic slope. Then, the water level was gradually increased to the water depth of 200±5 mm and was maintained throughout the current erosion test in the flume for slopes S30, S45, and S53, where the numbers represent the angle of slope in degrees. The hydraulic flow velocity in the flume was increased stepwise from 0.06±0.004 m/s to 0.62±0.033 m/s at intervals of a 5-minute for a total test duration of 40 minutes, as shown in Figure 3.3 (c). The erosion characteristics of the samples were analysed in terms of cumulative eroded depth, cumulative erosion rate, critical velocity, and soil mass loss. To minimise the influence of boundary conditions from the acrylic slope on the results, all samples were tested against the same flow conditions and the hydraulic velocity was measured at irregular time intervals utilising a pulse velocity meter. Figure 3.3 (a) shows the measurement points located 3 m apart.

The erosion characteristics of the samples were analysed in terms of cumulative eroded depth, cumulative erosion rate, critical velocity, and soil mass loss. The specific power (W/m^2) of the current impacting the soil specimen was calculated as the ratio of kinetic power and the area of exposed soil following equation (3.2) derived from Zdankus et al. (2014).

$$P_S = \frac{0.5\ \rho\ A(v^3)}{A_s} \qquad (3.2)$$

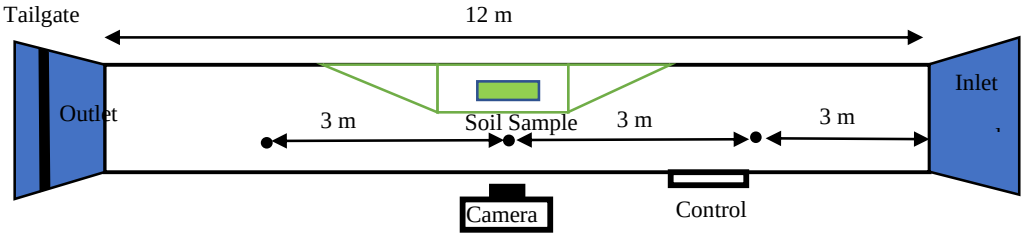

(a)

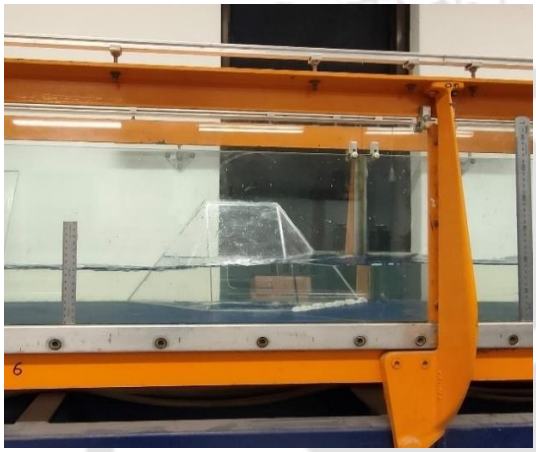

(b)

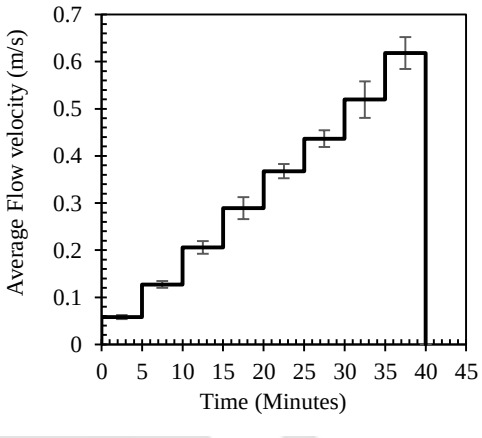

(c)

Figure 3.3 (a). Experimental schematics of the flume; (b). Front section photograph; and (c). Designed flow velocity profile.

Here, P_S is the specific power (W/m^2) for the corresponding hydraulic current velocity v (m/s) flowing through the cross-sectional area A (m^2) against the exposed soil specimen of surface area A_s (m^2). Here, ρ (kg/m^3) stands for the density of water.

The erosion was recorded with a video camera. The recording was processed using the open-source software ImageJ (version 1.53m) to obtain the eroded volume. The eroded volume was converted into cumulative eroded depth (mm) using equation (3.3).

$$D = \int_0^t \frac{dV.dt}{A_s} \qquad (3.3)$$

Here, D is the total eroded depth in time interval t, and V is the volume eroded, and. A_s is the surface area of the sample.

The cumulative erosion rate (E_R) at a particular velocity (v) was derived by calculating the total depth eroded per unit time interval (t) with equation (3.4).

$$E_R = \frac{D}{t} \tag{3.4}$$

The experiment was terminated when the average eroded volume exceeded 50% (average eroded depth>20 mm) to negate the undesired influence of boundary conditions from the soil containers.

3.2.7 Hydraulic wave-induced erosion tests

Hydraulic wave erosion tests were also simulated in the above-mentioned Armfield tilting flume. The soil samples were prepared in two distinct configurations to simulate tangential and perpendicular waves against the soil specimen, similar to the river and coastal waves. For the perpendicular waves test (P), the samples are prepared in an acrylic mould of dimensions 100 mm width, 100 mm length, and 100 mm depth, maintaining a 45° slope (1 horizontal to 1 vertical). For tangential wave tests (T), the soil samples were prepared in a container of dimension 92.5 mm in length, 58 mm in width, and 40 mm in depth. Later, the container was plugged into an acrylic slope of 45 degrees (1 horizontal to 1 vertical). The acrylic slope was gradually sealed along the walls of the flume with a smooth ramp to cause minimum interference to the flow. It must be noted that the initial volume was different for both tests as it required different kinds of setup/arrangements in the hydraulic flume to simulate the tangential and perpendicular wave. Only the surface of the soil specimens was exposed to flow for erosion in both scenarios. All the tests are conducted on triplicate samples, and the average values of results, along with deviations, have been reported.

Biocemented samples (BC1-BC4), biopolymer samples (BP1) and biopolymer-biocement composite samples (BP1BC1 and BP1BC2) were prepared for the hydraulic wave-induced erosion test in a flume. The samples subjected to tangential waves are labelled with a prefix T with the treatment nomenclature in the form of TBC0, TBC1-TBC4, and TBP1BC1- TBP1BC2. With a similar approach, the samples subjected to the perpendicular waves are labelled with the suffix P, namely PBC0, PBC1- PBC4, and TBP1BC1- TBP1BC2. After the flume erosion tests, needle penetration resistance and the microstructure of the treated soil samples were evaluated. The maximum test duration (30 minutes) was considered based on the trials on the cohesionless soil, which was heavily eroded as soon as the waves hit the specimens.

The plan and cross-section for the test configuration to simulate the perpendicular hydraulic waves are illustrated in Figures 3.4 (a) and (c). The waves were modelled based on the actual coastal 1waves at Rottenest Island (Shahin et al. 2020). The waves are generated on still water at depth (h) 50±5 mm in the hydraulic flume scaled at 1:250. The generated waves were set to propagate at a wave height (h_w) of 28 mm and wavelength (λ) of 1500 mm with a 0.33 Hz frequency (f). To ensure the generation of shallow surging erosional waves, three parameters were maintained, 1. $h > h_w/0.6$; 2. $h < \lambda/20$; and 3. $hw < \lambda/7$ (Flemming 2011, Shahin et al. 2020).

To simulate tangential waves, the alignment of the soil specimen is kept tangential with the flow to let the wave strike the soil in the intended tangential direction, as illustrated in Figures 3.4 (b) and (d). A gentle flow velocity was maintained at 0.06 m/s throughout the test with a constant water depth (h) of 50±5 mm. The hydraulic current is kept much slower than the theoretical critical velocity (V_c) to negate the hydraulic current-induced soil erosion, which is calculated as 0.175 m/s from Briaud's equation (Briaud 2008). The waves were produced utilising a pedal type of wave generator placed 1.5

meters from the inlet. The generated waves were set to propagate at a wave height (h_w) of 25 mm and wavelength (λ) of 1500 mm with a 0.33 Hz frequency. These parameters were adopted to mimic shallow wave conditions of the natural environment in the hydraulic flume fulfilling the three criteria of 1. (λ/h) in the range of 1 to 25; 2. (λ/h_w) in the range of 4 to 56, and 3. (kh)<(π/100) as recommended by few of the previous studies (Das et al. 2020), where k is the wavenumber.

The erosion was recorded with a Digital Single-Lens Reflex (DSLR) camera for image analysis. The stills of the recordings were used to evaluate the erosion characteristics of the treated soils with the open-source software ImageJ (version 1.53m).

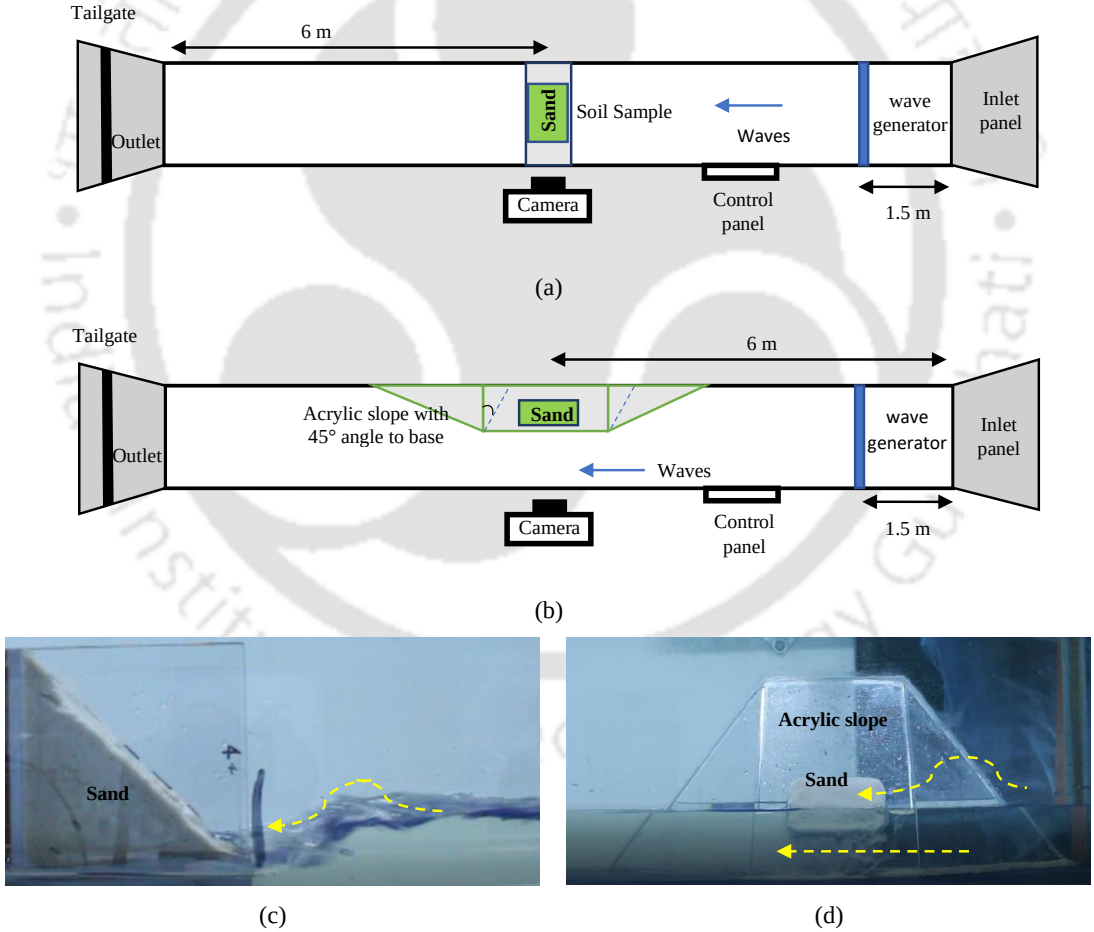

Figure 3.4 Schematics of the top view of configurations for (a). Perpendicular wave test, and (b). Tangential wave test; and corresponding front view photograph in (c) & (d).

The cumulative erosion rate (E_R) is defined as the total volume eroded within a time interval. The erosion rates are presented against the total applied wave energy density (E_D), which is evaluated from Equations 3.5 and 3.6.

$$E_w = \frac{\rho g {h_w}^2}{8} \tag{3.5}$$

$$E_D = \int_0^t \frac{E.f.}{A_S} dt \tag{3.6}$$

Where E_w is the wave energy as per linear shallow water wave theory, ρ is the density of the water, g is gravitational acceleration, h_w is the wave height, f is the frequency of waves, and A_s is the exposed surface area of the soil (Fredsøe and Deigaard 1992). For comparison of the efficiency of biocementation levels to improve erosion resilience, the soil mass loss is also compared.

3.2.8 Measurement of total eroded volume and soil mass loss

The erosion characteristics of the treated soils have been evaluated in terms of the total volume eroded and soil mass loss with the help of the hydraulic flume test in both the cases of current and wave-induced erosion. The stills of the recordings were used to evaluate the total volume eroded in the percentage of the initial volume (V) at different time intervals with the open-source software ImageJ. The eroded volume (V) of the sample at a particular E_D was calculated by following Equation (3.7).

$$V = \frac{V_i - V_t}{V_i} \times 100 \tag{3.7}$$

Where V_i is the initial volume of the treated specimen and V_t is the volume of retained soil at the time 't' responding to E_D.

After the erosion experiments, the specimen was dried in a fan-equipped oven at 40°C. The total eroded soil by the percentage of the weight of the initial specimen was determined based on the gravimetric differences. The soil mass loss (m_L) is also compared.

The soil mass loss (%) is calculated after drying the residual sample following Equation (3.8).

$$m_L = \frac{m_i - m_r}{m_i} \times 100 \quad (3.8)$$

Where m_i is the initial mass of treated soil and m_r is the mass of the residual soil after the erosion test.

3.2.9 Calcite content measurement

The calcite content of the MICP-treated soil was measured by the acid-washing method (Choi et al. 2017). For this purpose, the treated soil was washed in ultrapure water and then dried in a fan-equipped oven at 40°C. After this, 5-gram soil was collected in triplicates were washed with 25 ml of 1N HCl. The calcite content was determined based on their gravimetric difference. The calcite content was determined based on their gravimetric difference following Equation (3.9).

$$CaCO_3(\%) = \frac{m_i - m_a}{m_i} \times 100 \quad (3.9)$$

Where m_i is the initial mass of treated soil and m_a is the mass of the soil after acid-washing.

3.2.10 Microstructural and Mineralogical analysis of the treated soil

The recovered crystals collected from the flasks and the obtained chunks of biocemented soils were washed with ultrapure water and air-dried before spraying on the aluminium stub. The attached specimens were coated with a 10 nm platinum coating for their microstructural and elemental composition analysis. The microstructure analysis of the treated soil was evaluated with Scanning Electron Microscopy (SEM) and Energy-dispersive X-ray spectroscopy (EDX) on Tescan Vega 3 instrument (John de Laeter Research Centre, Curtin University) and ZEISS Neon 40 EsB instrument (Central Instrumentation Facility, IIT Guwahati). The SEM images were taken in secondary

electron and backscattered mode at intensities varying from 5kV to 15 kV and WD 5 to 20 mm. The size of the precipitates was analysed with the obtained images using the open-source software ImageJ (version 1.53m).

For quantitative EDX analysis, the samples were coated with 10 nm carbon coating and polished after mounting on epoxy resins. The EDX maps and spectrum for analysis of elements of the precipitates and sand were conducted utilising the Bruker-16 EDS analyser, which is a part of the Vega 3 SEM instrument.

For the mineralogical analysis of the precipitates, X-ray diffraction (XRD) analysis was conducted on Bruker D8 advanced diffractometer with Nickel filtered Cu-Kα radiation varying 2θ from 5° to 100° with a step size of 0.013°. All samples were micro-ionised (particle size < 10 microns) separately for the XRD analysis. The phase identification analysis was conducted utilising COD and ICDD databases with Bruker EVA.

3.2.11 Statistical analysis of experimental results

All experiments in this study were performed in triplicates. Standard deviations have been illustrated along with the results to decide on the repeatability of the experimental results. The data were analysed by one-way analysis of variance (ANOVA) in Microsoft excel, and means were compared by Tukey's test.

CHAPTER 4

ENRICHMENT, ISOLATION, AND CHARACTERISATION OF BIOCEMENTATION POTENT MICROBES FROM LOCAL SOILS

4.1 Introduction

It is evident from the literature that although there are several studies in the area of soil erosion control, most of them are focused on augmentation approaches utilising exogenous microbe *Sporosarcina pasteurii* (SP) due to its high biocementation potential (Maleki et al. 2016; Amin et al. 2017; Jiang and Soga 2017; Duo et al. 2018; Tian et al. 2018; Jiang et al. 2019; Zomorodian et al. 2019; Chung et al. 2021; Clarà Saracho et al. 2021; Do et al. 2021). The native microbial communities have better adaptability to the soil environment in terms of their survival and performance (Dhami et al. 2017; Gomez et al. 2017; Graddy et al. 2018; Graddy et al. 2021). Moreover, the presence of native biocementing microbes might lead to a reduction of transport-related costs for supplying healthy microbes to the site.

Within this context, an investigation of the biocementation potential of the native bacterial communities of the riverbank site in the Assam valley of the Brahmaputra River is investigated in this chapter by carrying out (a). Enrichment of ureolytic microbial communities from the natural riverbank soil, (b). Isolation and identification of ureolytic bacteria, (c). Characterisation of the isolated microbes via biochemical evaluations, (d). Comparison of their biocementation potential in terms of the urease activity and calcium utilisation rate with *Sporosarcina pasteurii* (SP), and (e). Microstructural and mineralogical analysis to confirm the precipitation of $CaCO_3$ crystals. A summary of the work plan can be comprehended by the flow chart in Figure 4.1.

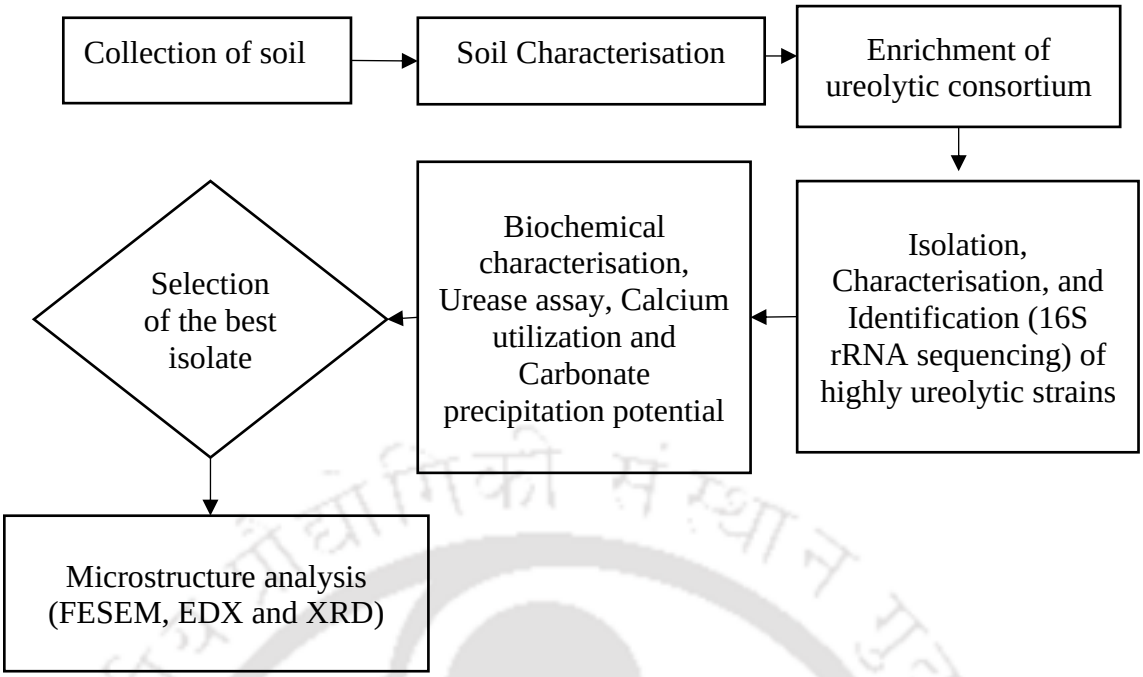

Figure 4.1 Summary of experiments to investigate and characterise the biocementation potent microbes in Brahmaputra soils.

4.2 Results and Discussion

4.2.1 Biostimulation of ureolytic communities

4.2.1.1 Enrichment

The native communities of the soils were successfully grown in the enrichment media (NB5U). The cultivated communities after two subcultures were serially diluted (10^{-2} to 10^{-6}) and were spread with a sterile loop over Nutrient agar plates supplemented with 2% urea. Later, 36 morphologically distinct single colonies were obtained on the urea agar base plates based on visual observation. Figure 4.2 illustrates the enriched soil in NB5U media, the third subculture and obtained single colonies on a few of the agar plates after the serial dilution.

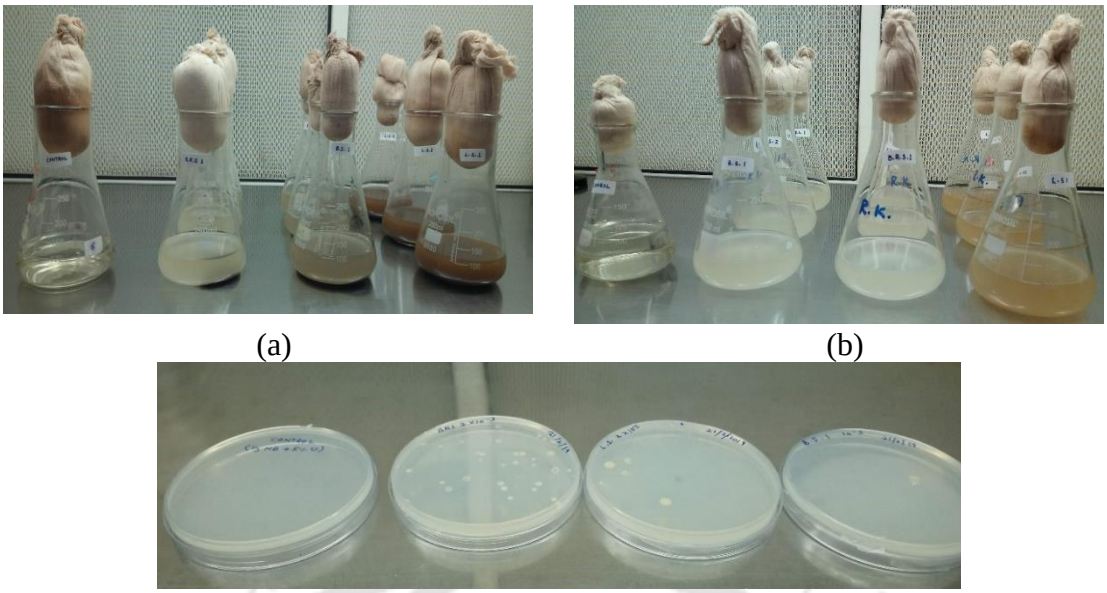

(a) (b)

(c)

Figure 4.2 (a). Enrichment of soil microbes in NB5U media, (b). Subculture of natural consortia and (c). Isolated pure colonies.

4.2.1.2 Isolation, identification, and characterisation of the ureolytic isolates

Out of 36 isolated bacteria, six isolates (BS1, BS2, BS3, BS4, LS1, and LS2) were selected after checking for the urease activity test on the urea agar base (UAB) plate. These selected isolates turned the colour of the UAB plate from orange to pink within 12 hours, as illustrated in Figure 4.3.

The first plate is negative control (without any bacteria), the second plate is positive control (*Bacillus pumilus*, a urease-negative bacteria), and the third plate belongs to the ureolytic bacteria used in the current study. Figure 4.3 (a). demonstrates the colour change in SP, while Figures 4.3 (b) to 4.3 (g) illustrate the colour changes in urea agar base plates for the isolated bacteria. All the isolates were rod-shaped. The Gram-staining revealed that all the isolates were Gram-positive as the isolates and SP exhibited blue-purple colour after the staining, as shown in Figure 4.4.

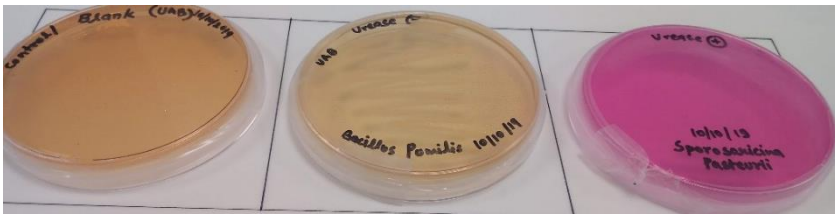

(a)

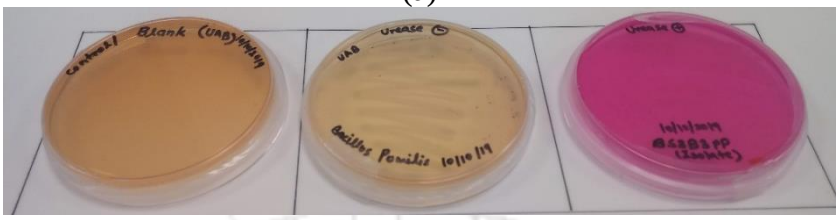

(b)

(c)

(d)

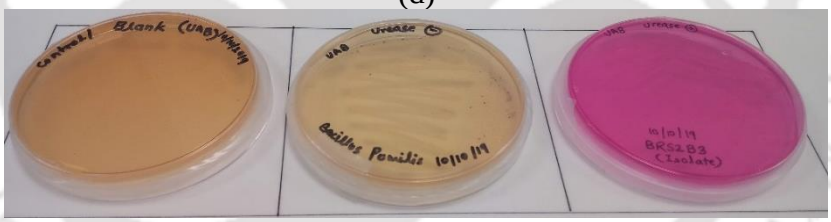

(e)

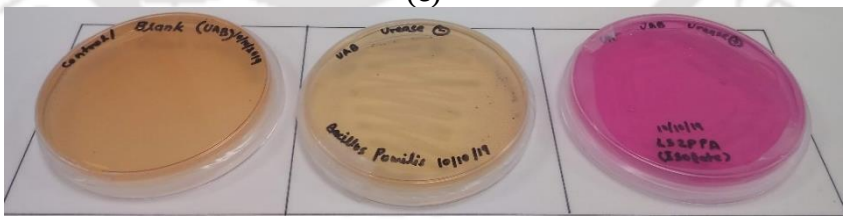

(f)

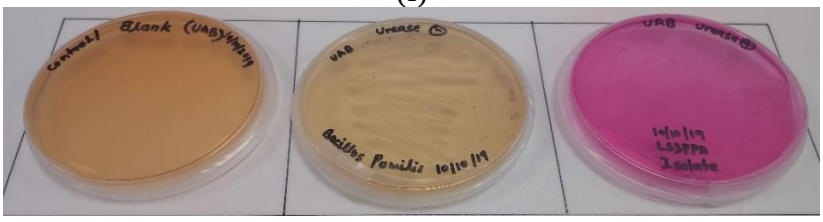

(g)

Figure 4.3 Colour change on urea agar base plates (a) SP, (b). BS1, (c). BS2, (d).BS3, (e). BS4, (f). LS1, and (g). LS2.

Bacteria	Gram Staining	Endospore Staining
SP		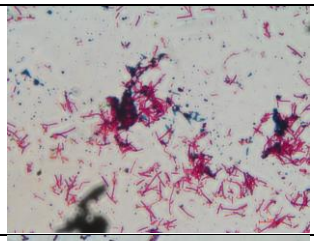
BS1	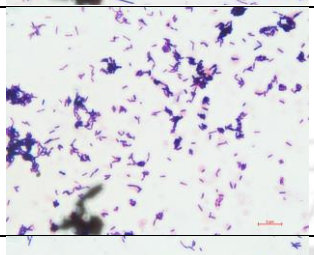	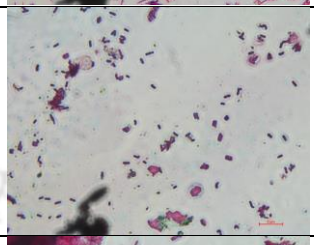
BS2	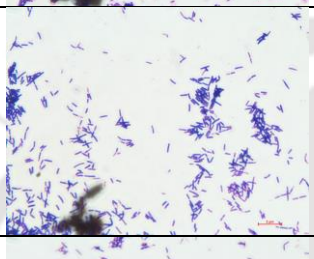	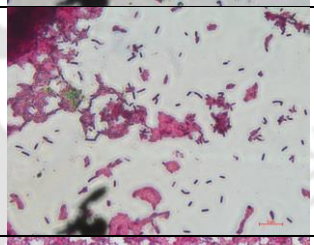
BS3	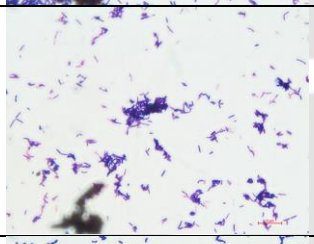	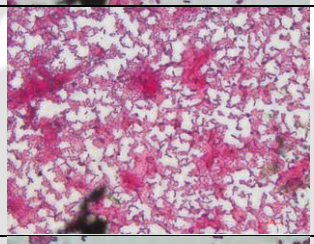
BS4	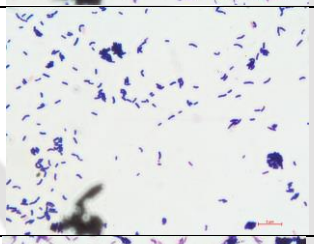	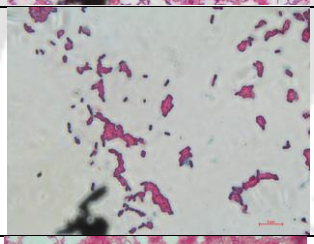
LS1	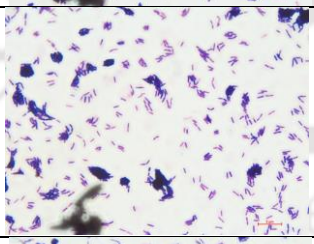	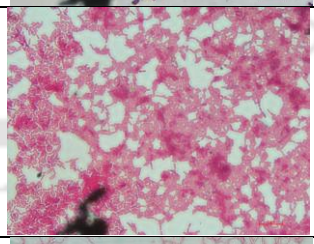
LS2	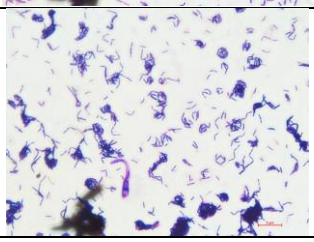	

Figure 4.4 Gram and Endospore-stained images of SP and the isolates.

Dark green spores were observed with vegetated pink bacterial cells after endospore staining in all the isolates. The capability of endospore formation indicates that the bacteria have the capability to undergo dormancy against harsh conditions such as heat (Hussey 2013). Further, the qualitative biochemical characterisation was conducted through the Microbact® kit, and the properties are tabulated as supplementary data in Appendix 1. Chiefly, all the isolates were not able to utilise the Lysine and ONPG, contrary to *Sporosarcina pasteurii* (SP).

The 16s rRNA sequence revealed the isolates as close relatives of SP. The details of the identified isolates are provided by NCMR. A further investigation of the isolated sequence was done via the NCBI database. The sequences were submitted to the GenBank database of the NCBI (National Centre for Biotechnology Information) under the accession number MW024144 to MW024149. The BLAST analysis revealed that these strains are novel strains of the *Sporosarcina* family. It was determined that isolates BS1 and BS2 had 96.62% (coverage 100%) and 96.22% (coverage 99%) identity with *Sporosarcina siberinisis* (NCBI accession number NR 134188). BS3 had 98.8 % identity (coverage 97%) with *Sporosarcina pasteurii* (NCBI accession number NR 104923). BS4 and LS1 had 97.4% (coverage 99%) and 97.37 % identity (coverage 100%) with *Sporosarcina soli* (NCBI accession number NR 043527). Contrarily, LS2 was found to be related to the *Pseudogracilibacillus* family. LS2 was observed to be closely related to *Pseudogracilibacillus auburnensis* P-207 with 97.06% identity (96% coverage). Based on these findings, the Phylogenetic tree was constructed with bootstrap (1000 replicates) considering the reference sequences obtained from the BLAST analysis, as shown in Figure 4.5.

The threshold criteria to differentiate two species is defined as a 98.65% similarity score with the reference culture from the databank (Kim et al. 2014), while another study

has suggested that in the case of similarity index is >99%, the unknown isolate should be assigned to a species, and if the unknown isolates have similarity score between 95 to 99% to a reference sequence, the isolate should be assigned to the genus (Bosshard et al. 2003). However, further investigation is suggested to conclude if the reported strains are novel or merely mutants of the reference strains of the databank.

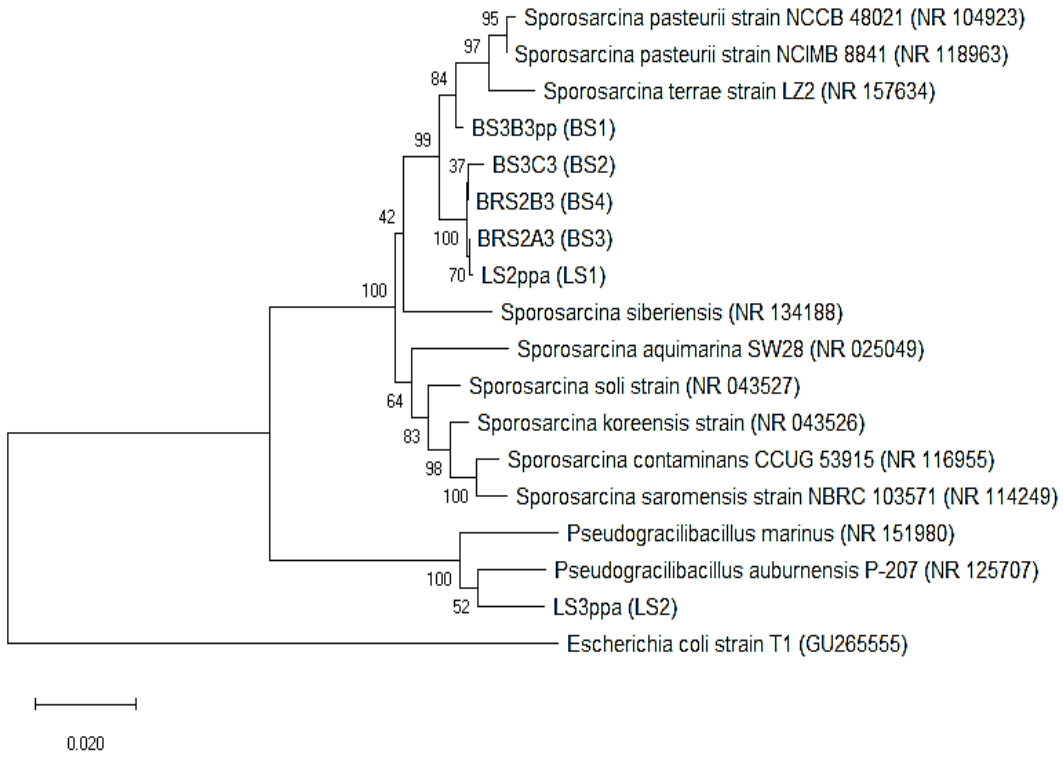

Figure 4.5 Neighbour-joining phylogenetic tree based on the 16S rRNA sequence of the isolates and reference sequence from the GenBank database (NCBI).

Similar observations were made by Graddy et al. (2018), where the majority of the isolated strains (47 out of 57) from the bio-stimulation soil tank were found to be strains of the Sporosarcina genus. It is worth noting that the soil enrichment media for stimulation was rich in urea, similar to Gomez et al. (2019) and Graddy et al. (2018), which is conditional stress for selective stimulation of ureolytic microorganisms.

4.2.2 Evaluation of biocementation potential of the isolated strains

4.2.2.1 Growth and pH

The various parameters of the biocementation potential of the isolated strains in comparison with *Sporosarcina pasteurii* (SP) have been plotted in Figure 4.6. The growth characteristics of the isolates in NBU media and pH during growth have been represented in Figures 4.6 (a) and 4.6 (b).

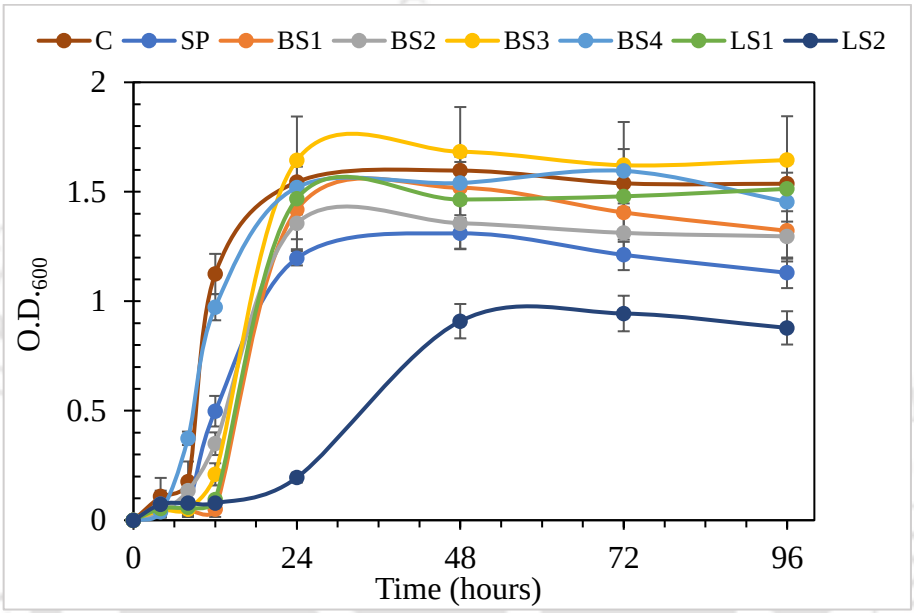

(a)

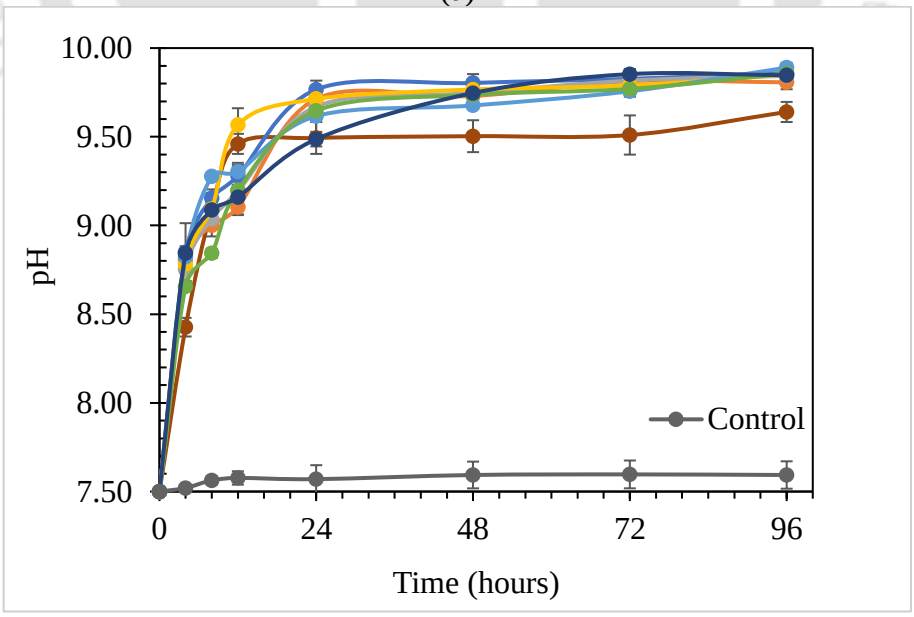

(b)

Figure 4.6 (a). Growth characteristics and (b). The pH of the isolates and consortia in comparison to SP.

The growth of the microbes was recorded in terms of the optical density of the cultivated solution at 600 nm ($O.D._{600}$). The serial dilution revealed that the cell numbers for a unit optical density varied in a narrow range of 11×10^7 cells/ml to 35×10^7 cells/ml. All the microbes reached the exponential growth phase within a 12 to 24 hours growth period. It is to be noted that 1% microbe ($O.D._{600}$ =1) was added to fresh NBU media to record their growth characteristics. Contrarily, LS2 demonstrated slow growth characteristics, possibly because it belongs to different genera.

The initial pH of the growth media was maintained at 7.5. It was observed that the pH of the growth media rises to 9.5 within 24 hours of growth, indicating that these strains favour an alkaline environment to grow, similar to SP (Whiffin 2004). All the isolates start growing when the pH of the media rises to 8.5 or above. Isolate LS2 was observed to have slower growth when compared with other isolates. This can be explained as LS2 belonging to different genera (*Psuedogracillibacillus)*.

4.2.2.2 Specific urease activity

The comparison of specific urease activity of the isolates has been compared with SP in Figure 4.7. The specific urease activities of the isolates were found to be comparable with SP. Based on the provided NBU media and growth condition, the specific urease activity of SP is found to be 173.44 mM urea hydrolysed h^{-1} $(O.D._{600})^{-1}$, which is around 2.9 mM urea hydrolysed min^{-1} $(O.D._{600})^{-1}$. The specific urease activity of BS3 was observed to be maximum as 186.6 mM urea hydrolysed h^{-1} $(O.D._{600})^{-1}$ during a growth period of 24 hours and pH> 9. Consortia (C) also demonstrated significant urease activity as 160 mM urea hydrolysed h^{-1} $(O.D._{600})^{-1}$ at a growth period of 48 hours. The maximum ureolytic activity in BS1 was observed after 72 hours of growth with a value of 106.67 mM urea hydrolysed h^{-1} $(O.D._{600})^{-1}$. Maximum specific urease activity of the isolate BS2, BS4, and LS1 was observed to be 160.2, 120-, and 173.4-mM urea hydrolysed h^{-1} $(O.D._{600})^{-1,}$ respectively, after a growth duration of 48 hours. LS2 demonstrated the

maximum specific urease activity of 146.4 mM urea hydrolysed h^{-1} $(O.D._{600})^{-1}$. The observed order of specific urease activity at 24 hours of the growth period is BS3>SP>C>LS1>BS2>BS4>LS2>BS1. As the urease activity of the strains depends on the growth media, urea content, and environmental conditions such as pH and temperature (Omoregie et al. 2017), we considered the conditions at the riverbank at the time of isolation and the pH and temperature of the growth media were set at 7.5 and 37 degrees Celsius. The specific urease measured by the electrical conductivity method is reported to be between 3 to 9.7 mM urea hydrolysed min^{-1} $(O.D._{600})^{-1}$ in yeast-extract urea media at pH 7.0 and a temperature of 30 degrees Celsius (Whiffin 2004). It is reported around 5 mM urea hydrolysed min^{-1} $(O.D._{600})^{-1}$ in the nutrient broth urea (2%) media at a temperature of 25 degrees Celsius (Omoregie et al. 2017). The comparative analysis of the urease activity (measured by the electrical conductivity method) was done, considering SP as a positive control in this study. The maximum specific urease activities of all isolates were found to be in a range of 106.67 to 186.67 mM urea hydrolysed h^{-1} $(O.D._{600})^{-1}$ (1.78 to 3.11 mM urea hydrolysed min^{-1} $O.D._{600}^{-1}$), which indicates that all of the isolated strains are capable of biocementation (Whiffin 2004; Jiang and Soga 2017).

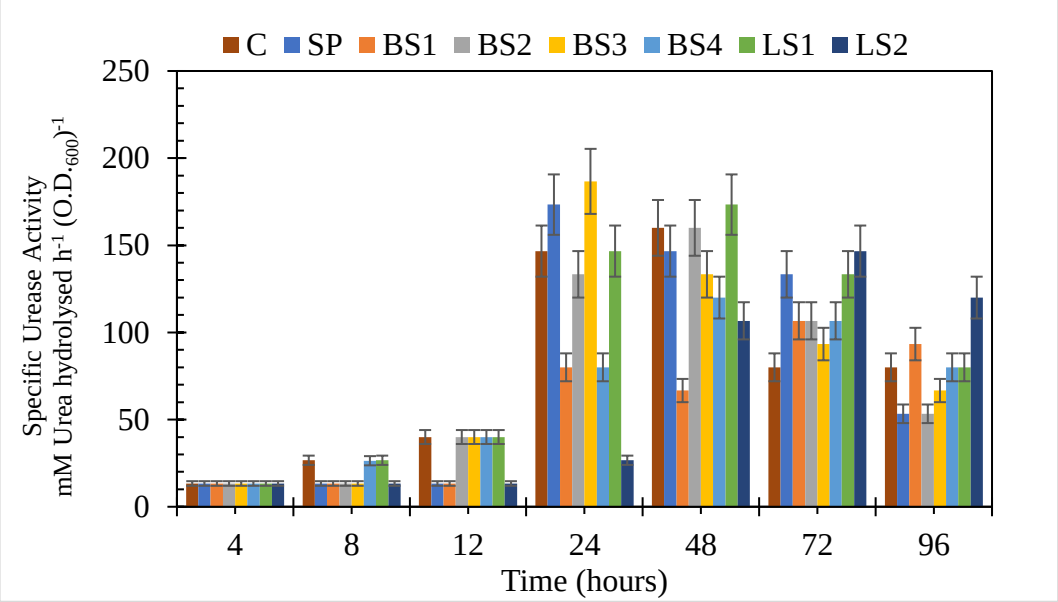

Figure 4.7 Specific urease activity of the isolates and consortia in comparison to SP.

4.2.2.3 Calcium utilisation and carbonate precipitation potential

It was experimentally observed that the depletion of the supplemented soluble calcium in the precipitation media (PM) corresponded to the ureolytic activities of the isolated strains. Within 48 hours of introducing 1% bacteria ($O.D._{600}$=1) in the precipitation media, the soluble calcium chloride (50 mM) was utilised to precipitate carbonate crystals, as illustrated in Figure 4.8 (a). Within 12 hours of the inoculation period, BS3 was able to utilise 75% of the supplied calcium, while SP was able to utilise only 62.5% of the soluble calcium. The order of the calcium utilisation potential in the isolates was observed as BS3≥LS2>LS1>C>SP>BS4>BS2>BS1 during the inoculation period. Contrarily, LS2, despite being a comparatively slow urease-producing bacteria, was able to utilise calcium ions at par with other isolates. Negligible changes were observed in the soluble calcium concentration of the control group eliminating the possibility of abiotic precipitation.

The carbonate precipitation rate for each isolate (1% at $O.D._{600}$=1) for the 50 mM cementation media is plotted in Figure 4.8 (b). The isolate BS3 with maximum ureolytic activity (specific urease activity 186.6 mM urea hydrolysed min^{-1} $O.D._{600}^{-1}$) precipitated the highest carbonate crystals after 96 hours of the incubation period. BS3 precipitated 438 mg/100 ml of carbonate crystals, which is around 87.66% precipitation from the total supplied $CaCl_2$, while precipitation with SP was quantified as 389 mg/100 ml (78%). The precipitation in consortia was observed to be 407 mg/100ml (81%), which is slightly higher than SP. Precipitation in other isolates was found to be significantly lower than in isolate BS3. Isolate BS1 and BS2 precipitated 334 mg/100ml (67%) and 343 mg/100ml (69%) of carbonate crystals, respectively, whereas isolate LS1 and LS2 precipitated around 357 mg/100 ml (71%) of carbonate crystals each. Isolate BS4 precipitated minimum carbonate crystals 292 mg/100 ml (58%). No precipitation was observed in the negative control set. Low concentrations of bacterial cells (1%) were considered in this

experiment to slow down the urea hydrolysis in order to differentiate the calcium utilisation potential of the isolated strains.

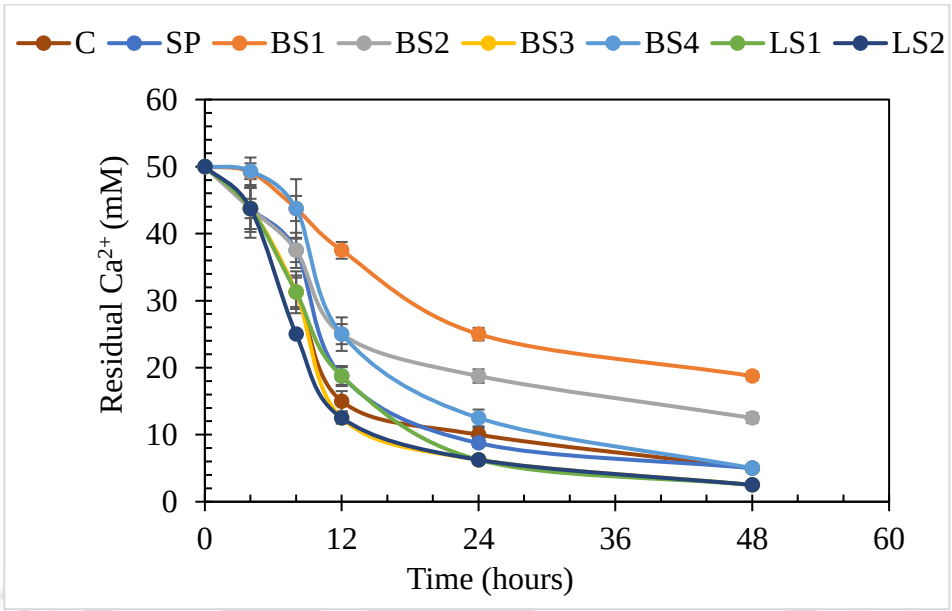

(a)

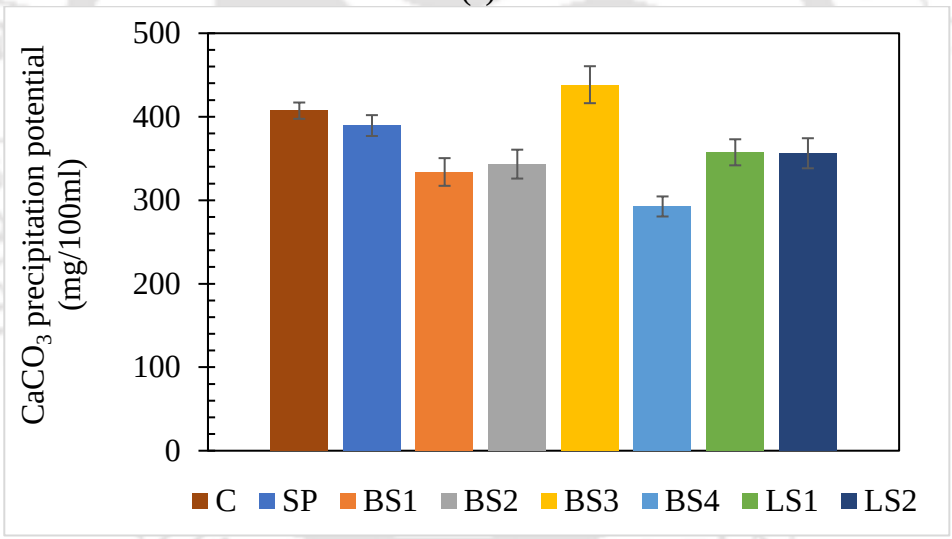

(b)

Figure 4.8 (a). Calcium utilisation rate, and (b). Carbonate precipitation rate of the isolates and consortia in comparison to SP.

This approach was modified by Dhami et al. (2016), and the results from the current study show agreement with their finding that 1% of SP cells deplete the 25 mM of $CaCl_2$ within 24 hours. It was observed that all the isolates took approximately 48 hours to deplete the 50 mM $CaCl_2$. The depletion of soluble calcium concentration was rapid in

the initial 24 hours in all the isolates. After 48 hours, the residual soluble calcium was observed to be in the range of 2.5-5 mM in all the isolates (except BS1 and BS2), which might be due to the loss of super-saturation caused by the unavailability of nutrients for bacterial cells to continue urea hydrolysis in the precipitation media (Whiffin 2004; Dhami et al. 2013a; Ramachandran et al. 2020). The mineralogy of precipitated carbonate polymorphs (calcite, aragonite, vaterite) and the residual calcium are also influenced by pH, temperature, saturation index, dissolved organic carbon concentration, and the Ca^{2+}/CO_3^{2-} ratio along with the presence of metabolites in the precipitation media (Rodriguez-Navarro et al. 2012; Dhami et al. 2013a; Ramachandran et al. 2020).

4.2.3 Microstructure analysis of the precipitates

The FESEM images of the precipitated carbonate crystals were investigated further. All the precipitates had a similar shape. The shape of the precipitated crystals was observed to be rhombohedral and trigonal (Figure 4.9 a). The average size of the crystals was observed in a range of 25 to 50 microns. The entrapped bacteria and rod-shaped bacterial imprints were identified (Figure 4.9 b), indicating that the bacteria acted as a nucleation site (Stocks-Fischer et al. 1999). The smaller crystals were observed to coagulate in layers to develop larger calcite crystals. The entrapped bacteria were noticed on the grown and coagulated calcite crystal in Figure 4.9 (c).

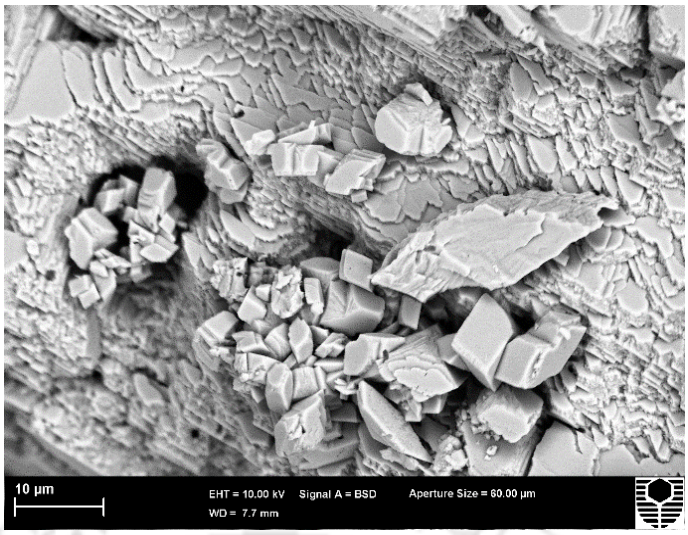

(a)

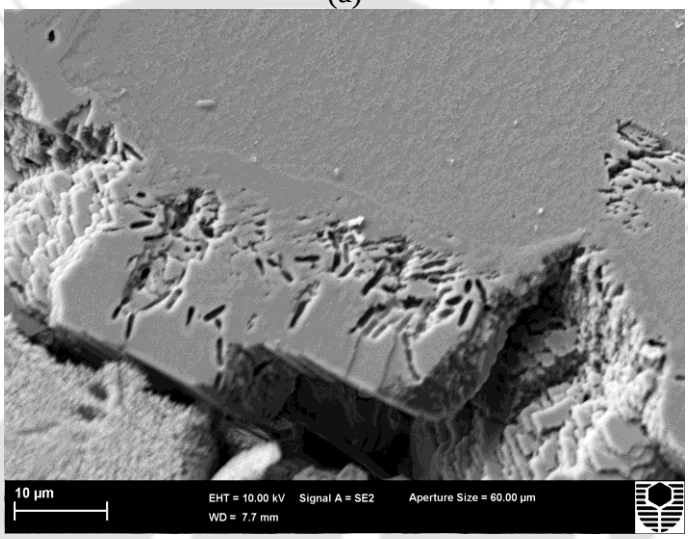

(b)

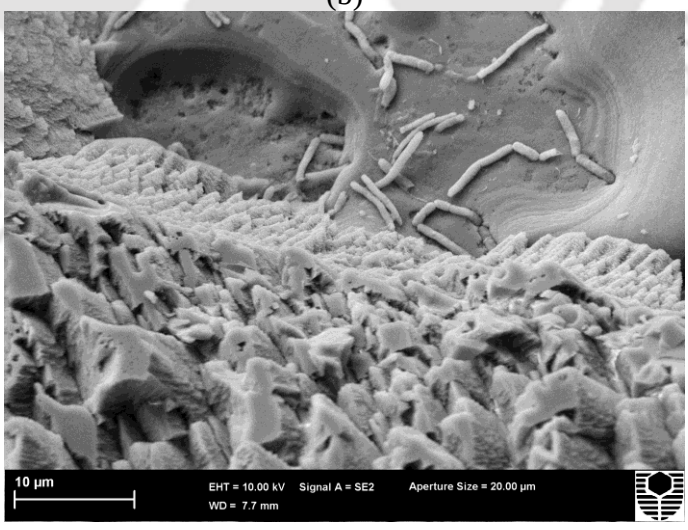

(c)

Figure 4.9 FESEM images of the calcite precipitated from BS3 (a). Coagulated crystals, (b) Bacterial imprints, (c). Entrapped bacteria on the precipitates.

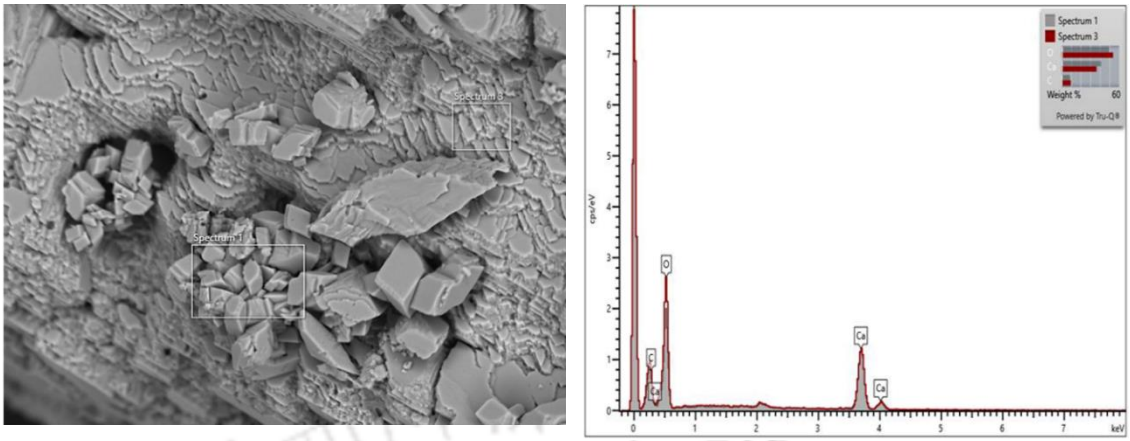

(a)

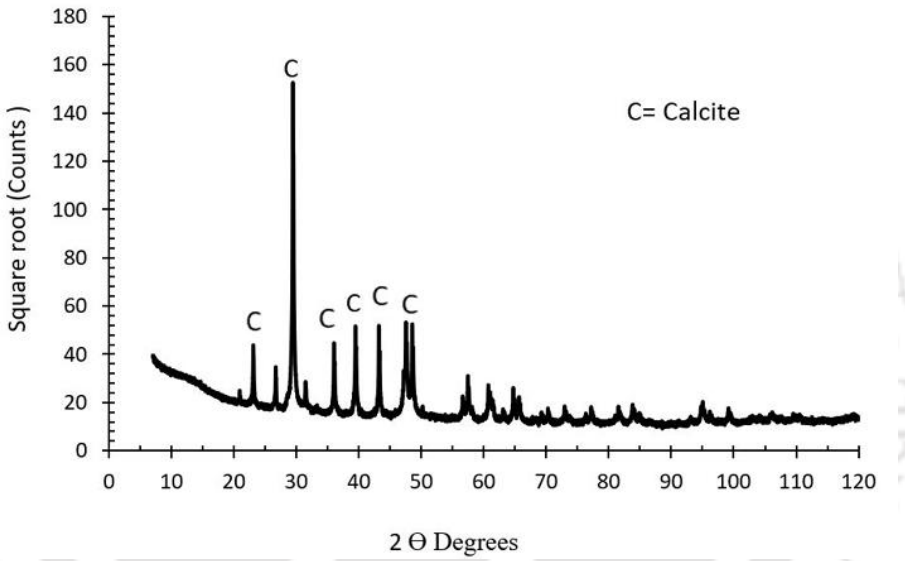

(b)

Figure 4.10 (a). EDX and (b). XRD analysis of the crystal precipitates from BS3.

4.3 Summary

Biostimulation of ureolytic carbonate precipitating communities from local soils, including Brahmaputra riverbank soil, was successfully conducted in this study. The major experimental observations from the study can be drawn as follows-

- Six highly biocement potent microbes with specific urease activity varying from 107 to 187 mM urea hydrolysed h^{-1} $(O.D._{600})^{-1}$ were isolated from

local soils. BS3 exhibited the highest specific urease activity with a value of 187 mM urea hydrolysed h^{-1} $(O.D._{600})^{-1}$.

- While most of the microbes belonged to *the Sporosarcina* genera, LS2 belonged to the *Pseudogracilibacillus* family. Soil improvement with *Pseudogracilibacillus* genera has been largely unaddressed. LS2 exhibited a specific urease activity of 147 mM urea hydrolysed h^{-1}.
- All the microbes were able to precipitate $CaCO_3$ in a range of 292 to 438 mg/100 ml of cementation media. BS3 exhibited the highest precipitation potential with 438 mg/100 ml, while LS2 precipitation potential was determined as 356 mg/100 ml of cementation media.
- Biogenic precipitation of rhombohedral calcite crystal was confirmed with microscopic and microstructural analysis.

In this study, MICP treatment was proposed as a potential eco-friendly erosion control technique with native bacteria so that there is a minimum intervention to the river ecology. However, there are numerous concerns about its field application. The alkalinity of growth media and ammonia generation are major concerns for the river ecology and geo-environment. There is a high possibility of ammonia being diluted to negligible levels at the riverbanks; however, this can be threatening to flora and fauna of the riparian zone. Therefore, potential strategies for minimising ammonia are of paramount importance, which is not addressed in this chapter. There are chances of the cementation media getting diluted in the saturated zones of the riverbanks. Therefore, it is essential to consider the application of the MICP for erosion control only in the low flood seasons to vulnerable riverbanks. A detailed investigation of MICP treatment of the riverbank soil will be critically useful in designing the field application strategy. Further investigations through

laboratory-scale erosion experiments in flume/wind tunnels are necessary to investigate the potential of this technology in the mitigation of various kinds of soil erosion.

4.4 Conclusion

This study provides promising evidence of the potential of native ureolytic communities from riverbank sites in their ability to mitigate soil erosion. Out of 36 bacteria, six were found to be highly biocementation potent. Five out of the six isolates belonged to the *Sporosarcina* genera highlighting the prevalence of these strains. One of the isolates (BS3), which is closely related to *Sporosarcina pasteurii*, was found to have marginally better biocementation potential than the pure culture of *Sporosarcina pasteurii* (ATCC 11859) in terms of specific urease activity and calcium utilisation. This implicates that the enrichment of native bacteria has definite advantages, along with reduced bacterial transport costs. Contrarily, LS2 belonged to the *Pseudogracilibacillus* family and exhibited lower growth characteristics and urease activity in comparison to the other five isolates. LS2 must be investigated further to ensure that the isolated microbes are capable of improving the soil properties. Overall, this study examined and modified the protocol for the isolation of biocementation-potent microbes from local soils.

CHAPTER 5

INFLUENCE OF BIOCEMENTATION ON GEOTECHNICAL PROPERTIES AND AEOLIAN EROSION CHARACTERISTICS OF DESERT SOIL

5.1 Introduction

The aeolian erosion impacts the residents adversely by causing 1. Respiratory-health issues due to eroded fine dust particles, 2. Loss of fertile land due to erosion, and 3. Interruption in regular infrastructure services such as transport, electricity and internet (Li et al. 2009; Ravi et al. 2011; Santra et al. 2013; Devrani et al. 2021). Therefore, mitigation of aeolian erosion is essential in the drylands. From the literature, it is evident that most of the studies have considered widely used exogenous pure culture *Sporosarcina pasteurii* (SP) for improving the resistance against wind-induced erosion. There are limited studies on the indigenous biocementation potent strains as their availability in desert soils is uncertain due to the harsh environment, low nutrient availability, and scarcity of moisture content (Bibi et al. 2018; Rajabi Agereh et al. 2019). Therefore, considering an alternative approach, a ureolytic soil microbe isolated from vegetative soil from the previous study (LS2) has been utilised for soil improvement in this chapter. LS2 belongs to the *Pseudogracilibacillus* species and has not been reported for biocementation in the literature.

In this chapter, the aeolian erosion characteristic of the soil collected from the erosion-prone Jaisalmer region of the Thar desert of India is investigated. A summary of the experimental plan is illustrated in Figure 5.1. The majority of the Thar Desert's area (~62% of India's total hot arid zone) is severely affected by the aeolian erosion due to arid sandy terrain and scarce vegetation cover (Kar et al. 2009). The biocementation potential of the isolated strain has been evaluated in terms of its influence on the permeability coefficient (k) and unconfined compressive strength (UCS) of the soil treated with a single

cycle of MICP at different levels of cementation (250, 500, and 1000 mM of equimolar urea and $CaCl_2$). For aeolian erosion mitigation application, the treated soil specimens were subjected to wind velocity in the range of 0 to 55 km/h in a lab-scale wind tunnel. The threshold detachment velocity (TDV), soil mass loss, and precipitated calcium carbonate content of the treated samples are reported as soil erosion characteristics. The developed soil crusts at different biocementation levels have been examined along with their microstructure.

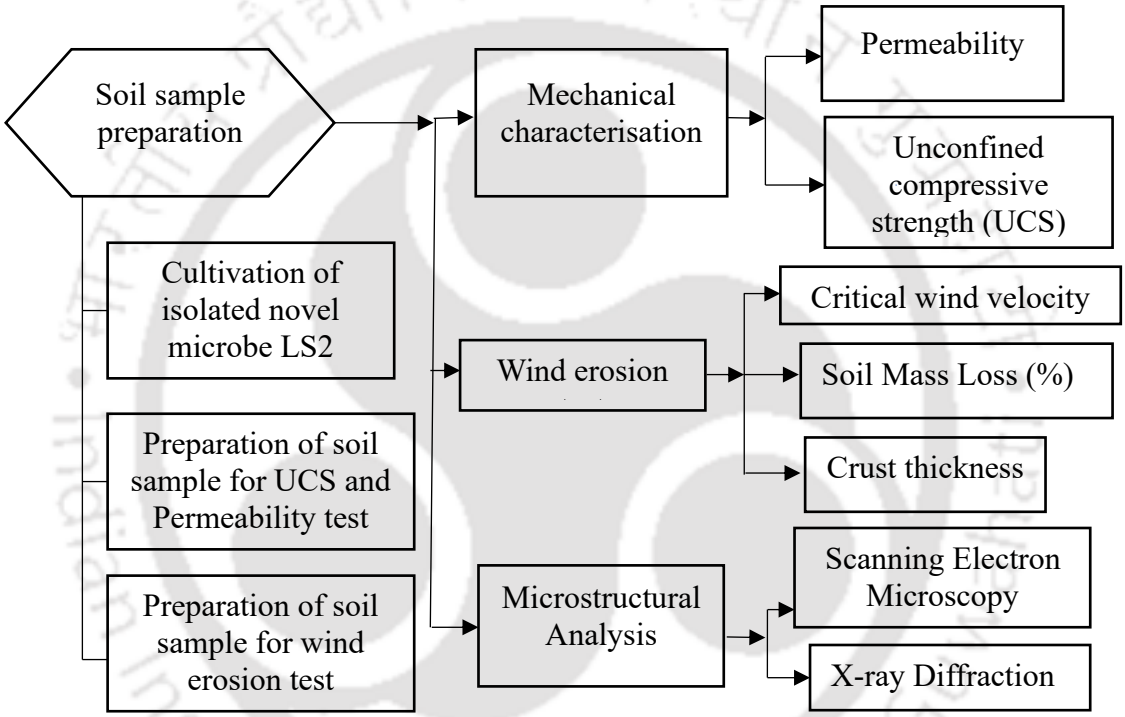

Figure 5.1 Summary of experiments to investigate the influence of biocementation on geotechnical and wind erosion characteristics of desert soil.

5.2 Results and Discussion

5.2.1 Hydraulic conductivity and unconfined compressive strength of the samples

The variation in hydraulic conductivity of the treated and untreated soil with the cementation solution concentration is presented in Figure 5.2 (a). The bare soil exhibited a hydraulic conductivity of 1.46×10^{-3} m/s, represented by the data point corresponding to the 0 concentration of cementation media. The hydraulic conductivity was reduced to

$4.67x10^{-4}$ m/s, $2.15x10^{-4}$ m/s, and $1.47x10^{-5}$ m/s with an increase in the cementation solution's concentration to 250 mM, 500 mM, and 1000 mM. The change in hydraulic conductivity was observed to be notable while comparing the bare desert sand and the biocemented sand treated with 1000 mM of cementation solution. The maximum reduction in hydraulic conductivity was observed to be of one order in the case of 1000 mM treatment. This is worth noting that MICP is reported as a potential tool to retain permeability with a substantial increase in soil strength (Chu et al. 2012; Al Qabany and Soga 2013; Mujah et al. 2017). However, only a few studies have reported bio-clogging of soil with repeated application of biocementation solution (Ivanov and Chu 2008; Chu et al. 2014). Chu et al. (2014) reported the reduction in hydraulic conductivity of untreated soil from $5x10^{-5}$ m/s to $1.6X10^{-7}$ m/s for the treated soil with a calcium carbonate content of 1.2%.

The soil was extruded after the treatment, and unconfined compressive strength was evaluated. The unconfined compressive strength of treated specimens is shown in Figure 5.2 (b).

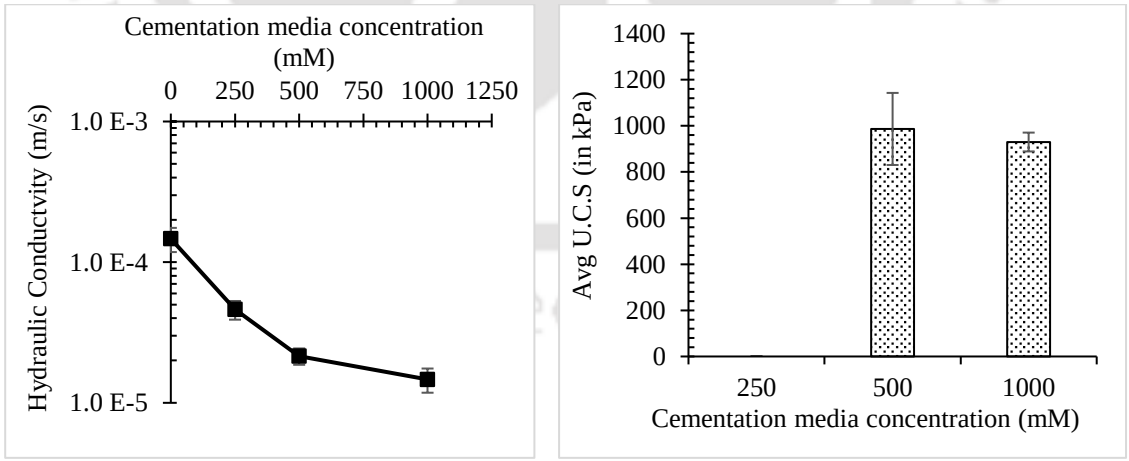

(a) (b)

Figure 5.2 Variation in (a). Hydraulic conductivity and (b) Unconfined compressive strength of bio-cemented soil samples.

The soil column with the 250 mM concentration was damaged while extruding because of the insufficient bonding of the soil grains. The UCS of the soil at 500 mM was observed to be 983 kPa, which is comparable with the 1000 mM treated soil sample (910 kPa), represented in figure 5.2 (b). The measured average calcium carbonate contents post-UCS testing are evaluated as 0.5%, 1.3%, and 2.1% for the sample treated with 250 mM, 500 mM, and 1000 mM of cementation solutions, respectively. The observed UCS value for the reported calcium carbonate content in the current study is unprecedentedly higher when compared to previously reported studies. Previous studies have reported the UCS value of around 1 MPa for calcium carbonate content in the range of 3% to 6% for fine sand (Cheng et al. 2013b; Al Qabany and Soga 2013; Terzis and Laloui 2018). However, Chu et al. (2014) also reported unconfined compressive strength of around 800 kPa for an average calcium carbonate content of 1.6%.

It is to be noted that apart from the calcium carbonate content parameter, the quality of crystal plays a vital role in the strength of treated soil, which is controlled by microbial urease activity. Low urease-producing microbes have been reported to induce larger crystals with higher nanoindentation moduli (Heveran et al. 2019). Chu et al. (2014) have also utilised low urease-producing strain *Bacillus sp*. like the current study. The specific urease activity of the isolated soil strain is around 2.45 mM urea hydrolysed per minute, which is significantly lower than the reported urease activities of the mostly reported exogenous culture *Sporosarcina pasteurii* (SP). The urease activity of SP is 8.62 mM urea hydrolysed per minute per ml for $O.D._{600} \geq 1.9$ (Duo et al. 2018; Tian et al. 2018).

5.2.2 Erosion Characteristics of the soil

The major visual observations have been photographed and illustrated in Figure 5.3.

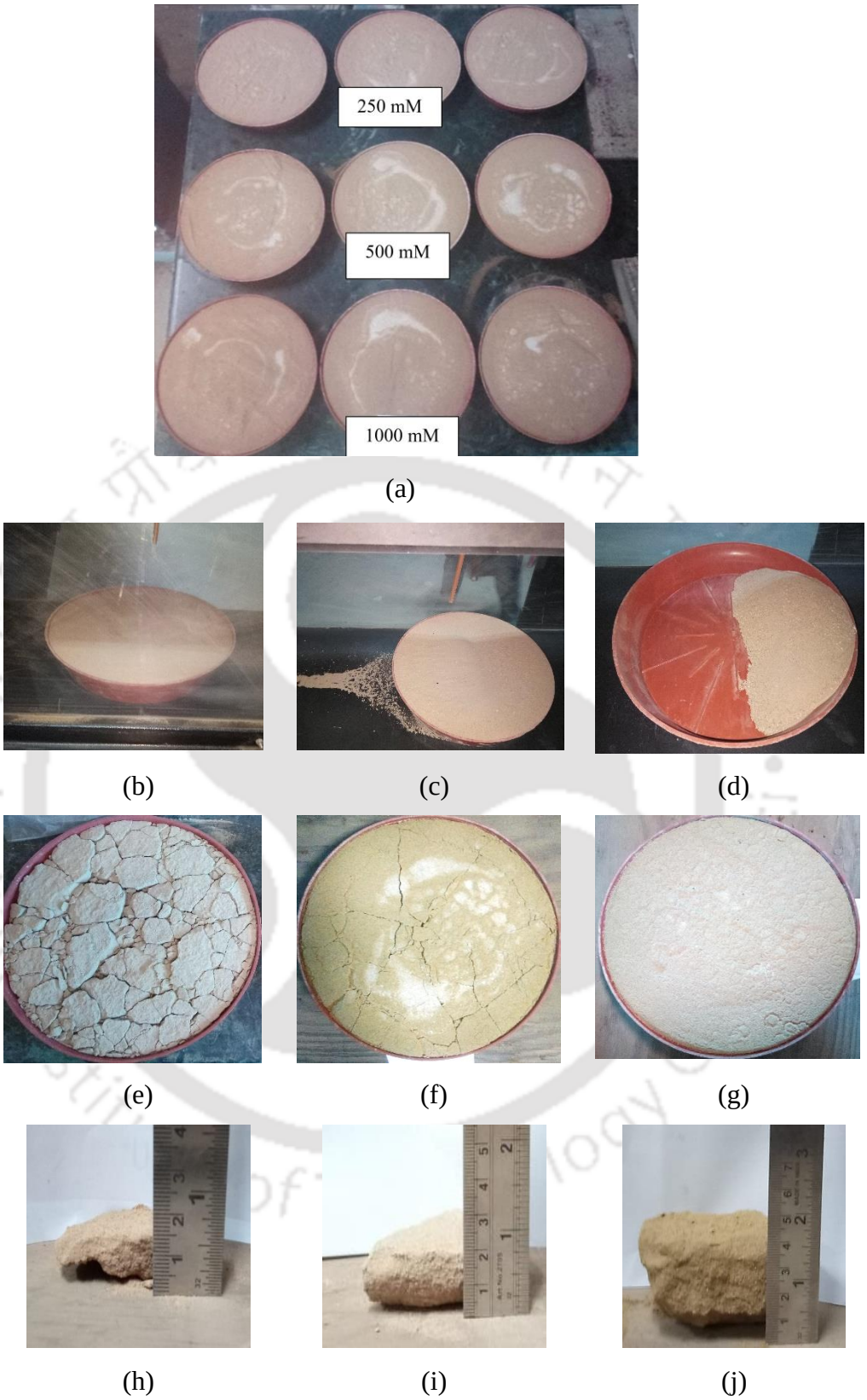

Figure 5.3 Visual observations through wind tunnel test (a). Treated specimen prior to erosion test, (b) Untreated sand, (c) Detachment of untreated sand at 20 km/h; and eroded samples and crust thickness after exposure to 55 km/h (d). Untreated, (e,h). 250 mM (f,i).500 mM, and (g,j). 1000 mM treated sand.

After the treatment, a crust was formed on the surface, and white spots were observed at the top of all the treated specimens, as shown in the photograph in Figure 5.3 (a). These white spots can either be precipitated calcium carbonate or ammonium chloride salt, which makes the deionised water wash for the treated soil specimen crucial prior to the acid washing protocol in order to avoid overestimation of calcium carbonate content. Later, these samples were exposed to the erosion test in the wind tunnel.

The visual inspection indicated the detachment of untreated sand particles was recorded at an early stage, as shown in Figures 5.3 (b) and 5.3 (c). The eroded sample after exposure to the wind tunnel test has been demonstrated in Figures 5.3 (d) to 5.3 (g). Figure 5.3 (d) shows the eroded untreated loose sand, which exhibits substantial mass loss due to the absence of soil particle bonding. Surficial cracks were noticed on the sand treated with 250 mM cementation solution, and the mass loss was significant, possibly due to weak and heterogenous biocementation, as shown in Figure 5.3 (e). The desert sand treated with a 500 mM cementation solution was found to have a more uniform binding of particles. Although there were noticeable cracks on the soil surface of 500 mM treated soil, the mass loss due to wind erosion was insignificant, as shown in Figure 5.3 (f). Surficial cracks were not observed on the soil samples treated with 1000 mM cementation solution, as shown in Figure 5.3 (g). The soil mass loss, crust thickness, calcium carbonate content, and TDV were recorded for each sample after the test. The photographs of the developed soil crust for 250, 500 and 1000 mM treated soil are presented in Figures 5.3 (h), (i), and (j) consecutively.

The average soil crust thickness for 250, 500, and 1000 mM treated soil was measured as 1 cm, 2 cm, and 3.5 cm consecutively, as plotted in Figure 5.4 (a). The recorded cumulative dry soil mass loss for different levels of biocementation is also plotted in Figure 5.4 (a). The soil mass loss for the untreated sand was 64% after the designed

wind flow profile. The 250 mM treated soil demonstrated significant resistance toward wind erosion with a soil mass loss of 19% only. The aeolian erosion ceased for the samples treated with 500 mM and 1000 mM of cementation.

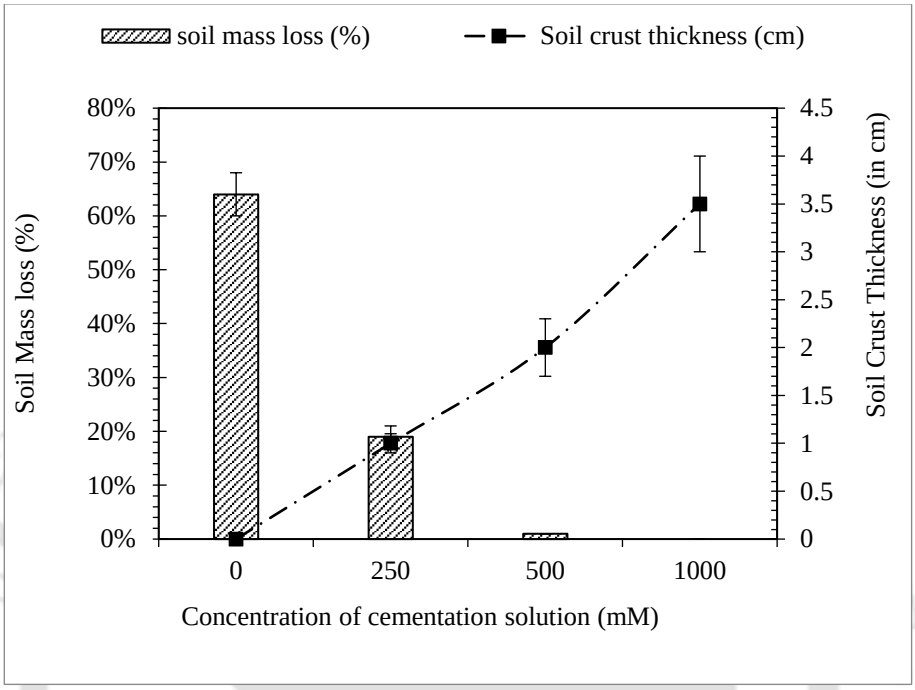

(a)

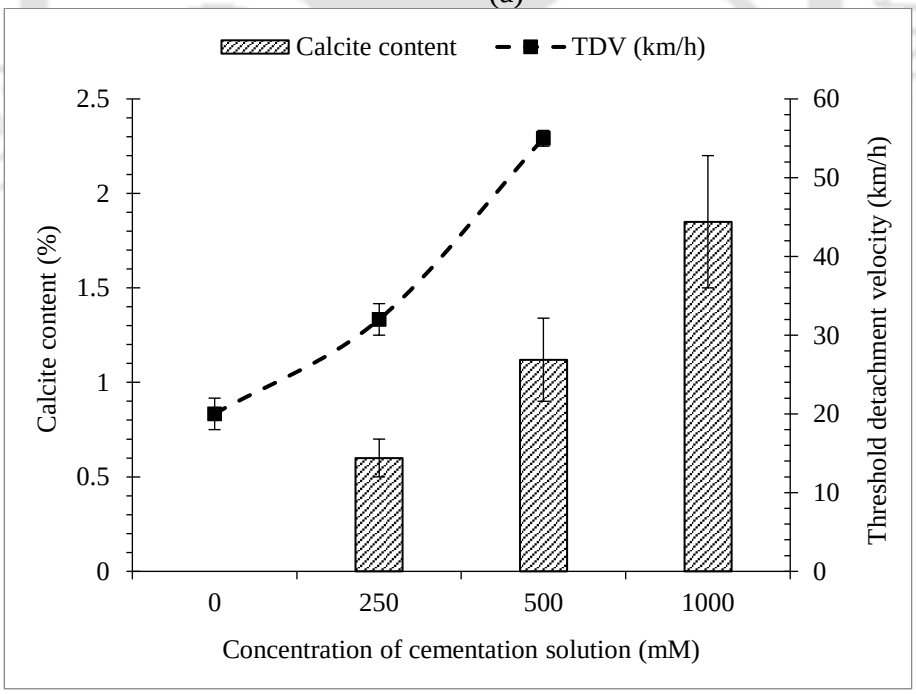

(b)

Figure 5.4 (a). Soil mass loss and soil crust thickness, and (b). Average calcium carbonate content and threshold detachment velocity (TDV) at different levels of bio-cementation.

The weight of the gravimetric calcium carbonate content (%) and the threshold detachment velocity of the samples treated with different levels of biocementation is plotted in Figure 5.4 (b). The TDV of the untreated soil was observed to be at 20 km/h. The TDV of the soil treated with 250 mM was observed to be 32 km/hr. The soil particles treated with 500 mM detached marginally with a wind velocity of 55 km/h, and a negligible mass loss (around 1%) was recorded. Samples treated with 1000 mM cementation media did not exhibit any detachment at 55 km/h, which is the highest wind speed attainable in the laboratory-scale wind tunnel utilised in this study. The average biogenic calcium carbonate content of the 250, 500, and 1000 mM treated soil was 0.5%, 1.1%, and 1.75%, consecutively.

Tian et al. (2018) reported the threshold velocity of untreated soil as 5.73 m/s (nearly 20 km/h) for China's Tengger Desert soil. They also reported no mass loss due to aeolian erosion for soil treated with three doses of 0.5 M (500 mM) cementation solution against the wind velocity of 16 m/s (57.6 km/h). The presented study revealed that single dosing of 500 mM and 1000 mM cementation solution could create a crust of depth 2 cm and 3.5 cm consecutively, which can effectively mitigate the erosion against the wind velocity up to 55 km/h.

This study's findings are also in agreement with the conclusions of Devrani et al. (2021), where 0.5 M cementation solution-based MICP via *Bacillus megaterium* (NCIM 5472) was found to be sufficient to mitigate the aeolian erosion up to wind velocity of 45 m/s. However, they reported biogenic calcium carbonate in the range of 1.94% to 4.1%, which is significantly higher when compared to the presented study (0.5% to 1.75%) despite the reported *Bacillus megaterium* (NCIM 5472) having slower urease activity when compared to the utilised soil isolate (LS2). This is most likely due to the difference in the availability of enzymes for urea hydrolysis, uniformity of precipitation, and

favourable conditions for the urease-producing microbe's survival (Whiffin et al. 2007; Harkes et al. 2010).

Moreover, the acid washing technique is reported to overestimate the calcium carbonate content (Choi et al. 2017) and may provide erroneous results in the case of non-uniform precipitation. It is to be noted as a limitation that this study does not consider gust and sandstorm wind velocity conditions as the impact of the highly accelerated wind are difficult to simulate in the laboratory scale wind tunnel, which had a limitation of maximum wind velocity of 55 km/h

The biocemented crust of depth of 3.5 cm with 1.75% average calcium carbonate content formed by spraying one pore volume of 1000 mM cementation solution was found to efficiently resist the maximum wind velocity of 55 km/h without any notable detachment of particles from the treated specimens suggesting promising potential for its field application. However, several factors, such as the biocementation potential of the microbes in the field, the strength of the precipitated crystals, the climate and actual wind velocities at the site, might influence the design of the biocementation procedures suggested in the current study. Continuous application of biocementation reagents along with bacterial solution employing irrigation like a micro-sprinkler spraying system (Zhang et al. 2020) is recommended for a large-scale application.

Another decisive factor for the field application of the proposed technique is the quantity of water required, as the desert regions are mostly water scarce. In the proposed biocementation technique, a considerable quantity of water was required to prepare the biocementation reagents (bacteria, fixation, and cementation solutions). The water required to prepare each solution per unit area is around 16 litres/m^2 water. Thus, the total quantity of water required per unit area to implement the technique at the site is estimated as 48 litres/m^2 from the protocols followed in the current study. However, the stabilised

sand with biocemented crust is most likely to prevent the aeolian erosion far more efficiently in the long-term when compared to other competitive techniques such as watering and biopolymers.

To form an equivalent crust by water and biopolymer treatment, the water requirement would be around 16 litres/m^2. The water treatment alone can alleviate the aeolian erosion temporarily; however, it would require a significantly higher quantity of water in the long run due to frequent drying in the arid regions triggered by the high evaporation rate. Moreover, after drying, the water treated sand behaves exactly like the untreated sand against wind-induced erosion, whereas the strength of the calcium carbonate scaffolding in the soil matrix develops with the drying and curing period (Zomorodian et al. 2019).

The bio-cementation-based mitigation techniques are quite-durable against the freeze-thaw cycles; however, they lose their strength significantly in acid-rain conditions (Cheng et al. 2013a). On the other hand, only biopolymer treated soils are reported to lose more than 50% strength with one wetting-drying cycle, raising concerns for their field application and long-term durability (Ramachandran et al. 2021). Consequently, a detailed investigation to optimise the required water quantity for field implementation of MICP and its comparison with other competitive techniques in terms of long-term durability is highly recommended.

5.2.3 Microstructural analysis of formed soil crust

The confirmation of calcite with FESEM and XRD has also been investigated in a similar fashion by Devrani et al. (2021) and Tian et al. (2018). However, the effect of interlocking and calcite bridging due to precipitated crystals on smooth surfaces of sand grains was unaddressed.

In the present study, the FESEM of the soil crust particles revealed that rhombohedral crystals of size 2 to 10 µm were grown on the smooth surface of the sand particles of all the treated sand. In the 250 mM treated soil sample (Figure 5.5 b), effective bridging of sand grains was not observed. The low calcite precipitation was also confirmed as 0.6% by the acid washing of the 250 mM treated sample. The insufficient bonding explains the failure of the sample during the extrusion of UCS samples.

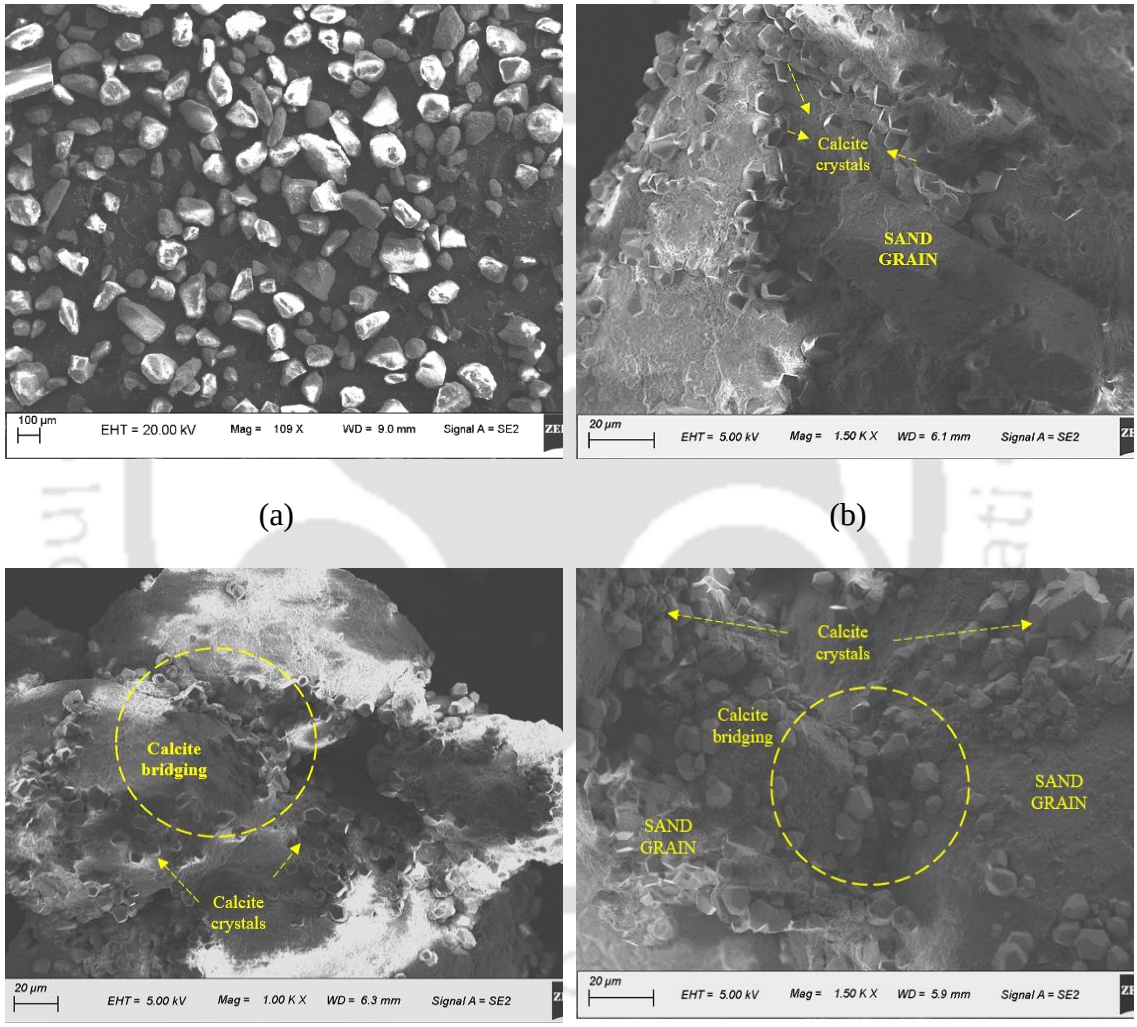

Figure 5.5 FESEM images of (a) Untreated sand, (b). 250 mM, (c). 500 mM and (d). 1000 mM treated sand.

However, with the mentioned low precipitation, 1 cm of soil crust was formed, as shown in Figure 5.3 (h), and the resistance against wind erosion increased due to better

interlocking of the sand particles (Feng and Montoya 2016). This increase in resistance against wind erosion was also observed during the lab-scale wind tunnel test as the TDV increased to 32 km/h from 20 km/h for 250 mM treated soil compared with the untreated soil.

In Figures 5.5 (c) and 5.5 (d), the FESEM images revealed a thick cluster of precipitated crystals in 500 mM and 1000 mM cementation solution-treated soil samples along with the sand grain bridging.

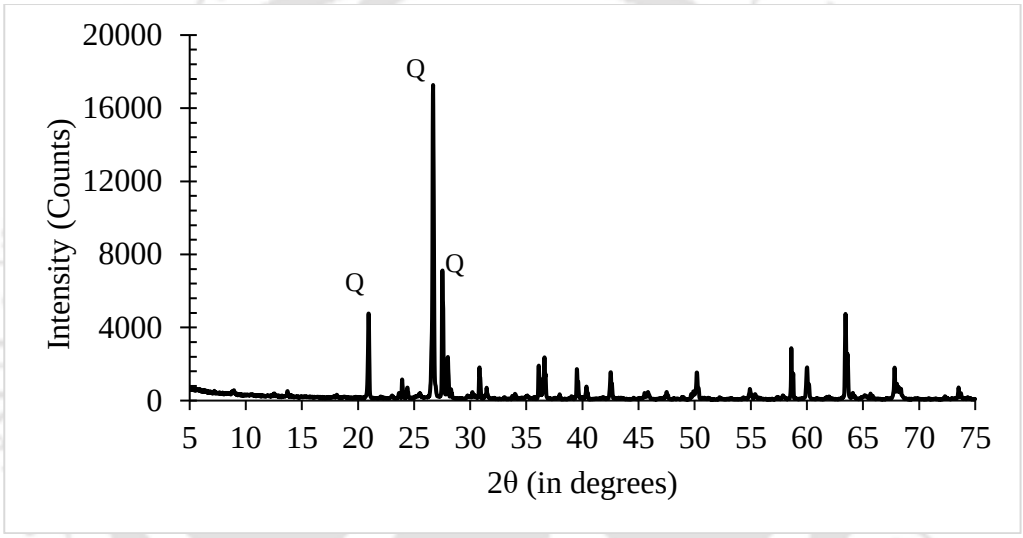

(a)

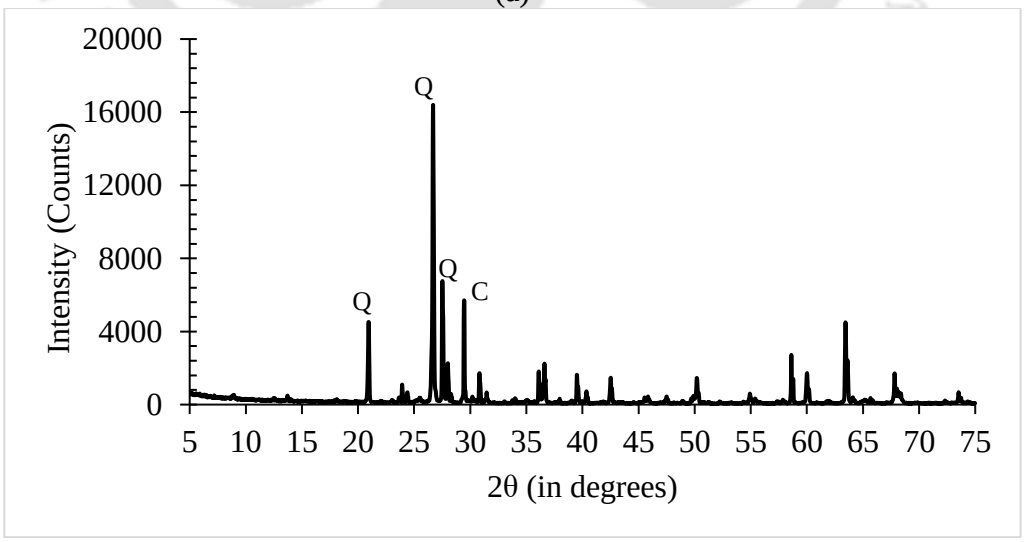

(b)

Figure 5.6 XRD patterns for (a). Untreated sand (b) Treated sand (500 M).

The bridging of the sand grains with thick clusters of precipitated crystals favours the development of the thick soil crust of 2 cm and 3.5 cm for the 500 mM, and 1000 mM treated soil specimens, respectively. This leads to the development of extreme resistance against wind erosion, and hence negligible soil mass loss was observed for the soil samples treated with 500 mM and 1000 mM treated soil. The untreated and MICP treated sand's XRD patterns are presented in Figures 5.6 (a) and 5.6 (b).

The XRD pattern of bare soil revealed the sand to be consisting of Quartz (Q) dominantly. Although the rhombohedral crystals with sharp edges were observed with FESEM indicating calcite precipitation, further investigation with XRD of the 0.5 M treated sand confirmed the prevalence of the calcite crystal along with an insignificant amount of vaterite in the treated sample.

5.3 Summary

This study investigated the application of an isolated soil strain of *Pseudogracilibacillus* species for the potential bio-mediated mitigation of the soil collected from one of the most erosion-prone zones of the Thar Desert (Jaisalmer) against the aeolian erosion. The results demonstrated promising potential for aeolian erosion control with the proposed methodology up to a certain extent. The main conclusion from this study can be summarised as follows-

- With a single dose of bio-cementation at different levels (250 mM, 500 mM, and 1000 mM), the hydraulic conductivity of the desert soil decreased notably. The maximum decrease of 1 order was observed with the 1000 mM cementation solution treatment. The unconfined compressive strength for the 500 mM and 1000 mM treated sand was evaluated to be in the range of 900 kPa.
- The Thar Desert soil obtained is highly erodible with a threshold detachment velocity of 20 km/h. With a small treatment of the bio-cementation solution of 250

mM, the erosion resistance improved drastically, and the threshold detachment velocity increased up to 32km/h with significantly low mass loss (19%) compared to untreated soil (64%). The soil mass loss ceased when the treatment level increased to 500 mM and 1000 mM cementation solution. No detachment of particles was observed for the sample treated with 1000 mM cementation solution at 55 km/h.

- The influence of rhombohedral calcite on enhancing erosion resistance by interlocking and sand grain bridging mechanisms has been confirmed with the microstructural analysis (FESEM and XRD).

The presented investigation is a preliminary step for site-specific bio-mediated erosion control practice. However, several aspects of the MICP-based treatments need to be addressed further, such as the influence of seasonal thermal variations, dry-wet cycles, and ammonia gas generation on its durability and applicability in the actual field conditions. The optimisation of the quantity of water required to prepare the biocementation reagents to control the depth of the crust is one of the crucial aspects to consider for future studies. This study recommends small-scale field trials to investigate further the ecological sustainability of the MICP-based treatment for erosion control in the actual environmental conditions of the Thar desert.

With the findings reported in the current chapter, it was established that the isolated soil microbes are capable of improving soil strength and erosion resistance of the soil. LS2 was a novel strain that was not reported for geotechnical application in the literature. The application of the isolated strains to improve the erosion resistance of soil is worth exploring. Moreover, the determined UCS was in a similar range for the 500 mM and 1000 mM cementation solution. Therefore, it is necessary to investigate the strength characteristics of the treated soil at various concentrations.

5.4 Conclusion

In this objective, it was established that the low-performing isolated strain LS2 was capable of improving the engineering properties of soil and aeolian erosion resistance. However, the UCS tests revealed that the soil treated with 500 and 1000 mM of cementation media exhibits similar strength, which can be due to heterogenous precipitation and a fall in the precipitation efficiency of the microbe to precipitate at higher concentrations of cementation media (1000 mM). Therefore, the suitable concentrations of cementation media for the microbes for soil improvement must be investigated further.

Moreover, in the aeolian erosion test in the wind-tunnel, it was revealed that with 500 mM of cementation media, a crust of 2 cm with 1.2% calcite content was formed, which was able to withstand erosion up to a wind velocity of 55 Km/h. However, the crust strength can not be represented with UCS strength due to different treatment strategies. The cylindrical samples for UCS tests were prepared with injection strategies, while the samples for wind erosion tests were prepared with a spraying strategy. The chances of heterogenous precipitation with a spraying strategy are higher, and therefore, the evaluation of local soil strength properties, such as needle penetration test, must be explored. The study adopted the spraying strategy as a shallow crust can improve the erosion resistance of soil significantly, and the spraying strategy is one of the most convenient approaches for field-scale applications.

CHAPTER 6

THE IMPACT OF CEMENTATION MEDIA CONCENTRATION ON BIOCEMENT PROPERTIES UNDER-STIMULATION AND AUGMENTATION

6.1 Introduction

The magnitude of soil strength improvement is dependent on the morphology, mineralogy and location of the precipitated calcium carbonate ($CaCO_3$), which is majorly controlled by the concentration of cementation solution and the urease activity of the employed biocementing microbe (Hammes et al. 2003; Dhami et al. 2013a; Al Qabany and Soga 2013; Zhao et al. 2014; Heveran et al. 2019; Mujah et al. 2019; Konstantinou et al. 2021; Sharma et al. 2021). While the augmentation and stimulation approaches have been investigated independently in previous studies, a comparative analysis of these techniques is lacking in the literature. Moreover, the response of liable microbial communities to the exposure of various concentrations of cementation solution to soil strength improvement has been largely unaddressed.

Within this context, microbes from different origins, including the soil isolate (BS3) and the consortium (C), both obtained from the bank material of Brahmaputra River, are compared for their biocementation potential with the standard exogenous biocementing microbe *Sporosarcina pasteurii* (SP). SP, BS3 and C are liable for augmentation, selective stimulation, and stimulation, respectively. The three communities are cultivated, and their growth characteristics and urease activities are measured. The specific urease activity of SP, BS3, and C was determined to be 173.44, 186.6, and 160-mM urea hydrolysed h^{-1} $(O.D._{600})^{-1}$, respectively. The obtained results from the specific urease assay suggest that all of them are efficient for hydrolysing urea in the soil at considerable rates (Jiang and Soga 2017; Konstantinou et al. 2021).

Later, the microbes were employed in the soil and treated with various levels of cementation solution. The considered range of the concentration of cementation media in this study is from 250 mM to 2000 mM. The strength of biocemented soil was evaluated with the needle penetration test to determine the heterogeneity in the local strength of the developed crust. The efficiency of the employed biocementation has been assessed by quantifying the precipitated $CaCO_3$ with the acid-washing protocol. In the second stage, the above-mentioned microbes were compared through a batch test at different levels of cementation solution. For this purpose, the biochemical reaction was examined at regular time intervals. The biocementation potential of the microbes was quantified by measuring the amount of hydrolysed urea, depleted calcium and precipitated $CaCO_3$ weight. The morphology of the precipitated was analysed by Scanning Electron Microscopy (SEM), and the size of the precipitated crystals was estimated using ImageJ. The schematic of the experimental program is summarised in Figure 6.1.

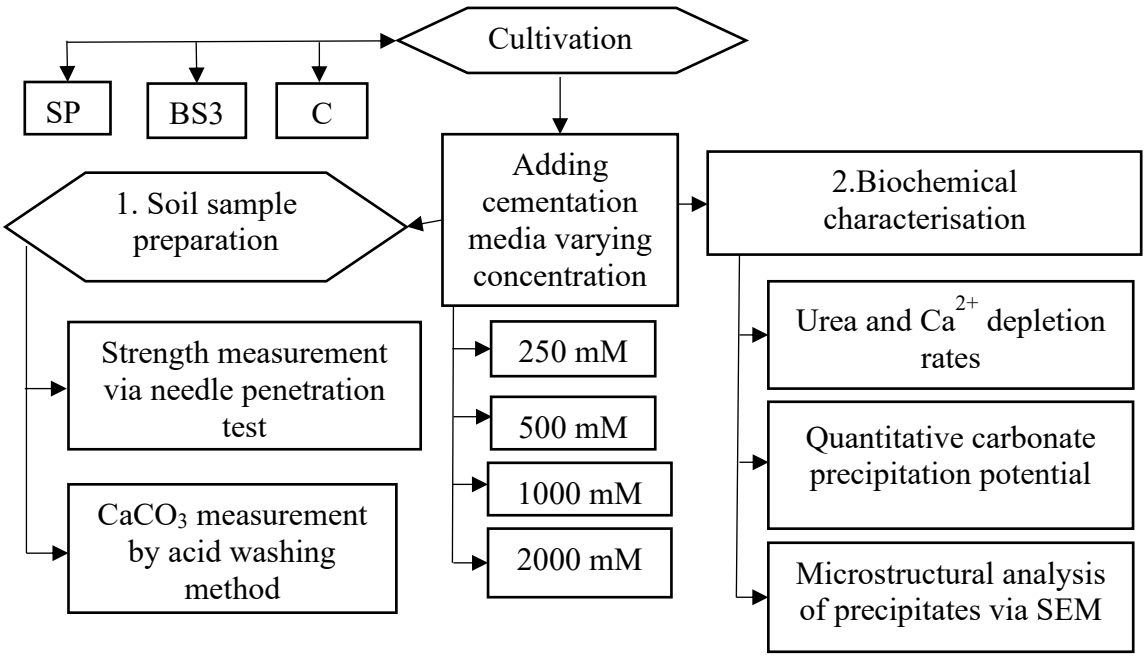

Figure 6.1 Summary of experiments to investigate the impact of cementation media concentration on properties of biocement.

6.2 Results and Discussion

6.2.1 Strength characteristics of the biocemented soil

6.2.1.1 Needle penetration test results

The variations in the needle penetration index with the concentration of cementation media are presented in Figure 6.2. At 250 mM concentration of CM, the needle penetration index (NPI) values for SP, BS3 and C were determined as 4.8, 5.8 and 3.8 N/mm. Maximum NPI was observed at 500 mM concentration of CM with more than 250% improvement for all three microbes. SP, BS3 and C exhibited NPI values of 13.1 N/mm, 17 N/mm, and 11.4 N/mm at 500 mM of CM. The NPI value for BS3 at 500 mM concentration was around 30% higher than SP and 54% higher than C. The NPI values decreased drastically at 1000 mM and 2000 mM concentrations of CM. The evaluated NPI at 1000 mM concentration for SP, BS3 and C were evaluated as 4.8, 12.2 and 8.7 N/mm. The maximum loss was observed in SP, where the NPI of 1000 mM of cementation media was observed to be equivalent to the 250 mM treated soil. For 2000 mM concentration, the NPI values were determined as 4.3, 6.8, and 6.9 N/mm for the SP, BS3 and C-treated samples, respectively.

Ideally, the NPI value should have been equivalent for all the samples. The disparities in the soil strength improvements are attributed to the reduced efficiency of the microbes for $CaCO_3$ precipitation with the multiple numbers of treatment cycles which might be influenced by their viability at low nutrient conditions during the extended treatment duration.

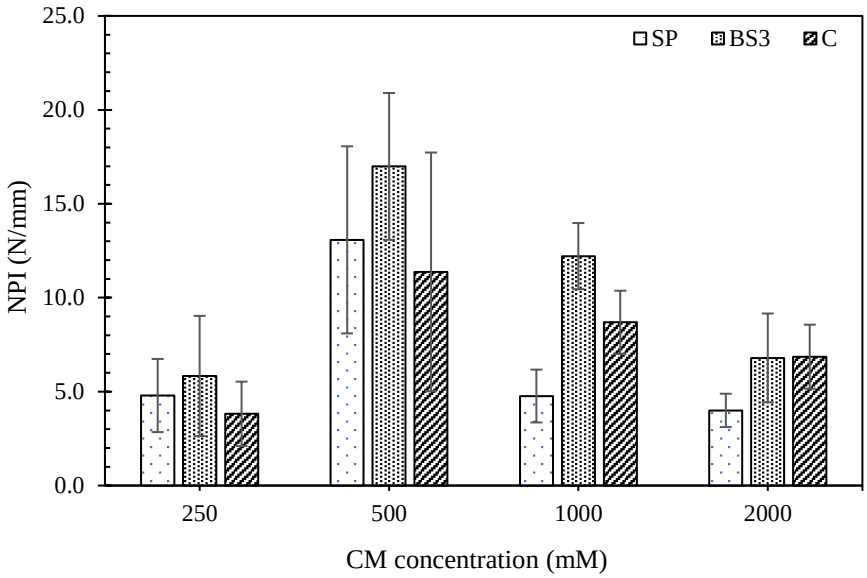

Figure 6.2 Needle penetration Index of the biocemented soil.

It is evident that the strength of the biocemented soil is majorly influenced by the concentration of cementation media. The maximum strength of the biocemented soil samples was observed with the 500 mM concentration of cementation solution, independent of the bacteria type. It should be noted that no recharge of the bacterial solution was applied to the soil in the present study. Mujah et al. (2019) have demonstrated that the $CaCO_3$ efficiency of the microbes decreases from 100% to less than 30% within four numbers of flushes of 0.25 M and 0.5 M concentration of CM. In this study, the number of applications of cementation solution for equivalent calcite with 250 mM and 500 mM concentration was eight and four, respectively. The substantial decrease in the biocementation efficiency of the microbes with multiple applications of cementation solution is most likely the major reason for the low precipitation and strength of the 250 mM cementation solution treated soil compared to the 500 mM cementation solution.

6.2.1.2 Calcium carbonate content

The measured calcium carbonate contents in the various biocemented soils are illustrated in Figure 6.3. Maximum precipitation was observed with the 500 mM treatment. For SP, BS3 and C, the precipitated $CaCO_3$ at 500 mM was observed as 5.5%, 6.8% and 5.1% by the weight of untreated soil. In all other concentrations, the precipitation was observed below 5%. For 250 mM of CM, the average precipitation for SP, BS3 and C was evaluated as 2%, 2.3% and 1.7%, respectively. It might be due to the multiple numbers of CM spray, which impact the microbial communities' $CaCO_3$ conversion efficiency adversely (Mujah et al. 2019). It is to be noted that the cementation treatments were sprayed daily for eight consecutive days to produce comparable calcite content for 250 mM concentration of CM over just one pore volume application of the microbial solution.

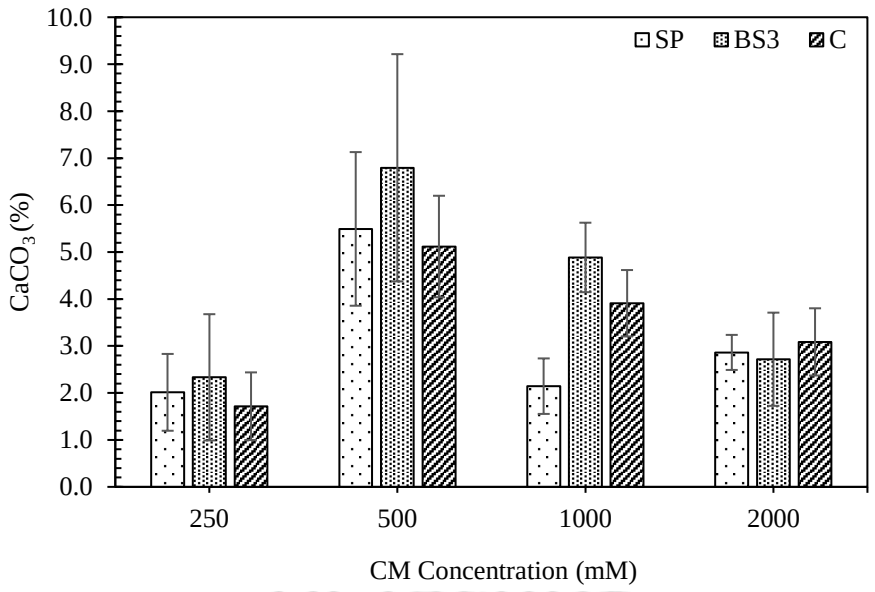

Figure 6.3 Average calcium carbonate content of the biocemented soil.

Whereas for 1000 mM concentration, 2.1%, 4.9% and 3.9% of $CaCO_3$ were precipitated for SP, BS3 and C, respectively. For 2000 mM concentration of CM, the precipitated $CaCO_3$ was observed as 2.9%, 2.7% and 3.1%, suggesting that a higher concentration of CM might be deteriorating the efficiency of microbes to precipitate.

Additionally, it is to be noted that for SP, the $CaCO_3$ content was notably high at 2000 mM than at 1000 mM concentration; however, the corresponding penetration resistance was lower, which is possibly due to the differences in the quality of the precipitates.

It is to be noted that Al Qabany and Soga (2013) reported inhomogeneity and null UCS strength with a 1 M cementation solution. In this study, inhomogeneity was observed almost in all the biocemented sand samples, as depicted by the deviation values of needle penetration resistance and $CaCO_3$ content.

6.2.2 Biochemical analysis of microbes' biocementation potential

To investigate the potential reasons behind the considerable variations in the soil strength and $CaCO_3$ contents, the mentioned microbes are scrutinised for their biocementation potential by monitoring the biochemical reactions during biocementation in the ideal conditions simulated in flasks. The urea hydrolysis was monitored at regular intervals by measuring the concentration of urea in the CM as illustrated in Figures 6.4 (a), (c), (e), and (g) for 250 mM, 500 mM, 1000 mM, and 2000 mM concentrations, respectively. The corresponding concentration of the depleting soluble Ca^{2+} ions has been plotted in Figures 6.4 (b), (d), (f) and (h).

The first measurements were carried out after 2 hours of adding the microbes to allow the added microbial community to settle in the cementation media environment. It is to be noted that at a lower concentration of CM, i.e., at 250 mm, the soil isolate BS3 was observed to be most effective in urea hydrolysis, and the depleted soluble Ca^{2+} concentration followed the trend.

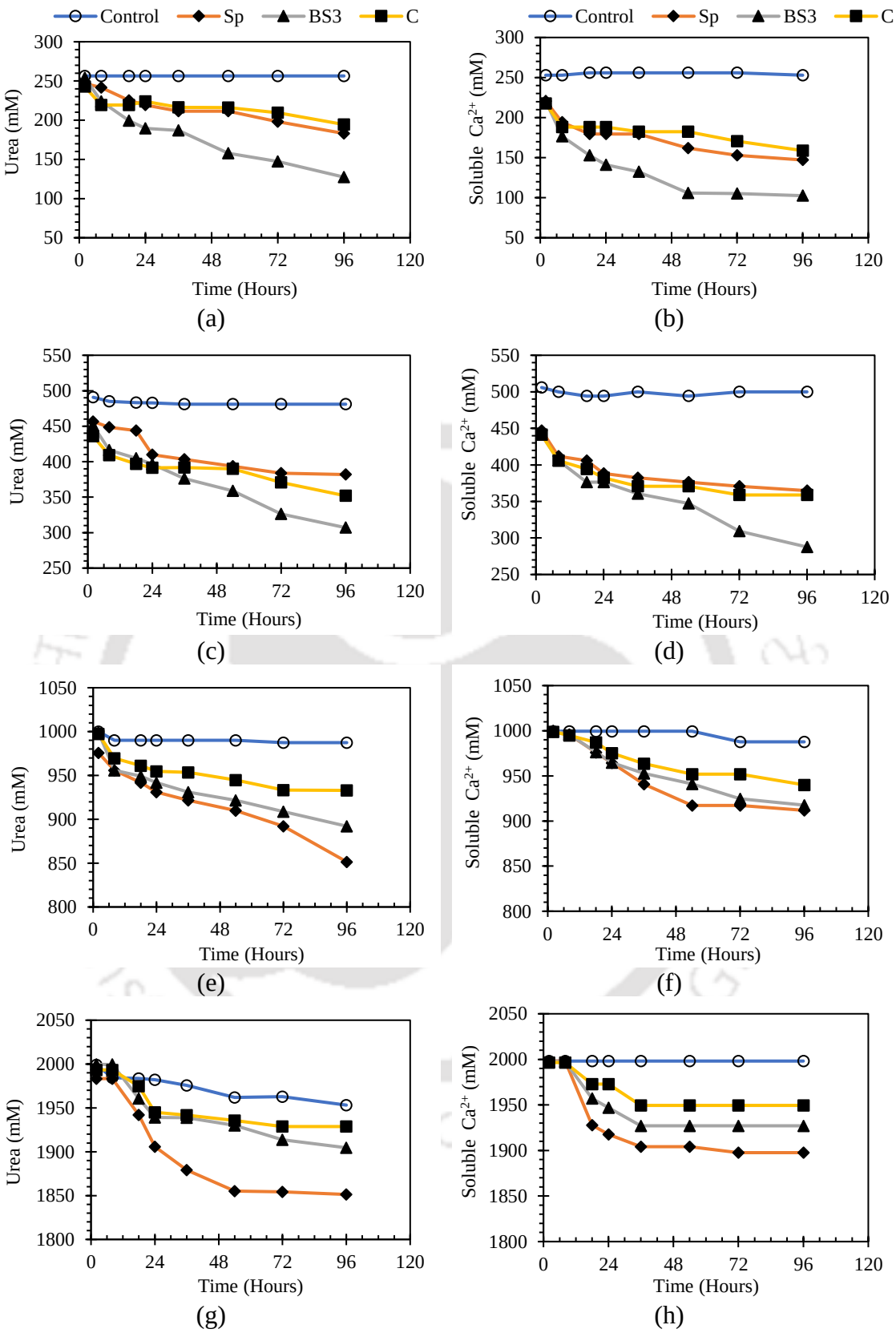

Figure 6.4 Urea and soluble Ca^{2+} concentration at (a-b).250 mM, (c-d).500 mM, (e-f).1000 mM, (g-h).2000 mM concentration of CM.

The net hydrolysed urea in SP, BS3, and C was 64, 127 and 48 mM, whereas the net depleted soluble Ca^{2+} ions were observed as 73, 118 and 59 mM, correspondingly at 250 mM concentration. The isolated soil strain was able to hydrolyse around 98% more urea, and 60% more soluble Ca^{2+} was depleted in comparison to SP. The consortium was observed to hydrolyse 24% less urea, and the subsequent soluble Ca^{2+} depletion was found to be 20% lower in comparison to SP. At 500 mM concentration of CM, the net urea hydrolysed in SP, BS3 and C was observed as 74 mM, 144 mM, and 84 mM, while the soluble Ca^{2+} depletion was 82, 153 and 82 mM. In this case, the urea hydrolysed and soluble Ca^{2+}depletion in BS3 flasks were observed to be 92% and 86% higher than SP. The net hydrolysed urea and depleted soluble Ca^{2+} were observed to be comparable for SP and C. Contrastingly, at higher concentrations, SP outperformed BS3 and C. At 1000 mM of CM, the net hydrolysed urea was evaluated as 124, 107, and 64 mM, whereas the net depleted soluble Ca^{2+} was observed as 88, 75 and 59 mM for SP, BS3 and C, respectively. The net urea hydrolysed for BS3 and C were 14% and 48% lower than SP, whereas the corresponding net depleted soluble Ca^{2+} for BS3 and C were 14% and 33% lower than SP at 1000 mM of CM. At 2000 mM concentration of CM similar trend was observed. The net hydrolysed urea was measured as 132, 95 and 65 mM, whereas the net depleted soluble Ca^{2+} was observed to be 101, 71 and 47 mM for SP, BS3 and C, respectively. The net hydrolysed urea for BS3 and C was 28% and 51% lower than SP, whereas the corresponding net depleted soluble Ca^{2+} was observed at 30% and 53% lower for BS3 and C in comparison with SP at 2000 mM of CM.

It is to be noted that only 2.5% of microbes at $O.D._{600}$ value 1 were added to cementation media, resulting in the dilution of cells to 1:40. This was done intentionally to slow down the hydrolysis to comparatively evaluate the biocementation potential of the different strains. A similar approach has been used for a 50 mM concentration of

cementation solution in a few previous studies to compare different strains, where 1% of the microbes at O.D.$_{600}$ values were added (Dhami et al. 2013a; Dhami et al. 2016).

The estimated average urea and soluble Ca^{2+} utilisation rates are illustrated in Figure 6.5. It was observed that the urea utilisation rate increased with an increase in the concentration of cementation solution for SP, indicating that SP was able to adapt to high-concentration conditions and metabolise urea accordingly. For SP, the urea utilisation rates were observed to increase in a range of 0.44 to 0.91 mM/minute/O.D.$_{600}$ in the concentration range of 250 to 2000 mM. The soluble Ca^{2+} utilisation rate followed the same trend, where the values ranged from 0.51 to 0.7 mM/minute/O.D.$_{600}$. In comparison, BS3 exhibited contrasting behaviour. The maximum value of urea utilisation rate was observed as 1 mM/minute/O.D.$_{600}$ at 500 mM of CM with a corresponding equivalent calcium utilisation rate. Both the average urea and soluble Ca^{2+} utilisation rates for soil isolate BS3 decreased at 1000 and 2000 mM of CM, indicating a lack of tolerance of the soil isolate in the higher calcium and urea concentrations.

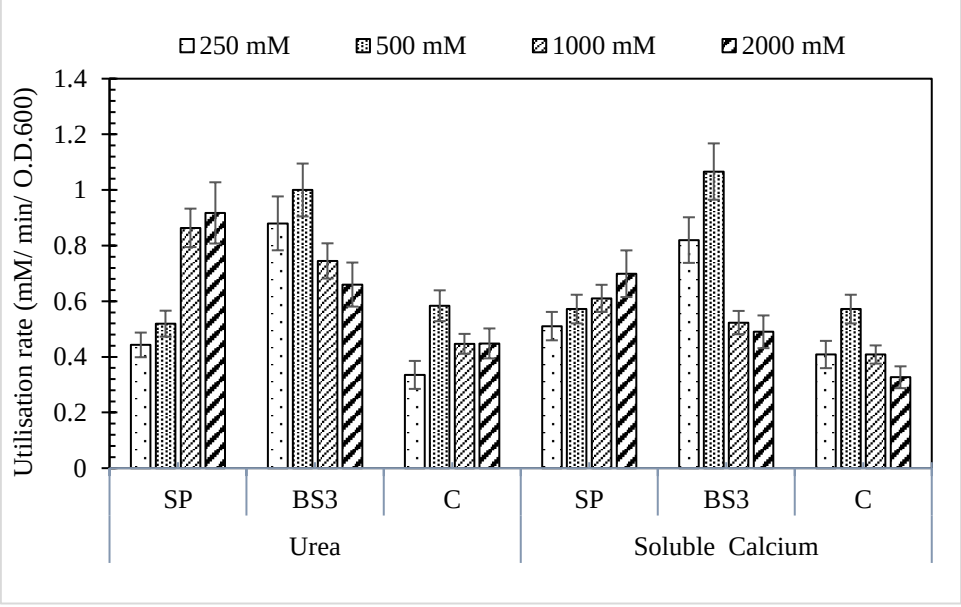

Figure 6.5 Estimated utilisation rates of urea and soluble calcium at various concentrations of CM.

For consortium C, the average urea utilisation rate was also observed at maximum for 500 mM concentration of CM with a value of 0.57 mM/minute/O.D.$_{600}$. It followed the same pattern as BS3; however, the urea and soluble calcium utilisation rates were significantly lower in comparison to SP and BS3.

It is to be noted that while the urease activity and urea utilisation rates are linked with the biocementation potential of the microbes (DeJong et al. 2010; Dhami et al. 2013b; Dhami et al. 2017; Mujah et al. 2017), the precipitation of calcium carbonate crystals may not be necessarily associated with it. The availability of calcium ions and the ambient environment play a crucial role in precipitation. In the present study, no pH adjustments were made in the flask experiments considering the pH of the soil. The measured pH increased in a narrow range of 7.0 to 7.5 for all the samples through the batch test duration. In contrast, an alkaline environment is reported to be favourable for precipitation (Ferris et al. 2004; Dhami et al. 2013a; Mujah et al. 2017). In the present study, notable differences were observed in the soluble calcium and urea utilisation rates at different levels of cementation solution with the different microbes. The differences suggest that even with equivalent specific urease activity, the response of the microbial communities may differ at different concentrations of cementation media. Their response may be based on their origin and adaptability to survive in different micro-environmental conditions.

The $CaCO_3$ precipitation potential for different microbes at varying concentrations of cementation media was observed to be consistent with the calcium depletion rates, as illustrated in Figure 6.6. For BS3, the maximum calcium carbonate precipitation potential was evaluated as 17% at 500 mM of CM. For the consortium, the precipitation potential was found comparable at 500 mM and 1000 mM cementation solution with values around 10%, respectively. For SP, the maximum precipitation was observed at around 10% at a 2000 mM concentration of CM. The quantity of recovered $CaCO_3$ precipitates is a small

portion of the theoretically anticipated calcite (<20%) as the added microbial quantity was substantially small to metabolise the whole amount of urea and precipitate $CaCO_3$. The application of the low quantity of the bacterial cells in this study was decided as the slow precipitation process is helpful to compare the biocement potential of strains, as discussed in some of the previous studies where 1% volume of the bacteria was added to 50 mM of cementation media (Dhami et al. 2013a; Dhami et al. 2017).

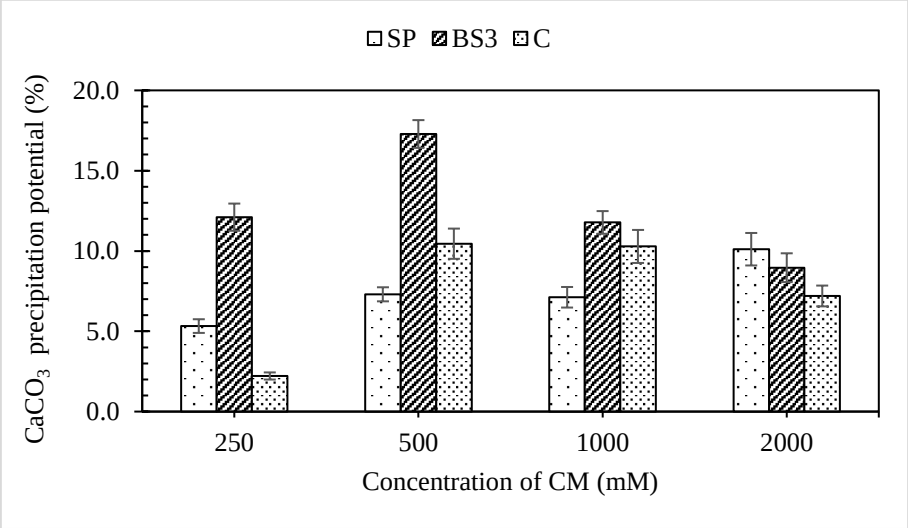

Figure 6.6 $CaCO_3$ precipitation potential of different strains at various concentrations of cementation media.

6.2.3 Microstructure of precipitates

The microstructures of the precipitated crystals were examined to anticipate their potential role in influencing the improvement in soil strength. It is well known that calcite, the most stable polymorph of $CaCO_3$, exhibits euhedral habit (Ševčík et al. 2018). The rhombohedral-shaped calcite with epitaxial growth is often observed with the MICP technique (Hammes et al. 2003; Cizer et al. 2012; Cuthbert et al. 2012). Vaterite is known for its cauliflower-like spheroidal morphology, and aragonite is identified by its morning-star shaped morphology bounded by curved prismatic faces (Mayorga et al. 2019).

The SEM micrographs of the precipitated crystals by SP at various concentrations of CM are plotted in Figure 6.7.

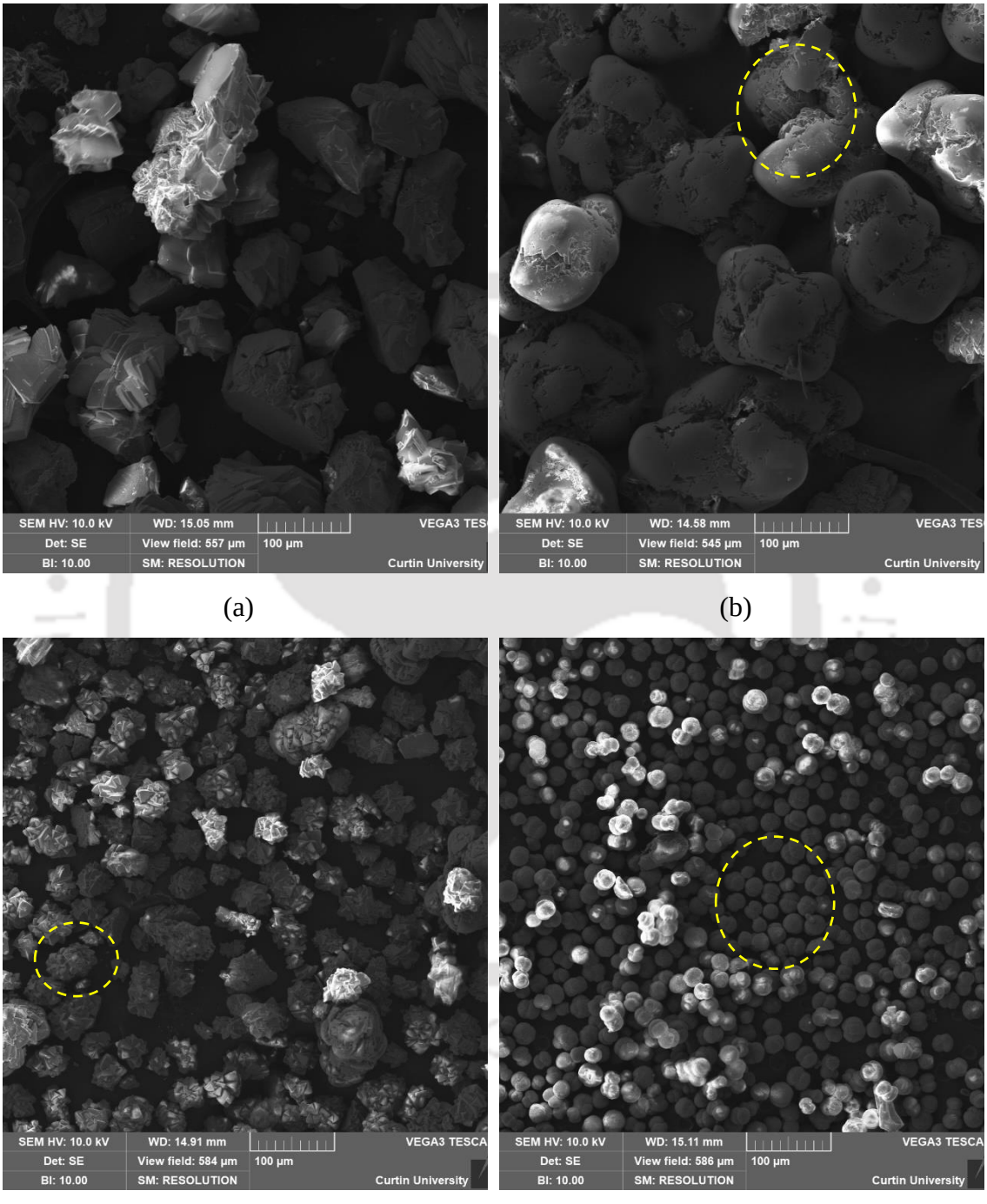

Figure 6.7 SEM micrographs of precipitates produced by SP at (a). 250 mM (b). 500 mM (c). 1000 mM (d) 2000 mM concentration of CM.

All the micrographs are taken at the same scale for visual comparison. The precipitates exhibited euhedral habit at 250 mM of CM in Figure 6.7 (a), suggesting the presence of calcite. The euhedral precipitates were observed to be formed in layers of rhombohedral and scalenohedral shapes. In Figure 6.7 (b), the largest crystal with a smooth texture was observed; however, fissure-like gaps were also noticed. Magnifying these images revealed that the precipitated crystals are packed up of small rhombohedral crystals, as illustrated in Figure 6.10 (a). At 1000 mM concentration of CM, the size of precipitates decreased when compared to 500 mM concentration of CM. The magnified image of the highlighted section in Figure 6.7 (c) is shown in Figure 6.10 (b), suggesting the epitaxial growth of rhombohedral calcite crystals. Whereas it was visually observed that at 2000 mM concentration of CM, spheroid crystals with cauliflower-like shape were precipitated, as illustrated in Figure 6.7 (d), suggesting the dominance of vaterite (Mayorga et al. 2019). The magnified image of these cauliflower-shaped precipitates is shown in Figure 6.10 (c).

The SEM micrographs of the precipitates from BS3 and C at various concentrations of cementation media are illustrated in Figure 6.8 and Figure 6.9. As it is deduced from Figures 6.8 (a) to 6.8 (d), the size of precipitates was maximum at 500 mM concentration of CM for BS3. At 250 mM and 1000 mM of CM, euhedral calcite with epitaxial growths was observed. Interestingly at 2000 mM, small rhombohedral crystals layered along with the spheroid-shaped precipitates were observed, as shown in Figure 6.8 (d). The highlighted section is magnified and shown in Figure 6.10 (d).

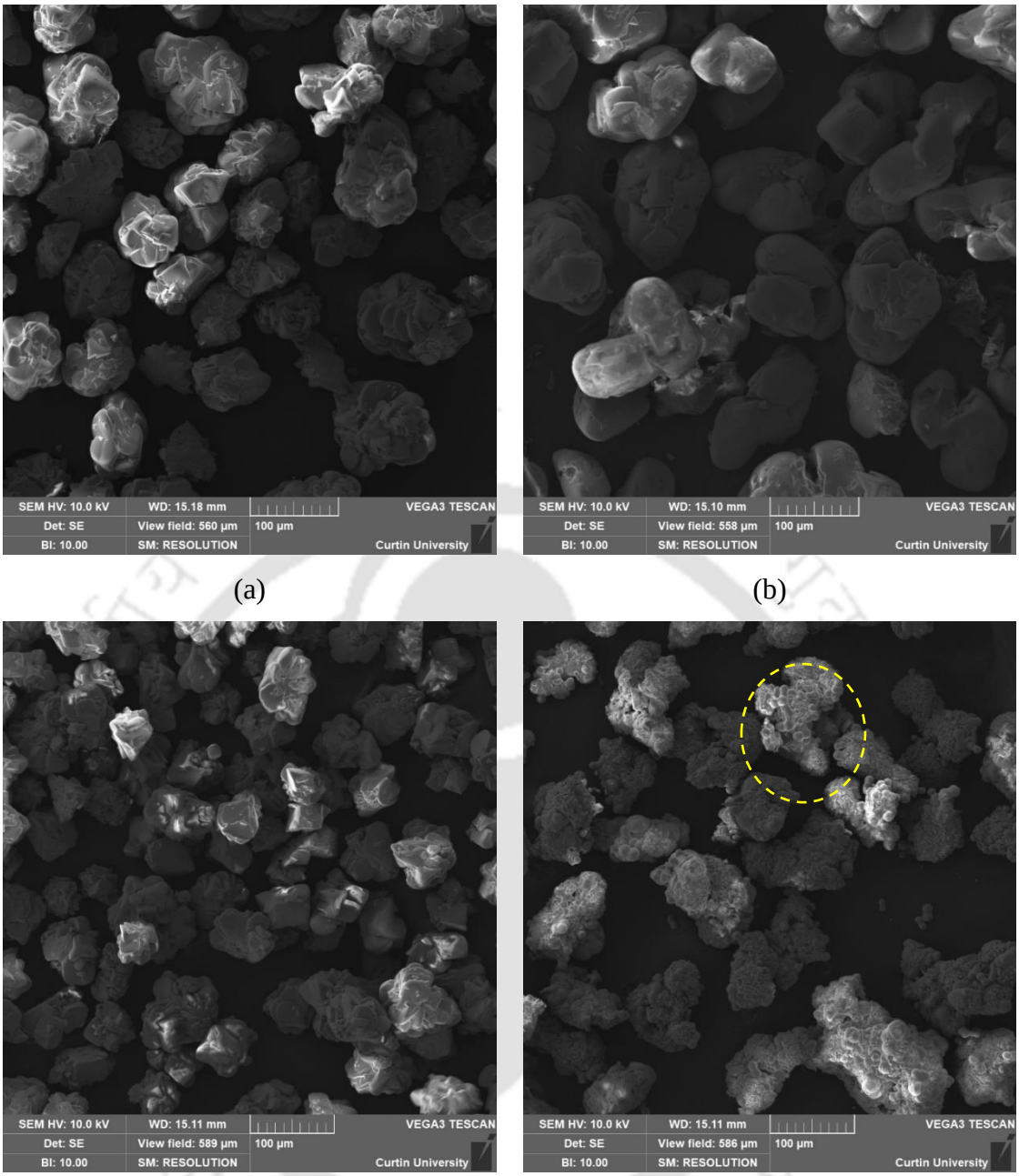

Figure 6.8 SEM micrographs of precipitates produced by BS3 at (a). 250 mM (b). 500 mM (c). 1000 mM (d) 2000 mM concentration of CM.

The variation in the size of the precipitates of consortium C at different concentrations of CM demonstrated a similar trend to BS3 (illustrated in Figure 6.9). However, the size of the precipitates was smaller in comparison to SP and BS3. For the consortium, the precipitated crystal at each concentration was observed to be euhedral and layered except 2000 mM. At a 2000 mM concentration of CM, significantly smaller

crystals amalgamated with spheroidal precipitates were observed, as shown in Figure 6.9 (d).

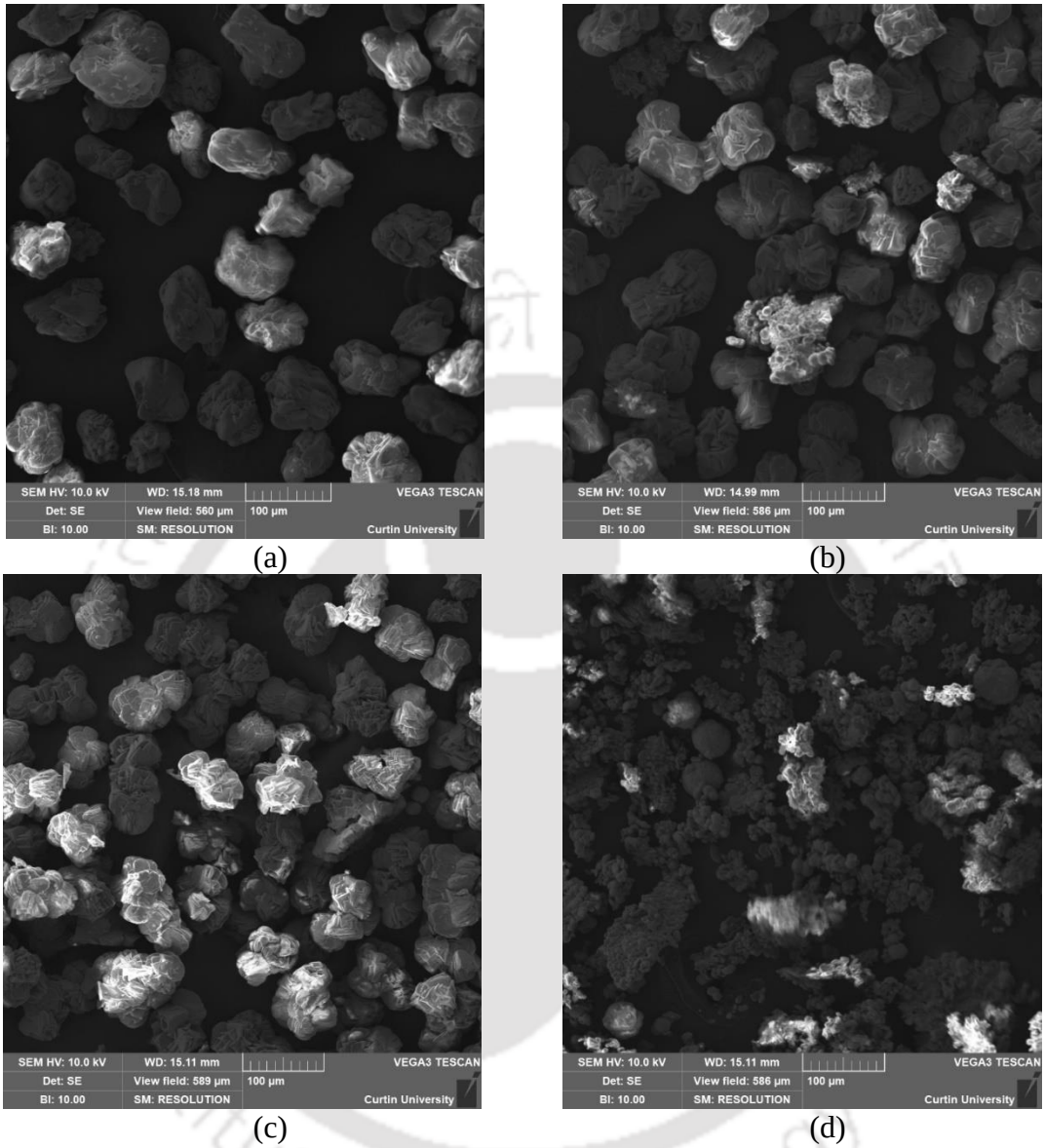

Figure 6.9 SEM micrographs of precipitates produced by C at (a). 250 mM (b). 500 mM (c). 1000 mM (d) 2000 mM concentration of CM.

It is to be noted that the large calcite crystals are reported to have a higher nanoindentation modulus and hardness (Heveran et al. 2019). Thus, the production of large $CaCO_3$ crystals is most likely to provide higher contributions to soil strength improvement than smaller crystals. Recalling the batch test results, the maximum carbonates were recovered at a 500 mM concentration of CM for BS3 and C. For SP, although the

maximum carbonates were recovered at a 2000 mM concentration of CM, the morphology of the precipitates suggests an abundance of small vaterite crystals.

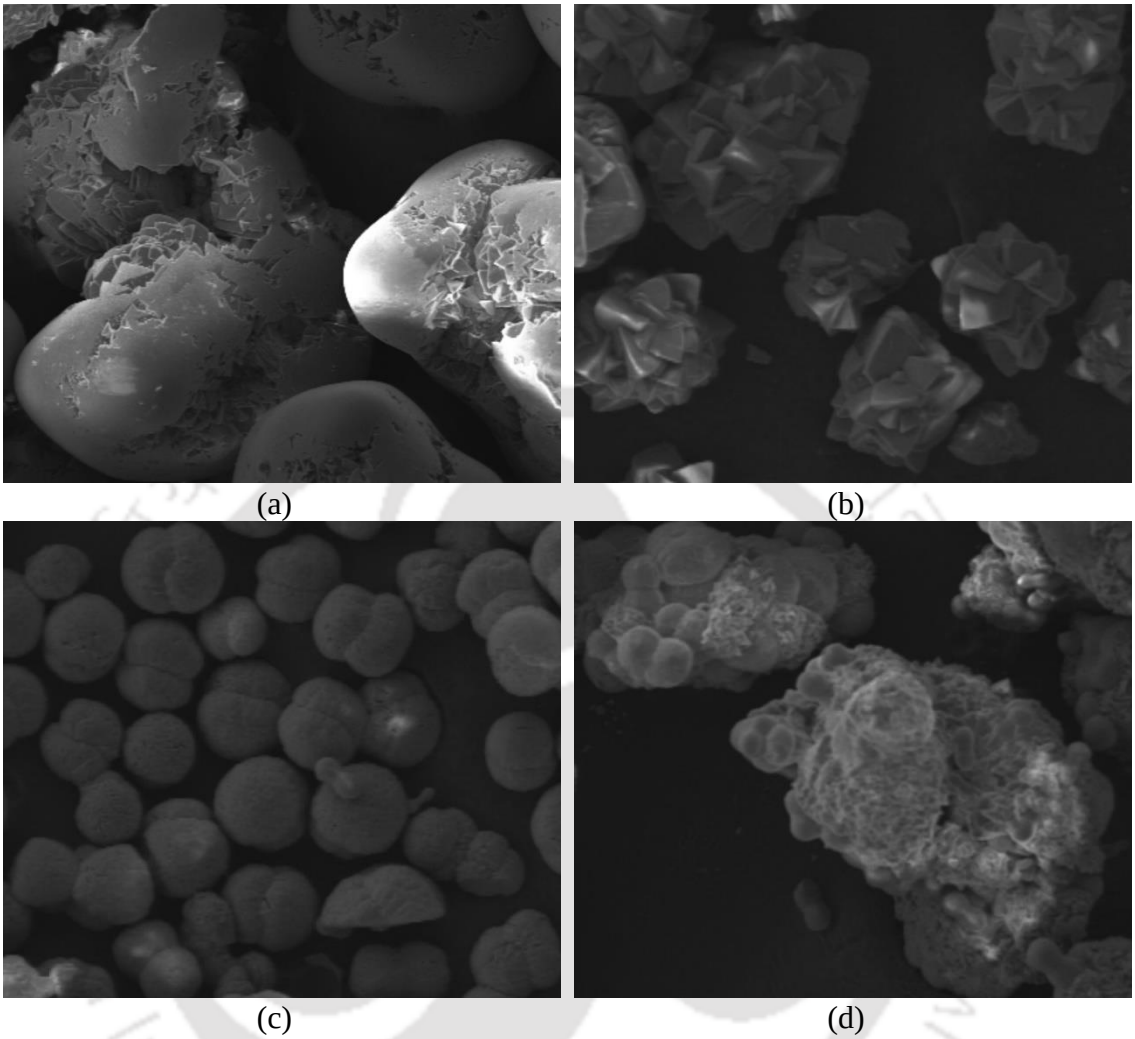

Figure 6.10 Magnified images of precipitates: (a) SP-500 mM; (b) SP-1000 mM; (c) SP-2000 mM; and (d) BS3-2000 mM.

It is to be noted that the maximum size of the precipitates was observed at 500 mM CM for SP too. The sizes of the precipitates analysed with the ImageJ are reported in Figure 6.11. The size of the precipitates for BS3 and SP both was observed in a range of 100-150 μm, whereas for C, the precipitates varied in a range of 60-100 μm at a 500 mM concentration of CM. At 2000 mM concentration of CM, the diameter of SP was measured as 20-30 μm, whereas for C, it was around 20-50 μm. Contrastingly, BS3 precipitated a relatively large size of crystal (75-100 μm) with 2000 mM cementation media. The

quantitative analysis of the precipitated crystals with X-Ray diffraction (XRD) was not considered in the current study due to the limited quantity of the precipitate, which was entirely used in the SEM analysis.

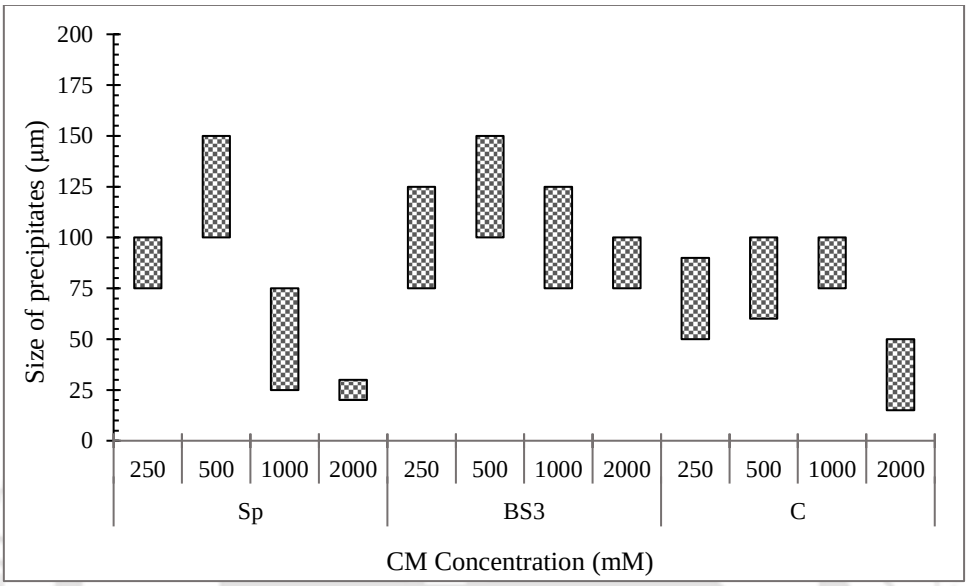

Figure 6.11 Size ranges of the precipitates produced by different microbial species at various concentrations of CM.

It was preliminary hypothesised that the potential reason for strength variation is the distinct response of microbes of different origins against the different levels of cementation media. To confirm this hypothesis, the biochemical reaction induced by the microbes was further assessed by simulating the biocementation process in flasks, and it was confirmed that the indigenous microbe, BS3 performed better in comparison to SP up to 500 mM concentration of cementation media. SP overtakes BS3 at higher concentrations (1000 mM and 2000 mM) of cementation media; however, the microstructure of the recovered precipitate revealed the precipitates to be small-size crystals. The large size and uniformity of the precipitated $CaCO_3$ with lower urease activity are associated with higher strength moduli (Chu et al. 2014; Heveran et al. 2019; Konstantinou et al. 2021). In the present study, the urease activity of the microbes was in

a similar range; however, their response in hydrolysing urea at different concentrations of cementation was dissimilar. The size of precipitates was found to be maximum at 500 mM of cementation media concentration for all the microbes. With a 2000 mM cementation solution, the size of $CaCO_3$ crystals was relatively smaller. The supporting findings from the biochemical analysis and microstructure confirm the ambient concentration of cementation solution to be 500 mM within the described experimental conditions. However, several other unaddressed critical parameters, such as the quantity of the available nutrient, dissolved oxygen, the viability of microbial cells and the evolution of the mineralogy of the precipitates during the biocementation process for different kinds of microbial strains, are recommended for future studies.

6.3 Summary

This study provides preliminary insights into the biocementation response of similar urease-producing microbes of different origins when exposed to various concentrations of cementation media. The standard biocementing microbe *Sporosarcina pasteurii* (SP), a soil isolate (BS3) that has 98% similarity in its genomic sequence to SP and a consortium, was scrutinised in two steps involving the quantification of the soil strength improvement and biochemical parameters. The major findings from the study can be encapsulated as follows-

- The maximum soil strength improvement was observed at 500 mM cementation media, irrespective of the microbial species. The indigenous soil isolate (BS3) exhibited 30% more resistance to needle penetration than the standard exogenous microbe (SP) at 500 mM of cementation media.
- The batch experiments revealed that soil isolate (BS3) outperformed the standard microbe SP in terms of precipitation potential at 250mM and 500mM cementation media. However, at higher concentrations, SP was observed to be more resilient.

- The microstructure analysis of the precipitated carbonate revealed that at 500 mM of cementation media, SP, BS3 and C precipitated larger crystals than the rest of the concentrations. At 2000 mM, the precipitation of relatively smaller spheroid crystals of 20-30μm was precipitated with SP, while BS3 and C had larger precipitates made up of both the spheroid and the rhombohedral crystals.

6.4 Conclusion

In this objective, it was determined that the 500 mM concentration of cementation solution is most ambient for the selected biocementing microbes to improve soil strength, regardless of the bacterial strain. The morphology of precipitates and $CaCO_3$ content primarily influences the strength of the soil. It is established that even microbes from the same genus and different origins have different biocementation behaviour at varying concentrations of cementation media, which might be helpful for the comprehension, design and control of bio-stimulation and bio-augmentation approach-based surficial erosion countermeasure.

It is to be noted that although the needle penetration test is a measure of soil strength and binding characteristics, it is not a measure of soil erodibility. The relationship of needle penetration resistance with $CaCO_3$ content and the erodibility of soil must be explored further.

CHAPTER 7

EVALUATION OF BIOCEMENT, BIOPOLYMER, AND THEIR COMPOSITES FOR MITIGATION OF CURRENT-INDUCED SOIL EROSION

7.1 Introduction

The findings from the prior chapters clearly indicate that MICP has great potential for the mitigation of riverbank erosion. However, it is necessary to quantify the influence of biocementation on the erosion resistance of riverbank soil via laboratory-scale physical models to facilitate its field application. Moreover, there are various challenges in the field application of conventional biocementation techniques. Transport of huge quantities of healthy biocementing microbes to the site and the produced by-product ammonia are the major challenges. The most often-used pathway of MICP breaks down urea, which releases ammonia into the environment. Some investigations have resorted to post-treatment of soil to remove the ammonia. Zeolites (Keykha et al. 2019), electro-bio-stabilisation (Keykha and Asadi 2017), and rinsing of the soil with a high pH and high ionic strength solution (Lee et al. 2019a) are attempted. Alternatively, the quantity of ammonia released is controlled by replacing urea with asparaginase (Li et al. 2015) and utilising ammonia to produce struvite (Yu et al. 2016).

In this chapter, a ureolytic bacterial strain (BS3) isolated from the riverbank site has been utilised in MICP. This technique is conducive to selective bio-stimulation, where the isolated strain can be reintroduced to the riverbank, avoiding the introduction of new species. The riverbank sand is treated with multiple cycles of biocementation of 500 mM cementation media. In the first stage, the strength of the treated samples was evaluated with the needle penetration test and correlated with the degree of cementation. In the second stage, a novel experimental program for simulating current erosion in a hydraulic flume has been developed. The treated samples have been subjected to current erosion at

varying slopes in a lab-scale hydraulic flume. The relationship between the current velocity and rate of erosion with varying levels of cementation has been examined. In the third stage, a new technique combining MICP with biopolymer spray is devised to utilise the virtues of both in the form of a bio-composite material. Their relative efficacies in terms of erosion mitigation vis-à-vis ammonia release have been explored. In the final stage of the study, extensive microstructural analysis was performed involving scanning electron microscopy (SEM), energy-dispersive X-ray spectroscopy (EDX), and X-Ray diffraction (XRD) to explain the phenomena observed in the erosion tests. In conclusion, a possible strategy for field-scale mitigation of riverbank erosion is presented.

The summary of the experimental program is illustrated in Figure 7.1. It is to be noted that the influence of the biocementation technique at different biocementation levels (BC) on the varying slopes (S30, S45 and S53) has been evaluated. Later, the three abovementioned soil binding techniques (BC, BP, and BPBC) are compared only at the steep slope (S53).

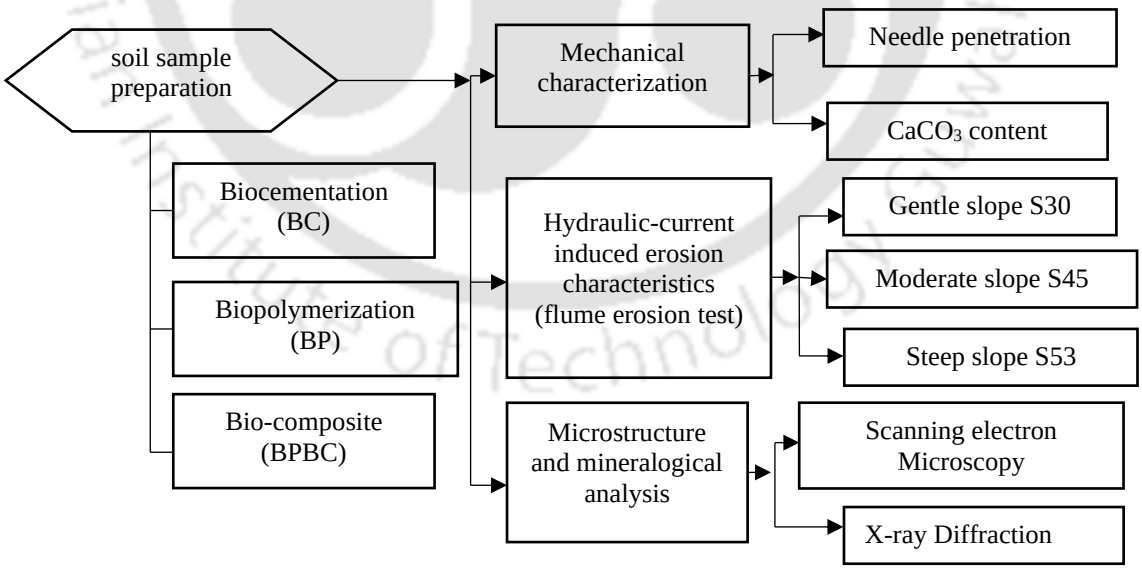

Figure 7.1 Experimental program to investigate mitigation of current-induced erosion with biocement and bio-composite treatment.

7.2 Results and Discussion

7.2.1 Mechanical characteristics of the treated soil

The needle penetration resistance of the biocemented soil specimens is plotted in Figure 7.2 (a, b). In Figure 7.2 (a), the response of the biocemented soil samples against the penetrated depth is plotted, whereas in Figure 7.2 (b), the needle penetration index (NPI) is reported. Samples BC0, BP1, BP2, and BP4, did not exhibit any noticeable resistance against the penetration (NPI<1 N/mm). This experiment demonstrates that biopolymer treatment does not add to the penetration resistance of the soil. The elastic moduli of biopolymer are significantly lower in comparison to that of the sand particles. Thus, they do not add penetration resistance. However, a steady increase in the penetration resistance was observed with the increase in the number of biocementation cycles, as shown in Figure 4 (a). The NPI of the biocemented samples BC1 was observed as 4.63 N/mm. Sample BC2 and BC3 exhibited 105% and 245% improvement compared to BC1, with NPI values of 9.47 and 15.93 N/mm. Interestingly, sample BC4 exhibited the highest NPI of 25.78 N/mm, which is 560% higher than the NPI of BC1. However, the sample failed at a penetration depth of 4.5 mm with a sudden propagation of crack on the crust. This phenomenon indicates the brittle nature of the heavily biocemented samples. Bio-composite samples BP1BC2 and BP2BC2 exhibited NPI values of 10.79 and 11.16 N/mm, respectively, which is in a comparable range of NPI with biocemented sample BC2, confirming that the low-viscosity biopolymer treated did not contribute to the needle penetration resistance. Contrarily, sample BP4BC2 exhibited a low NPI value of 7.32 N/mm. The reduction in the NPI value is likely due to the relatively higher biopolymer content. Another possible reason is disturbances to the biopolymer-biocement composite layer caused by the repeated spraying of biopolymer and biocementation solutions.

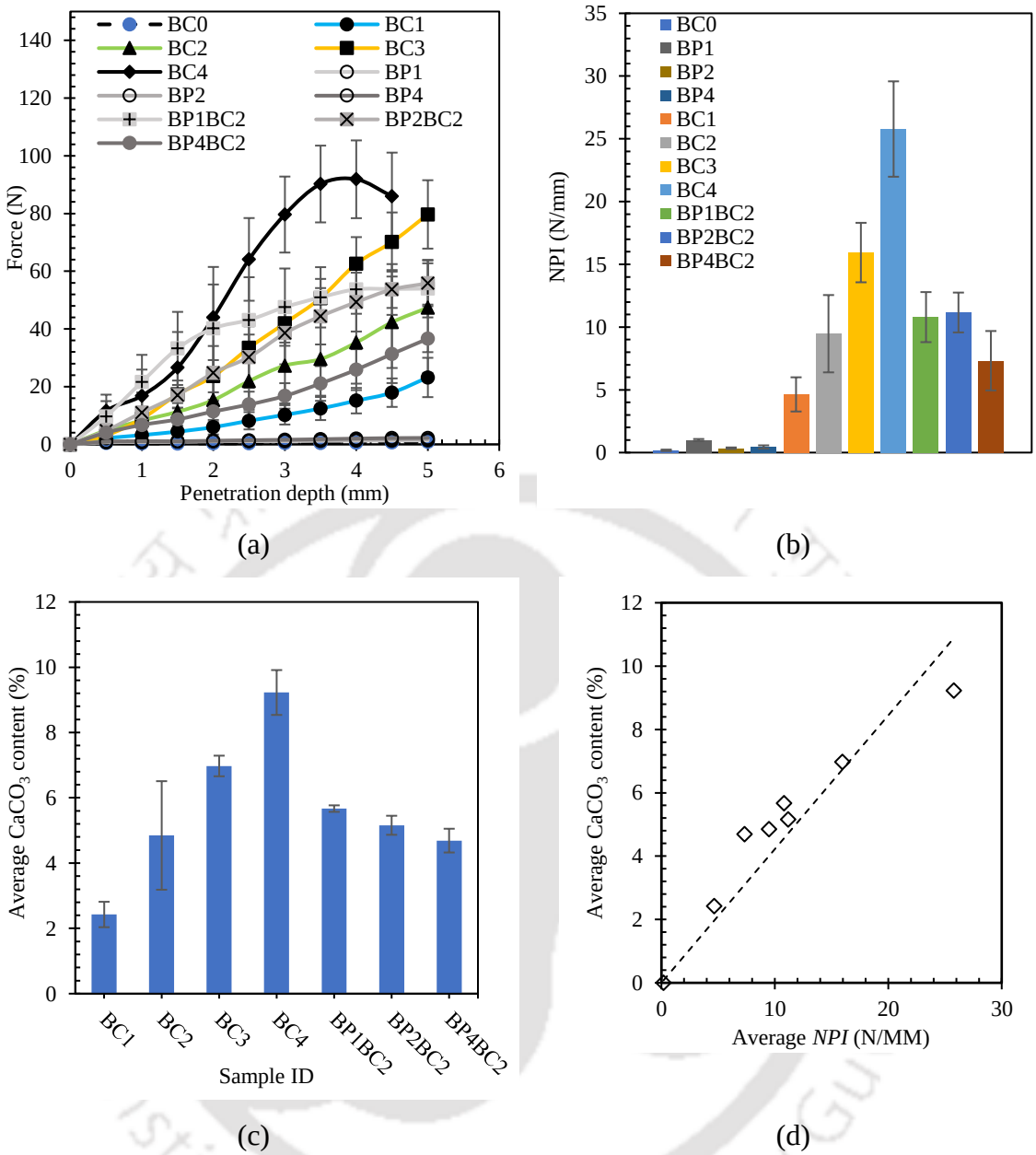

Figure 7.2 Measured (a) Needle penetration response; (b) Needle penetration indices; (c) Calcium carbonate content; and (d) Correlation between calcium carbonate content and NPI of the biocemented soil sample.

It should be noted that discernible non-uniformity was observed in the needle penetration resistance, as shown with the standard deviations in Figure 7.2 (b). Similar non-uniformity in the needle penetration response of the lime and cement-stabilised soil has also been observed by Dipova (2018), and to negate the uncertainty, large numbers of

tests on the sample have been recommended. Therefore, the needle penetration was conducted at 25 distinct points on each sample, and the non-uniformity was reported in the form of deviations. The spatial variation in the NPI is likely due to uncontrolled contact locations of the precipitates on the soil grains with the spraying strategy, which is incompetent to control the uniformity of soil bridging despite being the most convenient strategy for the field application (Cheng et al. 2013a; Mujah et al. 2017; Wang et al. 2018a; Chung et al. 2021).

Chung et al. (2020) reported penetration resistance in the range from 9.6 N/mm to 24.6 N/mm for fine-to-medium-grained sand treated with multiple cycles of MICP, producing calcium carbonate content of 85 mg/g of soil (around 8.5%). However, we detected with the needle penetration test that the increase in calcium carbonate content in the biocemented soil above a threshold might induce brittle behaviour despite leading to higher strength. Similar observations were made in the previous studies (Montoya and DeJong 2015; Clarà Saracho et al. 2021; Do et al. 2021). However, the address on the threshold is still largely unaddressed. Our study suggests a potential range between 7 to 9.2% of calcite content where the biocemented samples might be brittle.

The measured calcium carbonate content for all samples is reported in Figure 7.2 (c). The calcium carbonate content in samples BC1, BC2, BC3, and BC4 was evaluated as 2.42, 4.85, 6.97, and 9.22%, respectively. The bio-composite samples BP1BC2, BP2BC2, and BP4BC2 samples were observed to have calcium carbonate content of 5.67, 5.16, and 4.69%, respectively. The calcium carbonate content of samples BP1BC2 and BP2BC2 (5.67 and 5.15%) was found to be marginally more than the theoretically expected calcium carbonate (5%), most likely as the biopolymer arrests the precipitation within the surficial regions (Wang et al. 2018a). Abiogenic calcium carbonate was found to be negligible in the control sand. The average needle penetration index is plotted against

the average calcium carbonate content in Figure 7.2 (d). A linear relation between the needle penetration index and average calcium carbonate content is established with an R^2 value of 0.96, as follows:

$$C = 0.42\times NPI \quad (7.1)$$

Where C is the average calcium carbonate content in percentage (%) by the weight of soil and NPI is the needle penetration index in N/mm. Thus, NPI is a good index for field estimation of calcium carbonate deposition. It is worth mentioning that the above relationship is applicable only within the parameters of this experiment. It may be influenced by the type of soil and the biochemical parameters.

7.2.2 Flume erosion test

7.2.2.1 Performance of biocemented samples

The cumulative erosion depth (D) against flow velocity (v) and cumulative erosion rate (E_R) against specific power (P_S) are calculated from the video recordings as per equations (3.2), (3.3), and (3.4). The results are illustrated in Figure 7.3.

From Figure 7.3 (a), it was observed that for samples BC0, BC1 and BC2, the erosion triggers at a flow velocity (v) around 0.2 m/s, which is comparable with the theoretical critical velocity (0.175 m/s). The initiation of erosion was delayed in the case of BC3-BC4. The detachment of soil grains in samples BC3 and BC4 was initiated at a flow velocity of 0.29 m/s. At slope S30, the maximum D values for samples BC0, BC0, BC1, BC2, BC3, and BC4 were evaluated as 12, 10.7, 7.9, 3.9, and 2.4 mm, respectively.

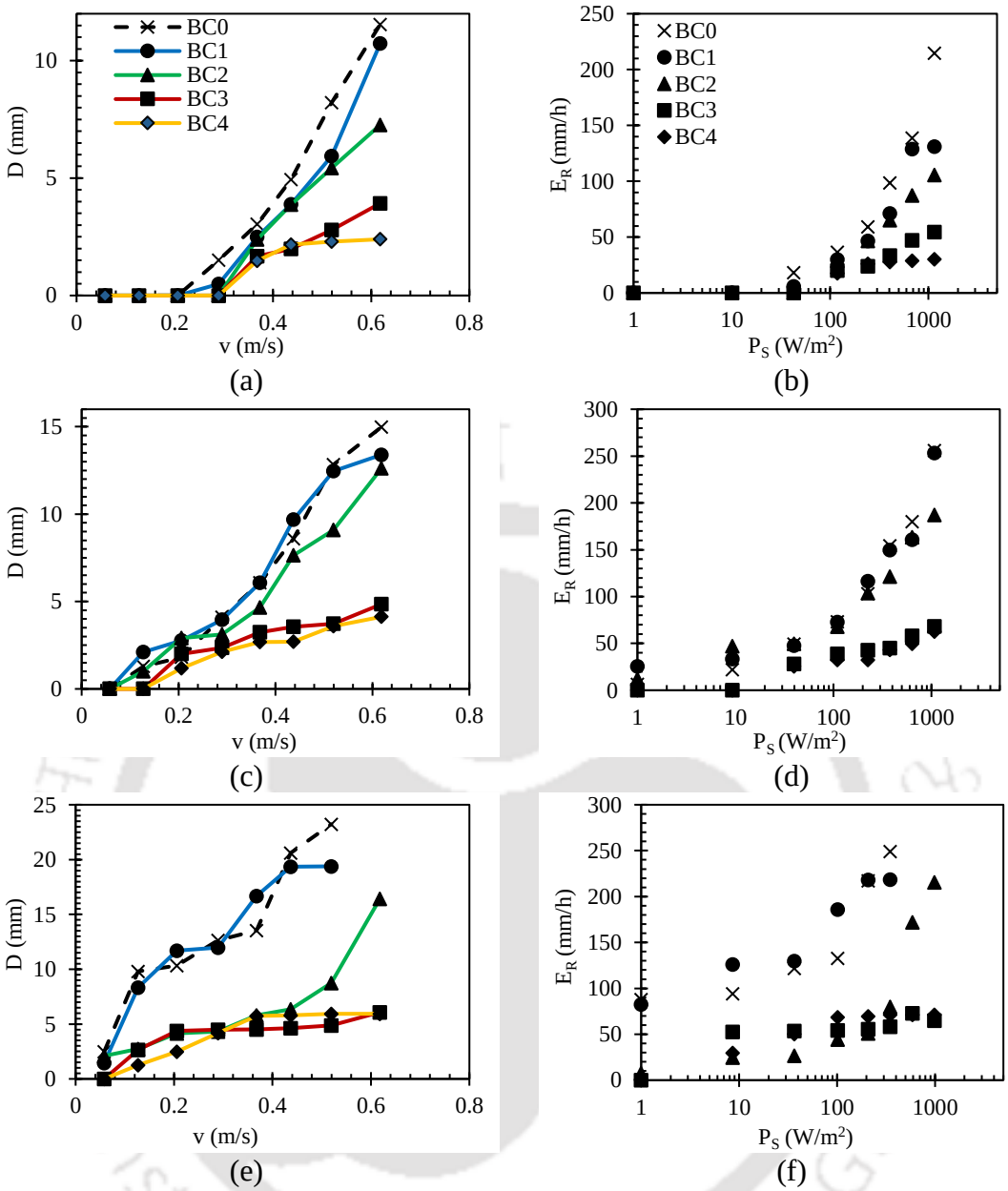

Figure 7.3 Cumulative eroded depths and erosion rates of biocemented soil samples at various slopes (S30; a-b), (S45; c-d), (S53; e-f).

At slope S45, the soil erosion was triggered at a flow velocity of 0.06 m/s for samples BC0, BC1, and BC2, whereas the initiation of erosion in samples BC3 and BC4 was observed at 0.127 m/s. At slope S45, the corresponding maximum D values for samples BC0, BC1, BC2, BC3 and BC4 were observed as 15, 13.3, 12.6, 4.9, and 4.1 mm, respectively. Whereas, at slope S53, the soil erosion for BC0, BC1 and BC2 was triggered as soon as the samples were plugged into the slope. At the same slope, the erosion was

triggered when the flow was imitated at a gentle velocity of 0.06 m/s for samples BC3 and BC4. The differences in the theoretical critical velocity and observed critical velocity values are mostly due to the instability of the loose sand particles caused by the steepness of slopes (S45 and S53). At the S53 slope, the corresponding maximum D values for samples BC0, BC1, BC2, BC3 and BC4 were observed as >23, >19.4, 16.4, 6, and 5.9 mm, respectively. BC0 and BC1 failed in the same manner before reaching the flow velocity of 0.52 m/s, as the maximum value of D exceeded 50% of the sample depth. Sample BC2 exhibited comparatively resilient behaviour against erosion. A substantial reduction of more than three folds in the maximum D values was observed in biocemented samples BC3 and BC4 compared to untreated samples (BC0).

Similar patterns were observed in the E_R values of the biocemented samples against the P_S, as plotted in Figure 7.3 (b, d, f). A significant reduction in the erosion rate (E_R) for heavily biocemented soil (BC3) was observed compared to the untreated sand (BC0). The maximum E_R for samples BC0, BC1, BC2, BC3, and BC4 at slope S30 were observed to be 215, 131, 106, 54, and 30 mm/h, respectively, against the maximum P_S 1 kW/m^2. The corresponding E_R values at slope S45 were observed as 255, 253,186, 68, and 63 mm/h, respectively. For slope S53, samples BC2, BC3, and BC4 exhibited relatively higher E_R values of 216, 65, and 71 mm/h, respectively, against the maximum P_S value of around 1 kW/m^2, whereas samples BC0 and BC1 failed at P_S 350 W/m^2 with E_R values of 249 and 214 mm/h. Broadly, a four-fold reduction was observed in the E_R values for all the slopes with samples BC3 and BC4 compared to untreated sample BC0. Previous studies have demonstrated that the detachment of loose sand occurs at specific stream power of around 35 W/m^2 (Zdankus et al. 2014). In the present study, we observed that the specific power required to detach the sand particles and trigger erosion at the gentle

slope is around 42 W/m^2. However, with the increase in steepness, the detachment in the loose sand initiated at specific power below 10 W/m^2.

In summary, the low biocementation treatment (BC1) did not have any noticeable improvement in the erosion characteristics except at slope S30. In comparison, a considerable improvement in erosion resistance was observed with the samples BC2. The inadequate bonding of the grains due to low calcium carbonate content is one of the potential reasons for marginal or no improvement, which has also been reported in a few of the previous studies against other hydraulic erosion induced by rainfall, piping, and tangential flow (Jiang and Soga 2017; Jiang et al. 2019; Chung et al. 2021; Clarà Saracho et al. 2021; Do et al. 2021). The improvement against erosion with increased levels of biocementation does not follow a direct relationship, as samples BC3 and BC4 have practically non-significant differences in their erosion characteristics. Sample BC4 performance against hydraulic current-induced erosion was found to be comparable with sample BC3, despite having significantly higher calcium carbonate content, as illustrated in Figure 7.2 (c). Therefore, it is crucial to investigate the mechanical characteristics of biocemented samples. The investigation of the local strength of the bonded grains via needle penetration resistances unravelled that BC4 samples exhibited brittle nature despite inhering greater strength in comparison to sample BC3, which is most likely responsible for the erosion resistance of the soil to be independent of the quantity of calcium carbonate in the higher ranges of biocementation.

The images in Figure 7.4 were taken after drying the specimens post-flume experiments. The images show severe erosion of the untreated soil on all the slopes. There is an undiscernible improvement with one cycle of biocementation (BC1). Sample BC1 exhibited a failure pattern similar to the untreated sand at all the slopes as insufficiently bonded particles get eroded in particulate mode. However, with the increase in

biocementation degree (for samples BC2, BC3, and BC4), slab failures were evident with biocemented chunks.

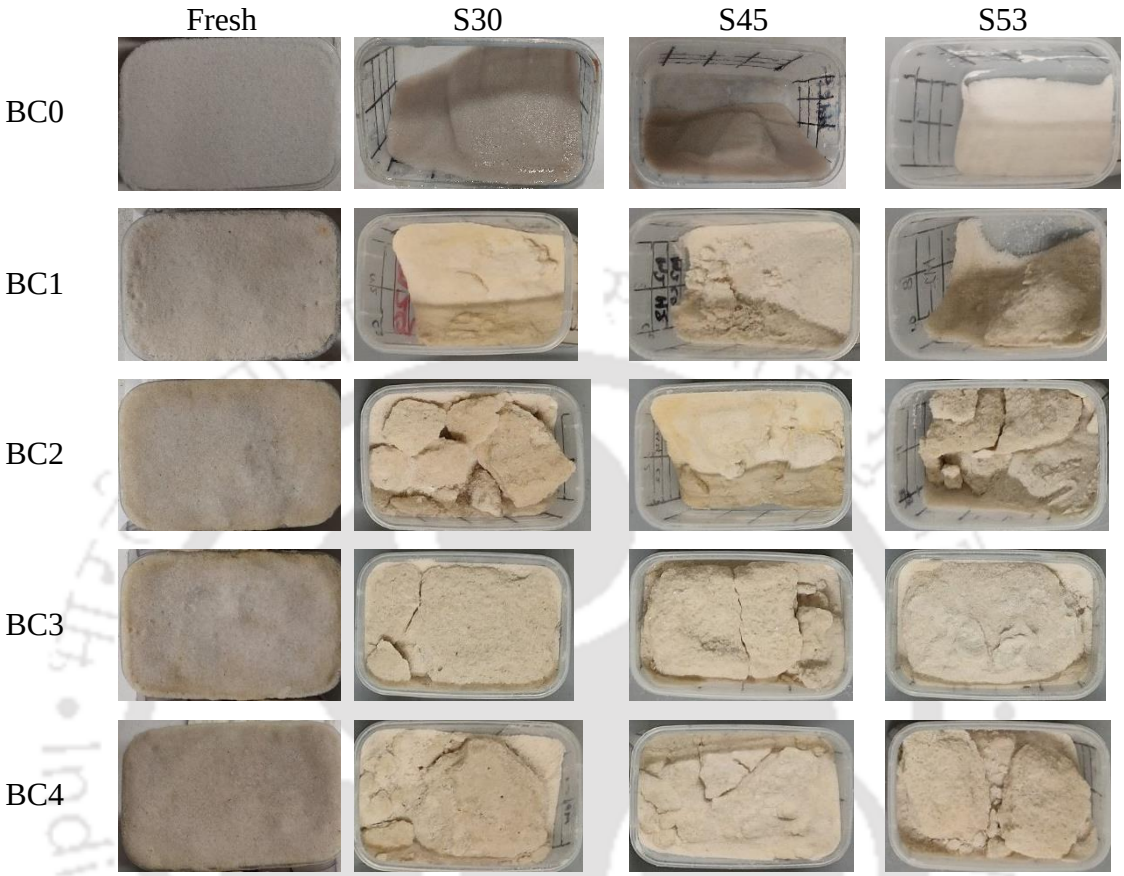

Figure 7.4 Biocemented samples at different slopes after erosion exposure.

Clarà Saracho et al. (2021) reported that the erodibility of biocemented soil is independent of calcium carbonate content in the higher ranges of precipitation. The study revealed that a 10-cycle treatment of 0.08 M cementation solution ceased the erosion in a tangential flow ranging from 0.033 to 0.185 m/s. The biocemented samples were recognised to erode in block failure rather than particulate mode, as observed in the untreated specimen. Do et al. (2021) have also reported the formation of brittle chunks and erosion of agglomerated clusters rather than smooth particle transport while investigating scour mitigation for soil treated with 0.25 M cementation solution (Ca^{2+}) with an injection strategy against a surface flow velocity of 0.25 m/s for a 20-hour test

duration. In another study by Jiang et al. (2019), the samples were tested against rainfall intensity of 300 mm/h. The sample treated with a 2 M cementation solution was found to be ineffective in controlling erosion. Considering the findings from the previous studies, we have considered a repetitive treatment of up to four cycles with a cementation solution of 0.5 M. The spraying strategy was adopted, considering a pragmatic approach for field application. Moreover, the bacteria were resupplied after each cycle of cementation solution to maintain effective and uniform $CaCO_3$ conversion. However, when the samples were tested against a tangential current ranging from 0.06-0.62 m/s, it was observed that the sample cracks propagate in the direction of flow and the dislodged biocemented chunks are transported almost immediately, which indicates that although the current-induced erosion can be restricted up to a great extent with a biocemented crust, it cannot be ceased entirely.

7.2.2.2 Performance of biopolymer and bio-cement composite

The biopolymer spray treated samples BP1, BP2, and BP4 were evaluated first. With the visual observation during the flume erosion test, a sheet-like layer of biopolymer treated soil getting eroded at amended critical velocity was observed, as illustrated in Figure 7.5.

Figure 7.5 Photographs of the dislodging sheet-like biopolymerised layer.

The evaluated D and E_R values for the bio-composite samples against the designed hydraulic current are plotted in Figure 7.6 (a, b). The maximum D values were found to

be 22, 21, and 17.5 mm for BP1, BP2, and BP4, respectively, at a flow velocity of 0.62 m/s. The maximum D value for untreated sand (BC0) was observed to be 23 mm at a flow velocity of 0.52 m/s. The corresponding maximum E_R values for samples BP1, BP2, and BP4 were 283, 250, and 218 mm/h, respectively, at maximum P_S value (≈1kW/m^2). Although the reduction in D values was observed to be marginal with the repeated biopolymer sprays for samples BP1, BP2, and BP4, the v_c required for soil erosion improved with the increase in biopolymer content considerably. The flow required to trigger the erosion process in BP4 was around 228% higher in comparison with the samples BP1 and BP2. For samples BP1 and BP2, the erosion was triggered at a flow velocity of 0.127 m/s, whereas for sample BP4 the erosion was triggered at 0.29 m/s. However, once the biopolymer layer was dislodged, the soil eroded in the same manner as the untreated sample BC0, suggesting that the biopolymer treatment may not be effective at higher flow velocities.

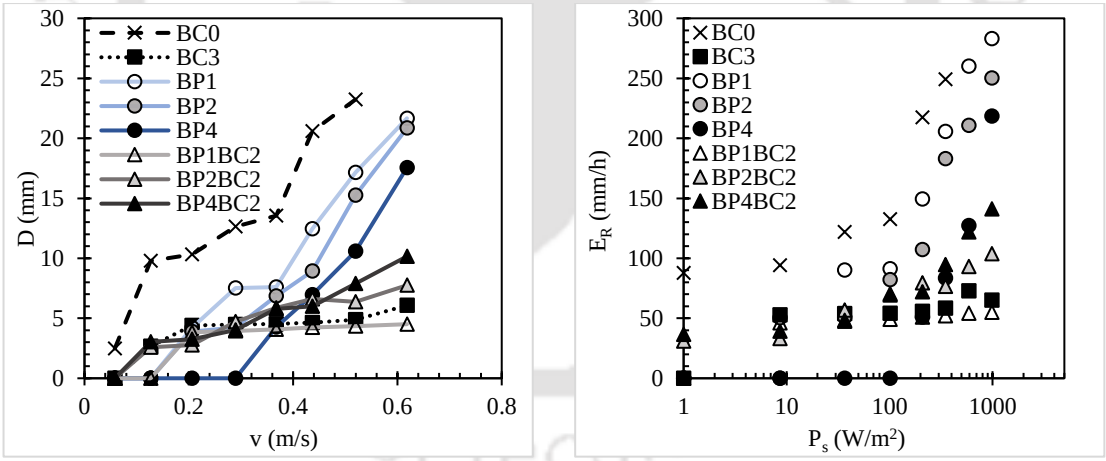

Figure 7.6 Cumulative eroded depths and erosion rate of biopolymer and bio-composite samples at slopes S53.

On the contrary, in all bio-composite samples, the erosion was initiated at a flow velocity of 0.06 m/s, except for sample BP1BC2, where the erosion was initiated at a flow velocity of 0.127 m/s. However, bio-composite specimens BP1BC2, BP2BC2, and

BP4BC2 were found to be more resilient as the maximum E_R values were significantly lower when compared to biopolymer treated samples. The failure of the sheet-like biopolymer layer was observed in bio-composite samples also, however, as the erosion is prevented due to the biocemented layer beneath. The maximum values of D for samples BP1BC2, BP2BC2 and BP4BC2 were observed to be 4.5, 7.75, and 10.15 mm, respectively. The corresponding maximum E_R values were determined as 55, 104, and 141 mm/h. The E_R values were observed to be minimum in the sample BP1BC2 (55 mm/h), which is lower when compared to samples BC3 (65 mm/h) and BC4 (71 mm/h). The samples BC3 and BC4 have calcite content of around 6.97% and 9.22%, while sample BP1BC2 possesses calcite content of around 5.6%. Therefore, it can be assumed that sample BP1BC2 outperformed sample BC3 and BC4, as lower quantities of reagents are required for bio-composite materials for producing an equally efficient erosion-resistant material, and this would also lead to a reduction in the quantity of generated ammonia. Samples BC3 and BC4 exhibited higher NPI of 16 and 26 N/mm in comparison to BP1BC2 (10.79 N/mm), indicating that even though the bio-composite material is a softer material compared to biocement, it can prevent soil erosion with equivalent efficiency.

In Figure 7.7, the photos of specimens post-flume erosion tests are illustrated. In the images post flume experiment, the specimens BP1, BP2 and BP4 are observed the same as the untreated sand. The biopolymer treated specimens are reported to lose more than 50% of their strength after one wetting-drying cycle (Ramachandran et al. 2021) at biopolymer concentrations ranging from 0.5% to 1.5% (by weight of the soil). As we used a significantly lower concentration of biopolymer (1g/l) and the biopolymer treated sample was continuously interacting with the flowing water, a drastic failure was anticipated once the stabilised layer was dislodged. In the case of the bio-composite material, negligible soil chunks were observed, suggesting that the bio-composite material

inherits the advantageous characteristics of the biopolymer and the biocement both. The stabilised soil matrix is less brittle than the conventionally biocement-treated samples.

Figure 7.7 Biopolymer and bio-composite samples at slope S53 post erosion exposure.

Overall, the flume test revealed the erosion mechanism of biocemented sand against the tangential current. Although the study presented valuable insights, there were several restrictions to implicating the results in the field directly. Only one type of soil was used in this study, considering a particular bank site of the Brahmaputra River. In the field, complex soil exists, including different proportions of sand, clay and gravel. Moreover, the current coexists with waves and turbulence in Nature, which has not been considered in the present study. Another crucial point to consider for future studies is the scaling effects taking the geometric scaling into account and fulfilling the Froude ratio for designing procedures (Aminoroayaie Yamini et al. 2019).

7.2.2.3 Eroded weight of treated soil samples

The eroded weights of the treated soil with different techniques are reported in Figure 7.8. The soil mass loss data is consistent with the presented erosion characteristics. In Figure 7.8 (a), it is evident that the soil mass loss is affected adversely by the increase in slope. Whereas with the increase in the biocementation level, the soil mass loss decreased for all the slopes. The mass loss for the control soil at slopes S30, S45, and S53 was evaluated to be around 56%, 78%, and 86%, respectively, which reduced around four-

fold for BC3 with values of 12%, 19%, and 22% corresponding to slopes S30, S45, and S53, respectively. However, the increased eroded weight for sample BC4 was recorded as 20%, 27%, and 30% for slopes S30, S45, and S53, respectively, which can possibly be attributed to the block failure of the developed crust caused by the propagation of tangential cracks.

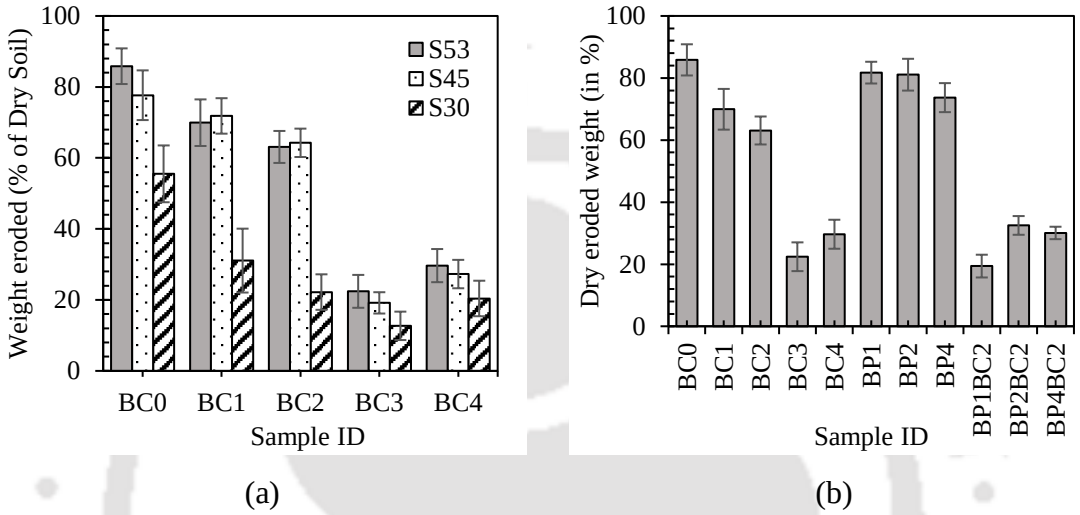

Figure 7.8 Dry eroded weight (%) of the biocemented samples: (a) At various slopes; and (b) Comparison of biopolymer, biocement and bio-composite treated samples at slope S53.

Figure 7.8 (b) shows the soil mass loss in the case of bio-composite samples against hydraulic current-induced erosion on slope S53. The total dry eroded weight of samples BC0, BC1, BC2, BC3, and BC4 is 86%, 70%, 63%, 22%, and 30%, respectively, which shows significant improvement in the erosion resistance of the biocemented soil with the increase biocementation levels. The biopolymer-treated samples BP1, BP2, and BP4 yielded an erosion of 82%, 81%, and 73% of soil, respectively, showing negligible improvement in the erosion resistance of the treated soil. However, the improvement in terms of critical velocity has been observed too. The soil mass loss in bio-composite samples BP1BC2, BP2BC2, and BP4BC2 due to the hydraulic current was observed as

19%, 32%, and 30%, respectively. The minimum soil mass loss was recorded for bio-composite sample BP1BC2, which is comparable with biocement-treated specimen BC3.

7.2.3 Microstructure analysis of treated soils

The SEM images of treated soil samples are illustrated in Figures 7.9 and 7.10. In Figures 7.9 (a, d), the SEM of sample BC1 is shown. With the lower magnified image, rhombohedral mesocrystals of calcium carbonate in the grooves and around the sand grains are observed. These clusters of precipitated calcium carbonate lacked effective bridging over the sand grains, as shown in the image with higher magnification, i.e., Figure 7.9 (d). The presence of the calcium carbonate bridges and their location is critical for the effective bonding of soil grains to improve the mechanical properties of the soil (Cheng et al. 2013a; Porter et al. 2017b). Figure 7.9 (b, e) represents the low and high-magnification SEM images of sample BC2. With these images, the initial phase of calcium carbonate bridging is emphasised. Moreover, bacterial imprints were observed in the image shown in Figure 7.9 (e), confirming the biogenic precipitation of calcium carbonate and the role of bacteria as nucleation sites (Stocks-Fischer et al. 1999). In sample BC3, the bridging of sand grains with the heavy biocementation (BC3) was observed, as shown in Figure 7.9 (c, f).

The microstructural images of treated soils are consistent with the results of the flume erosion tests and needle penetration tests. As the effective bridging was absent from the soil matrix of sample BC1, it did not exhibit improvement in erosion resistance. However, as the mesocrystals contribute to enhancing the packing and friction of the soil matrix, improvement in the needle penetration index was detected. Whereas the initiation of grain bridging was observed in sample BC2, contributing to a notable improvement in the needle penetration and flume erosion resistance. As the grains of sample BC3 were

well-packed with the biocement, the sample performed as the most resilient against fluvial erosion.

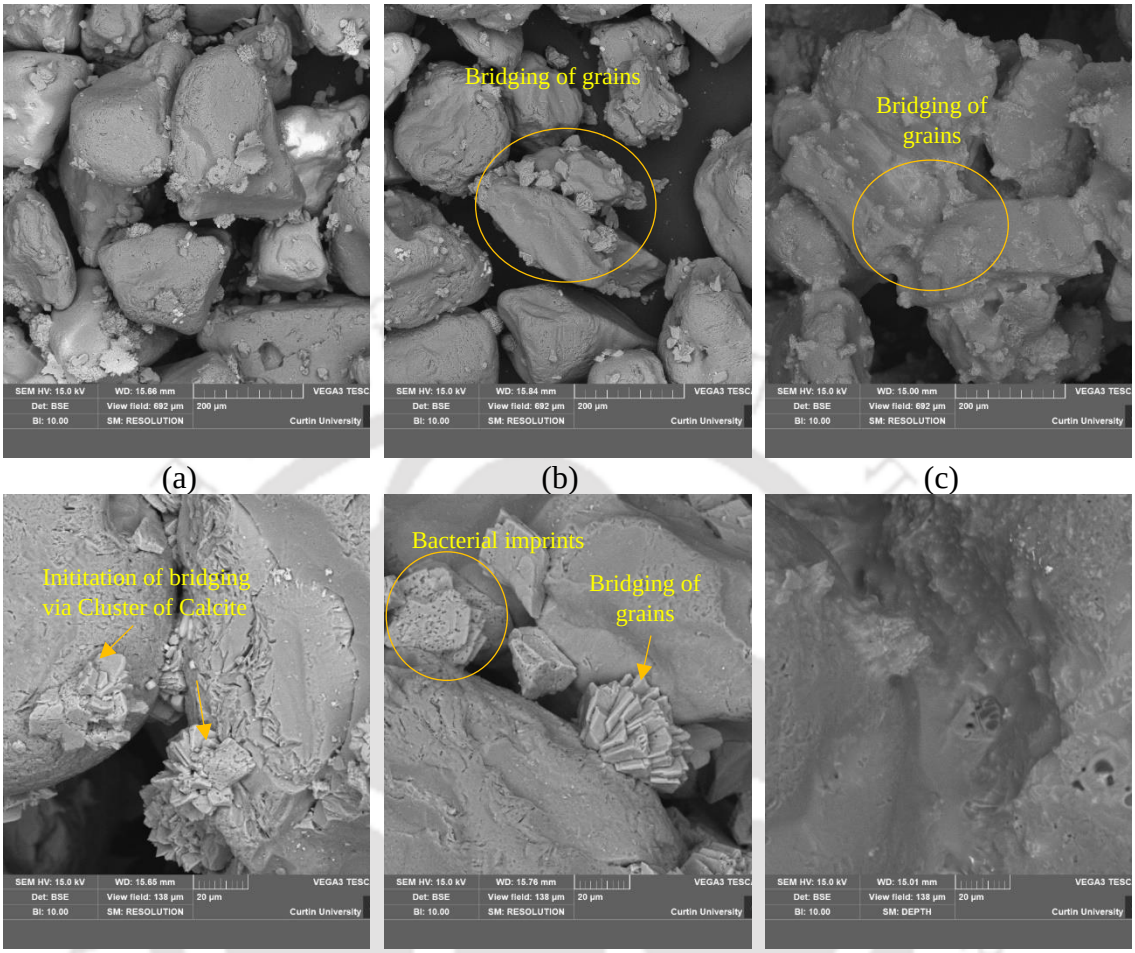

Figure 7.9 SEM images of treated specimens: sample BC1 (a, d); sample BC2 (b, e), sample BC3 (c, f).

Similar to sample BC3, sample BC4 was also observed to be covered in the biocement, as shown in Figure 7.10 (a, c). The clusters of calcium carbonate crystals were visible at the edges of sand grains, as shown in Figure 7.10 (c). The polymer addition in the bio-composite material is expected to support urea-hydrolysis-based biocementation (Wang et al. 2018a). In the bio-composite samples BP1BC2, the collaborative influence of the biopolymer and biocement treatment was detected, as shown in Figure 7.10 (b, d). The sand grains were bridged together with the biopolymer strings and anchored with

calcium carbonate, which validates the idea of the bio-composite material taking advantage of both the biocement and the biopolymer.

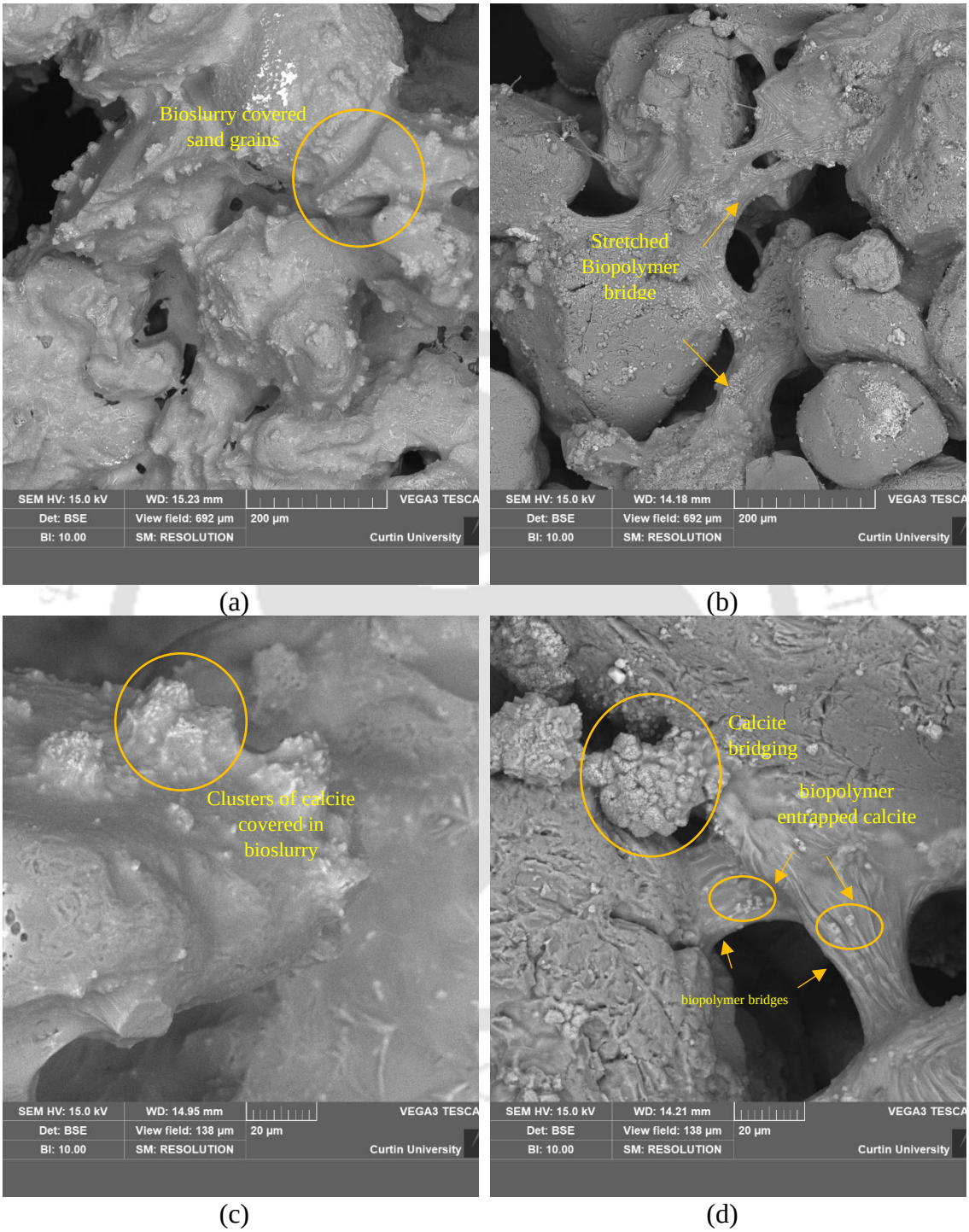

Figure 7.10 SEM of treated specimens: sample BC4 (a, c); and sample BP1BC2 (b, d).

The elemental composition and mineralogy of treated soil specimens were scrutinised with Energy-dispersive X-ray spectroscopy (EDS) and X-Ray diffraction

(XRD). The EDS analysis of the treated soil sample BC3 revealed the abundance of silicon and oxygen at spectrum 1, suggesting the predominance of silica, as shown in Figure 7.11 (a, c). The elemental analysis at site 2 treated soil samples revealed the presence of calcium, carbon, and oxygen, as shown in Figure 7.11 (d). The presence of calcium carbonate bridges at the acute corners of sand grains is a topologically optimal configuration to prevent the dislodgement of sand particles due to intergranular slip or rotation (Porter et al. 2017a).

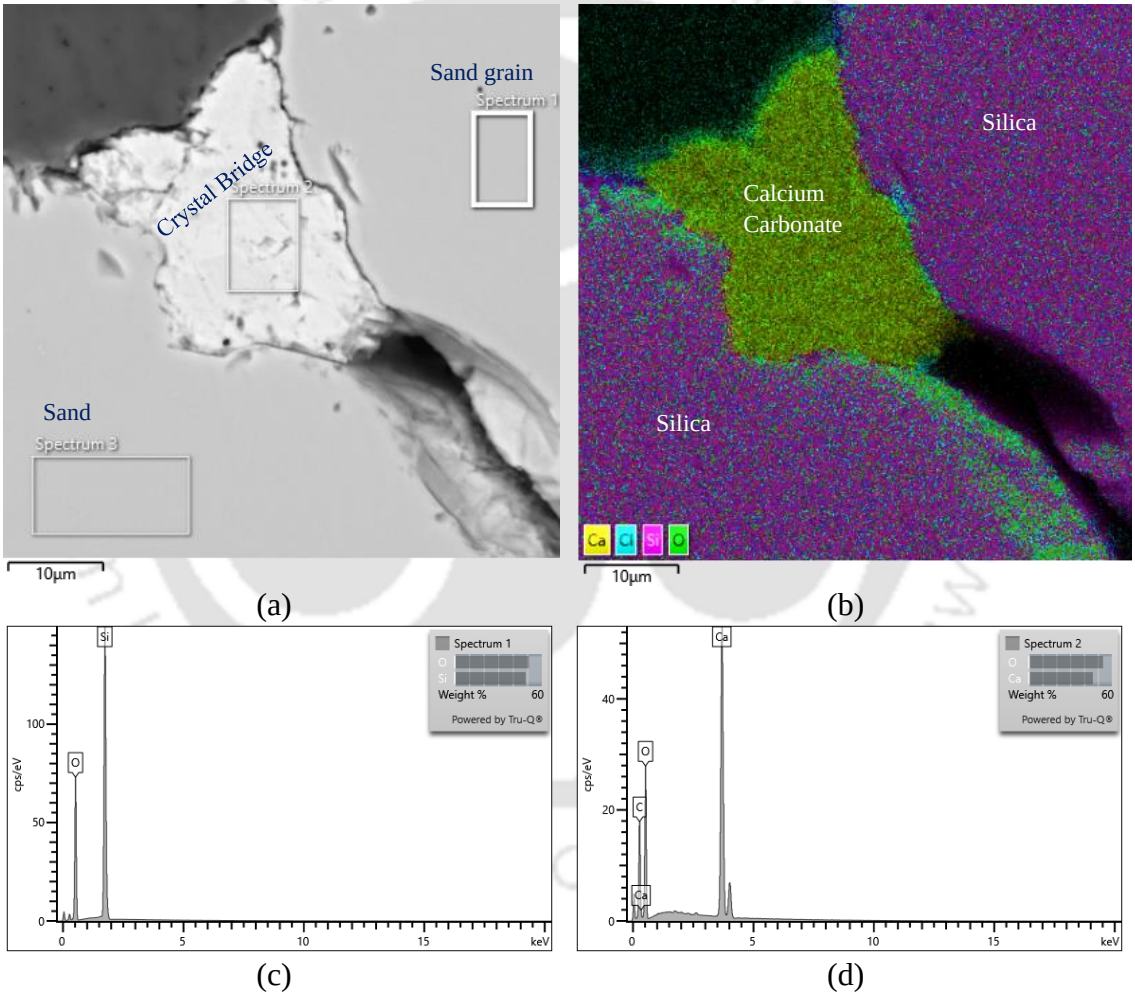

Figure 7.11 ESD maps and spectrum of sample BC3.

The XRD plots of samples BC3 and BP1BC2 in comparison with the untreated sand (BC0) are presented in Figure 7.12 (a, b). The XRD analysis confirmed the

predominance of quartz (Q) and the absence of calcium carbonate (C) in the untreated sand. Noticeable peaks corresponding to calcite were observed in samples BC3 and BP1BC2. One of the major peaks responded to calcite, C(104), at a 2θ value of 29.4° (Wen et al. 2020).

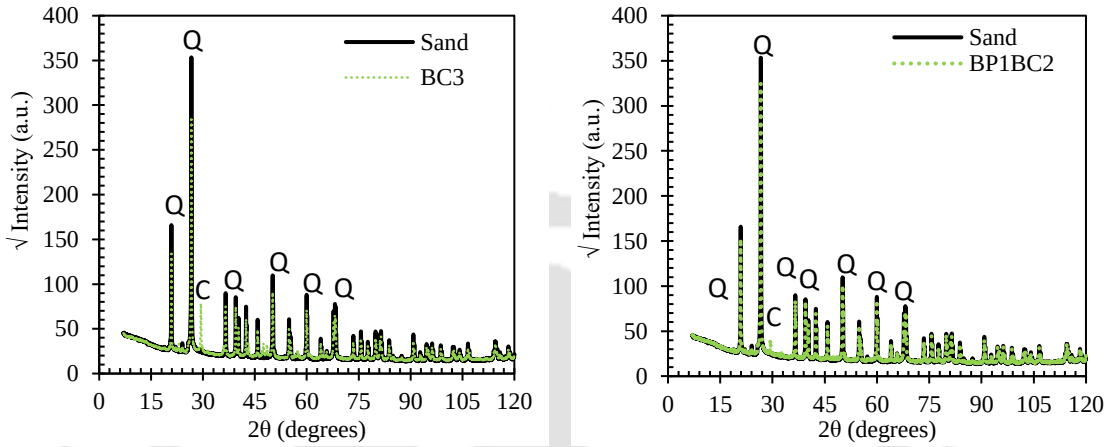

Figure 7.12 XRD plots of treated samples BC3 and BP1BC2.

7.2.4 Generation of Ammonia

The experiments suggest that biocementation has a great potential to control hydraulic-current-induced erosion for field application. However, the ureolytic reaction generates ammonia which can be harmful. The acceptable limit of ammonia in the surface water is recommended as 17mg/l for acute exposure and 1.9 mg/l for chronic exposure to protect the aquatic life in the freshwater (USEPA 2013). Thus, ammonia generation vis-à-vis erosion resistance achieved is calculated. The kg (kilograms) of ammonia produced per kg of soil retained for various specimen treatments is presented in Figure 1. The percentage of soil retained is also presented for comparison. It can be seen that among the biocemented samples, BC3 has the least ammonia generated. This is due to the higher resistance to erosion in the case of BC3. It may be recalled that BC4 had lower resistance

to erosion due to brittle fracturing. The bio-composite BP1BC2 outperformed BC3. It generated 36% less ammonia than BC3. Thus, a bio-composite with a judicious proportion of biocement and biopolymer is likely to offer the best erosion resistance with the least risk of harming the river ecology.

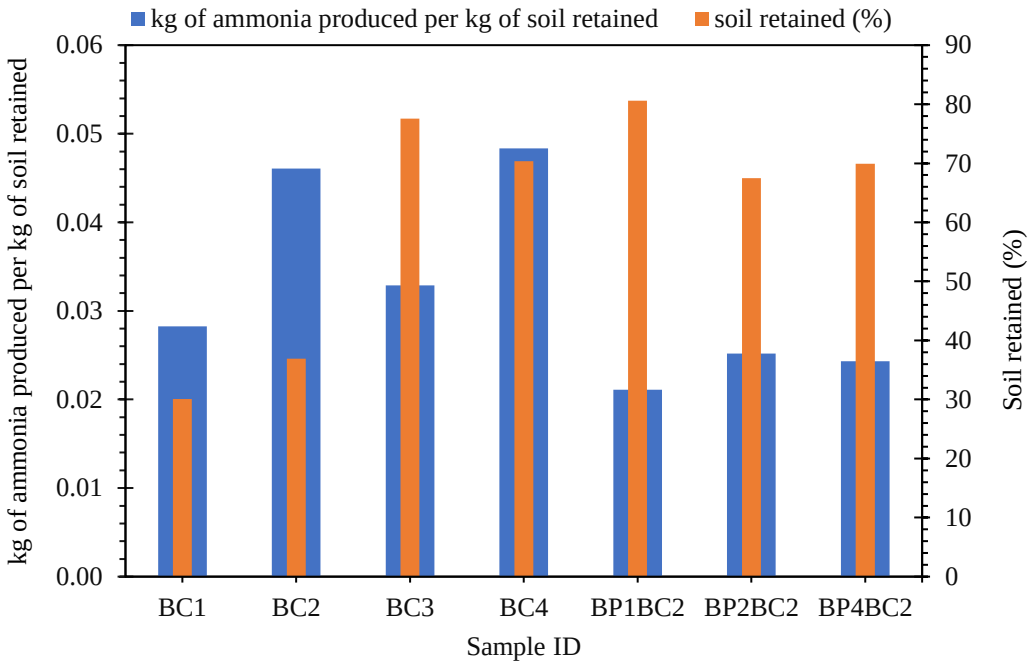

Figure 7.13 Comparison of ammonia generated (%) by weight of retained soil for treated soil specimens.

It must be noted that the biopolymer (xanthan gum) is biodegradable. However, previous studies have reported that the rate of degradation by biological activity is quite slow (Lee et al. 2019b). The biopolymer was selected based on the rationale that it can provide a micro-ambient environment to the microbes in terms of long-term moisture retention (Wang et al. 2018a) and complex carbohydrate availability for their survival. Moreover, the biocement precipitated by the microbes after the biopolymer application is expected to make the bio-composite treatment more durable. The concentration of the proposed preapplication of xanthan gum powder was 1g/l for the bio-composite treatment, which provides it with a water-like consistency for permeation in soil media via a spraying

strategy for field application. The proposed application is for in-situ application via spraying strategy, where the existing soil can be improved without the disturbing it. On the other hand different types of fibres have also been reported to improve MICP treatment significantly (Spencer et al. 2020; Liang et al. 2022), but these kinds of applications are suited more toward geotechnical applications needing soil replenishment and/or replacement, such as embankments and highways subgrade.

7.3 Summary

This investigation addresses the challenge of riverbank erosion through an environmentally benign biogenic stabilisation. A flume test was designed to study erosion at riverbanks due to hydraulic current and its potential mitigation with bio-based stabilisers. Biocement, biopolymer, and their combination resulting in a bio-composite have been investigated. The erosion resistance of sand equivalent to the Brahmaputra riverbank material was improved by the treatment. The native bacterium BS3 was utilised for biocementation. The use of the native bacterium in the field leads to selective biostimulation that combines the advantages of bioaugmentation and biostimulation. A bio-composite material prepared with low-viscosity biopolymer and biocement is tested for its efficacy against hydraulic erosion for the first time with the aim of alleviating the environmental impact by minimising the production of ammonia and maximising erosion resistance. The following major findings can be drawn from the results of the present study:

- The needle penetration indices of the treated samples were found to be linearly dependent on the calcium carbonate content within the experimental range for the used fine sand. The proposed equation should be useful to monitor the biocementation process in the field and predict the quantity of calcium carbonate precipitates non-destructively.

- The results demonstrate a promising control over soil erosion with the increase in biocementation levels. An approximately four-fold reduction in erosion rate was observed for biocemented samples BC3 and BC4. Up to 6.97% of calcium carbonate content, the erosion resistance improved consistently with the increase in the biocementation levels. However, in the case of BC4, the sand broke down into fragments. Thus, beyond the limit of cementation, brittle fragmentation is expected.
- The application of low-viscosity biopolymer solution via spraying strategy was intended to provide immediate stability against hydraulic erosion. It is observed that the critical velocity required to erode biopolymer-treated samples improves considerably. However, once the sheet-like biopolymerised layer is dislodged, the soil erosion rate is found to be equivalent to the untreated sand.
- The bio-composite sample outperformed the biocemented or biopolymer samples. Moreover, the bio-composite produces 36% less ammonia stoichiometrically than an equally efficient biocemented sample. This implies that the application of biopolymer along with biocementation not only assists in the survival of bacteria and managing the brittleness of the soil matrix but also reduces ammonia generation. The synergy of biopolymer and biocement in the bio-composite specimens is confirmed in SEM imaging.

It must be noted that biopolymer is biodegradable in nature. The durability of the proposed treatments must be investigated in future studies. A large-scale test is necessary to validate the efficiency and viability of the proposed technique in terms of cost-efficiency, performance, and durability in real-field conditions. The proposed selective biostimulation needs validation through bacterial community dynamics studies

7.4 Conclusion

In this objective, incremental levels of biocement treatment of sand were investigated for their local strength and erosion characteristics. It was observed that the needle penetration strength improved consistently with the number of treatment cycles; however, the erosion resistance is adversely impacted for samples with $CaCO_3$ content above 7% due to brittle fragmentation. The brittle fragmentation could be attributed to heterogenous precipitation or indued brittleness in the soil matrix at higher $CaCO_3$ content. Therefore, a biopolymer-biocement composite was devised with a preapplication of low-viscosity Xanthan Gum solution, which helped to anchor microbes due to the ambient micro-environment. The bio-composite exhibited promising erosion resistance with lower biocementation cycles resulting in lesser ammonia and quantity of materials required.

It is to be noted that in rivers, erosion occurs due to tangential flow. However, during high tides and flooding, waves also accompany the tangential flow. Moreover, coastal erosion occurs due to waves attacking perpendicular to the shoreline. The proposed techniques can be further tested against such scenarios.

CHAPTER 8

EVALUATION OF BIOCEMENT, BIOPOLYMER, AND THEIR COMPOSITES FOR MITIGATION OF HYDRAULIC WAVE INDUCED SOIL EROSION

8.1 Introduction

The increased frequency of extreme weather events has made the conservation of riverbanks and coastlines a global concern. Natural soil erosion of coasts and riverbanks is a complex phenomenon that occurs with the interaction of currents, waves, tides and wind (van Rijn et al. 2007). Soil erosion occurs due to several factors, such as internal hydraulic pressure (internal erosion), current as experienced in riverbanks (current erosion) as well as waves as in seacoasts (wave erosion). Generally, they have been studied separately. To simulate coastal conditions, laboratory tests have been performed in hydraulic flumes by estimating soil erosion against perpendicular waves (Skafel and Bishop 1994; Faure et al. 2010; Gu et al. 2020; Kou et al. 2020; Shahin et al. 2020; Liu et al. 2021b). In the case of riverbank erosion, bridge scours, and earth-filled embankment dams, a tangential current without waves has been employed (Wang et al. 2018a; Clarà Saracho et al. 2021). In reality, a complex interaction of current and wave erosion is experienced. When the waves hit the coastline at an oblique angle, nearshore wave breaking produces shore parallel current (Ashton et al. 2002), while in the riverbanks, the shallow waves coexist with tangential current (Das et al. 2020). Therefore, it is crucial to consider both forms of erosion for its successful mitigation.

The present chapter evaluates biocemented soil against both current and wave loads. Two sets of experiments with perpendicular waves and tangential waves in conjunction with current have been conducted. For scaling the experimental results up to field conditions, the excitation parameters must be quantified in a judicious way. In this investigation, the cumulative erosion rates of different levels of biocemented sand slopes have been plotted against the total wave energy density. The plots are of much importance for achieving soil

stabilisation for a specific field condition. In addition, the level of stabilisation of the soil has been estimated through a needle penetration test that can be applied in the field. Moreover, the biopolymer-biocement composite has been compared with the standard biocementation for its efficacy in preventing wave-induced erosion. The average erosion rates are correlated with Needle Penetration Index (NPI) within the viewpoint of potential field application. A summary of the conducted experiment has been illustrated in Figure 8.1.

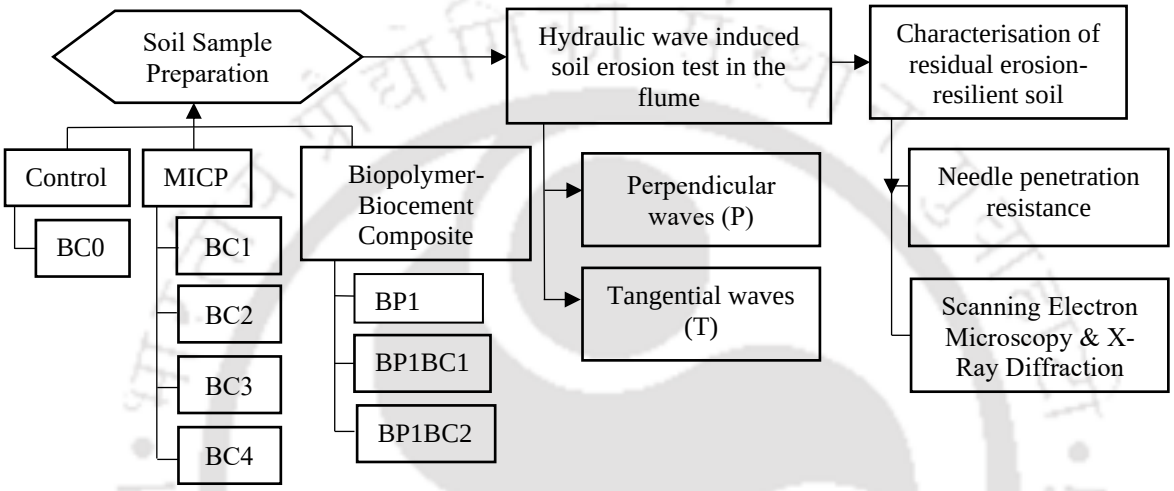

Figure 8.1 Experimental summary to investigate mitigation of wave-induced erosion with biocementation and bio-composite treatment

8.2 Results and Discussion

8.2.1 Flume erosion test

8.2.1.1 Performance of biocemented sample

Figure 8.2 (a) shows the percentages of soil volume eroded (V) with the increasing energy density of the perpendicular waves (E_D). The corresponding cumulative erosion rates (E_R) are shown in Figure 8.2 (b). The graphs are plotted until either 65% of the volume is eroded or the maximum wave energy is reached. The threshold E_D is defined as the wave energy density at which soil erosion initiates.

The biocement treatment prevents erosion till the wave energy reaches to threshold E_D. Once the threshold E_D is reached, soil erodes rapidly. Eventually, the soil loss plateaus and the

biocemented specimen takes a shape that minimises the impact of waves. Another possible reason for plateauing might be that the weakly biocemented grains at the top surface got eroded first as they were continuously disturbed due to the multiple spraying of treatment solutions. Therefore, the soil volume loss and cumulative erosion rates exhibit the S shape curve for most of the specimens against the applied wave energy.

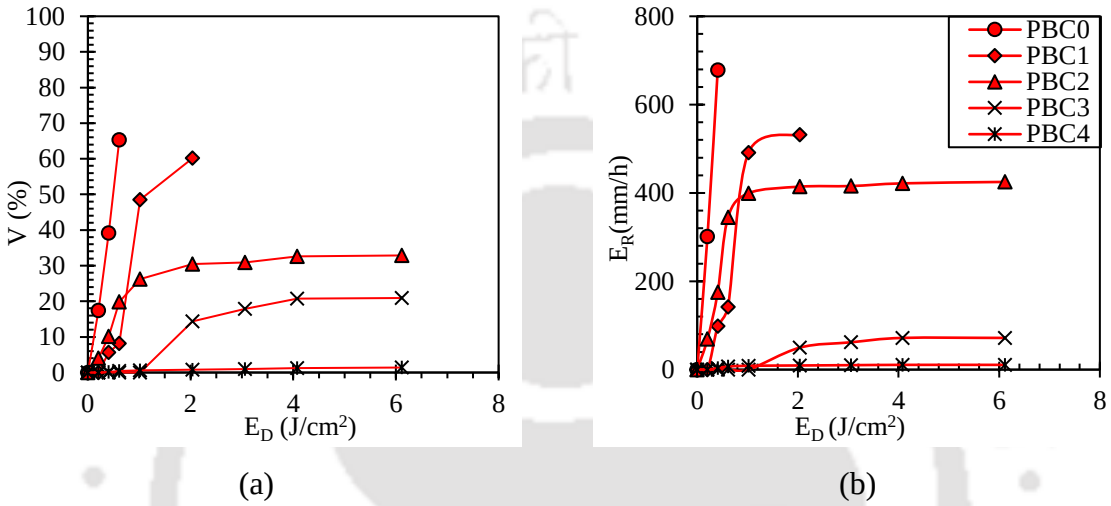

Figure 8.2 Comparison of (a). Percentage volume eroded and (b). Cumulative erosion rates for different levels of the biocemented soil against perpendicular waves.

The untreated sample PBC0 lost 65% of mass at a low E_D (0.6 J/cm^2). Thus, unstabilised sand has a high rate of erosion, as shown in Figure 8.2 (b). The rate of erosion is reduced substantially with biocementation. The threshold E_D goes higher with increasing cementation. For the same E_D (0.6 J/cm^2), PBC1, treated with the lowest level of biocementation, had only 8% erosion. Thus, even with a relatively low biocementation, erosion from a moderate E_D can be mitigated. However, with increasing E_D, the sample experienced an increasing rate of erosion. Finally, it lost 65% of its volume at E_D 2 J/cm^2. Thus, it is clear that higher levels of cementation would be required as wave energy increases. In comparison, PBC2 lost only 32% of its volume when the maximum E_D of around 6 J/cm^2 was reached. The maximum rate of erosion (E_R) for PBC2 was observed as 421 mm/h as compared to 524 mm/h in PBC1. Sample PBC3 exhibited a maximum of 21% V with a much-reduced E_R value of 71 mm/h. For sample

PBC4, there was negligible erosion. Sample PBC4 exhibited a maximum V of only 1.4% with E_R of 10.7 mm/h. It is evident that a biocementation of sand for a target erosion control can be designed.

The V and E_R values against E_D for the tangential waves are plotted in Figures 8.3 (a) and (b). Although the nature of the curves was similar to that of the perpendicular waves, there are significant differences. TBC0 lost more than 65% of its volume at a low E_D of 1 J/cm^2. TBC0 displayed a high erosion rate of around 338 mm/h. At the same E_D, the eroded volume of samples TBC1, TBC2, TBC3, and TBC4 were observed as 38.9, 37.5, 30, and 19%, respectively. Thus, biocementation is effective against the tangential flow as well. However, in this experiment, tangential waves caused a higher level of erosion than the perpendicular waves for the corresponding level of wave energy. This is due to the drag force exerted on the sample by the tangential wave. This force creates shear stress on the samples, which tends to dislodge their upper crust.

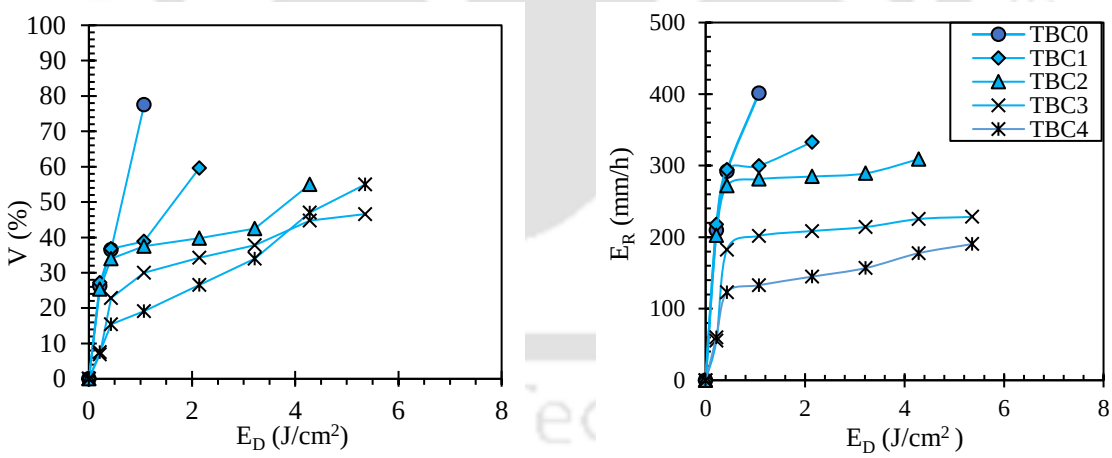

Figure 8.3 Comparison of (a). Percentage volume eroded and (b). Cumulative erosion rates for different levels of the biocemented soil against tangential waves.

TBC1 exhibited a maximum V of 60% at a twofold E_D. TBC2 was significantly more erosion resistant than TBC1. TBC2 lost around 55% of its volume with E_R of 284 mm/h at a fourfold E_D than TBC1. TBC3 and TBC4 endured the maximum designed E_D of 5.3 J/cm^2. The

total eroded volume for TBC3 was observed to be 46% at the maximum E_D. Interestingly, TBC4 lost 9% more volume than TBC3 despite having the highest level of biocementation treatment. Clarà Saracho et al. (2021) and Do et al. (2021) state that the samples may become brittle after a threshold level of cementation is crossed. This aspect is investigated in the next section by visually comparing the samples.

Photographs of biocemented samples post-erosion exposure are presented in Figures 8.4 (a-l). With the introduction of biocementation, the aggregation of sand particles can be easily identified in Figure 8.4 (f). PBC1 and TBC1 were identified with the lightly biocemented sand (LBS) aggregates. At this stage, although aggregation was observed on the surface of the specimens, it was not uniformly distributed. With the increasing number of treatments, a biocemented crust (C) was observed. TBC2 was observed to have a relatively thin crust, which was dislodged by the higher energy tangential waves. With the visual observation of the images of residual samples, it was noticed that the thickness of the biocemented crust increased. The increased crust thickness in PBC3 and PBC4 protected them from erosion to a great extent despite getting subjected to much higher E_D. Contrary to TBC2, the dislodgement of the deteriorated crust did not occur in PBC2 and PBC3, possibly due to the distinct nature of the impacting perpendicular waves. The perpendicular waves break upon hitting the soil, producing uprush and backwash currents. The uprush current detaches the weak soil grains, and the backwash current transports the detached grains with the induced drag (Ashton et al. 2002). On the other hand, in the case of tangential flow, the waves flowing over the fluvial current induce additional shear on the bank material, resulting in severe soil erosion. The eroded material is immediately transported by the tangential current. PBC4 exhibited negligible erosion confirming that in the case of perpendicular waves, the soil erosion decreased consistently with the increase in biocementation. Contrarily, TBC4 was observed to be more

weathered than TBC3. Brittle chunks of the cracked biocemented layers from TBC3 and TBC4 were observed to be drawn away with the tangential flow.

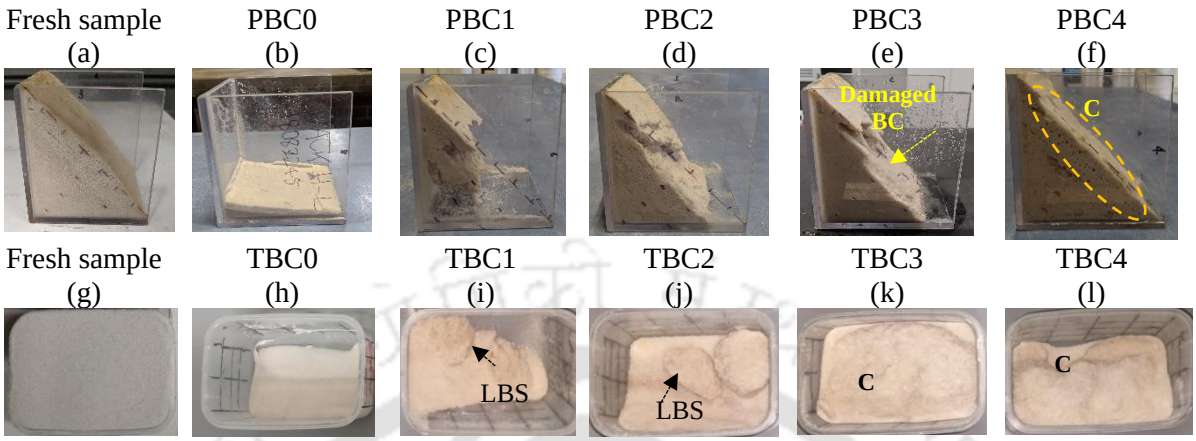

Figure 8.4 Biocemented soil samples post-erosion exposure against (a-e) perpendicular and (g-l) tangential waves.

The soil mass loss post-erosion exposure is reported in Figures 8.5 (a) and (b). The protection against soil loss improved with the increase in biocementation levels. PBC0 and PBC2 demonstrated a massive soil mass loss of around 90%. However, it is to be recalled from Figure 8.2 (a) that the required wave energy to erode the equivalent amount of soil was notably higher for PBC1 than PBC0. Thus, although light biocementation is effective for moderate waves, higher levels of treatment would be necessary against high wave energy. The soil mass loss receded with the increase in biocementation levels. PBC2 and PBC3 lost only 32% and 20% of soil mass loss. Soil erosion against the perpendicular waves was negligible (1.4%) after eight cementation cycles.

In the case of tangential waves, the soil mass loss for TBC0 was recorded at around 90%, the same as PBC0. However, the rest of the samples exhibited different responses against erosion. The soil mass loss for TBC2 and TBC4 was observed at around 75%. Minimum soil mass loss was recorded for TBC3 as 46% as the soil was protected with a thick biocemented crust, as illustrated in Figure 8.4 (k). TBC4 exhibited a mass loss of 57%, more than TBC3.

The increase in soil mass loss in TBC4 indicates that an increase in biocementation levels does not essentially lead to improvement in the erosion resilience of the soil in the case of the tangential flow.

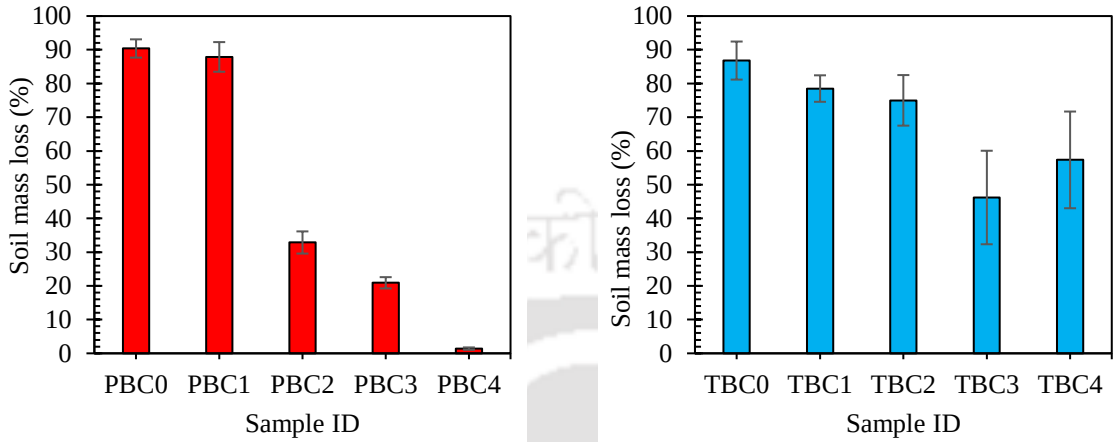

Figure 8.5 Comparison of soil mass loss with the various biocemented soil against (a). perpendicular and (b). tangential waves.

In previous studies on hydraulic wave-induced erosion, the erosion characteristic of the biocemented samples is reported in terms of soil mass loss and decline in the slope angle of the bank against the duration and number of erosional waves. Shahin et al. (2020) exposed biocemented sand to erosional waves of height 6.9 cm and wavelength 23 cm for two hours and reported less than 5% soil mass loss with a calcite content of 1.52%. Kou et al. (2020) have reported that the minimum soil erosion in terms of decline in slope angle at various slopes (10°, 20° and 35°) with a sample containing 30.1% calcite content in the residual soil against the hydraulic wave amplitude around 4 cm and frequency of 1 cycle per minute for a 30-minute test. On the other hand, Liu et al. (2021b) compared MICP with EICP (enzyme induced calcite precipitation) treated calcareous sand (98% carbonate) and reported that for a 2-hour duration of wave action of the height of 0.4 cm and 0.8 cm with a frequency of 2.2 Hz, both the treatments were inefficient to prevent long-term erosion on steep slopes. Both MICP and EICP samples were treated soils with two cycles of cementation solutions that failed when exposed

to the hydraulic waves for a longer duration. However, the calcite content was not quantified in the study. The inefficiency of the MICP and EICP to prevent erosion might be due to low $CaCO_3$ precipitation. In the present study, the samples treated with low levels of biocementation (BC1) also failed at a relatively low wave energy impact. Behzadipour and Sadrekarimi (2021) have employed biochar assisted biocementation for erosion mitigation on a physical model of riverbank slope of Karoon river, Iran against wave-action and demonstrated that a heavily biocemented sample treated with 20 cycles of cementation solution remained largely stable against the impact of 600 strong waves of height 7 cm and frequency two cycles per second. The features of waves such as wave dimension, frequency and test duration were different in the aforementioned studies, which is most likely the reason for the differences in the findings. This study is the first to report the erosion characteristics against the cumulative wave energy density, which could be a more practical parameter for designing the required levels of biocementation for erosion mitigation at the field. However, a field-scale trial is necessitated to verify the applicability of the proposed experimental findings.

8.2.1.2 Performance of biopolymer-biocement composite

The erosion characteristics of samples that received a biopolymer pre-treatment have been reported in Figures 8.6 and 8.7, along with the dotted lines denoting results with no such pre-treatment. In this case, the experiments were also halted either in case of 65% of the volume was lost or once the maximum wave energy was achieved. The curves followed a similar S pattern as in the case of MICP-treated specimens. However, the biopolymer-biocement composite treatment (continuous lines) was observed to be more resistant to soil erosion than the plain MICP treatment (dotted lines).

Figures 8.6 (a) and (b) illustrate the erosion behaviour of the bio-composite treated specimens against the perpendicular waves in terms of V (%) and E_R (mm/h) against E_D (J/cm^2). It was observed that the sample treated only with the biopolymer (PBP1) resisted erosion better

than PBC0. Thus, biopolymer treatment alone does improve erosion resistance. PBP1 lost 57.5% of its initial volume, with a high E_R of 489 mm/h at the E_D value of 2 J/cm^2. With the introduction of MICP treatment to the biopolymerised specimen, erosion was reduced substantially. PBP1BC1 and PBP1BC2 endured the maximum wave energy. Plateauing of erosion curves of PBP1BC1 and PBP1BC2 was also observed in this case; however, PBP1BC1 and PBP1BC2 were observed to outperform their counterparts, PBC1 and PBC2. PBP1BC1 eroded only 34% against the same wave energy. Most of the soil loss in PBPBC1 occurred against E_D, varying in the narrow range of 0.6 to 2 J/cm^2. After the E_D value reaches 2 J/cm^2, erosion almost ceases. Soil loss in PBPBC1 increased to 44% at the maximum E_D, clearly indicating the biopolymer-biocement composite treatment controls soil erosion. PBP1BC2 exhibited a fourfold reduction in the eroded volume in comparison with PBP1BC1. PBP1BC2 eroded only 11% of the total volume at the maximum E_D value of 6 J/cm^2. The corresponding E_R values reduced from 229 mm/h to 30 mm/h while comparing PBP1BC1 and PBP1BC2.

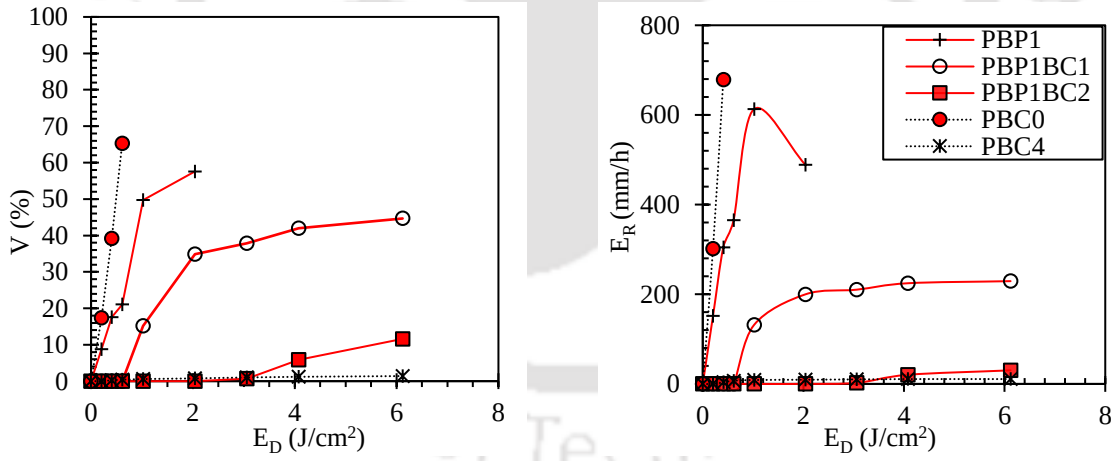

Figure 8.6 Comparison of (a). Percentage volume eroded and (b). Cumulative erosion rates for different levels of biopolymer-biocement composite treated soil samples against perpendicular waves.

These findings clearly demonstrate that the erosion resilience of PBP1BC1 and PBP1BC2 were significantly higher than their counterparts, PBC1 and PBC2. The erosion

resilience of heavily biocemented sample PBC4 was found to be comparable with the biopolymer-aided moderately biocemented PBP1BC2.

The erosion characteristics of the biopolymer-biocement composite treated specimens against the tangential waves are reported in Figures 8.7 (a) and (b). TBP1 was eroded around 65% of its volume at a low E_D of 1 J/cm^2, similar to the untreated sample TBC0, indicating that mere low-viscosity biopolymer treatment might not be enough to prevent soil erosion against high-energy tangential waves. Biopolymer stabilised (0.5% of soil weight) poorly-graded sand without any fine content has been reported to lose its strength after interaction with moisture (Ramachandran et al. 2021). A high E_R of 439 mm/h was observed in TBP1. Conversely, the soil treated with biopolymer-aided biocement exhibited considerably high erosion resistance. TBP1BC1 and TBP1BC2 lost around 13% of the initial volume at the E_D 1 J/cm^2, which is around one-fifth of that in TBC0 and TBP1. The erosion resistance of TBP1BC1 and TBP1BC2 surpassed the best-performing conventionally biocemented samples, TBC3 and TBC4. The Maximum V for TBP1BC1 was observed as 52.75% at the maximum E_D. TBP1BC2 exhibited a more than threefold reduction in erosion in terms of the total volume eroded when compared to TBP1BC1.

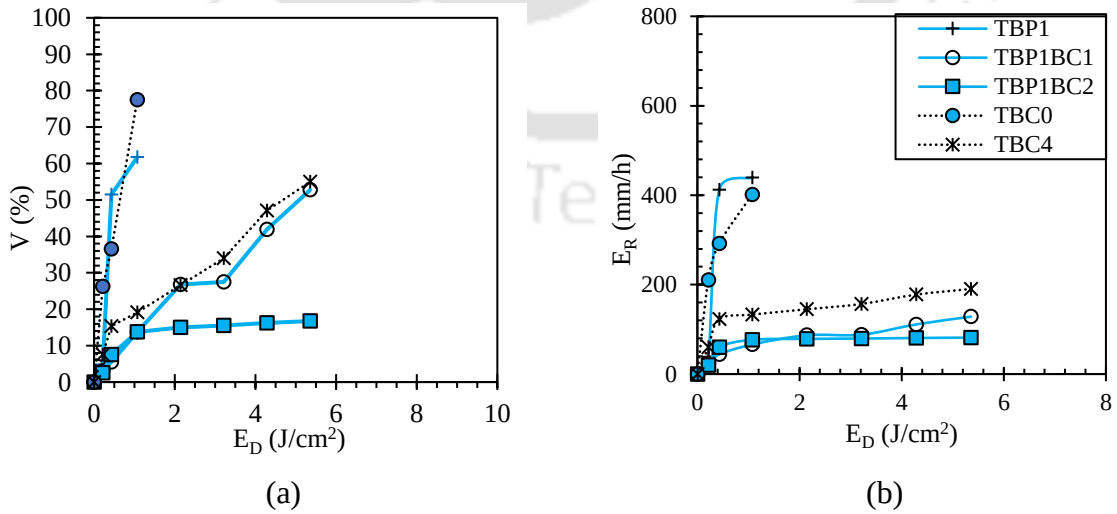

Figure 8.7 Comparison of (a). Percentage volume eroded and (b). Cumulative erosion rates for different levels of biopolymer-biocement composite treated soil samples against tangential waves.

The maximum V for TBP1BC2 was observed as 16.75% at the maximum E_D. The maximum E_R of TBP1BC1 and TBP1BC1were estimated as 128 and 81 mm/h. These observations clearly demonstrate the efficacy of biopolymer pre-treatment before MICP.

Figures 8.8 (a-h) are photographs of the samples before and after the erosion test. It is evident that biopolymer pre-treatment has prevented fragmentation, as observed in MICP samples. The biopolymer-biocement crust (BBC) is clearly more resilient than the biocement crust (BC). PBP1BC1 was damaged somewhat at high-energy waves (Figure 8.8 c). Comparatively, TBP1BC1 provided appreciable protection against erosion induced by the tangential waves. A thick protective BBC was observed for TBP1BC2 and PBP1BC2 samples, which resulted in marginal soil loss against the eroding waves.

A visual comparison between biopolymer-biocement composite treated specimens TBP1BC2 and plain biocemented specimens TBC2 from Figure 8.8 and Figure 8.4 indicates that comparatively, a more uniform distribution of carbonates happened in the biopolymer-biocement composite-treated specimens, which led to the development of a biocemented crust. On the other hand, the plain biocemented specimens TBC2 only exhibit aggregation of sand due to biocementation.

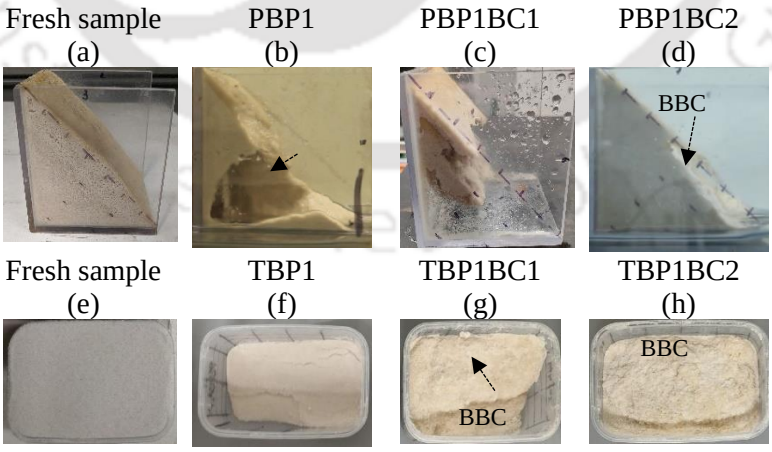

Figure 8.8 Biopolymer-biocement composite samples post erosion exposure against (a-d) perpendicular and (e-h) tangential waves.

It is to be noted that Wang et al. (2018a) have considered making the cementation solution in polyvinyl alcohol (PVA) to control the location of precipitation to the intended depth. In this study, instead of modifying the cementation reagent, the soil was supplemented with one pore volume of low-viscosity biopolymer solution (Xanthan Gum) prior to biocementation for the same purpose. However, further investigations are required to find the best approach to control the uniformity of $CaCO_3$ precipitation. Different biopolymers at varying viscosities must be investigated to determine the best suitable combinations for the biopolymer-biocement composite. Continuous application of low-concentration biocementation reagents along with bacterial solution employing irrigation like micro-sprinkler spraying system is suggested for future studies. Continuous micro-sprinkler spraying systems are often used in irrigation (Zhang et al. 2020) to supply the water uniformly to the field, which might also be suitable for a field-scale MICP application.

The performance of the biopolymer-biocement-treated specimens in terms of soil mass loss is reported in Figure 8.9. The soil mass loss observed for PBP1, PBP1BC1, and PBP1BC2 were 76, 62 and 24%, whereas the observed soil mass loss for TBP1, TBP1BC1, and TBP1BC2 were 83, 45, and 21%.

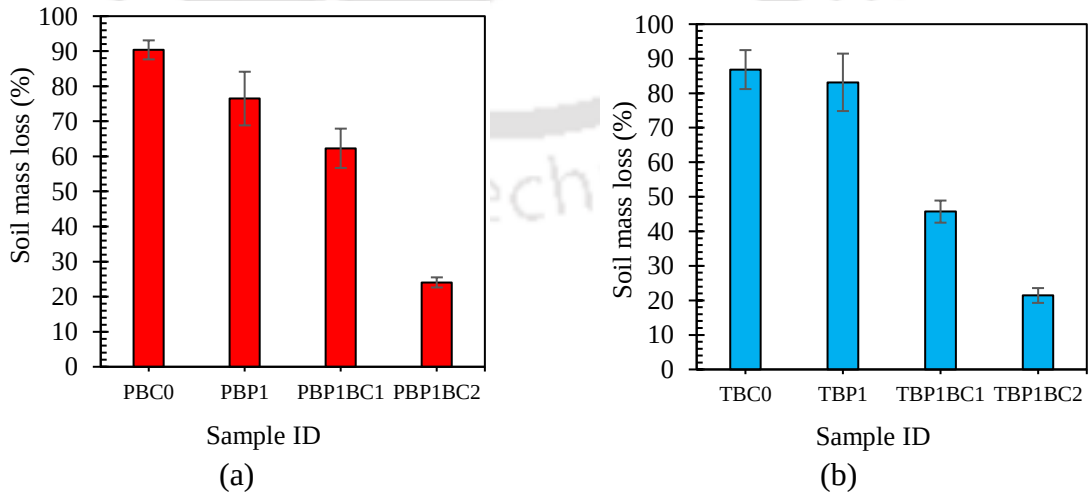

Figure 8.9 Comparison of soil mass loss with the various biopolymer-biocement composite soil against (a). Perpendicular and (b). Tangential waves.

From Fig. 8.9, it is evident that with the biopolymer-biocement treated soil samples, the erosion resilience improved consistently with the increase in MICP levels. It may be recalled that with MICP treatment alone, brittle behaviour was observed in the case of a relatively high level of biocementation. Such behaviour was avoided with biopolymer pre-treatment.

Apart from the enhanced erosion resistance, there are several other benefits of using the biopolymer as an aid to conventional biocementation. Application of biopolymer would be helpful to substantially reduce the required materials' quantity, associated cost and environmental impact of the conventional biocementation. The bio-composite material has been reported to produce 36% less ammonia for an equally efficient erosion-resistant biocemented specimen against the hydraulic current varying from 0.06 to 0.62 m/s. In this study, the authors observed that stoichiometrically, only half of the biocementation reagents would be required for the best performing biopolymer-biocement composite treated specimen (PBP1BC2) in comparison to the best performing MICP treated specimen (PBC4) with similar performance for erosion control. Theoretically, it will also reduce the generation of harmful by-product ammonia by 50%, making the proposed biopolymer-aided biocementation treatment a preferred alternative over the conventional MICP. In the case of tangential waves, 33.33% lesser chemical reagents would be required for preparing TBP1BC2, considering TBC3 the best-performing soil specimen. Interestingly, a threefold erosion-resilient material will be produced with TBP1BC2 in comparison with TBC3, considering the total volume eroded (V).

8.2.2 Needle penetration index of residual specimens

The needle penetration index (NPI) values of the residual samples are presented in Figures 8.10 (a) and (b). As the samples for both sets were treated with the same methodology,

comparable NPI values for the counterparts were expected. The NPI values for samples prepared for perpendicular setup (PBC1-PBC4) varied from 9 N/mm to 21 N/mm, respectively. The NPI values for samples prepared for tangential setup (TBC1-TBC4) were found in a range of 5.5 to 21 N/mm, respectively. A notable difference was observed only in TBC1 and PBC1, which could possibly be due to the use of residual samples that have undergone different wave actions. Biopolymer-biocement composite-treated specimens displayed NPI in a similar range to the equivalent biocemented specimens. Negligible NPI values were recorded for TBP1 and PBP1, indicating that the biopolymer in the present concentration does not contribute to improving the stiffness of the soil. PBP1BC1 and PBP1BC2 exhibited NPI values of 10.58 and 15.38 N/mm. At the same time, the NPI values for TBP1BC1 and TBP1BC2 were evaluated as 10.3 and 14.63 N/mm. It is well known that the polymer has a considerably lower elastic modulus in comparison to either sand or biocement. Thus, it does not add significantly to the penetration resistance.

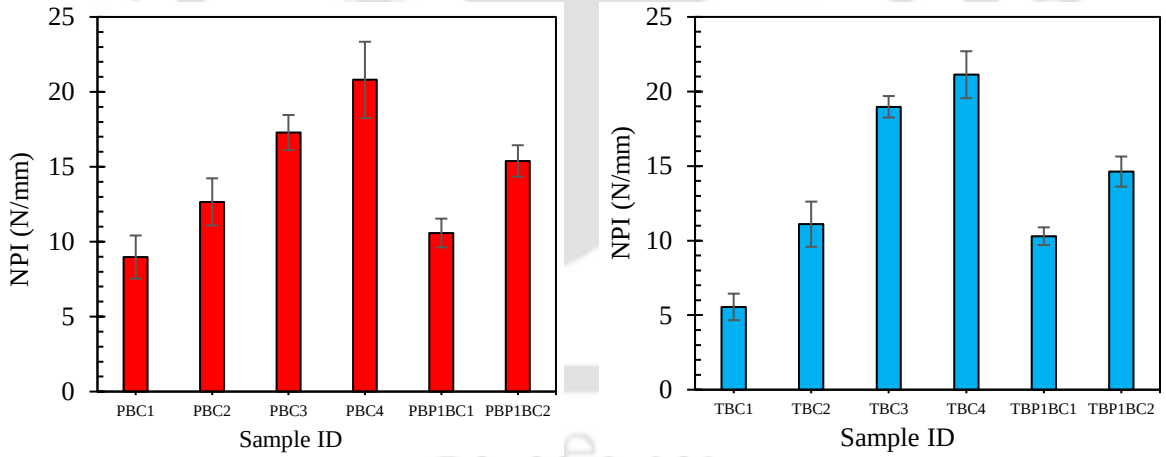

Figure 8.10 Needle penetration index (NPI) of the residual samples.

8.2.3 Correlation of average erosion rate with NPI

The average erosion rate (mm/h) with respect to the average NPI values of the treated soils is presented in Figure 8.11. The average erosion rate (mm/h) is defined as the total volume

eroded (V_e) during the experimental duration (T) per unit surface area (A_s) of the specimen, as shown in Equation 8.1.

$$E_{avg} = \frac{V_e}{A_s \times T} \tag{8.1}$$

With vegetation-based bank protection against surficial erosion, several researchers have correlated the erosion rate in exponentially declining models considering several controlling parameters such as vegetation cover (%), root length and root density (Zuazo and Pleguezuelo 2008). In a recent study, the soil erosion rate is reported to decline exponentially with root density against the hydraulic wave-like impact (Scheres and Schüttrumpf 2020). Adopting a similar model, the average erosion rates (E_{avg}) and the NPI values are correlated in Equation 8.2.

$$E_{avg} = A.\, e^{-B.(NPI)} \tag{8.2}$$

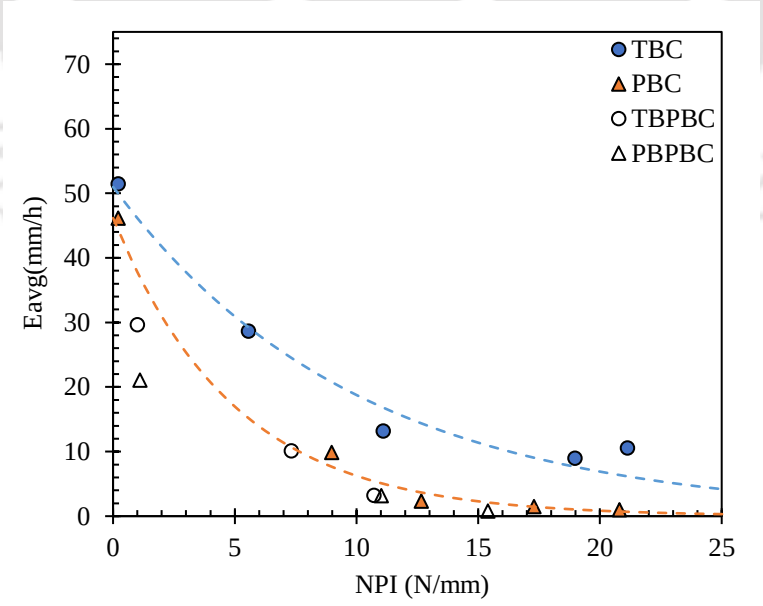

Figure 8.11 Correlation of average erosion rate with needle penetration index (NPI).

Here A (mm/h) and B (mm/N) are the fitting parameters. A is set as the maximum erosion rate for the untreated soil. While the fitted parameter B, which derives the decline rate of the erosion curve, is dependent on material strength properties as well as the applied hydraulic conditions. For tangential wave experiments, the A and B values were obtained as 51 mm/h and -0.1 mm/N from the numerical fitting. For the perpendicular wave experiment, the A and B values were obtained as 46.17 mm/h and -0.2 mm/N, indicating that the decline in average erosion rate with the increase in biocementation levels was more drastic in the case of perpendicular waves than the tangential waves.

8.2.4 Microstructure analysis

To illustrate the mechanism of grain binding, optical microscope images along with SEM micrographs of the samples treated with moderate (BC2) and extreme levels (BC4) of MICP are presented in Figure 8.12. Untreated sand gains were observed with smooth surfaces, as illustrated in Figures 8.12 (a) and (d). The clusters of rhombohedral $CaCO_3$ crystals (CC) were observed in the moderately biocemented sand over the smooth surface and grooves of the sand grains making the surface rough, as illustrated in Figures 8.12 (b) and (e). The resulting interparticle locking of the sand grains is most likely the reason for the notable improvement in the erosion resistance of the soil.

The increased roughness leading to an improved interparticle locking of the grains has been reported to improve the shear strength of the soil. For extreme biocementation, residual samples from PBC4 and TBC4 were considered. The heavily biocemented sand grains were observed to be covered and bridged with biocement, as illustrated in Figures 8.12 (c) and (f). The substantial precipitation of $CaCO_3$ over sand grains has led to grain bridging and significant improvement of erosion resistance. However, at high wave energy, these samples fragmented into large chunks. Excessive precipitation around the $CaCO_3$ bridging is possibly the major contributor to the brittleness in the heavily biocemented samples.

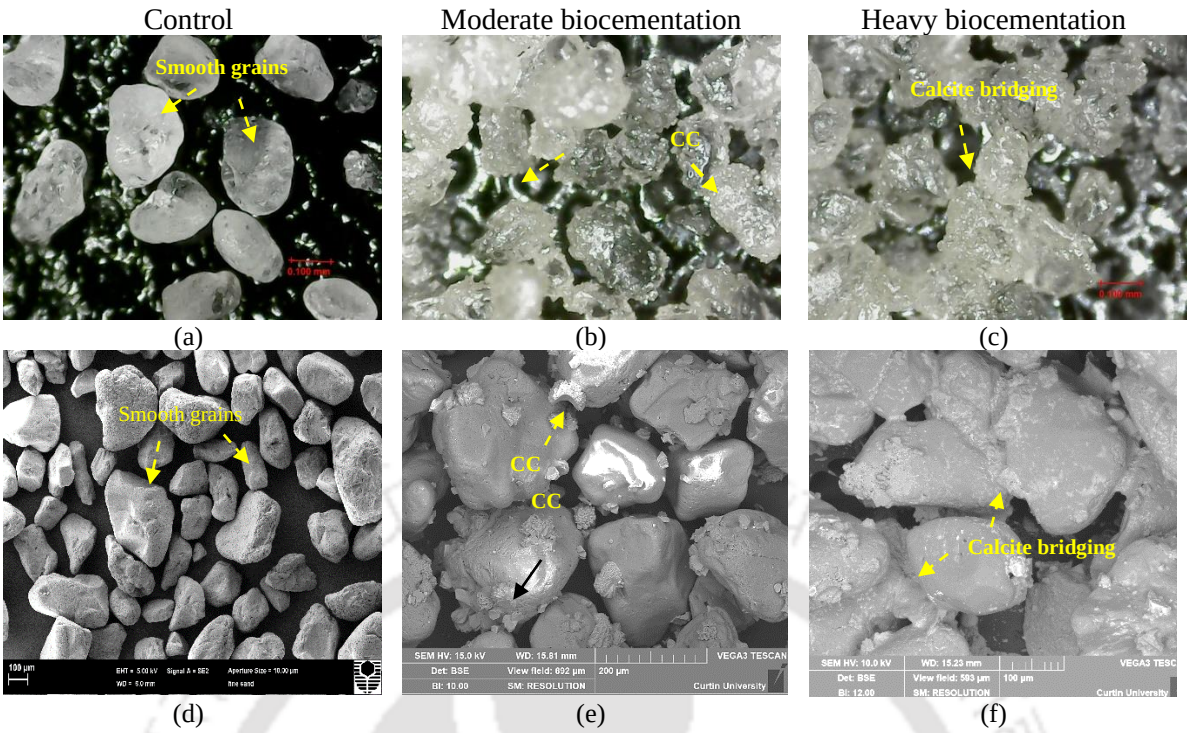

Figure 8.12 Optical and Scanning Electron Microscope images of (a, d). Untreated sand-BC0; (b, e). Moderately biocemented specimens- BC2; and (c, f). Heavily biocemented specimens-BC4.

In Figure 8.13, the microscopic images of biopolymer-biocement composite treated specimens are shown. Figures 8.13 (a) and (d) represent the control samples PBP1 and TBP1, which are devoid of calcium carbonate crystals. The SEM image in Figure 8.13 (d) demonstrates a thin biopolymer (Bp) bridging between two sand grains. In PBP1BC1 and TBP1BC1, the $CaCO_3$ crystals were detected along with the stretched threads of biopolymer (Bp) on sand grains, as shown in Figures 8.13 (b) and (e).

On the other hand, PBP1BC2 and TBP1BC2 were observed to be covered in biocement, as illustrated in Figures 8.13 (c) and (f). The threads of the biopolymer were also observed in PBP1BC2 and TBP1BC2. With higher magnification images, the structure of the biopolymer-modified composite bridging (BMC) was discovered.

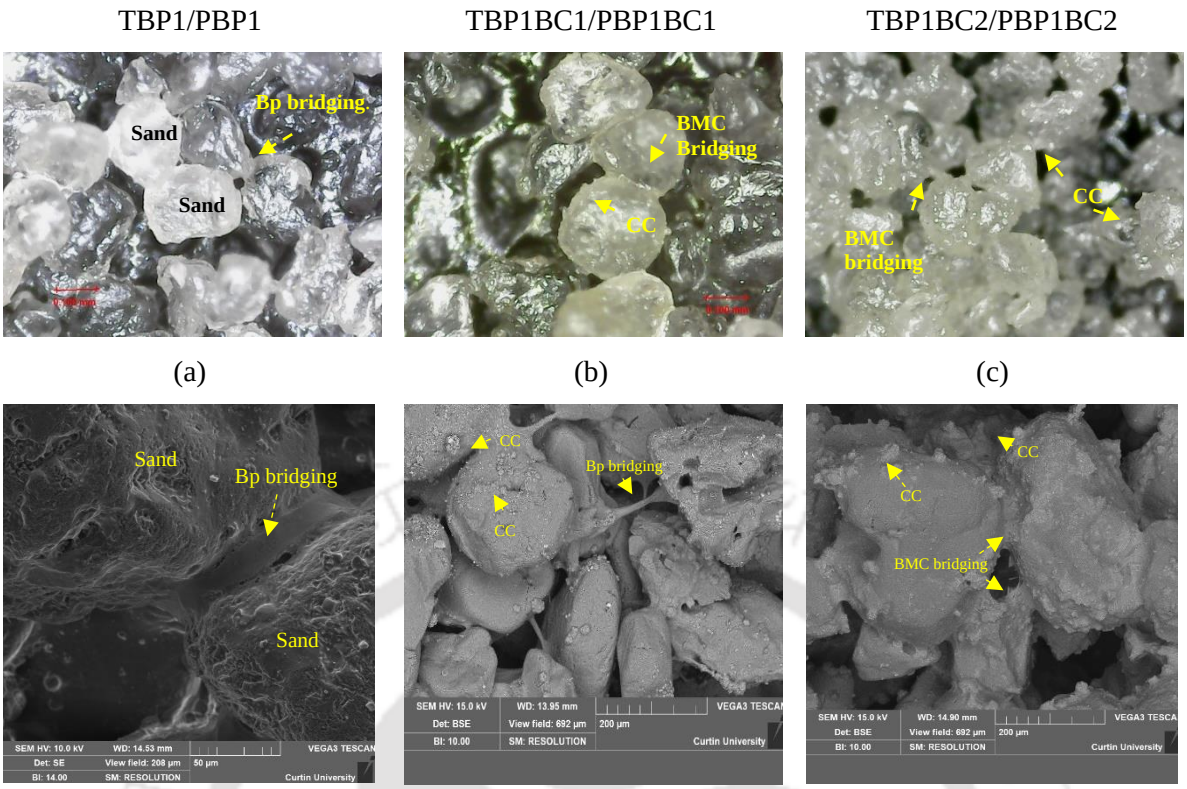

Figure 8.13 Optical and Scanning Electron Microscope images of (a, d). Plain biopolymer treated sand- BP1; and Biopolymer-biocement composite treated specimen (b, e). BP1BC1; and (c, f). BP1BC2.

Figure 8.14 illustrates an SEM micrograph of the PBP1BC2 samples. A thick cluster of rhombohedral precipitates anchoring on the biopolymer layer was observed, confirming that biopolymer assists in localising the precipitation.

Since biopolymers are known to improve the shear strength of soil, maintaining ductility (Lee et al. 2019b), the composite of biopolymer and biocement lead to the unparalleled erosion resilience of TBP1BC2 and PBP1BC2, despite having lesser $CaCO_3$ content than the conventionally biocemented samples TBC3/PBC3 and TBC4/PBC4.

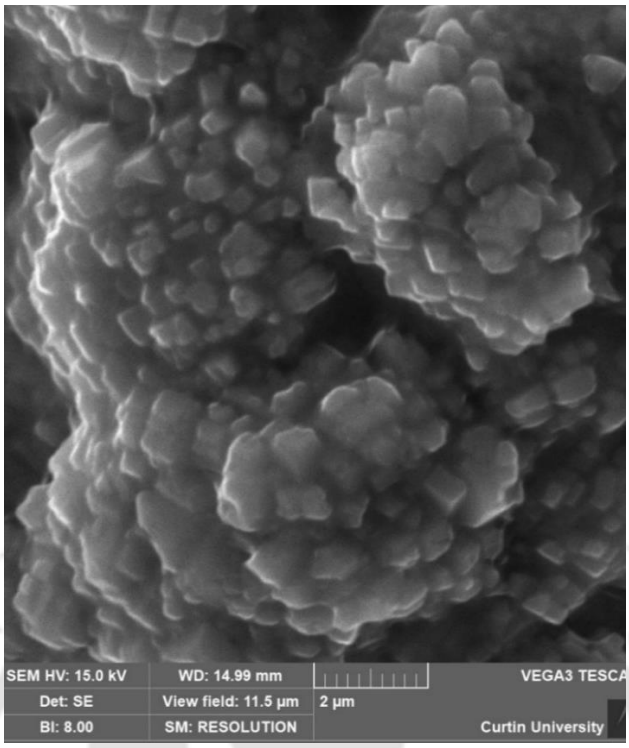

Figure 8.14 Anchored $CaCO_3$ cluster in the BMC bridge (Sample BP1BC2).

The mineralogical analysis with the XRD plots verified the presence of different polymorphs in the precipitated $CaCO_3$. The predominance of quartz (Q) was detected in the untreated sand. No peaks responding to $CaCO_3$ crystals were observed in the untreated sand. All the biocemented samples and bio-composite-treated specimens exhibited peaks of calcite (C104), confirming the presence of calcite (Wen et al. 2020). The plots of XRD were coinciding for all the samples. Therefore, plots corresponding to TBC4 and TBC0 are presented in Figure 8.15. Smaller peaks of vaterite were also observed for samples TBC3/PBC3 and TBC4/PBC4.

Calcite, vaterite and aragonite are the three anhydrous polymorphs of $CaCO_3$, which could be precipitated with any modification of the MICP process (Hammes et al. 2003; Rodriguez-Navarro et al. 2012). Calcite is the most stable polymorph of $CaCO_3$ that exhibits euhedral shapes, whereas vaterite is known to have a spheroid cauliflower-like shape. Aragonite is rarely reported in MICP and has morning star-like morphology (Rodriguez-Navarro et al. 2012). Calcite bridging is reported to induce higher strength in soils than vaterite.

In the current study, the mineralogical analysis along with the microstructural analysis assisted in confirming that inclusion of a biopolymer treatment prior to biocementation does not alter the morphologies of precipitated carbonate crystals.

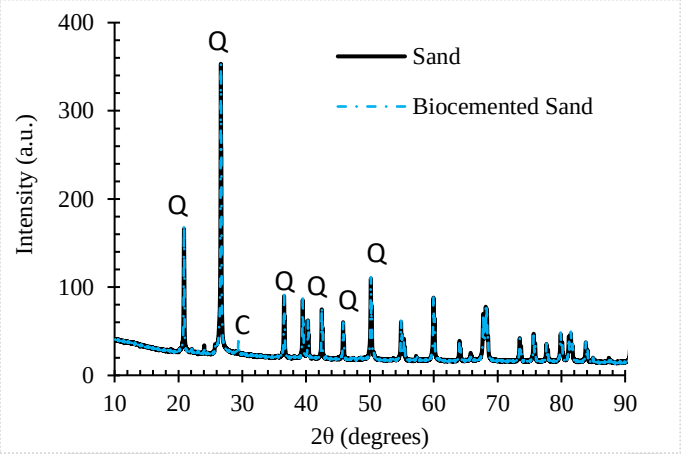

Figure 8.15 Comparison of XRD plots of untreated (TBC0) and biocemented sand (TBC4).

8.2.5 Cost and Construction-Efficiency

DeJong et al. (2013) reported that the cost of implementing conventional MICP for soil improvement in the field might vary from US$ 75/m^3 to US$ 500/m^3, which depends on the levels of biocementation, quality of cementation reagents, and cost of implementation, including electricity, labour & transport. Ivanov and Chu (2008) reported that the material cost for conventional MICP can vary from US$ 0.5/m^3 to US$ 9/m^3, while conventional soil grouting materials such as acrylamide, polyurethane, phenoplast and sodium silicate costs are reported in a range of from US$ 2/m^3 to US$ 72/m^3. As per the current rates for industrial grade biocementing reagents (>95% purity), the costs for proposed strategies BC4 and BP1BC2 were estimated at around US$ 9/m^2 and US$ 4.6/ m^2, respectively. The estimates are for a 5 cm target depth of biocemented crust. The cost can be reduced further by utilising commercially available low-cost biocementation reagents. The material costs for conventionally used

temporary/flexible erosion control products (Aussie Environmental, Australia, Certified Professionals in Erosion and Sediment Control) are given in Table 8.1.

Table 8.1 Comparison of costs of existing erosion control products.

Products	Market Price/Unit (US$)	Dimension (m×m)	Cost (US$/m^2)
Filled Sandbags (Poly-woven)	5.95	0.42×0.3	34
Jute Textile	142	1.8×25	3.15
Coir Mesh Brick (700 GSM)	115	2×25	2.3
Geofabric (140 GSM)	95	2×50	0.95

On the other hand, a report by the environmental agency UK (Hudson et al. 2015) described that rigid concrete structures such as sea defences, retaining walls and sea walls may cost as high as 750 US$/m^2 to 7500 US$/m^2 (543 to 5467 £/m²). The flexible erosion control systems do not exhibit strength characteristics, but it is the most used product due to their low cost, as mentioned in Table 8.1.

The proposed method in the current study aims to replace the soil grouting materials. The water-like permeability of the reagents and low-viscosity biopolymer solution allows the proposed method for a convenient field application by spraying strategy. Although the findings from the current study suggested that the proposed composite treatment could prevent wave erosion to a great extent, a meter-scale pilot study is necessary to determine its feasibility in terms of cost-effectiveness and construction efficiency. It is critical to evaluate the long-term performance of meter-scale biocemented soil against different types of waves to determine the design period of the proposed treatment.

8.3 Summary

Soil erosion at beaches and riverbanks leads to an enormous loss of infrastructure. The conservation of soil with natural aggregation processes has a significant potential for developing an ecologically conscious alternative to current practices. In the present study,

various levels of biocementation are compared against perpendicular and tangential flowing hydraulic waves in a lab-scale flume. The potential of bio-composite treatment for improving the erosion resistance of the soil against hydraulic waves is tested for the first time. The strength of the biocemented soil is evaluated with a non-destructive needle penetration test and is correlated with precipitated calcium carbonate content. The behaviour of the biocemented sand is also interpreted by its microstructure and mineralogy. The major findings from the present study are as follows:

- In the case of perpendicular waves, the erosion declined consistently with the increase in biocementation levels. Within the investigated $CaCO_3$ precipitation range, the specimen with an NPI of 21 N/mm was found to be most effective in ceasing the soil erosion against imparted wave energy density of 6 J/cm^2 with the conventional biocementation approach.
- In the case of tangential waves, the erosion decreased considerably with an increase in biocementation levels. However, the erosion did not completely cease. Even with a high NPI value of around 21 N/mm, the biocemented sand eroded more than 40% of its initial volume at a wave energy density of 5.3 J/cm^2.
- The composite with biopolymer-aided biocement had lower erosion compared to conventional biocement against both perpendicular and tangential waves. A sample with an NPI of 10.7 N/mm was observed to bring down the eroded volume to 20% against the tangential hydraulic wave of energy density 5.3 J/cm^2.
- The collaborative influence of biopolymer-biocement composites was analysed with microstructure analysis. Clusters of rhombohedral calcite crystals were observed to be anchored in the biopolymer layer, which provided enhanced efficiency against erosion.

8.4 Conclusion

In this objective, it was determined that the biocementation technique might not be a panacea against wave-induced soil erosion, specifically against the tangential flow. The composite with biopolymer- biocement composite had lower erosion rates compared to conventional biocement against both perpendicular and tangential waves. The biocomposite was observed to bring down the eroded volume to 20% against the tangential hydraulic wave of energy density 5.3 J/cm^2. Moreover, the erosion characteristics are reported against the wave energy density parameter, which can be helpful for the researchers to design the pilot scale future studies.

There are several challenges in the application of the proposed technology for ecologically sensitive coastal and riverbank zones (including the quantity of generated ammonia and the brittle nature of biocemented soil). Many of these factors can be tackled up to a certain extent with the proposed bio-composite treatment. Further research on large-scale setups is advised with real-time monitoring of biogeochemical reactions for the optimisation of treatment protocols.

CHAPTER 9

CONCLUSIONS AND RECOMMENDATIONS

9.1 Conclusions

Biocementation through microbially induced carbonate precipitation (MICP) is a powerful technique that has established its applicability in soil improvement and erosion control. Previous studies have demonstrated their efficacy in the control of aeolian, rainfall-induced, tidal, surficial flow-induced and coastal erosion. Most of these studies have utilised the standard biocementing microbe *Sporosarcina Pasteurii*. Soil is known to be rich in microbial biodiversity, and the urease enzyme is common in a wide variety of such microorganisms. Therefore, the ability of bacteria isolated from local soil environments was assessed for their biocementation potential and various kinds of erosion mitigations. The major findings from the current study can be encapsulated as follows-

- Brahmaputra riverbank soil and the selected local soil were found to be rich in biocement potent ureolytic bacteria. Thirty-six ureolytic bacteria were isolated and screened. Out of 36 bacteria, six were found to be highly biocementation potent with specific urease activity varying from 107 to 187 mM urea hydrolysed h^{-1} $(O.D._{600})^{-1}$. Their genomic sequences revealed them to be Firmicutes of the *Sporosarcina* family. The urease activity and calcium carbonate conversion efficiency were observed to be comparable with the standard biocementing microbe *Sporosarcina pasteurii* (ATCC 11859).
- One of the soil isolates (LS2) from local soil was investigated for its efficiency in controlling wind erosion. It was observed that with a mere calcium carbonate content of below 2%, the soil withstood against a wind velocity up to 55 m/s without any particle detachment. The unconfined compressive strength was

found to be around 900 kPa for biocementation treatment with 500 mM and 1000 mM cementation solution.

- While investigating the surface strength characteristics with needle penetration tests, it was found that the optimum concertation of cementation media is 500 mM regardless of the bacteria. It was also observed that the ureolytic bacteria liable for augmentation and stimulation responds distinctively to the various concentration of cementation media.
- With microstructure and mineralogical analysis, several interesting findings were obtained. It was confirmed that different kinds of microbes (SP, BS3 and Consortia) precipitate different-sized crystals at various concentrations of cementation solutions. Epitaxial growth of rhombohedral crystals was the most dominant class of observed $CaCO_3$ crystals. The size of precipitates was observed to influence their NPI strength. At a higher concentration of cementation solution, the morphology of the precipitates changed from rhombohedral to cauliflower-shaped crystals suggesting the presence of vaterite.
- A numerical correlation between $CaCO_3$ contents and NPI was observed for poorly graded fine sand within the proposed range of precipitation (up to around 10% $CaCO_3$ content). The proposed equation can be useful for monitoring the degree of cementation with a pocket penetrometer having a similar configuration to the experimental setup.
- The hydraulic current test revealed that the biocemented sample with around 7% of $CaCO_3$ and an NPI value of 16 N/mm resisted erosion effectively up to flow 0.62 m/s. Biopolymer treatment resulted in notable improvement in the critical velocity. However, once the sheet-like biopolymerised layer is

dislodged, the soil erosion rate is found to be equivalent to the untreated sand. The biopolymer-biocement composite samples were found to produce 36% lesser ammonia than an equally efficient biocemented sample, making it more suitable for applications in ecologically sensitive zones such as riverbanks.

- A biocemented specimen with an NPI of 21 N/mm was found to be most effective in ceasing soil erosion against the energy density of 6 J/cm^2 imparted by perpendicular waves. However, in the case of tangential setup, the erosion did not completely cease. Even with a high NPI value of around 21 N/mm, the biocemented sand eroded more than 40% of its initial volume at a wave energy density of 5.3 J/cm^2. The bio-composite treated sample with an NPI of 10.7 N/mm was observed to bring down the eroded volume to 20% against the tangential hydraulic wave of energy density 5.3 J/cm^2. The biopolymer-aided biocemented samples are found to be more effective in terms of material requirement, ammonia generation and erosion mitigation efficiency.
- With the microstructure and mineralogical analysis, it was confirmed that the pre-treatment of biopolymer did not influence the morphology of the desired calcite crystals. Instead, the calcite crystals were observed to form a matrix with biopolymer, which provided the composite effect, which is mostly the reason for the superior performance of the biopolymer-biocement composite treated soils.

9.2 Recommendations

While the present study has several valuable conclusions, future research is necessary to explore the extent of the proposed treatments. The major areas which are recommended for future studies are as follows-

- This study is focused chiefly on the biocementation technique based on urea hydrolysis. However, there are other biocementation techniques, especially denitrification and ammonification, that must be considered for future investigations considering the naturally available cementation sources.
- In this study, the soil was selected from a few preferred sites for microbial isolation. A urea hydrolysis screening was conducted only to choose biocementation-potent microbes. However, the local biodiversity was not explored. The influence of urea hydrolysis on the viability of other microbial strains must be considered for future investigations. Furthermore, the isolated strains can be mutated for better control of the biocementation process.
- Alternative techniques for a complete capture of generated by-product ammonia, such as struvite precipitation, zeolites and electrokinetic stabilisation, are recommended to be explored along with the biostimulation approach.
- The bio-composite developed in the current study is based on the pre-application of a hydrophilic and biodegradable polymer. Since the quantity of biopolymer applied for the development of the composite is very low, the author hypothesises the influence of their degradation to be minimum. However, the durability and long-term performance of the bio-composite must be comprehensively investigated in future studies for their field applications.
- The scales of the experiments in the present study were mostly constrained due to the dimensions of the wind tunnel and hydraulic flume. Therefore, scaling effects could not be considered in the present study. Although the experiments provide valuable insights for comparative analysis of the untreated and treated soil in a lab-scale environment, these results are not directly extendable to the field scale. Therefore, a large-scale investigation of the proposed treatments

must be carried out before the field trials to confirm the viability of the proposed biopolymer-biocement composite treatment in terms of cost, durability, and long-term performance. The cost can be reduced with commercial-grade reagents.

- For practical implementation of the proposed treatment method over a large scale, a continuous micro-sprinkler-based spraying system is recommended for future studies. For mitigating the hydraulic-current and wave-induced soil erosion, the treatment would require to be in low-tide/low-flood conditions so that the bacterial/cementation solutions are not diluted with the flow compared to the mitigation of aeolian erosion where rain and daily temperature variation might derive the biocementation purpose. To monitor the performance of the proposed treatment, non-destructive approaches such as bender elements and needle penetration tests could be adopted. For assessing erosion for large-scale samples over a long period, the change in elevation and cross-section of the eroded landmass can be monitored via measuring bars and photogrammetry.

References

Achal, V., Pan, X., Fu, Q. and Zhang, D. 2012. Biomineralization based remediation of As(III) contaminated soil by Sporosarcina ginsengisoli. Journal of Hazardous Materials 201–202, pp. 178–184. DOI: 10.1016/j.jhazmat.2011.11.067

Ali, M.B., Saidur, R. and Hossain, M.S. 2011. A review on emission analysis in cement industries. Renewable and Sustainable Energy Reviews 15(5), pp. 2252–2261. DOI: 10.1016/j.rser.2011.02.014

Alshalif, A.F., Irwan, J.M., Othman, N. and Anneza, L.H. 2016. Isolation of Sulphate Reduction Bacteria (SRB) to Improve Compress Strength and Water Penetration of Bio-Concrete. Abd Rahman, N., Mohd Jaini, Z., Yunus, R., and Rahmat, S. N. eds. MATEC Web of Conferences 47, p. 01016. Available at: http://www.matec-conferences.org/10.1051/matecconf/20164701016

Altermann, W., Kazmierczak, J., Oren, A. and Wright, D.T. 2006. Cyanobacterial calcification and its rock-building potential during 3.5 billion years of Earth history. Geobiology 4(3), pp. 147–166. DOI:10.1111/j.1472-4669.2006.00076.x

Amin, M., Zomorodian, S.M.A. and O'Kelly, B.C. 2017. Reducing the hydraulic erosion of sand using microbial-induced carbonate precipitation. Proceedings of the Institution of Civil Engineers: Ground Improvement 170(2), pp. 112–122. DOI: 10.1680/jgrim.16.00028

Aminoroayaie Yamini, O., Mousavi, S.H. and Kavianpour, M.R. 2019. Experimental investigation of using geo-textile filter layer in articulated concrete block mattress revetment on coastal embankment. Journal of Ocean Engineering and Marine Energy 5(2), pp. 119–133. DOI: 10.1007/s40722-019-00133-y

Arp, G., Reimer, A. and Reitner, J. 1999. Calcification in cyanobacterial biofilms of alkaline salt lakes. European Journal of Phycology 34(4), pp. 393–403. DOI: 10.1080/09670269910001736452

Ashton, A., Murray, A.B. and Arnoult, O. 2002. Formation of coastline features by large-scale instabilities induced by high-angle waves. Nature 415(6872), pp. 666–666. Available at: http://www.nature.com/articles/415666a

ASTM D4254-16 2006. Standard Test Methods for Minimum Index Density and Unit Weight of Soils and Calculation of Relative Density. ASTM International, West Conshohocken, PA. I(Reapproved 2006), p. 9. DOI: 10.1520/D4254-16

ASTM D4972-19 2019. Standard Test Methods for pH of Soils. ASTM International, West Conshohocken, PA. 01(10). DOI: 10.1520/D4972-19

ASTM D6913/D6913M-17 2017. Standard Test Methods for Particle-Size Distribution (Gradation) of Soils Using Sieve Analysis. ASTM International, West Conshohocken, PA. , pp. 1–34. DOI: 10.1520/D6913-17

ASTM D854-14 2014. Standard Test Methods for Specific Gravity of Soil Solids by Water Pycnometer. ASTM International, West Conshohocken, PA. , pp. 1–7. DOI: 10.1520/D0854-10.2

Bagnold, R.A. 1984. The Physics of Blown Sand and Desert Dunes. John Wiley & Sons, Inc.

Baskar, S., Baskar, R., Lee, N. and Theophilus, P.K. 2009. Speleothems from Mawsmai and Krem Phyllut caves, Meghalaya, India: Some evidences on biogenic activities. Environmental Geology 57(5), pp. 1169–1186. DOI: 10.1007/s00254-008-1413-y

Behzadipour, H. and Sadrekarimi, A. 2021. Biochar-assisted bio-cementation of a sand using native bacteria. Bulletin of Engineering Geology and the Environment. DOI: 10.1007/s10064-021-02235-0

Benini, S., Borsari, M., Ciurli, S., Dikiy, A. and Lamborghini, M. 1998. Modulation of Bacillus pasteurii cytochrome C553 reduction potential by structural and solution parameters. Journal of Biological Inorganic Chemistry 3(4), pp. 371–382. DOI: 10.1007/s007750050247

Bibi, S., Oualha, M., Ashfaq, M.Y., Suleiman, M.T. and Zouari, N. 2018. Isolation, differentiation and biodiversity of ureolytic bacteria of Qatari soil and their potential in microbially induced calcite precipitation (MICP) for soil stabilization. RSC Advances 8(11), pp. 5854–5863. DOI: 10.1039/C7RA12758H

Bindschedler, S., Cailleau, G. and Verrecchia, E. 2016. Role of fungi in the biomineralization of calcite. Minerals 6(2), pp. 1–19. DOI: 10.3390/min6020041

Bosshard, P.P., Abels, S., Zbinden, R., Böttger, E.C. and Altwegg, M. 2003. Ribosomal DNA sequencing for identification of aerobic gram-positive rods in the clinical laboratory (an 18-month evaluation). Journal of Clinical Microbiology 41(9), pp. 4134–4140. DOI: 10.1128/JCM.41.9.4134-4140.2003

Briaud, J.-L. 2008. Case Histories in Soil and Rock Erosion: Woodrow Wilson Bridge, Brazos River Meander, Normandy Cliffs, and New Orleans Levees. Journal of Geotechnical and Geoenvironmental Engineering 134(10), pp. 1425–1447. DOI: 10.1061/(ASCE)1090-0241(2008)134:10(1425)

Briaud, J.-L. 2013. Geotechnical Engineering: Unsaturated and Saturated Soils. John Wiley & Sons, Inc

Burbank, M.B., Weaver, T.J., Green, T.L., Williams, B. and Crawford, R.L. 2011. Precipitation of calcite by indigenous microorganisms to strengthen liquefiable soils. Geomicrobiology Journal 28(4), pp. 301–312. DOI: 10.1080/01490451.2010.499929

Burbank, M.B., Weaver, T.J., Williams, B.C. and Crawford, R.L. 2012. Urease Activity of Ureolytic Bacteria Isolated from Six Soils in which Calcite was Precipitated by Indigenous Bacteria. Geomicrobiology Journal 29(4), pp. 389–395. DOI: 10.1080/01490451.2011.575913

Burrell, A.L., Evans, J.P. and De Kauwe, M.G. 2020. Anthropogenic climate change has driven over 5 million km2 of drylands towards desertification. Nature Communications 11(1), pp. 1–11. DOI: 10.1038/s41467-020-17710-7

Caesar, K.H., Kyle, J.R., Lyons, T.W., Tripati, A. and Loyd, S.J. 2019. Carbonate formation in salt dome cap rocks by microbial anaerobic oxidation of methane. Nature Communications 10(1). DOI: 10.1038/s41467-019-08687-z

Casas, J.A., Santos, V.E. and García-Ochoa, F. 2000. Xanthan gum production under several operational conditions: Molecular structure and rheological properties. Enzyme and Microbial Technology 26(2–4), pp. 282–291. DOI: 10.1016/S0141-0229(99)00160-X

Castro-Alonso, M.J., Montañez-Hernandez, L.E., Sanchez-Muñoz, M.A., Macias Franco, M.R., Narayanasamy, R. and Balagurusamy, N. 2019. Microbially induced calcium carbonate precipitation (MICP) and its potential in bioconcrete: Microbiological and molecular concepts. Frontiers in Materials 6(June), pp. 1–15. DOI: 10.3389/fmats.2019.00126

Chang, I., Im, J. and Cho, G.C. 2016. Introduction of microbial biopolymers in soil treatment for future environmentally-friendly and sustainable geotechnical engineering. Sustainability (Switzerland) 8(3). DOI: 10.3390/su8030251

Chang, I., Im, J., Prasidhi, A.K. and Cho, G.-C. 2015. Effects of Xanthan gum biopolymer on soil strengthening. Construction and Building Materials 74(x), pp. 65–72. DOI: 10.1016/j.conbuildmat.2014.10.026

Chek, A., Crowley, R., Ellis, T.N., Durnin, M. and Wingender, B. 2021. Evaluation of Factors Affecting Erodibility Improvement for MICP-Treated Beach Sand. Journal of Geotechnical and Geoenvironmental Engineering 147(3), p. 04021001. DOI: 10.1061/%28ASCE%29GT.1943-5606.0002481

Chekroun, K.B., Rodri, C., Teresa Gonza, M., Maria Arias, J., Cultrone, G. and Rodri, M. 2004. Precipitation and Growth Morphology of Calcium Carbonate Induced By Myxococcus Xanthus: Implications for Recognition of Bacterial Carbonates. Journal of Sedimentary Research 74(6), pp. 1527–1404

Cheng, L. and Cord-Ruwisch, R. 2012. In situ soil cementation with ureolytic bacteria by surface percolation. Ecological Engineering 42, pp. 64–72. DOI: 10.1016/j.ecoleng.2012.01.013

Cheng, L. and Cord-Ruwisch, R. 2014. Upscaling Effects of Soil Improvement by Microbially Induced Calcite Precipitation by Surface Percolation. Geomicrobiology Journal 31(5), pp. 396–406. DOI: 10.1080/01490451.2013.836579

Cheng, L., Cord-Ruwisch, R. and Shahin, M.A. 2013a. Cementation of sand soil by microbially induced calcite precipitation at various degrees of saturation. Canadian Geotechnical Journal 50(1), pp. 81–90. DOI: 10.1139/cgj-2012-0023

Cheng, L. and Shahin, M.A. 2016. Urease active bioslurry: a novel soil improvement approach based on microbially induced carbonate precipitation. Canadian Geotechnical Journal 53(9), pp. 1376–1385. DOI: 10.1139/cgj-2015-0635

Cheng, L., Shahin, M.A., Addis, M., Hartanto, T. and Elms, C. 2014. Soil Stabilisation by Microbial-Induced Calcite Precipitation (MICP): Investigation into Some Physical and Environmental Aspects. In: 7th International Congress on Environmental Geotechnics, At Melbourne, Australia., pp. 10–14

Cheng, L., Shahin, M.A. and Chu, J. 2019. Soil bio-cementation using a new one-phase low-pH injection method. Acta Geotechnica 14(3), pp. 615–626. DOI: 10.1007/s11440-018-0738-2

Cheng, X., Yang, Z., Zhang, Z. and Wang, H. 2013b. Modeling of microbial induced carbonate precipitation in porous media. Journal of Pure and Applied Microbiology 7(1), pp. 449–458

Chlachula, J. 2021. Between sand dunes and hamadas: Environmental sustainability of the thar desert, West India. Sustainability (Switzerland) 13(7). DOI: 10.3390/su13073602

Choi, S.G., Park, S.S., Wu, S. and Chu, J. 2017. Methods for calcium carbonate content measurement of biocemented soils. Journal of Materials in Civil Engineering 29(11). DOI: 10.1061/(ASCE)MT.1943-5533.0002064

Christensen, W.B. 1946. Urea Decomposition as a Means of Differentiating Proteus and Paracolon Cultures from Each Other and from Salmonella and Shigella Types. Journal of bacteriology 52(4), pp. 461–466

Chu, J., Ivanov, V., Naeimi, M., Stabnikov, V. and Liu, H.-L. 2014. Optimization of calcium-based bioclogging and biocementation of sand. Acta Geotechnica 9(2), pp. 277–285. DOI: 10.1007/s11440-013-0278-8

Chu, J., Stabnikov, V. and Ivanov, V. 2012. Microbially Induced Calcium Carbonate Precipitation on Surface or in the Bulk of Soil. Geomicrobiology Journal 29(6), pp. 544–549. DOI: 10.1080/01490451.2011.592929

Chung, H., Kim, S.H. and Nam, K. 2021. Application of microbially induced calcite precipitation to prevent soil loss by rainfall: effect of particle size and organic matter content. Journal of Soils and Sediments 21(8), pp. 2744–2754. DOI: 10.1007/s11368-020-02757-2

Cizer, Ö., Rodriguez-Navarro, C., Ruiz-Agudo, E., Elsen, J., Van Gemert, D. and Van Balen, K. 2012. Phase and morphology evolution of calcium carbonate precipitated by carbonation of hydrated lime. Journal of Materials Science 47(16), pp. 6151–6165. DOI: 10.1007/s10853-012-6535-7

Clarà Saracho, A., Haigh, S.K. and Ehsan Jorat, M. 2021. Flume study on the effects of microbial induced calcium carbonate precipitation (MICP) on the erosional behaviour of fine sand. Géotechnique 71(12), pp. 1135–1149. DOI: 10.1680/jgeot.19.P.350

Colica, G., Li, H., Rossi, F., Li, D., Liu, Y. and De Philippis, R. 2014. Microbial secreted exopolysaccharides affect the hydrological behavior of induced biological soil crusts in desert sandy soils. Soil Biology and Biochemistry 68, pp. 62–70. DOI: 10.1016/j.soilbio.2013.09.017

Cuthbert, M.O., Riley, M.S., Handley-Sidhu, S., Renshaw, J.C., Tobler, D.J., Phoenix, V.R. and Mackay, R. 2012. Controls on the rate of ureolysis and the morphology of carbonate precipitated by S. Pasteurii biofilms and limits due to bacterial encapsulation. Ecological Engineering 41(April), pp. 32–40. DOI: 10.1016/j.ecoleng.2012.01.008

D'Odorico, P., Bhattachan, A., Davis, K.F., Ravi, S. and Runyan, C.W. 2013. Global desertification: Drivers and feedbacks. Advances in Water Resources 51, pp. 326–344. DOI: 10.1016/j.advwatres.2012.01.013

Das, T.K., Haldar, S.K., Gupta, I. Das and Sen, S. 2014. River bank erosion induced human displacement and its consequences. Living Reviews in Landscape Research 8(1), pp. 1–35. DOI: 10.12942/lrlr-2014-3

Das, V.K., Roy, S., Barman, K., Chaudhuri, S. and Debnath, K. 2020. Cohesive river bank erosion mechanism under wave-current interaction: A flume study. Journal of Earth System Science 129(1), p. 99. DOI: 10.1007/s12040-020-1363-7

DeJong, J.T. et al. 2013. Biogeochemical processes and geotechnical applications: progress, opportunities and challenges. Géotechnique 63(4), pp. 287–301. DOI: 10.1680/geot.SIP13.P.017

DeJong, J.T., Fritzges, M.B. and Nüsslein, K. 2006. Microbially Induced Cementation to Control Sand Response to Undrained Shear. Journal of Geotechnical and Geoenvironmental Engineering 132(11), pp. 1381–1392. DOI: 10.1061/(asce)1090-0241(2006)132:11(1381)

DeJong, J.T., Mortensen, B.M., Martinez, B.C. and Nelson, D.C. 2010. Bio-mediated soil improvement. Ecological Engineering 36(2), pp. 197–210. DOI: 10.1016/j.ecoleng.2008.12.029

Devrani, R., Dubey, A.A., Ravi, K. and Sahoo, L. 2021. Applications of bio-cementation and bio-polymerization for aeolian erosion control. Journal of Arid Environments 187(December 2020), p. 104433. DOI: 10.1016/j.jaridenv.2020.104433

Dhami, N.K., Alsubhi, W.R., Watkin, E. and Mukherjee, A. 2017. Bacterial community dynamics and biocement formation during stimulation and augmentation: Implications for soil consolidation. Frontiers in Microbiology 8(JUL). DOI: 10.3389/fmicb.2017.01267

Dhami, N.K., Mukherjee, A. and Reddy, M.S. 2016. Micrographical, minerological and nano-mechanical characterisation of microbial carbonates from urease and carbonic anhydrase producing bacteria. Ecological Engineering 94, pp. 443–454. DOI: 10.1016/j.ecoleng.2016.06.013

Dhami, N.K., Reddy, M.S. and Mukherjee, A. 2013a. Biomineralization of calcium carbonate polymorphs by the bacterial strains isolated from calcareous sites. Journal of Microbiology and Biotechnology 23(5), pp. 707–714. DOI: 10.4014/jmb.1212.11087

Dhami, N.K., Reddy, M.S. and Mukherjee, A. 2013b. Biomineralization of calcium carbonates and their engineered applications: A review. Frontiers in Microbiology 4(OCT), pp. 1–13. DOI: 10.3389/fmicb.2013.00314

van Dijk, W.M., Teske, R., Van De Lageweg, W.I. and Kleinhans, M.G. 2013. Effects of vegetation distribution on experimental river channel dynamics. Water Resources Research 49(11), pp. 7558–7574. DOI: 10.1002/2013WR013574

Dipova, N. 2018. Nondestructive Testing of Stabilized Soils and Soft Rocks via Needle Penetration. Periodica Polytechnica Civil Engineering, pp. 539–544. DOI: 10.3311/PPci.11874

Do, J., Montoya, B.M. and Gabr, M.A. 2021. Scour Mitigation and Erodibility Improvement Using Microbially Induced Carbonate Precipitation. Geotechnical Testing Journal 44(5), p. 20190478. DOI: 10.1520/GTJ20190478

Duo, L., Kan-liang, T., Hui-li, Z., Yu-yao, W., Kang-yi, N. and Shi-can, Z. 2018. Experimental investigation of solidifying desert aeolian sand using microbially induced calcite precipitation. Construction and Building Materials 172, pp. 251–262. DOI: 10.1016/j.conbuildmat.2018.03.255

Erşan, Y.Ç., Belie, N. de and Boon, N. 2015. Microbially induced CaCO3 precipitation through denitrification: An optimization study in minimal nutrient environment. Biochemical Engineering Journal 101, pp. 108–118. DOI: 10.1016/j.bej.2015.05.006

Fattahi, S.M., Soroush, A., Huang, N., Zhang, J. and Abbasi, S.J. 2020. Laboratory study on biophysicochemical improvement of desert sand. Catena 190(August 2019), p. 104531. DOI: 10.1016/j.catena.2020.104531

Faure, Y.H., Ho, C.C., Chen, R.H., Le Lay, M. and Blaza, J. 2010. A wave flume experiment for studying erosion mechanism of revetments using geotextiles. Geotextiles and Geomembranes 28(4), pp. 360–373. DOI: 10.1016/j.geotexmem.2009.11.002

Feng, K. and Montoya, B.M. 2016. Influence of Confinement and Cementation Level on the Behavior of Microbial-Induced Calcite Precipitated Sands under Monotonic Drained Loading. Journal of Geotechnical and Geoenvironmental Engineering 142(1), p. 04015057. DOI: 10.1061/(ASCE)GT.1943-5606.0001379

Ferris, F.G., Phoenix, V., Fujita, Y. and Smith, R.W. 2004. Kinetics of calcite precipitation induced by ureolytic bacteria at 10 to 20°C in artificial groundwater. Geochimica et Cosmochimica Acta 68(8), pp. 1701–1710. DOI: 10.1016/S0016-7037(03)00503-9

Florsheim, J.L., Mount, J.F. and Chin, A. 2008. Bank Erosion as a Desirable Attribute of Rivers. BioScience 58(6), pp. 519–529. DOI: 10.1641/b580608

Fredsøe, J. and Deigaard, R. 1992. Mechanics of Coastal Sediment Transport. World Scientific. DOI: 10.1142/1546

Fujita, Y., Taylor, J.L., Wendt, L.M., Reed, D.W. and Smith, R.W. 2010. Evaluating the potential of native ureolytic microbes to remediate a 90Sr contaminated environment. Environmental Science and Technology 44(19), pp. 7652–7658. DOI: 10.1021/es101752p

Ganendra, G. et al. 2014. Formate oxidation-driven calcium carbonate precipitation by Methylocystis parvus OBBP. Applied and Environmental Microbiology 80(15), pp. 4659–4667. DOI: 10.1128/AEM.01349-14

Gao, Y., Wang, L., He, J., Ren, J. and Gao, Y. 2022. Denitrification-based MICP for cementation of soil : treatment process and mechanical performance. Acta Geotechnica 6. DOI: 10.1007/s11440-022-01489-6

García-Ruiz, J.M., Beguería, S., Nadal-Romero, E., González-Hidalgo, J.C., Lana-Renault, N. and Sanjuán, Y. 2015. A meta-analysis of soil erosion rates across the world. Geomorphology 239, pp. 160–173. DOI: 10.1016/j.geomorph.2015.03.008

Gomez, M.G., Anderson, C.M., Graddy, C.M.R., DeJong, J.T., Nelson, D.C. and Ginn, T.R. 2017. Large-Scale Comparison of Bioaugmentation and Biostimulation Approaches for Biocementation of Sands. Journal of Geotechnical and Geoenvironmental Engineering 143(5), p. 04016124. DOI: 10.1061/(ASCE)GT.1943-5606.0001640

Gomez, M.G., Graddy, C.M.R., DeJong, J.T. and Nelson, D.C. 2019. Biogeochemical Changes During Bio-cementation Mediated by Stimulated and Augmented Ureolytic Microorganisms. Scientific Reports 9(1), pp. 1–15. DOI: 10.1038/s41598-019-47973-0

Gomez, M.G., Martinez, B.C., Dejong, J.T., Hunt, C.E., Devlaming, L.A., Major, D.W. and Dworatzek, S.M. 2015. Field-scale bio-cementation tests to improve sands. Proceedings of the Institution of Civil Engineers: Ground Improvement 168(3), pp. 206–216. DOI: 10.1680/grim.13.00052

Graddy, C.M.R., Gomez, M.G., DeJong, J.T. and Nelson, D.C. 2021. Native Bacterial Community Convergence in Augmented and Stimulated Ureolytic MICP Biocementation. Environmental Science & Technology , p. acs.est.1c01520. DOI: 10.1021/acs.est.1c01520

Graddy, C.M.R., Gomez, M.G., Kline, L.M., Morrill, S.R., Dejong, J.T. and Nelson, D.C. 2018. Diversity of Sporosarcina -like Bacterial Strains Obtained from Meter-Scale Augmented and Stimulated Biocementation Experiments. Environmental Science and Technology 52(7), pp. 3997–4005. DOI: 10.1021/acs.est.7b04271

Gu, J., Liu, G., ABD Elbasit, M.A.M. and Shi, H. 2020. Response of slope surface roughness to wave-induced erosion during water level fluctuating. Journal of Mountain Science 17(4), pp. 871–883. DOI: 10.1007/s11629-019-5745-8

Habert, G., Billard, C., Rossi, P., Chen, C. and Roussel, N. 2010. Cement production technology improvement compared to factor 4 objectives. Cement and Concrete Research 40(5), pp. 820–826. DOI: 10.1016/j.cemconres.2009.09.031

Hammes, F., Boon, N., De Villiers, J., Verstraete, W. and Siciliano, S.D. 2003. Strain-specific ureolytic microbial calcium carbonate precipitation. Applied and Environmental Microbiology 69(8), pp. 4901–4909. DOI: 10.1128/AEM.69.8.4901-4909.2003

Harkes, M.P., van Paassen, L.A., Booster, J.L., Whiffin, V.S. and van Loosdrecht, M.C.M. 2010. Fixation and distribution of bacterial activity in sand to induce carbonate precipitation for ground reinforcement. Ecological Engineering 36(2), pp. 112–117. DOI: 10.1016/j.ecoleng.2009.01.004

Heveran, C.M. et al. 2019. Engineered Ureolytic Microorganisms Can Tailor the Morphology and Nanomechanical Properties of Microbial-Precipitated Calcium Carbonate. Scientific Reports 9(1), pp. 1–13. DOI: 10.1038/s41598-019-51133-9.

Heveran, C.M. et al. 2020. Biomineralization and Successive Regeneration of Engineered Living Building Materials. Matter 2(2), pp. 481–494. DOI: 10.1016/j.matt.2019.11.016

Hudson, T., Keating, K. and Petit, A. 2015. Cost estimation for coastal protection - Summary of evidence. Environment Agency, Horizon House, Deanery Road, Bristol, BS1 5AH , p. 37.

Hussey, M.A. 2013. Endospore Stain Protocol. American Society for Microbiology (September 2007), pp. 1–11.

Intergovernmental Panel on Climate Changes; United Nations 2018. Summary for Policymakers of IPCC Special Report on Global Warming of 1.5°C approved by governments. IPCC Secretariat (October), pp. 1–4

IS:1479-1 1960. Methods of test for dairy industry, Part 1: Rapid examination of milk. Bureau of Indian Standards, New Delhi

Ivanov, V. and Chu, J. 2008. Applications of microorganisms to geotechnical engineering for bioclogging and biocementation of soil in situ. Reviews in Environmental Science and Bio/Technology 7(2), pp. 139–153. DOI: 10.1007/s11157-007-9126-3

Ivanov, V. and Stabnikov, V. 2017. Construction Biotechnology. Singapore: Springer Singapore. DOI: 10.1007/978-981-10-1445-1

Jain, S. and Arnepalli, D.N. 2019. Biochemically Induced Carbonate Precipitation in Aerobic and Anaerobic Environments by Sporosarcina pasteurii. Geomicrobiology Journal 36(5), pp. 443–451. DOI: 10.1080/01490451.2019.1569180

Jain, S., Fang, C. and Achal, V. 2021. A critical review on microbial carbonate precipitation via denitrification process in building materials. Bioengineered 12(1), pp. 7529–7551. DOI: 10.1080/21655979.2021.1979862

Jiang, N.-J. and Soga, K. 2017. The applicability of microbially induced calcite precipitation (MICP) for internal erosion control in gravel–sand mixtures. Géotechnique 67(1), pp. 42–55. DOI: 10.1680/jgeot.15.P.182

Jiang, N.-J., Tang, C.-S., Yin, L.-Y., Xie, Y.-H. and Shi, B. 2019. Applicability of Microbial Calcification Method for Sandy-Slope Surface Erosion Control. Journal of Materials in Civil Engineering 31(11), pp. 1–11. DOI: 10.1061/(ASCE)MT.1943-5533.0002897

Jiang, N.J., Yoshioka, H., Yamamoto, K. and Soga, K. 2016. Ureolytic activities of a urease-producing bacterium and purified urease enzyme in the anoxic condition: Implication for subseafloor sand production control by microbially induced carbonate precipitation (MICP). Ecological Engineering 90(October 2017), pp. 96–104. DOI: 10.1016/j.ecoleng.2016.01.073

Kar, A. et al. 2009. Desertification and its control measures. Trends in Arid Zone Research in India (October), pp. 1–47.

Karol, R.H. 2003. Chemical Grouting And Soil Stabilization. Third. Marcel Dekker, New York. Available at: https://www.taylorfrancis.com/books/9780203911815

Kavazanjian, E., Iglesias, E. and Karatas, I. 2009. Biopolymer soil stabilization for wind erosion control. Proceedings of the 17th International Conference on Soil Mechanics and Geotechnical Engineering: The Academia and Practice of Geotechnical Engineering 1, pp. 881–884. DOI: 10.3233/978-1-60750-031-5-881

Keykha, H.A. and Asadi, A. 2017. Solar Powered Electro-Bio-Stabilization of Soil with Ammonium Pollution Prevention System. Advances in Civil Engineering Materials 6(1), p. 20170001. DOI: 10.1520/ACEM20170001

Keykha, H.A., Asadi, A. and Zareian, M. 2017. Environmental Factors Affecting the Compressive Strength of Microbiologically Induced Calcite Precipitation-Treated Soil. Geomicrobiology Journal 34(10), pp. 889–894. DOI: 10.1080/01490451.2017.1291772

Keykha, H.A., Mohamadzadeh, H., Asadi, A. and Kawasaki, S. 2019. Ammonium-Free Carbonate-Producing Bacteria as an Ecofriendly Soil Biostabilizer. Geotechnical Testing Journal 42(1), p. 20170353. DOI: 10.1520/GTJ20170353

Kim, M., Oh, H.S., Park, S.C. and Chun, J. 2014. Towards a taxonomic coherence between average nucleotide identity and 16S rRNA gene sequence similarity for species demarcation of prokaryotes. International Journal of Systematic and Evolutionary Microbiology 64(PART 2), pp. 346–351. DOI: 10.1099/ijs.0.059774-0

Konhauser, K. 2007. Introduction to Geomicrobiology. Blackwell Science Ltd. DOI: 10.1111/j.1365-2389.2007.00943_4.x

Konstantinou, C., Wang, Y., Biscontin, G. and Soga, K. 2021. The role of bacterial urease activity on the uniformity of carbonate precipitation profiles of bio-treated coarse sand specimens. Scientific Reports 11(1), pp. 1–17. DOI: 10.1038/s41598-021-85712-6

Kou, H., Wu, C., Ni, P. and Jang, B. 2020. Assessment of erosion resistance of biocemented sandy slope subjected to wave actions. Applied Ocean Research 105(October), p. 102401. DOI: 10.1016/j.apor.2020.102401

Krzeminska, D., Kerkhof, T., Skaalsveen, K. and Stolte, J. 2019. Effect of riparian vegetation on stream bank stability in small agricultural catchments. Catena 172(August 2018), pp. 87–96. DOI: 10.1016/j.catena.2018.08.014

Kumar, S., Stecher, G., Li, M., Knyaz, C. and Tamura, K. 2018. MEGA X : Molecular Evolutionary Genetics Analysis across Computing Platforms. 35(May), pp. 1547–1549. DOI: 10.1093/molbev/msy096

Kwon, Y.M., Chang, I., Lee, M. and Cho, G.C. 2019. Geotechnical engineering behavior of biopolymer-treated soft marine soil. Geomechanics and Engineering 17(5), pp. 453–464. DOI: 10.12989/gae.2019.17.5.453

Lai, H.J., Cui, M.J., Wu, S.F., Yang, Y. and Chu, J. 2021. Retarding effect of concentration of cementation solution on biocementation of soil. Acta Geotechnica 16(5), pp. 1457–1472. DOI: 10.1007/s11440-021-01149-1

Latrubesse, E.M. 2008. Patterns of anabranching channels: The ultimate end-member adjustment of mega rivers. Geomorphology 101(1–2), pp. 130–145. DOI: 10.1016/j.geomorph.2008.05.035

Lee, M., Gomez, M.G., San Pablo, A.C.M., Kolbus, C.M., Graddy, C.M.R., DeJong, J.T. and Nelson, D.C. 2019a. Investigating Ammonium By-product Removal for Ureolytic Bio-cementation Using Meter-scale Experiments. Scientific reports 9(1), p. 18313. DOI: 10.1038/s41598-019-54666-1

Lee, S., Chung, M., Park, H.M., Song, K.-I. and Chang, I. 2019b. Xanthan Gum Biopolymer as Soil-Stabilization Binder for Road Construction Using Local Soil in Sri Lanka. Journal of Materials in Civil Engineering 31(11), p. 06019012. DOI: 10.1061/(ASCE)MT.1943-5533.0002909

Li, C., Yao, D., Liu, S., Zhou, T., Bai, S., Gao, Y. and Li, L. 2018. Improvement of Geomechanical Properties of Bio-remediated Aeolian Sand. Geomicrobiology Journal 35(2), pp. 132–140. DOI: 10.1080/01490451.2017.1338798

Li, L., Du, S., Wu, L. and Liu, G. 2009. An overview of soil loss tolerance. Catena 78(2), pp. 93–99. DOI: 10.1016/j.catena.2009.03.007

Li, M., Fu, Q.L., Zhang, Q., Achal, V. and Kawasaki, S. 2015. Bio-grout based on microbially induced sand solidification by means of asparaginase activity. Scientific Reports 5, pp. 1–9. DOI: 10.1038/srep16128

Li, Q., Csetenyi, L. and Gadd, G.M. 2014. Biomineralization of metal carbonates by Neurospora crassa. Environmental Science and Technology 48(24), pp. 14409–14416. DOI: 10.1021/es5042546

Liang, S., Xiao, X., Wang, J., Wang, Y., Feng, D. and Zhu, C. 2022. Influence of Fiber Type and Length on Mechanical Properties of MICP-Treated Sand. Materials 15(11), p. 4017. DOI: 10.3390/ma15114017

Lipar, M. and Webb, J.A. 2015. The formation of the pinnacle karst in Pleistocene aeolian calcarenites (Tamala Limestone) in southwestern Australia. Earth-Science Reviews 140, pp. 182–202. DOI: 10.1016/j.earscirev.2014.11.007

Liu, B. et al. 2021a. Bio-mediated method for improving surface erosion resistance of clayey soils. Engineering Geology 293(November 2020), p. 106295. DOI: 10.1016/j.enggeo.2021.106295

Liu, K.-W., Jiang, N.-J., Qin, J.-D., Wang, Y.-J., Tang, C.-S. and Han, X.-L. 2021b. An experimental study of mitigating coastal sand dune erosion by microbial- and enzymatic-induced carbonate precipitation. Acta Geotechnica 16(2), pp. 467–480. DOI: 10.1007/s11440-020-01046-z

Lowenstam, H.A. 1981. Minerals formed by organisms. Science 211(4487), pp. 1126–1131. DOI: 10.1126/science.7008198

Ma, G., He, X., Jiang, X., Liu, H., Chu, J. and Xiao, Y. 2021. Strength and permeability of bentonite-assisted biocemented coarse sand. Canadian Geotechnical Journal 58(7), pp. 969–981. DOI: 10.1139/cgj-2020-0045

Maleki, M., Ebrahimi, S., Asadzadeh, F. and Emami Tabrizi, M. 2016. Performance of microbial-induced carbonate precipitation on wind erosion control of sandy soil. International Journal of Environmental Science and Technology 13(3), pp. 937–944. DOI: 10.1007/s13762-015-0921-z

Martin, D., Dodds, K., Ngwenya, B.T., Butler, I.B. and Elphick, S.C. 2012. Inhibition of sporosarcina pasteurii under anoxic conditions: Implications for subsurface carbonate precipitation and remediation via ureolysis. Environmental Science and Technology 46(15), pp. 8351–8355. DOI: 10.1021/es3015875

Mayorga, I.C., Astilleros, J.M. and Fernández-Díaz, L. 2019. Precipitation of CaCO3 polymorphs from aqueous solutions: The role of ph and sulphate groups. Minerals 9(3), pp. 1–16. DOI: 10.3390/min9030178

Mitchell, A.C., Espinosa-Ortiz, E.J., Parks, S.L., Phillips, A.J., Cunningham, A.B. and Gerlach, R. 2019. Kinetics of calcite precipitation by ureolytic bacteria under aerobic and anaerobic conditions. Biogeosciences 16(10), pp. 2147–2161. DOI: 10.5194/bg-16-2147-2019

Mitchell, J.K. and Santamarina, J.C. 2005. Biological Considerations in Geotechnical Engineering. Journal of Geotechnical and Geoenvironmental Engineering 131(10), pp. 1222–1233. DOI: 10.1061/(ASCE)1090-0241(2005)131:10(1222)

Moharana, P.C., Santra, P., Singh, D. V., Kumar, S., Goyal, R.K., Machiwal, D. and Yadav, O.P. 2016. ICAR-Central Arid Zone Research Institute, Jodhpur: Erosion processes and

desertification in the Thar Desert of India. Proceedings of the Indian National Science Academy 82(3), pp. 1117–1140. DOI: 10.16943/ptinsa/2016/48507

Montoya, B.M. and DeJong, J.T. 2015. Stress-Strain Behavior of Sands Cemented by Microbially Induced Calcite Precipitation. Journal of Geotechnical and Geoenvironmental Engineering 141(6), p. 04015019. DOI: 10.1061/(ASCE)GT.1943-5606.0001302

Mortensen, B.M., Haber, M.J., Dejong, J.T., Caslake, L.F. and Nelson, D.C. 2011. Effects of environmental factors on microbial induced calcium carbonate precipitation. Journal of Applied Microbiology 111(2), pp. 338–349. DOI: 10.1111/j.1365-2672.2011.05065.x

Mujah, D., Cheng, L. and Shahin, M.A. 2019. Microstructural and Geomechanical Study on Biocemented Sand for Optimization of MICP Process. Journal of Materials in Civil Engineering 31(4), p. 04019025. DOI: 10.1061/(asce)mt.1943-5533.0002660

Mujah, D., Shahin, M.A. and Cheng, L. 2017. State-of-the-Art Review of Biocementation by Microbially Induced Calcite Precipitation (MICP) for Soil Stabilization. Geomicrobiology Journal 34(6), pp. 524–537. DOI: 10.1080/01490451.2016.1225866

Murugan, R., Suraishkumar, G.K., Mukherjee, A. and Dhami, N.K. 2021. Insights into the influence of cell concentration in design and development of microbially induced calcium carbonate precipitation (MICP) process. PLoS ONE 16(7 July). DOI: 10.1371/journal.pone.0254536

Nassar, M.K. et al. 2018. Large-Scale Experiments in Microbially Induced Calcite Precipitation (MICP): Reactive Transport Model Development and Prediction. Water Resources Research 54(1), pp. 480–500. DOI: 10.1002/2017WR021488

Omoregie, A.I. 2016. Characterization of ureolytic bacteria isolated from Limestone Caves of Sarawak and evaluation of their efficiency in Biocementation. PhD thesis. Swinburne University of Technology.

Omoregie, A.I., Khoshdelnezamiha, G., Senian, N., Ong, D.E.L. and Nissom, P.M. 2017. Experimental optimisation of various cultural conditions on urease activity for isolated Sporosarcina pasteurii strains and evaluation of their biocement potentials. Ecological Engineering 109(September), pp. 65–75. DOI: 10.1016/j.ecoleng.2017.09.012

van Paassen, L.A. 2011. Bio-Mediated Ground Improvement: From Laboratory Experiment to Pilot Applications. Geo-Frontiers 2011 41165(February), pp. 4099–4108. DOI: 10.1061/41165(397)419

van Paassen, L.A., Daza, C.M., Staal, M., Sorokin, D.Y., van der Zon, W. and van Loosdrecht, M.C.M. 2010a. Potential soil reinforcement by biological denitrification. Ecological Engineering 36(2), pp. 168–175. DOI: 10.1016/j.ecoleng.2009.03.026

van Paassen, L.A., Ghose, R., van der Linden, T.J.M., van der Star, W.R.L. and van Loosdrecht, M.C.M. 2010b. Quantifying Biomediated Ground Improvement by Ureolysis: Large-Scale Biogrout Experiment. Journal of Geotechnical and Geoenvironmental Engineering 136(12), pp. 1721–1728. DOI: 10.1061/(asce)gt.1943-5606.0000382

Phukan, A., Goswami, R., Borah, D., Nath, A. and Mahanta, C. 2012. River Bank Erosion and Restoration in the Brahmaputra River in India. The Clarion 1(1), pp. 1697–2277.

Porter, H., Dhami, N.K. and Mukherjee, A. 2017a. Sustainable road bases with microbial precipitation. Proceedings of the Institution of Civil Engineers - Construction Materials 171(3), pp. 95–108. DOI: 10.1680/jcoma.16.00075

Porter, H., Dhami, N.K. and Mukherjee, A. 2017b. Synergistic chemical and microbial cementation for stabilization of aggregates. Cement and Concrete Composites 83, pp. 160–170. DOI: 10.1016/j.cemconcomp.2017.07.015

Al Qabany, A. and Soga, K. 2013. Effect of chemical treatment used in MICP on engineering properties of cemented soils. Géotechnique 63(4), pp. 331–339. DOI:10.1680/geot.SIP13.P.022

Rajabi Agereh, S., Kiani, F., Khavazi, K., Rouhipour, H. and Khormali, F. 2019. An environmentally friendly soil improvement technology for sand and dust storms control. Environmental Health Engineering and Management 6(1), pp. 63–71. DOI: 10.15171/ehem.2019.07

Ramachandran, A.L., Dubey, A.A., Dhami, N.K. and Mukherjee, A. 2021. Multiscale Study of Soil Stabilization Using Bacterial Biopolymers. Journal of Geotechnical and Geoenvironmental Engineering 147(8), p. 04021074. DOI: 10.1061/(ASCE)GT.1943-5606.0002575

Ramachandran, A.L., Polat, P., Mukherjee, A. and Dhami, N.K. 2020. Understanding and creating biocementing beachrocks via biostimulation of indigenous microbial communities. Applied Microbiology and Biotechnology 104(8), pp. 3655–3673. DOI: 10.1007/s00253-020-10474-6

Ravi, S. et al. 2011. Aeolian processes and the biosphere. Reviews of Geophysics 49(3), pp. 1–45. DOI: 10.1029/2010RG000328

Ravi, S., Zobeck, T.M., Over, T.M., Okin, G.S. and D'Odorico, P. 2006. On the effect of moisture bonding forces in air-dry soils on threshold friction velocity of wind erosion. Sedimentology 53(3), pp. 597–609. DOI: 10.1111/j.1365-3091.2006.00775.x

Rebata-Landa, V. 2007. Microbial Activity in Sediments: Effects on Soil Behavior. Doctoral dissertation, Georgia Institute of Technology Atlanta, GA

van Rijn, L.C., Walstra, D.-J.R. and van Ormondt, M. 2007. Unified View of Sediment Transport by Currents and Waves. IV: Application of Morphodynamic Model. Journal

of Hydraulic Engineering 133(7), pp. 776–793. DOI: 10.1061/(ASCE)0733-9429(2007)133:7(776)

Rodríguez-Martínez, M., Sánchez, F., Walliser, E.O. and Reitner, J. 2012. An Upper Turonian fine-grained shallow marine stromatolite bed from the Muñecas Formation, Northern Iberian Ranges, Spain. Sedimentary Geology 263–264, pp. 96–108. DOI: 10.1016/j.sedgeo.2011.06.014

Rodriguez-Navarro, C., Jroundi, F., Schiro, M., Ruiz-Agudo, E. and González-Muñoz, M.T. 2012. Influence of substrate mineralogy on bacterial mineralization of calcium carbonate: Implications for stone conservation. Applied and Environmental Microbiology 78(11), pp. 4017–4029. DOI: 10.1128/AEM.07044-11

Rodriguez-Navarro, C., Rodriguez-Gallego, M., Chekroun, K. Ben and Gonzalez-Muñoz, M.T. 2003. Conservation of ornamental stone by Myxococcus xanthus-induced carbonate biomineralization. Applied and Environmental Microbiology 69(4), pp. 2182–2193. DOI: 10.1128/AEM.69.4.2182-2193.2003

Rosalam, S. and England, R. 2006. Review of xanthan gum production from unmodified starches by Xanthomonas comprestris sp. Enzyme and Microbial Technology 39(2), pp. 197–207. DOI: 10.1016/j.enzmictec.2005.10.019

Salifu, E., MacLachlan, E., Iyer, K.R., Knapp, C.W. and Tarantino, A. 2016. Application of microbially induced calcite precipitation in erosion mitigation and stabilisation of sandy soil foreshore slopes: A preliminary investigation. Engineering Geology 201, pp. 96–105. DOI: 10.1016/j.enggeo.2015.12.027

Sánchez-Román, M., Romanek, C.S., Fernández-Remolar, D.C., Sánchez-Navas, A., McKenzie, J.A., Pibernat, R.A. and Vasconcelos, C. 2011. Aerobic biomineralization of Mg-rich carbonates: Implications for natural environments. Chemical Geology 281(3–4), pp. 143–150. DOI: 10.1016/j.chemgeo.2010.11.020

Santra, P., Mertia, R.S., Kumawat, R.N. and Sinha, N.K. 2013. Loss of Soil Carbon and Nitrogen through Wind Erosion in the Indian Thar Desert. Journal of Agricultural Physics 13(1), pp. 13–21

Sarma, J.N. 2005. Fluvial process and morphology of the Brahmaputra River in Assam, India. Geomorphology 70(3-4 SPEC. ISS.), pp. 226–256. DOI: 10.1016/j.geomorph.2005.02.007.

Scheres, B. and Schüttrumpf, H. 2020. Investigating the Erosion Resistance of Different Vegetated Surfaces for Ecological Enhancement of Sea Dikes. Journal of Marine Science and Engineering 8(7), p. 519. DOI: 10.3390/jmse8070519

Ševčík, R., Šašek, P. and Viani, A. 2018. Physical and nanomechanical properties of the synthetic anhydrous crystalline CaCO3 polymorphs: vaterite, aragonite and calcite. Journal of Materials Science 53(6), pp. 4022–4033. DOI: 10.1007/s10853-017-1884-x

Shahin, M.A., Jamieson, K. and Cheng, L. 2020. Microbial-induced carbonate precipitation for coastal erosion mitigation of sandy slopes. Géotechnique Letters 10(2), pp. 1–5. DOI: 10.1680/jgele.19.00093

Sharma, M., Satyam, N. and Reddy, K.R. 2020. Strength Enhancement and Lead Immobilization of Sand Using Consortia of Bacteria and Blue-Green Algae. Journal of Hazardous, Toxic, and Radioactive Waste 24(4), p. 04020049. DOI: 10.1061/(ASCE)HZ.2153-5515

Sharma, M., Satyam, N. and Reddy, K.R. 2021. Effect of freeze-thaw cycles on engineering properties of biocemented sand under different treatment conditions. Engineering Geology 284(November 2020), p. 106022. DOI: 10.1016/j.enggeo.2021.106022

Singh, C., Osbahr, H. and Dorward, P. 2018. The implications of rural perceptions of water scarcity on differential adaptation behaviour in Rajasthan, India. Regional Environmental Change 18(8), pp. 2417–2432. DOI: 10.1007/s10113-018-1358-y

Skafel, M.G. and Bishop, C.T. 1994. Flume experiments on the erosion of till shores by waves. Coastal Engineering 23(3–4), pp. 329–348. DOI: 10.1016/0378-3839(94)90009-4

Smith, A.C. and Hussey, M.A. 2005. Gram stain protocols. American Society for Microbiology (September 2005), p. 14

Smith, R.W., Fujita, Y., Hubbard, S.S. and Ginn, T.R. 2012. Field Investigations of Microbially Facilitated Calcite Precipitation for Immobilization of Strontium-90 and Other Trace Metals in the Subsurface. Final report for United States Department of Energy (DOE) Grant No. DE-FG02-07ER64404 (October)

Soon, N.W., Lee, L.M., Khun, T.C. and Ling, H.S. 2014. Factors Affecting Improvement in Engineering Properties of Residual Soil through Microbial induced calcite precipitation. 04014006(11), pp. 1–11. Available at: DOI: 10.1061/(ASCE)GT.1943-5606.0001089

Spencer, C.A., van Paassen, L. and Sass, H. 2020. Effect of jute fibres on the process of MICP and properties of biocemented sand. Materials 13(23), pp. 1–24. DOI: 10.3390/ma13235429

Stabnikov, V., Ivanov, V. and Chu, J. 2015. Construction Biotechnology: a new area of biotechnological research and applications. World Journal of Microbiology and Biotechnology 31(9), pp. 1303–1314. DOI: 10.1007/s11274-015-1881-7

Stocks-Fischer, S., Galinat, J.K. and Bang, S.S. 1999. Microbiological precipitation of CaCO3. Soil Biology and Biochemistry 31(11), pp. 1563–1571. DOI: 10.1016/S0038-0717(99)00082-6.

Tambunan, T., Juki, M.I. and Othman, N. 2019. Mechanical properties of sulphate reduction bacteria on the durability of concrete in chloride condition. Awaludin, A., Matsumoto, T., Pessiki, S., Jonkers, H., Siswosukarto, S., Fajar Setiawan, A., and Nur Rahma Putri, K. eds. MATEC Web of Conferences 258(S5), p. 01024. Available at: https://www.matec-conferences.org/10.1051/matecconf/201925801024

Terzis, D. and Laloui, L. 2017. On the Application of Microbially Induced Calcite Precipitation for Soils: A Multiscale Study. In: Advances in Laboratory Testing and Modelling of Soils and Shales. Springer Series in Geomechanics and Geoengineering, pp. 388–394. DOI: 10.1007/978-3-319-52773-4_46

Terzis, D. and Laloui, L. 2018. 3-D micro-architecture and mechanical response of soil cemented via microbial-induced calcite precipitation. Scientific Reports 8(1), pp. 1–11. DOI: 10.1038/s41598-018-19895-w

Terzis, D. and Laloui, L. 2019. A decade of progress and turning points in the understanding of bio-improved soils: A review. Geomechanics for Energy and the Environment 19(March), p. 100116. DOI: 10.1016/j.gete.2019.03.001

Tian, K., Wu, Y., Zhang, H., Li, D., Nie, K. and Zhang, S. 2018. Increasing wind erosion resistance of aeolian sandy soil by microbially induced calcium carbonate precipitation. Land Degradation & Development 29(12), pp. 4271–4281. DOI: 10.1002/ldr.3176

Tiwari, N., Satyam, N. and Sharma, M. 2021. Micro-mechanical performance evaluation of expansive soil biotreated with indigenous bacteria using MICP method. Scientific Reports 11(1), pp. 1–12. DOI: 10.1038/s41598-021-89687-2

Tobler, D.J., Cuthbert, M.O., Greswell, R.B., Riley, M.S., Renshaw, J.C., Handley-Sidhu, S. and Phoenix, V.R. 2011. Comparison of rates of ureolysis between Sporosarcina pasteurii and an indigenous groundwater community under conditions required to precipitate large volumes of calcite. Geochimica et Cosmochimica Acta 75(11), pp. 3290–3301. DOI: 10.1016/j.gca.2011.03.023

Ulusay, R. et al. 2014. ISRM suggested method for the needle penetration test. Rock Mechanics and Rock Engineering 47(3), pp. 1073–1085. DOI: 10.1007/s00603-013-0534-0

Ulusay, R. and Erguler, Z.A. 2012. Needle penetration test: Evaluation of its performance and possible uses in predicting strength of weak and soft rocks. Engineering Geology 149–150, pp. 47–56. DOI: 10.1016/j.enggeo.2012.08.007

United Nations 2019. Global perspective Human stories, U.N. news. pp. 1–6. Available at: https://news.un.org/en/story/2019/06/1040561

USEPA 2013. Aquatic Life Ambient Water Quality Criteria for Ammonia – Freshwater. Available at: https://www.epa.gov/sites/production/files/2015-08/documents/aquatic-life-ambient-water-quality-criteria-for-ammonia-freshwater-2013.pdf

Velayati, A.A. et al. 2015. Identification and genotyping of Mycobacterium tuberculosis isolated from water and soil samples of a metropolitan city. Chest 147(4), pp. 1094–1102. DOI: 10.1378/chest.14-0960

Wang, X., Tao, J., Bao, R., Tran, T. and Tucker-Kulesza, S. 2018a. Surficial Soil Stabilization against Water-Induced Erosion Using Polymer-Modified Microbially Induced Carbonate Precipitation. Journal of Materials in Civil Engineering 30(10), p. 04018267. DOI: 10.1061/(ASCE)MT.1943-5533.0002490

Wang, Y.-J., Jiang, N.-J., Han, X.-L., Liu, K. and Du, Y.-J. 2022. Biochemical, Strength and Erosional Characteristics of Coral Sand Treated by Bio-Stimulated Microbial Induced Calcite Precipitation. Acta Geotechnica 0123456789. DOI: 10.1007/s11440-022-01491-y

Wang, Y., Soga, K., DeJong, J.T. and Kabla, A.J. 2021. Effects of Bacterial Density on Growth Rate and Characteristics of Microbial-Induced CaCO3 Precipitates: Particle-Scale Experimental Study. Journal of Geotechnical and Geoenvironmental Engineering 147(6), pp. 1–13. DOI: 10.1061/(asce)gt.1943-5606.0002509

Wang, Z., Zhang, N., Ding, J., Lu, C. and Jin, Y. 2018b. Experimental Study on Wind Erosion Resistance and Strength of Sands Treated with Microbial-Induced Calcium Carbonate

Precipitation. Advances in Materials Science and Engineering 2018, pp. 1–10. DOI: 10.1155/2018/3463298

Weatherburn, M.W. 1967. Phenol-Hypochlorite Reaction for Determination of Ammonia. Analytical Chemistry 39(8), pp. 971–974. DOI: 10.1021/ac60252a045

Wen, K., Li, Y., Amini, F. and Li, L. 2020. Impact of bacteria and urease concentration on precipitation kinetics and crystal morphology of calcium carbonate. Acta Geotechnica 15(1), pp. 17–27. DOI: 10.1007/s11440-019-00899-3

Whiffin, V.S. 2004. Microbial CaCO3 Precipitation for the Production of Biocement. Murdoch University, Western Australia. DOI: http://researchrepository.murdoch.edu.au/399/2/02Whole.pdf

Whiffin, V.S., van Paassen, L.A. and Harkes, M.P. 2007. Microbial carbonate precipitation as a soil improvement technique. Geomicrobiology Journal 24(5), pp. 417–423. DOI: 10.1080/01490450701436505

Won, J., Jeong, B., Lee, J., Dai, S. and Burns, S.E. 2021. Facilitation of microbially induced calcite precipitation with kaolinite nucleation. Geotechnique 71(8), pp. 728–734. DOI: 10.1680/jgeot.19.P.324

Wu, S., Li, B. and Chu, J. 2021. Stress-Dilatancy Behavior of MICP-Treated Sand. International Journal of Geomechanics 21(3), p. 04020264. DOI: 10.1061/(asce)gm.1943-5622.0001923

Yang, J. et al. 2016. Bioimmobilization of heavy metals in acidic copper mine tailings soil. Geomicrobiology Journal 33(3–4), pp. 261–266. DOI: 10.1080/01490451.2015.1068889

Yu, X., Qian, C. and Xue, B. 2016. Loose sand particles cemented by different bio-phosphate and carbonate composite cement. Construction and Building Materials 113, pp. 571–578. DOI: 10.1016/j.conbuildmat.2016.03.105

Zdankus, N., Punys, P. and Zdankus, T. 2014. Conversion of lowland river flow kinetic energy. Renewable and Sustainable Energy Reviews 38, pp. 121–130. DOI: 10.1016/j.rser.2014.05.074

Zeng, C., Veenis, Y., Hall, C.A., Young, E.S., van der Star, W.R.L., Zheng, J. and van Paassen, L.A. 2021. Experimental and Numerical Analysis of a Field Trial Application of Microbially Induced Calcite Precipitation for Ground Stabilization. Journal of Geotechnical and Geoenvironmental Engineering 147(7), p. 05021003. DOI: 10.1061/(asce)gt.1943-5606.0002545

Zhang, M. et al. 2020. Effect of Microsprinkler Irrigation under Plastic Film on Photosynthesis and Fruit Yield of Greenhouse Tomato. Journal of Sensors 2020, pp. 1–14. DOI: 10.1155/2020/8849419

Zhao, Q., Li, L., Li, C., Li, M., Amini, F. and Zhang, H. 2014. Factors Affecting Improvement of Engineering Properties of MICP-Treated Soil Catalyzed by Bacteria and Urease. Journal of Materials in Civil Engineering 26(12), p. 04014094. DOI: 10.1061/(ASCE)MT.1943-5533.0001013

Zhu, C., Vail, M., Tang, C.S., Anderson, L., Moroski, M. and Montalbo-Lomboy, M.T. 2019. Desiccation cracking behavior of MICP-treated bentonite. Geosciences (Switzerland) 9(9), pp. 1–16. DOI: 10.3390/geosciences9090385

Zomorodian, S.M.A., Ghaffari, H. and O'Kelly, B.C. 2019. Stabilisation of crustal sand layer using biocementation technique for wind erosion control. Aeolian Research 40(March), pp. 34–41. DOI: 10.1016/j.aeolia.2019.06.001

Zuazo, V.H.D. and Pleguezuelo, C.R.R. 2008. Soil-erosion and runoff prevention by plant covers. A review. Agronomy for Sustainable Development 28(1), pp. 65–86. DOI: 10.1051/agro:2007062

List of Publications

A. Peer-reviewed Journals

Dubey, A.A., Ravi, K., Mukherjee, A., Sahoo, L., Abiala, M.A. and Dhami, N.K. 2021. Biocementation mediated by native microbes from Brahmaputra riverbank for mitigation of soil erodibility. Scientific Reports 11(1), p. 15250. DOI: 10.21203/rs.3.rs-235959/v1.

Dubey, A.A., Devrani, R., Ravi, K., Kaur, N., Mukherjee, A. and Sahoo, L. 2021. Experimental investigation to mitigate aeolian erosion via biocementation employed with a novel ureolytic soil isolate. Aeolian Research 52(July), p. 100727. DOI: 10.1016/j.aeolia.2021.100727.

Dubey, A.A., Murugan, R., Ravi, K., Mukherjee, A. and Dhami, N.K. 2022. Investigation on the Impact of Cementation Media Concentration on Properties of Biocement under Stimulation and Augmentation Approaches. Journal of Hazardous, Toxic, and Radioactive Waste 26(1), pp. 1–13. DOI: 10.1061/(ASCE)HZ.2153-5515.0000662

Dubey, A.A., Ravi, K., Shahin, M.A., Dhami, N.K. and Mukherjee, A. 2021. Bio-composites treatment for mitigation of current-induced riverbank soil erosion. Science of The Total Environment 800, DOI: 10.1016/j.scitotenv.2021.149513.

Dubey, A.A., Hooper-Lewis, J., Ravi, K., Dhami, N.K. and Mukherjee, A. 2022. Biopolymer-biocement composite treatment for stabilisation of soil against both current and wave erosion. Acta Geotechnica. D: 10.1007/s11440-022-01536-2.

Dubey, A.A., Ravi, K., Dhami, N.K. and Mukherjee, A. 202X Biocementation and its potential in mitigation of soil erosion: A review on applications, limitations and future directions. Under preparation.

B. Conferences proceedings, Book Chapters and Workshops

Dubey, A.A., Devrani, R., Ravi, K., Dhami, N.K. and Mukherjee, A. 2022. Influence of Single-Dose Biocement Treatment on the Hydraulic Conductivity of the Riverbank Sand. In: Proceedings of the 7th World Congress on Civil, Structural, and Environmental Engineering.

Dubey, A.A., Devrani, R., Ravi, K. and Sahoo, L. 2021. Investigation of the Microstructure of Brahmaputra Sand Treated with Bacillus megaterium-Mediated Single-Dosed Bio-Cementation. In: Lecture Notes in Civil Engineering., pp. 549–555. Available at: https://link.springer.com/10.1007/978-981-33-6444-8_49.

Dubey, A.A., Ravi, K., Dhami, N.K. and Mukherjee, A. 2020 Evaluation of potential bio-stimulation for landslide mitigation by native high urease producing microbe, 1st International Conference on Microbial Biotechnology in Construction Materials and Geotechnical Engineering, Nanjing, China.

Dubey, A.A., Borthakur, A., Rathore, S., and Ravi, K. 2017 Sustainable ground improvement by means of bio-engineered geo-microbial activities-A critical review, Workshop on sustainable geotechnics, IGS Kanpur chapter, IIT Kanpur, India.

Appendix 1

Qualitative evaluation of the Physicochemical Properties of the isolates (P=positive, N= negative) in comparison to *Sporosarcina pasteurii* (SP)

Tests*/ Microbe	**U**	**O**	**L**	**Or**	**H2S**	**G**	**M**	**X**	**ONPG**	**I**	**VP**	**C**	**TDA**	**G**	**Ma**	**In**	**S**	**R**	**Su**	**Ar**	**Ad**	**Ra**	**Sal**	**Arg**
SP	P	P	**P**	N	N	N	N	N	**P**	N	P	N	P	N	N	N	N	N	N	N	N	N	N	N
BS1	P	P	**N**	N	N	N	N	N	**N**	N	P	N	P	N	N	N	N	N	N	N	N	N	N	N
BS2	P	P	**N**	N	N	N	N	N	**N**	N	P	N	P	N	N	N	N	N	N	N	N	N	N	N
BS3	P	P	**N**	N	N	N	N	N	**N**	N	P	N	P	N	N	N	N	N	N	N	N	N	N	N
BS4	P	P	**N**	N	N	N	N	N	**N**	N	P	N	P	N	N	N	N	N	N	N	N	N	N	N
LS1	P	P	**N**	N	N	N	N	N	**N**	N	P	N	P	N	N	N	N	N	N	N	N	N	N	N
LS2	P	P	**N**	N	N	N	N	N	**N**	N	P	N	P	N	N	N	N	N	N	N	N	N	N	N

Where, biochemical qualitative tests, U= Urease; O=Oxidase; L=Lysine; Or= Ornithine; H2S= Hydrogen sulphide production; G= Glucose; M= Mannitol; X=Xylose; ONPG= ortho-Nitrophenyl-β-galactoside; I=Indole; VP= Voges–Proskauer; C=Citrate; TDA= Tryptophan Deaminase Reaction; Ge= Gelatin; Ma= Malonate; In= Inositol; S= Sorbitol; R= Rhamose; Su= Sucrose; Ar= Arabinose, Ad= Adonitiol; Ra= Raffinose; Sal= Salicin; Arg= Arginine.